Els quàdruplex de guanina: Estudis estructurals i diana farmacològica

Rubén Ferreira Aguilera

ADVERTIMENT. La consulta d'aquesta tesi queda condicionada a l'acceptació de les següents condicions d'ús: La difusió d'aquesta tesi per mitjà del servei TDX (**www.tdx.cat**) ha estat autoritzada pels titulars dels drets de propietat intel·lectual únicament per a usos privats emmarcats en activitats d'investigació i docència. No s'autoritza la seva reproducció amb finalitats de lucre ni la seva difusió i posada a disposició des d'un lloc aliè al servei TDX. No s'autoritza la presentació del seu contingut en una finestra o marc aliè a TDX (framing). Aquesta reserva de drets afecta tant al resum de presentació de la tesi com als seus continguts. En la utilització o cita de parts de la tesi és obligat indicar el nom de la persona autora.

ADVERTENCIA. La consulta de esta tesis queda condicionada a la aceptación de las siguientes condiciones de uso: La difusión de esta tesis por medio del servicio TDR (**www.tdx.cat**) ha sido autorizada por los titulares de los derechos de propiedad intelectual únicamente para usos privados enmarcados en actividades de investigación y docencia. No se autoriza su reproducción con finalidades de lucro ni su difusión y puesta a disposición desde un sitio ajeno al servicio TDR. No se autoriza la presentación de su contenido en una ventana o marco ajeno a TDR (framing). Esta reserva de derechos afecta tanto al resumen de presentación de la tesis como a sus contenidos. En la utilización o cita de partes de la tesis es obligado indicar el nombre de la persona autora.

WARNING. On having consulted this thesis you're accepting the following use conditions: Spreading this thesis by the TDX (**www.tdx.cat**) service has been authorized by the titular of the intellectual property rights only for private uses placed in investigation and teaching activities. Reproduction with lucrative aims is not authorized neither its spreading and availability from a site foreign to the TDX service. Introducing its content in a window or frame foreign to the TDX service is not authorized (framing). This rights affect to the presentation summary of the thesis as well as to its contents. In the using or citation of parts of the thesis it's obliged to indicate the name of the author.

UNIVERSITAT DE BARCELONA

FACULTAT DE FARMÀCIA

DEPARTAMENT DE FARMÀCOLOGIA I QUÍMICA TERAPÈUTICA

"Els quàdruplex de guanina: Estudis estructurals i diana farmacològica"

Rubén Ferreira Aguilera

2012

UNIVERSITAT DE BARCELONA

FACULTAT DE FARMÀCIA

DEPARTAMENT DE FARMÀCOLOGIA I QUÍMICA TERAPÈUTICA

"Els quàdruplex de guanina: Estudis estructurals i diana farmacològica"

Memòria presentada per:

Rubén Ferreira Aguilera

Per optar al títol de Doctor per la Universitat de Barcelona
Programa de doctorat: Química Orgànica a la Indústria Químico-farmacèutica
Bienni 2008-10

Dirigida per: Dr. Ramon Eritja Casadellà i Dra. Anna Aviñó Andrés

Tutor: Dr. Joan Bosch Cartes

Barcelona, 2012

Volia agrair a tothom qui ha contribuït professionalment a la tesis, especialment al meus supervisors Ramon Eritja i Anna Aviñó. També voldria agrair als meus companys de laboratori i als investigadors que m'han rebut a les estades a l'estranger o durant les col·laboracions.

A la meva família i als meus amics, pel seu suport i ànims.

El treball descrit en aquesta memòria ha estat realitzat a l'Institut de Recerca Biomèdica (IRB) situat al Parc Científic de Barcelona de la Universitat de Barcelona. Aquest ha gaudit dels ajuts que es detallen a continuació.

Beca predoctoral del Ministeri de Ciència i Innovació d'Espanya, FPI (BES-2008-009315). Beques per realitzar estades breus a Milà (Italia), Liège (Belgica) i Minneapolis (USA) del Ministeri de Ciència i Innovació (SEST1000I000028XV0; EEBB-2011-44445 i EEBB-I-12-05224). Beques finançades pel COST (*European Cooperation in Sciencie and Technology*) per participar a un workshop a Spa (Belgica) i una estada breu a Liège.

ÍNDEX

ÍNDEX D'ABREVIATURES

Abs: Absorbància
ACN: Acetonitril
Ac2O: Anhídrid acètic
AcOEt: Acetat d'etil
Aeg: (2-Aminoetil)-glicina
Boc: *tert*-Butoxicarbonil
CCS: Secció eficaç de col·lisió (*Collision cross section*)
CD: Dicroisme circular
COSY: Espectroscòpia de correlació
CPG: Vidre de porus controlat
DACA: N-[2-(Dimetilamino)etil]acridina-4-carboxamida
DCM: Diclorometà
DDS: 2,2-Dimetil-2-silapentà-5-sulfonat de sodi perdeuterat
DIEA: Diisopropiletilamina
DIPCDI: N,N'-Diisopropilcarbodiimida
DIPEA: Diisopropiletilamina
DMAP: 4-Dimetilaminopiridina
DMEM: Medi de cultiu d'Eagle modificat per Dulbecco
DMF: *N*,*N*-Dimetilformamida
DMSO: Dimetilsufòxid
DMT: 4,4-O-Dimetoxitritil
DNA: Àcid desoxiribonucleic
DQF: Seqüència de polsos (filtre de doble quantum)
EDTA: Àcid etilendiaminotetracètic
ESI: Ionització per electrosprai
EtOH: Etanol
FBS: Sèrum fetal boví
Fmoc: 9-Fluorenilmetoxicarbonil
GLC-4 clon: Línea cel·lular humana de càncer de pulmó
HBT-38: Línea cel·lular humana de càncer colon
HIV: Virus de la immunodeficiència humana
HOBt: 1-Hidroxibenzotriazole
HPLC: Cromatografia líquida d'alta pressió
IC: Concentració inhibitòria
IMS: Espectroscòpia iònica de masses
iPrOH: Isopropanol
Jurkat clone E6-1: Línea cel·lular humana de càncer de leucèmia
LGA: Algoritme genètic de Lamarckian
LV: Columna de baix volum per sintetitzar oligonucleòtids
MALDI-TOF: Ionització per desorció laser assistida per matriu – Temps de vol
MBHA: Metilbenzildrilamina
MD: Dinàmica molecular
mdeg: Miligraus
MM: Mecànica molecular
MeOH: Metanol
mRNA: Àcid ribonucleic missatger
MS: Espectroscòpia de masses
MTT: Bromur de 3-(4,5-dimetiltiazol2-il)-2,5-difeniltetrazol
m/z: Relació massa/càrrega
NAP: Columna de Sephadex
NH4OAc: Acetat d'amoni
NIHT-3T3: Línea cel·lular de ratolí
NMR: Ressonància magnètica nuclear
NOE: Efecte Overhausser Nuclear
NOESY: Espectroscòpia per efecte Overhausser nuclear
OD: Densitat òptica
ODN: Oligonucleòtid
PAGE: Electroforesi en gel de poliacrilamida

PBS: Tampó fosfat salí
PNA: Àcid nucleic peptídic
PDB: Base de dades d'estructures tridimensional de proteïnes i àcids nucleics
PS: Poliestirè
PyBOP: Hexafluorofosfat de (benzotriazol-1-iloxi)tripirrolidinofosfoni
Pyr: Piridina
QM: Mecànica quàntica
rmsd: Desviació per la mitjana quadràtica
RNA: Àcid ribonucleic
RPMI: Medi Roswell Park Memorial Institute
r.t.: Temperatura ambient
Sar: Sarcosina
SDS: Dodecasulfat de Sodi
TAE: Solució tampó formada per Tris, Acetat i EDTA
TB: Trebler, reactiu per generar tres cadenes de DNA
TCA: Àcid tricloroacètic
TEAA: Acetat de trietilamoni
TFA: Àcid trifluoroacètic
TLC: Cromatografia en capa fina
TOCSY: Espectroscòpia de correlació total
Tris: Tris(hidroximetil)aminometà
UV: Ultravioleta
WC: Watson-Crick

ÍNDEX DE FIGURES

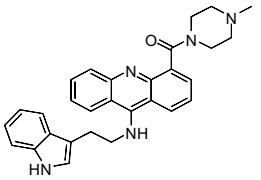

1 BBA (2012)

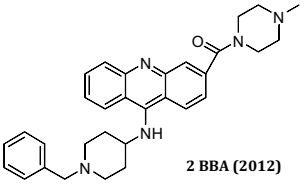

2 BBA (2012)

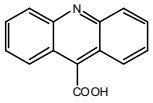

acridine-9-carboxylic acid
J. Nucleic acids
1 BBA (2011)
1 Molecules

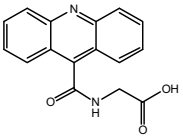

2-(acridine-9-carboxamide)
acetic acid J. Nucleic acids
2 BBA (2011)

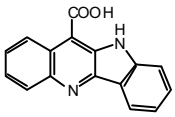

3 BBA (2011)

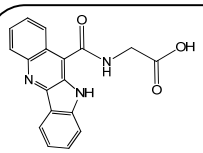

4 BBA (2011)

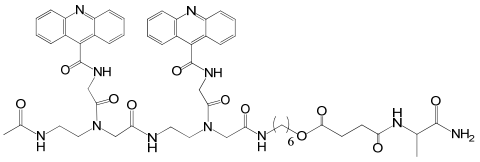

Dimer 1 J. Nucleic acids

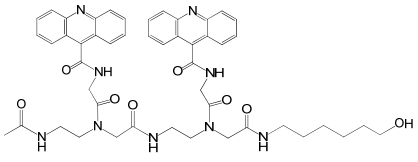

Dimer 2 J. Nucleic acids

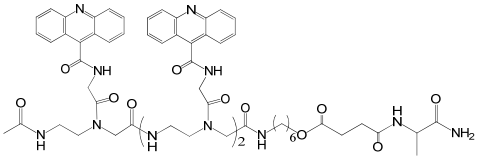

Trimer 3 J. Nucleic acids

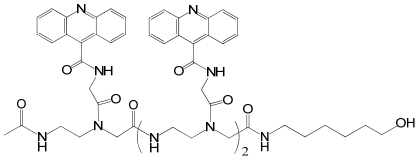

Trimer 4 J. Nucleic acids

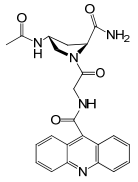

5 BBA (2011)

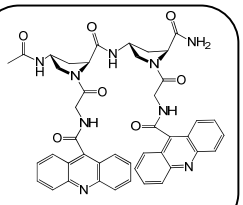

6 BBA (2011)

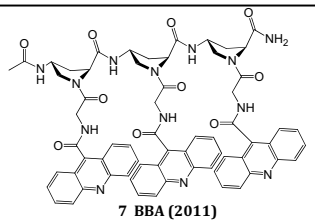

7 BBA (2011)

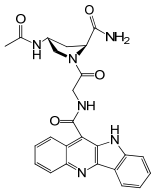

8 BBA (2011)

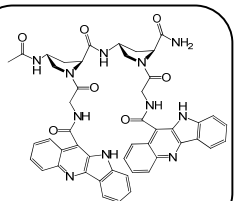

9 BBA (2011)

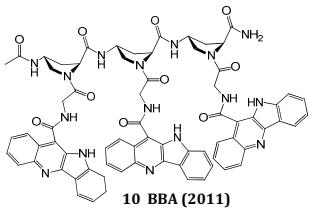

10 BBA (2011)

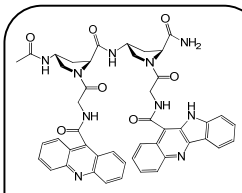

11 BBA (2011)

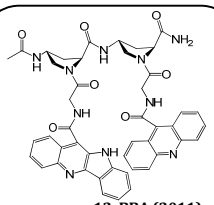

12 BBA (2011)

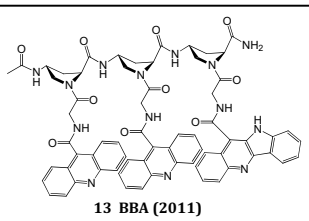

13 BBA (2011)

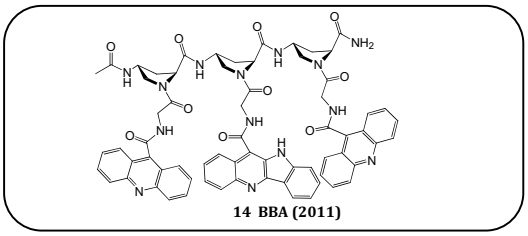

14 BBA (2011)

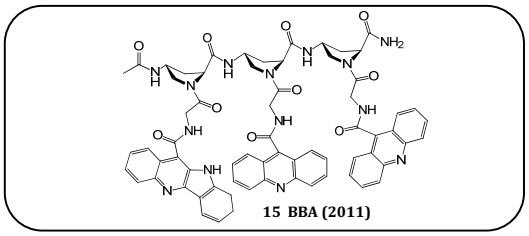

15 BBA (2011)

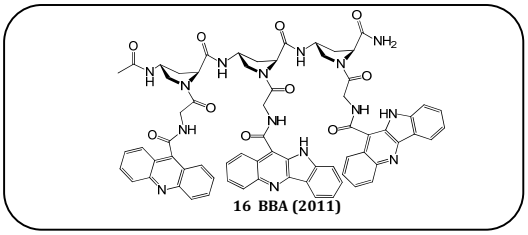

16 BBA (2011)

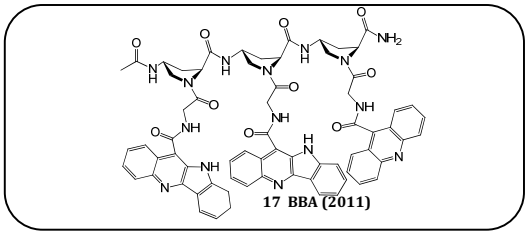

17 BBA (2011)

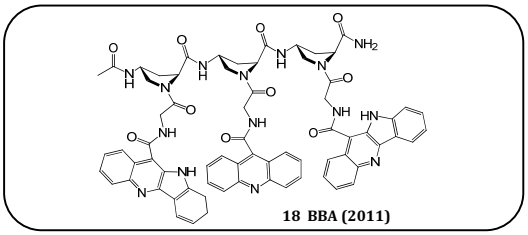

18 BBA (2011)

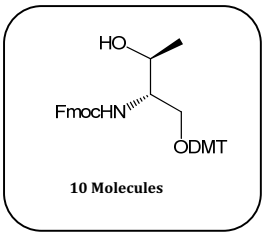

10 Molecules

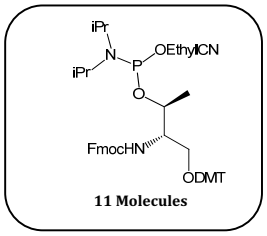

11 Molecules

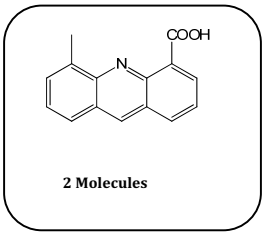

2 Molecules

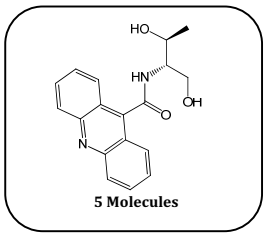

5 Molecules

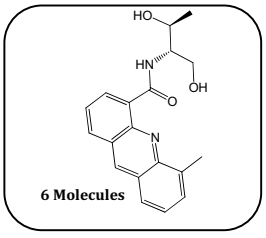

6 Molecules

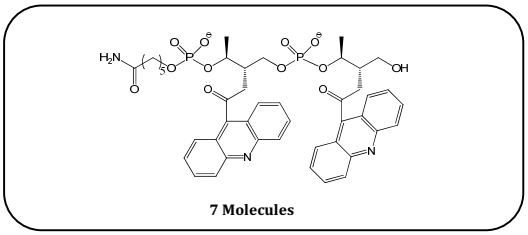

7 Molecules

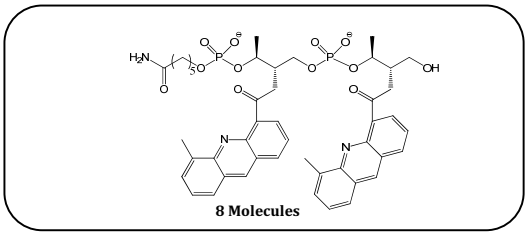

8 Molecules

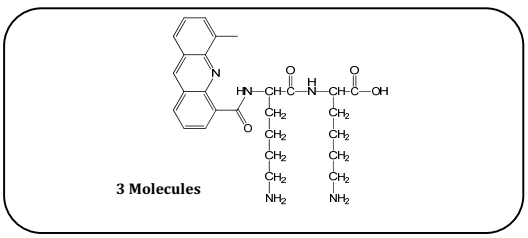

3 Molecules

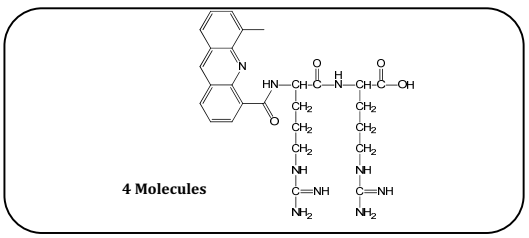

4 Molecules

Introducció i objectius

INTRODUCCIÓ

La diversitat conformacional dels àcids nucleics

El descobriment de l'estructura del DNA com un dúplex helicoïdal de polímers de nucleòtids, per James Watson i Francis Crick el 1953 [1], ha permès als científics reexaminar la majoria dels fenòmens biològics. Així, en les últimes cinc dècades, s'ha formulat una visió general de l'herència biològica i de la transferència d'informació genètica, que ha permès establir l'anomenat "Dogma central de la Biologia Molecular" [2].

La doble hèlix de DNA està estabilitzada principalment per les interaccions de pont d'hidrogen que s'estableixen entre les nucleobases de cada cadena (Figura 1). Entre les dues cadenes també es formen interaccions de tipus hidrofòbic i interacció d'apilament entre les nucleobases [3].

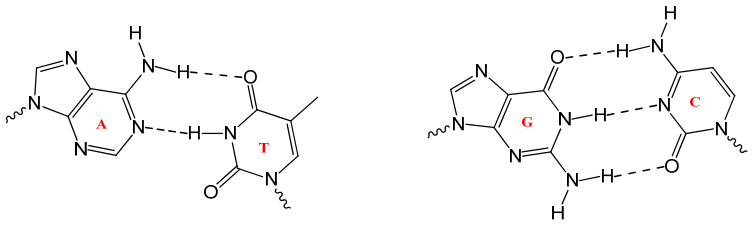

Figura 1. Enllaços de pont d'hidrogen de tipus Watson-Crick entre A-T i G-C.

En els sistemes biològics s'han identificat tres conformacions fonamentals per la doble hèlix de DNA, anomenades A-DNA, B-DNA i Z-DNA (Figura 2) [3].

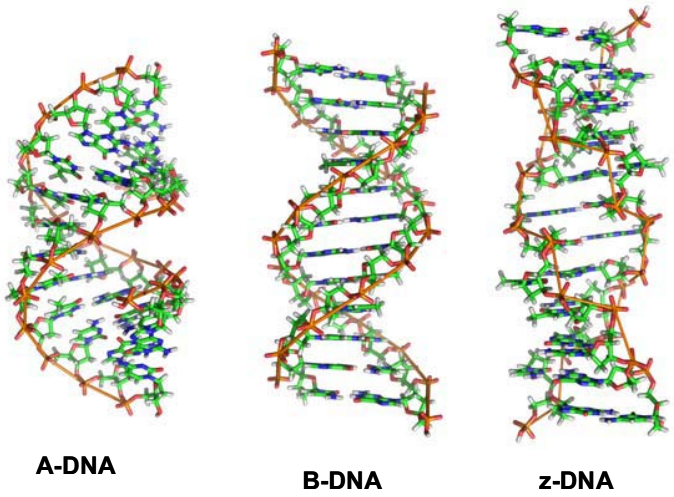

Figura 2. Conformacions bàsiques de la doble hèlix de DNA: B-DNA, A-DNA i Z-DNA.

La conformació helicoïdal B-DNA [3], descrita per James Watson i Francis Crick, és la forma predominant en els organismes vius. La forma A [4] és adoptada pels fragments de doble cadena d'RNA i essencialment pels híbrids DNA-RNA [3], també es pot donar en dúplexs de DNA en condicions d'alta concentració de cations o baixa hidratació [5]. La conformació A presenta diferències respecte la B, és més compacta i els solcs són diferents [3]. Aquestes diferències són crucials pel reconeixement de certes proteïnes [5]. El primer cristall de DNA que es va aconseguir resoldre, va mostrar un dúplex levogir i per la seva forma en zig-zag va ser anomenat Z-DNA [6]. Aquest dúplex levogir és allargat i prim i només presenta un solc estret i profund [3]. La conformació de Z-DNA existeix *in vivo*, como ho demostra l'existència de proteïnes que el reconeixen amb una gran afinitat i especificitat [7].

La notable flexibilitat conformacional dels àcids nucleics els ha permès formar una gran varietat d'estructures, a més a més de la doble hèlix, com ara els tríplex, els *i-motifs* i els quàdruplex de guanina (G-quàdruplex). Aquesta flexibilitat prové en gran part de la llibertat conformacional de l'anell de ribosa i, en menor grau, de la rotació entorn l'enllaç glicosídic i les rotacions de l'esquelet fosfat [3].

L'any 1957 Rich i col·laboradors van demostrar la formació d'estructures de triple cadena o tríplex de DNA [8] en mescles de poliuridines i poliadenines. L'interès per aquestes estructures va augmentar a finals dels 80, degut al potencial ús d'oligonucleòtids que poden formar tríplex (TFO) com agents inhibidors de l'expressió gènica a nivell de traducció (estratègia antigen) [9] i com a eines en la investigació biomèdica [10]. En el tríplex de DNA, l'oligonucleòtid que forma el tríplex s'uneix al solc major del dúplex estàndard Watson-Crick, mitjançant enllaços d'hidrogen. Els tríplex poden ser paral·lels o antiparal·lels, segons l'orientació de la tercera cadena que forma el tríplex. Els oligonucleòtids formadors de tríplex (TFO) d'homopirimidines s'uneixen paral·lelament a la cadena de purina del dúplex per enllaços d'hidrogen Hoogsteen per formar els tríplets T·AT i C^+·GC (Figura 3A). En canvi, el TFO d'homopurines s'uneixen antiparal·lelament mitjançant enllaços Hoogsten reversos i formen els tríplets G·GC i T·AT (Figura 3B). La formació de tríplex paral·lel requereix pH àcids per protonar la citosina i això el fa poc útil en entorns fisiològics. En el DNA biològic es poden formar tríplex hèlixs locals, anomenades H-DNA, en situacions d'estrès superhelicoïdal o a baix pH [11]. La seva funció biològica no és clara, però l'abundància de seqüències formadores d'aquest motiu és molt major en eucariotes que en procariotes i en general es troben en introns o regions no traduïdes. És per aquesta raó, que s'ha hipotetitzat que l'H-DNA pot tenir un paper important com a senyal regulador de la replicació o en la transcripció en eucariotes [11].

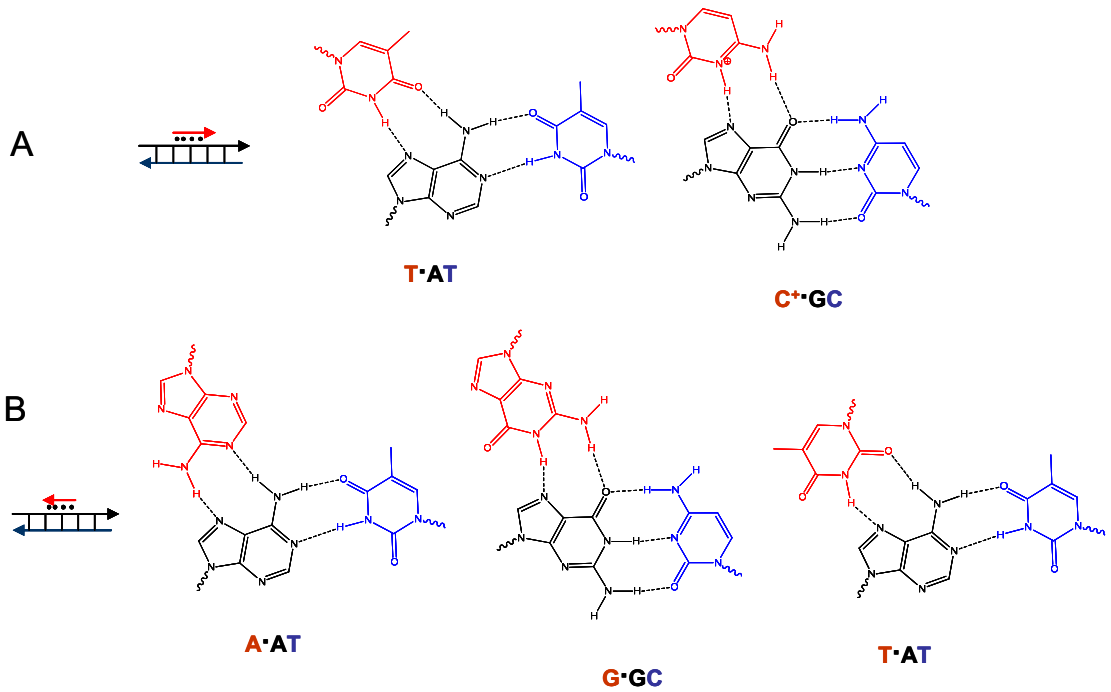

Figura 3. A) Estructures de les triades T·AT i C⁺·GC presents en els triplex paral·lels. B) Estructures dels triades A·AT, G·GC i T·AT presents en els tríplex antiparal·lels.

Les cadenes riques en citosines poden formar una estructura de quatre cadenes anomenada *i-motif* (Figura 4B). Aquestes estructures, que varen ser descobertes a l'any 1993 per Gehring [12] i col·laboradors, revelen que dos dúplex paral·lels es poden intercalar l'un amb l'altre mitjançant ponts d'hidrogen C:C+ (Figura 4A).

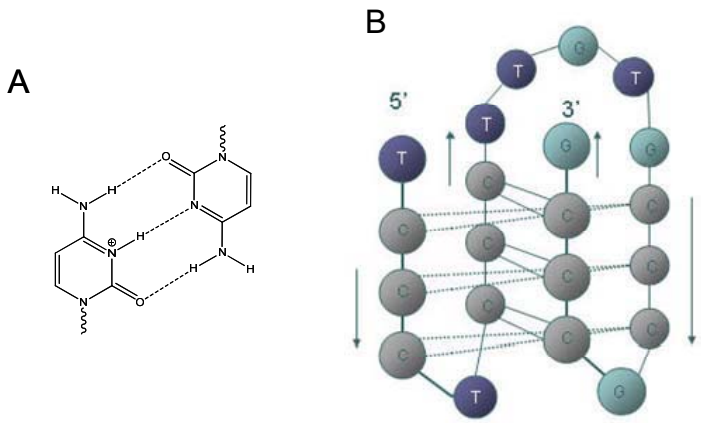

Figura 4. A) Interaccions per ponts d'hidrogen en C-C⁺. B) Representació esquemàtica del *i-motif*.

L'any 1910, Bang va publicar que una solució concentrada d'àcid guanílic formava un gel, però no va ser fins l'any 1962 que Gellebert va determinar que es tractava d'una estructura de quàdruplex. D'altra banda, Sen and Gilbert varen observar que seqüències riques en guanines presentaven una electroforesis en gel inusual i varen predir que podria ser degut a la formació d'enllaços Hoogsten [13]. En realitat les guanines poden establir uns enllaços d'hidrogen Hoogsten formant unes estructures anomenades G-tètrades [14] (Figura 5A). Aquestes tètrades són un arranjament co-planar on cada guanina accepta i dóna dos enllaços d'hidrogen. Aquesta disposició forma una cavitat central que permet incorporar un metall, que estabilitza l'estructura [14]. Quan dos o més G-tètrades estan apilades es formen unes estructures anomenades G-quàdruplex [14]. La primera estructura resolta de G-quàdruplex va ser publicada l'any 1992 per la seqüència telomèrica de la *Oxytricha* ($G_4T_4G_4$) per cristal·lografia i per RMN [15].

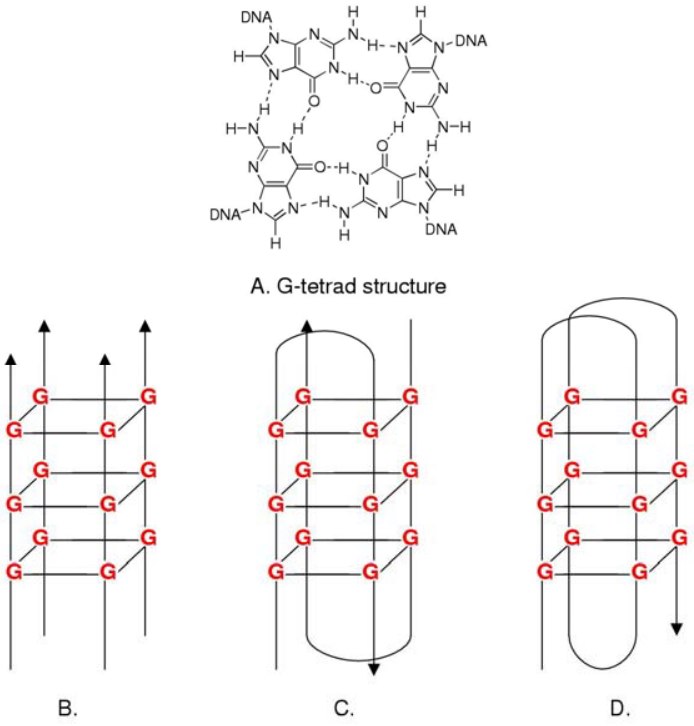

Figura 5. A) Tètrada formada per quatre guanines B) Quàdruplex tetramolecular C) Quàdruplex bimolecular D) Quàdruplex monomolecular

Els quàdruplex es poden formar amb vàries estequiometries de cadena. Els quàdruplex intramoleculars (Figura 5D) es formen amb una cadena senzilla, en canvi, una seqüència amb dues parts riques en guanines poden formar una forqueta i associar-se per generar un quàdruplex dimèric

(Figura 5C) intermolecular. Quatre cadenes separades també poden combinar-se i formar un quàdruplex tetramolecular (Figura 5B).

Les múltiples estructures determinades fins al moment present, han mostrat que el quàdruplex de guanina és altament polimòrfic, amb diferents topologies respecte al nombre i l'orientació de les cadenes, conformació *syn* o *anti* de l'enllaç glicosídic de les guanines i disposició dels enllaços [16]. Mentre que els quàdruplex intermoleculars normalment tenen les quatre cadenes en una orientació paral·lela, els bimoleculars i els intramoleculars poden presentar diferents topologies, definides pel tipus de unió (Figura 6).

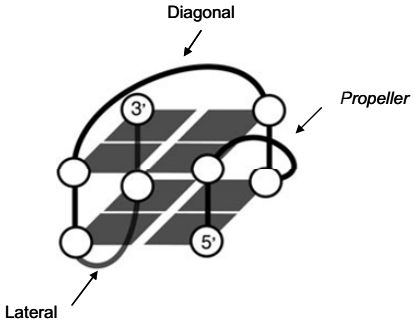

Figura 6. Diferents tipus de unions per connectar les guanines en un quàdruplex.

Les unions laterals connecten les bases de la mateixa tètrada que comparteixen enllaços, les unions diagonals connecten les bases de la mateixa tètrada que no estan unides per enllaços i les unions *propellers* connecten guanines que no estan en la mateixa tètrada però si en el mateix solc (Figura 6). En el cas dels quàdruplex unimoleculars, segons el tipus de unions es podrien formar 27 tipus d'estructures, però només 13 són estèricament permeses. Les conformacions més comunes són les de cadira (Figura 7, 6a i 6b) i les de cistella (Figura 7, 11a i 11b). En les estructures de quàdruplex, els enllaços fosfodiester defineixen els solcs, que poden ser de tres tipus: gran, mitja o petit.

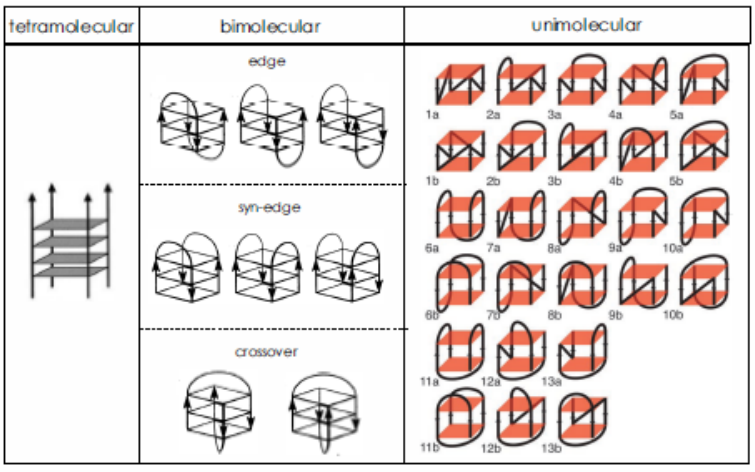

Figura 7. Diferents estructures de G-quàdruplex intermolecular, bimolecular i intramolecular.

Moltes seqüències poden formar més d'una estructura de quàdruplex, atorgant als quàdruplex un gran polimorfisme. Per exemple, s'han descrit diferents estructures intramoleculars per l'oligonucleòtid telomèric $AGGG(TTAGGG)_3$ per RMN o Cristal·lografia [17]. La seqüència telomèrica presenta una estructura tipus cistella (Figura 8B) en una solució de sodi per RMN mentre que l'estructura del cristall, en potassi, presenta una estructura paral·lela (Figura 8C). Estudis posteriors mostren que les dues estructures es poden presentar alhora en condicions properes a les fisiològiques i es poden interconvertir en una escala de temps de minuts [18, 19]. Recentment s'ha descrit per aquesta seqüència un altra estructura, en solució de potassi, del tipus *dog-eared* (Figura 8A).

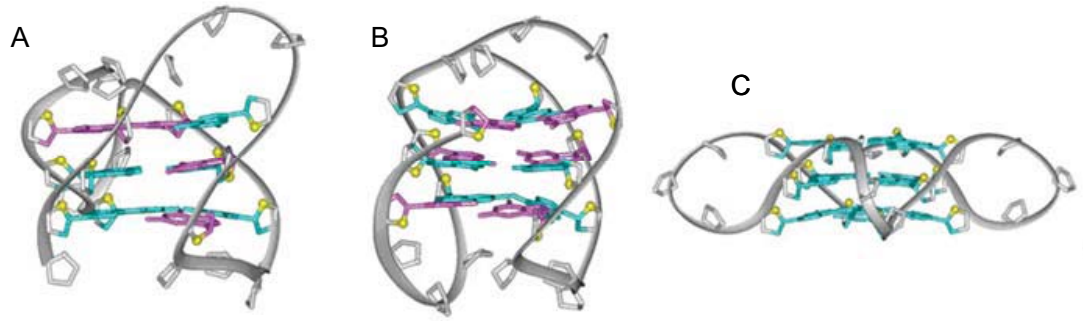

Figura 8. Estructures de la seqüència telomèrica 24-mer. A) Tipus dog-eared. B) tipus cistella. C) Paral·lela.

L'estabilitat d'una conformació depèn de molts factors, com ara la concentració, el nombre de cadenes, el nombre de G-tètrades, el tipus i seqüència de les unions i les condicions de solució [20]. El tipus i la concentració del catió és un dels factors més influent en l'estabilització d'una estructura particular de quàdruplex. L'estabilitat general dels quàdruplex pels cations segueix aquesta tendència: $Sr^{2+}>K^{+}>Rb^{+}\sim Ba^{2+}>NH^{4+}>Ca^{2+}>Na^{+}>Mg^{2+}\sim Cs^{+} >>Li^{+}$ [21]. Els cations també poden afectar el polimorfisme dels quàdruplex i afavorir la conversió de dúplex a quàdruplex .

Rellevància biològica dels quàdruplex

Hi han evidències que els G-quàdruplex es formen *in vivo* [22-23] i que presenten una gran rellevància biològica.

Els telòmers es troben al final dels cromosomes dels eucariotes i contenen un tàndem de seqüències riques en guanines no codificables. La repetició telomèrica en els humans és entre 2 i 10 Kb de longitud i consisteix en repeticions de la seqüència (TTAGGG). També es coneixen altres seqüències

telomèriques en altres espècies com ara la *Tetrahymena* i l'*Oxytricha nova* (TTTTGGGG) o la *S. Cerevisiae* (TG_{1-3}). Els telòmers ajuden a prevenir la degradació i la fusió dels extrems dels cromosones. En humans, aproximadament entre 50-200 parells de bases en els telòmers es perden després de cada cicle de replicació. Degut a aquest fet, els telòmers tenen un paper important en la regulació de la longevitat i la mort cel·lular. La mort cel·lular programada es pot produir quan la seqüència telomèrica es redueix a una determinada longitud [24]. D'altra banda, la telomerasa és un enzim que insereix una repetició telomèrica addicional al DNA. Williamson i col·laboradors van observar que les seqüències telomèriques formen estructures de quàdruplex *in vitro* [14] i des de llavors, la formació d'estructures de quàdruplex per seqüències telomèriques *in vitro* s'han estudiat per diverses tècniques.

Un altre tret sobre la rellevància biològica dels quàdruplex és que s'han observat un nombre important de proteïnes que s'uneixen a les estructures de quàdruplex [25].

Així mateix, s'han trobat seqüències que poden formar G-quàdruplex en zones promotores de gens, suggerint que la seva funció podria estar relacionada amb la regulació gènica a nivell de la transcripció. Aquest ha estat el punt de partida de moltes investigacions sobre el paper del quàdruplex en la regulació de proto-oncogens com el *c-myc* [26], *VEGF* [27], *HIF-1α*, [28], *bcl-2* [29] o *c-Kit* [30].
Hi ha estudis que demostren que el nivell d'alguns ions, com el potassi o el sodi, poden afectar l'expressió gènica o l'apoptosis, i es troben alterats en alguns tumors cel·lulars [31]. La modificació de la relació entre aquests cations en les cèl·lules cancerígenes podrien provocar canvis conformacionals en les estructures de quàdruplex i alterar la funció dels telòmers o la transcripció gènica. Es pot hipotetitzar que les estructures de quàdruplex podrien actuar com a interruptors biològics en la transcripció (Figura 9).

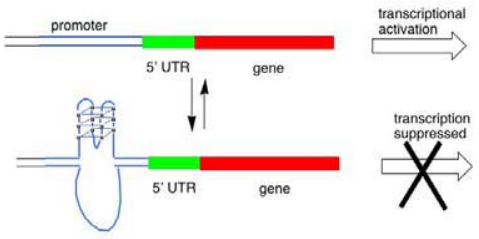

Figura 9. Esquema que representa el rol del G-quàdruplex en la regulació gènica.

Els G-quàdruplexs també formen part de la família de biomolècules actives que s'uneixen a proteïnes, aquests oligonucleòtids es coneixen com aptàmers. Els aptàmers són oligonucleòtids que han estat seleccionats mitjançant uns cicles repetitius de selecció *in vitro* per unir-se a unes dianes biològiques [32]. Un dels aptàmers més conegut és l'aptàmer que s'uneix a la trombina (TBA, *Thrombing Binding*

Aptàmer). El TBA forma un quàdruplex intramolecular amb dos G-tetràdes i tres diferents unions (Figura 10) [33, 34]. La seva estructura i activitat biològica depèn de la concentració de K^+. Altres exemples són els aptàmers de DNA que inhibeixen l'integrasa del HIV humà [35]. Estudis cristal·logràfics mostren que la topologia dels quàdruplex és crucial pel reconeixement amb la proteïna.

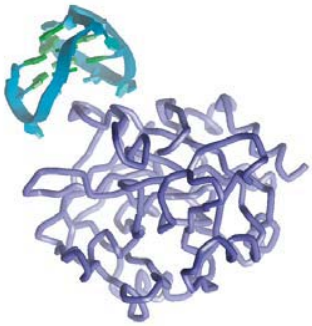

Figura 10. L'aptàmer de la trombina (blau) s'uneix específicament amb la proteïna trombina (lila).

Els àcids nucleics com a diana farmacològica

Degut a la gran rellevància biològica del DNA, no és sorprenent que existeixin fàrmacs, d'ús clínic o en fases clíniques avançades, relacionats amb els àcids nucleics [36]. Els compostos que interaccionen amb els àcids nucleics poden alterar l'expressió gènica o induir l'apoptosis, degut a que interfereixen en els processos de replicació, transcripció o traducció cel·lular. Les aplicacions terapèutiques de fàrmacs que interaccionen amb el DNA poden presentar un ampli espectre d'activitats com ara antivirial, antifungicida, antibiòtica o antineoplàstica. Les molècules que interaccionen amb el DNA són particularment importants com agents anticancerígens.

Normalment les interaccions de molts compostos amb el DNA són covalents i irreversibles, però poden ser útils en tractaments de tumors, processos virals o bacterians. Aquests compostos provoquen la mort cel·lular degut a les lesions provocades al DNA, però, generalment són tòxics i poden tenir efectes secundaris importants que redueixen l'ús clínic. Un exemple de fàrmac anticancerigen que s'uneix covalentment és el *cis*-platí (Figura 11)

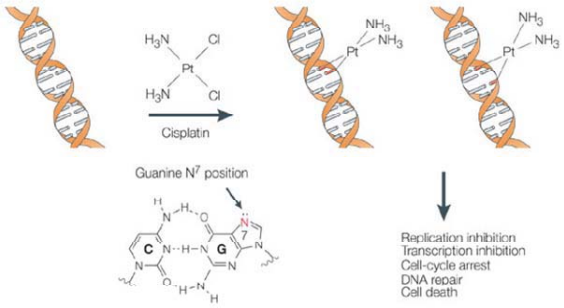

Figura 11. Representació dels tipus d'unió covalent del cis-platí amb el DNA.

Una altra forma d'interacció amb el DNA és mitjançant la intercalació. Els compostos que s'intercalen al DNA normalment són sistemes policíclics, aromàtics i plans que s'encaixen entre els parells de bases del DNA [37]. Existeixen un considerable nombre d'intercalants amb potencial farmacològic antiviral, antibiòtic [38] o antitumoral, com algunes acridines [39]. Un exemple de fàrmac que s'intercala al DNA és la daunomicina. La daunomicina (Figura 12) és un agent quimioterapèutic de la família de les antraciclines utilitzat pel tractament d'alguns càncers [40].

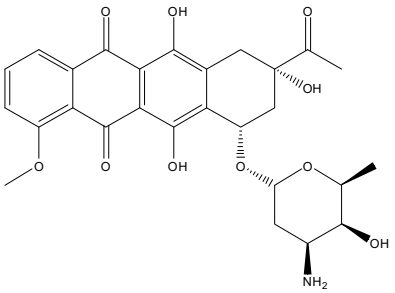

Figura 12. Estructura de la daunomicina

També existeixen molècules que interaccionen al solc major o menor del DNA. Normalment són anells simples o fusionats connectats per enllaços amb llibertat de moviment [41]. Aquests lligands poden desplaçar els cations o les molècules d'aigua dels solcs i interaccionar amb el parell de bases, això fa que puguin ser selectius en el reconeixement de la seqüència. Un exemple és la distamicina [42, 43], un producte natural format per tres anells de pirrol que s'uneix al solc petit del DNA. El grup terminal amidínic serveix per atraure el compost al DNA carregat negativament, i el grup 2-amino els hi proporciona una selectivitat pel parell de bases AT (Figura 13)

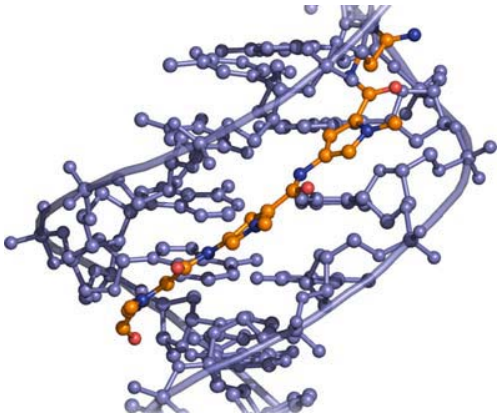

Figura 13. Estructura tridimensional del complex format per la distamicina (taronja) i un dúplex de DNA (lila).

L'estabilització del quàdruplex podria estar relacionada amb la regulació transcripcional d'alguns gens. En els últims anys, ha sorgit un gran interès en el disseny de molècules que tenen afinitat pels G-quàdruplex presents en els promotors d'oncogens, per tal d'obtenir nous fàrmacs contra el càncer [44].

Per una altra banda, la majoria de les cèl·lules somàtiques tenen un baix nivell de l'enzim telomerasa i cessen de proliferar quan els telòmers arriben a una determinada longitud. En canvi, més d'un 85% de les cèl·lules cancerígenes presenten un gran nivell d'aquest enzim [45]. Inhibir l'activitat de la telomerasa és una estratègia pel disseny de fàrmacs. Una estratègia per dissenyar inhibidors de l'enzim és prendre com a diana terapèutica les estructures de quàdruplex que es formen amb les seqüències telomèriques. Zahler i col·laboradors van observar que l'estabilització de les estructures de quàdruplex formades per seqüències telomèriques inhibia l'elongació dels telòmers per la telomerasa [46].

Degut a l'estructura plana de les tètrades de guanina, els compostos que interaccionen amb les estructures de quàdruplex són normalment lligands aromàtics policíclics amb diverses substitucions [47]. L'estabilització del quàdruplex pels lligands generalment és deguda per les interaccions π-π en la tètrada de guanina i per les electrostàtiques en els solcs del quàdruplex. La interacció exterior del lligand amb el quàdruplex sembla ser la única manera de reconeixement estructural pel quàdruplex [47].

Els lligands selectius a quàdruplex es podrien classificar en quatre categories segons la seva naturalesa catiònica [47].

Els lligands protonables *in situ* són compostos que presenten cadenes secundàries, normalment de naturalesa amínica, que en medi fisiològic es troben protonades. Un exemple és l'acridina trisubstituïda BRACO-19 (Figura 14) optimitzada per Neidel, Hurley i col·laboradors [48]. Aquest compost estabilitza fortament l'estructura de quàdruplex i presenta una gran una selectivitat pel quàdruplex *vs* dúplex. Així mateix, és un potent inhibidor de la telomerasa i presenta activitat antitumoral. La part aromàtica del BRACO-19 interacciona amb les G-tètrades mentre que les tres cadenes ho fan pels solcs del quàdruplex.

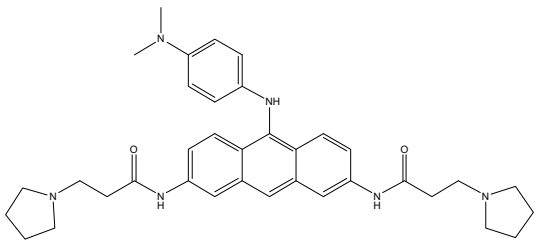

Figura 14. Estructura del BRACO-19.

En els lligands aza-aromàtics N-metilats, el caràcter catiònic del lligand s'obté pel nitrogen quaternari de l'anell aromàtic. Aquesta estratègia permet obtenir compostos hidrosolubles amb una gran habilitat per formar interaccions π-π, reduint la densitat electrònica de la part aromàtica. Un exemple és el TMPyP4 (Figura 15A), àmpliament estudiada per Hurley's i col·laboradors, que presenta una gran afinitat pels G-quàdruplex, una eficient inhibició de la telomerasa i regulen l'expressió d'oncogens [27]. Un altre exemple són les antraquinones, compostos desenvolupats originalment per interaccionar amb el DNA i que presenten activitat antitumoral [49]. Sun i col·laboradors van demostrar que la antraquinona BSU1051 (Figura 15B) interacciona i estabilitza les estructures de G-quàdruplex, inhibint la telomerasa. L'acridina pentacíclica RHPS4 (Figura 15C) també és un potent inhibidor de la telomerasa i inhibeix la proliferació cel·lular [50].

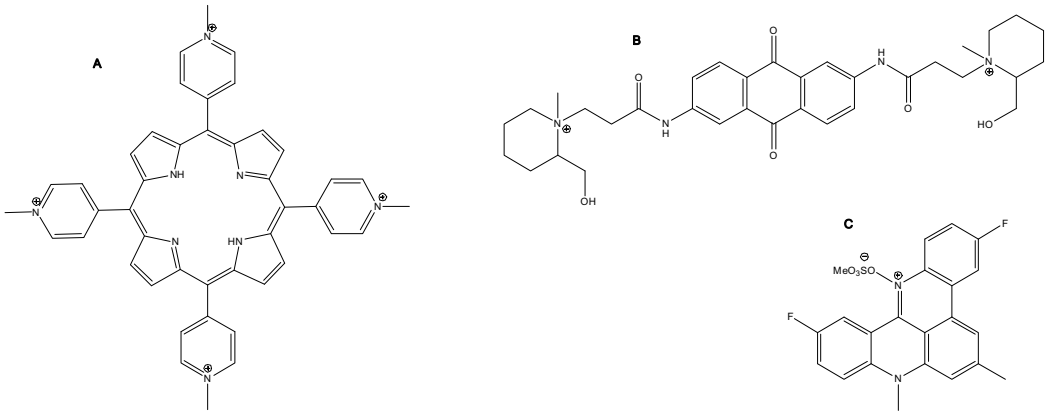

Figura 15. Estructures del A) TMPyP4 B) BSU1051 C) RHPS4

Els lligands metal·lo-orgànics [51] són interessants degut a que es poden obtenir fàcilment per síntesi i s'ha demostrat que poden tenir una bona capacitat d'unió a quàdruplex de guanina. El metall del lligand podria ocupar la posició central de la G-tètrada, afavorint la interacció mitjançant quel·lació. Aquesta naturalesa catiònica o altament polaritzada és un clar avantatge per promoure l'associació amb el G-quàdruplex. Un dels primers lligands metal·lo-organics publicats va ser el TMPyP4 amb Cu(II) (Figura 16A) [52]. Aquest presenta una preferència pel quàdruplex *vs* el dúplex i una modesta inhibició de la telomerasa. Un altre exemple són els complexes metàl·lics desenvolupats per Vilar i col·laboradors (Figura 16B) que interaccionen amb els G-quàdruplex telomèrics i presenten activitat antitumoral i inhibidora de la telomerasa [53, 54].

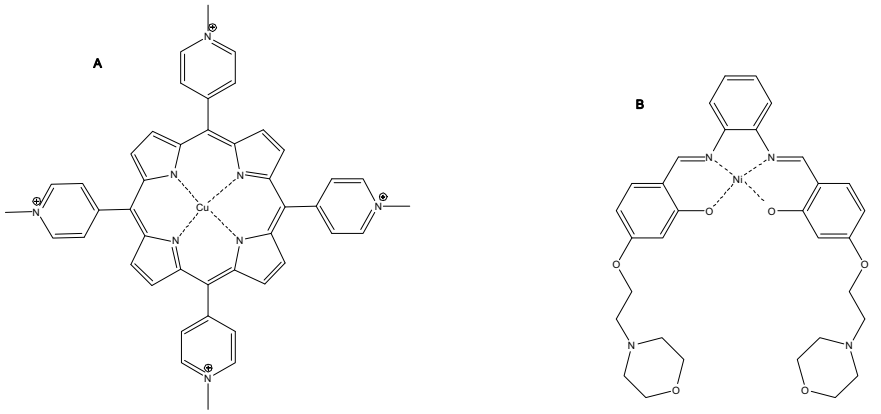

Figura 16. Estructures del A) CuTMPyP4 B) Ni(II)Salphen

La telomastatina [55] (Figura 17A) està inclosa en la categoria dels lligands macrocíclics. Aquesta molècula natural va ser aïllada del *Streptomyces annulatus* l'any 2001 pel grup del Shinya. Posteriorment va ser molt estudiada pel seu potencial com a lligand de quàdruplex, degut a la seva completa absència d'interacció amb el dúplex i per inhibir la telomerasa. Però el seu inconvenient més gran és la dificultat per obtenir-la, per tant, s'han desenvolupat altres derivats sintètics de la telomestatina, com el macrocíclic hexaoxazol HXDV (Figura 17B) o l'acetat de bistrioxazol (Figura 17C) [56, 57].

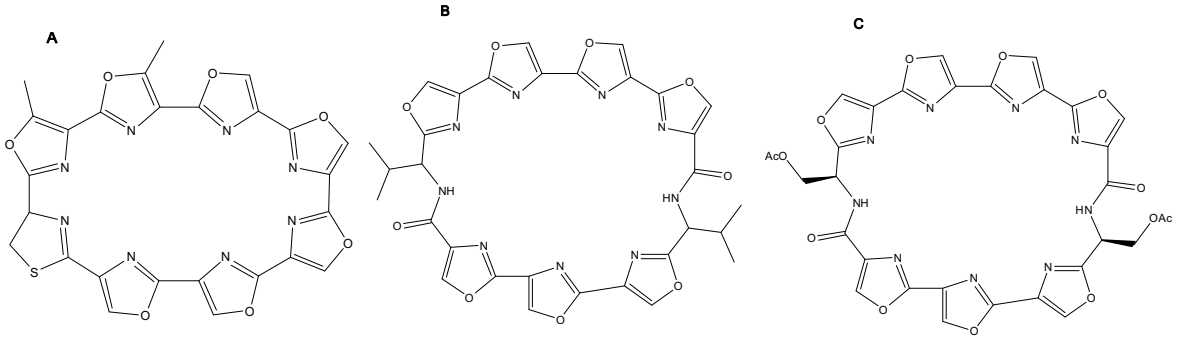

Figura 17. Estructures del A) Telomastatina B) HXDV C) bistrioxazol.

Últimament l'interès per obtenir lligands capaços de discriminar entre quàdruplex *vs* dúplex s'ha desplaçat pel disseny de compostos capaços de diferenciar entre diverses topologies de quàdruplex [58]. Alguns d'aquests lligands selectius a G-quàduplex tenen un gran potencial per entrar en estudis clínics [58].

El Quarfloxin (Figura 18) és un derivat del Norfloxacin, una fluoroquinolona que presenta afinitat per la topoisomerasa II i pels G-quàdruplex [59]. Cylene Pharmaceutical el va optimitzar per eliminar l'activitat inhibidora de la topoisomerasa II i maximitzar la selectivitat pels G-quàdruplex. El

Quarfloxin presenta una gran selectivitat per tots els G-quàdruplex paral·lels, com els formats als promotors *c-myc*, *VEGF* i *T30695* [59]. Tot i això, estudis posteriors demostren que les propietats biològiques del Quarfloxin són degudes a la interacció al complex proteic del quàdruplex *c-myc* [60]. Encara que el Quarfloxin no va superar els estudis clínics de Fase II per la seva biodisponibilitat, el seu perfil terapèutic aviva l'interès per optimitzar els lligands de G-quàdruplex pel seu ús farmacològic.

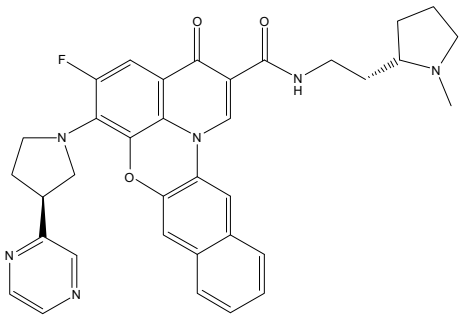

Figura 18. Estructura del Quarfloxin.

OBJECTIUS

L'objectiu general d'aquesta tesis és l'estudi estructural d'oligonucleòtids que formen quadruplex de guanina i la síntesis de lligands selectius per aquestes estructures amb finalitats terapèutiques. Els objectius es poden resumir en 3 objectius principals:

1. L'estudi estructural d'oligonucleòtids naturals i modificats que formen quàdruplex de guanina.

1.1. Concretament un dels objectius d'aquesta tesi és la síntesi d'uns oligonucleòtids ramificats que estan constituïts per 4 cadenes riques en guanina lligades per un dels extrems. D'aquesta manera es persegueix produir estructures de quàdruplex unimoleculars altament estabilitzades de conformació i associació intermolecular restringida (Capítol 1).

1.2. Un segon objectius es basa en l'estudi de l'associació bimolecular de seqüències de DNA naturals presents en els telòmers humans. S'ha descrit que aquestes seqüències formen quàdruplex de guanina que poden ser de dos tipus diferents: una forma en la que les quatre cadenes son paral·leles i una altra en la que hi ha dos cadenes paral·leles i dos antiparal·leles. Aquest equilibri, de gran interès per l'estabilitat i funció biològica dels telòmers, és estudiat en detall per espectroscòpia de masses i dicroisme circular (Capítol 2).

2. Avaluació de les propietats d'unió al DNA d'inhibidors de les topoisomerases que estan en avaluació preclínica. Aquest objectiu ha comportat la utilització de tècniques de diàlisis competitiva, espectroscòpia de RMN i modelatge molecular per tal de definir l'estructura del complex format pel quàdruplex de guanina i els inhibidors (Capítol 3).

3. Síntesis de nous compostos amb afinitat pel DNA, estudi de l'afinitat i elucidació estructural dels complexes formats. El tret comú que tenen els compostos estudiats es que estan formats per diverses unitats de compostos heterocíclics que poden unir-se al DNA per intercalació. Per tal d'unir els compostos intercalants s'han estudiat diversos espaiadors com per exemple (2-aminoetil)-glicina (Capítol 4), 4-aminoprolina (Capítol 5) i treoninol-fosfat (Capítol 6). Aquests espaiadors tenen la particularitat d'unir derivats d'acridina i quindolina a una distancia compatible amb el DNA de doble cadena per tal d'aconseguir l'apilament múltiple de les unitats intercalants .

Bibliografia

[1] Watson, J. D.; Crick, F. H. Molecular structure of nucleic acids: A structure for deoxyribose nucleic acid, *Nature*, **1953**, 171, 737-738.

[2] Lehninger, A. L., *Biochemistry: The molecular basis of cell structure and function*, Worth publischers, **1970**.

[3] Saenger W., *Principles of nucleic acids structure*, Springer-Verlag, New York, **1984**.

[4] Wahl, M.C.; Sundaralingam, M., Crystal structures of A-DNA duplexes, *Biopolymers*, **1997**, 44, 45–63.

[5] Blackburn, G. M.; Gait, M.J., *Nucleic acids in chemistry and biology*, IRL Press, Oxford, **1999**.

[6] Rich, A.; Zhang, S., Z-DNA: the long road to biological function, *Nat. Rev. Genet.*, **2003**; 4, 566–572.

[7] Nordheim, A.; Tesser, P.; Azorin, F.; Kwon, Y. H.; Möller, A.; Rich, A. Isolation of drosophila proteins that bind selectively to left-handed Z-DNA, *Proc. Natl. Acad. Sci. USA.*, **1982**, 79, 7729-7733.

[8] Felsenfeld, G.; Davies, D. R.; Rich, A., Formation of a three-stranded polynucleotide molecule. *J. Am. Chem. Soc.*, **1957**, 79, 2023-2024

[9] Moser, H. E.; Dervan, P. B., Sequence-specific cleavage of double helical DNA by triple helix formation, *Science*, **1987**, 238, 645-650.

[10] Grigoriev, M.; Praseuth, D.; Guieysee, A. L.; Robin, P.; Thuong, N.T.; Hélène, C.; Harel-Beellan, A., Inhibition of gene expression by triple helix-directed DNA cross-linking at specific sites, *Proc. Natl. Acad. Sci. U. S. A.,* **1993**, 90, 3501-3505.

[11] Sun, J.S.; Garestier, T.; Hélène, C., Oligonucleotide directed triple helix formation. *Curr. Opin. Struct. Biol*., **1996**, 6, 327-333.

[12] Gehring, K.; Leroy, J.L; Guéron, M., A tetrameric structure with protonated cytosinecytosine base pairs. *Nature*, **1993**, 363, 561-565.

[13] Sen, D.; Gilbert, W., Formation of parallel four-stranded complexes by guanine-rich motifs in DNA and its implications for meiosis, *Nature*, **1988**, 334, 364-366.

[14] Williamson, J.R.; Raghuraman, M.K.; Cech, T.R., Monovalent cation-induced structure of telomèric DNA: the G-quartet model, *Cell*, **1989**, 59, 871-880.

[15] Kang, C.H.; Zhang, X.; Ratliff, R.; Moyzis, R.; Rich, A., Crystal structure of four-stranded Oxytricha telomèric DNA. *Nature*, **1992**, 356, 126-131.

[16] Webba da Silva, M., Geometric formalism for DNA quadruplex folding. *Chem. Eur. J.*, **2007**, 13, 9738-9745.

[17] Li, J.; Correia, J.J.; Wang, L.; Trent, J. O.; Chaires, J. B., Not so crystal clear: the structure of the human telòmere G-quadruplex in solutions differs from that present in a crystal, *Nucleic Acids Res.*, **2005**, 33, 4649-47659.

[18] Lee, J. Y.; Okumus, B.; Kim, D.S.; Ha, T., Extreme conformational diversity in human telomèric DNA, *Proc Natl Acad Sci U S A,* **2005**, 102, 18938-18943.

[19] Ying, L.; Green, J.J.; Li, H.; Klenerman, D,; Balasubramanian, S., Studies on the structure and dynamics of the human telomèric G quadruplex by single-molecule fluorescence resonance energy transfer, *Proc Natl Acad Sci U S A*, **2003**, 100, 14629-14634.

[20] Gilbert, D.E.; Feigon, J., Multistranded DNA structures, *Curr Opin Struc Biol*, **1999**, 9, 305-314.

[21] Guschlbauer, W.; Chantot, J.F.; Thiele, D., Four-stranded nucleic acid structures 25 years later: from guanosine gels to telòmere DNA, *J Biomol Struct Dyn*, **1990**, 8, 491-511.

[22] Oganeisian, L.; Bryan, T.M., Physiological relevance of telomèric G-quadruplex formation: a potential drug target, *Bioessays*, **2007**, 29, 155-165

[23] Duquette, M.L.; Handa, P.; Vincent, J.A.; Taylor, A.F.; and Maizels, N. Intracellular transcription of G-rich DNAs induces formation of G-loops, novel structures containing G4 DNA, *Genes Dev*, **2004**, 18, 1618-1629.

[24] Greider, C.W., Mammalian telòmere dynamics: healing, fragmentation sortening and stabilization, *Curr. Opin. in Genet. Dev.,* **1994**, 4, 203–211

[25] Fry, M., Tetraplex DNA and its interacting proteins., *Frontiers in bioscience*, **2007**, 12, 4336-4351.

[26] Simonsson, T.; Pecinka, P.; Kubista, M., DNA tetraplex formation in the control region of c-myc. *Nucleic Acids Res*., **1998**, 26, 1167-1172.

[27] Sun,D.; Guo,K.; Rusche,J.J; Hurley,L.H., Facilitation of a structural transition in the polypurine/polypyrimidine tract within the proximal promoter region of the human VEGF gene by the presence of potassium and G-quadruplex-interactive agents. Nucleic Acids Res., **2005**, 33, 6070–6080.

[28] De Armond, R.; Wood, S.; Sun, D.; Hurley, L.H; Ebbinghaus, S.W., Evidence for the presence of a guanine quadruplex forming region within a polypurine tract of the hypoxia inducible factor 1alpha promoter. *Biochemistry*, **2005**, 44, 16341–16350.

[29] Dexheimer,T.S.; Sun,D.; Hurley,L.H., Deconvoluting the structural and drug-recognition complexity of the G-quadruplex-forming region upstream of the bcl-2 P1 promoter., *J. Am. Chem. Soc.*, **2006**, 128, 5404–5415.

[30] Rankin, S.; Reszka, A.P.; Huppert, J.; Zloh, M.; Parkinson, G.N.; Todd, A.K.; Ladame, S.; Balasubramanian, S.; Neidle, S., Putative DNA quadruplex formation within the human c-Kit oncogene. *J. Am. Chem. Soc.*, **2005**, 127, 10584–10589.

[31] Nagy, I.; Lustyik, G.; Lukacs, G.; Nagy, V.; Balzs, G., Correlation of malignancy with the intracellular Na^+:K^+ ratio in human thyroid tumors, *Cancer res,* **1983**, 43, 5395-5402.

[32] Brody, E. N.; Gold, L., Aptàmers as Therapeutic and Diagnostic Agents. *Reviews in Molecular Biotechnology*. **2000**, 74, 5-13.

[33] Padmanabhan, K.; Tulinsky, A., An ambiguous structure of a DNA 15-mer thrombin complex, *Acta crystallogr. Sect. D*, **1996**, 52, 272-282.

[34] Kelly, J. A.; Feigon, J.; Yeates, T. O., Reconciliation of the X-Ray and NMR structures of the Thrombin-Binding Aptamer d(GGTTGGTGTGGTTGG). *J. Mol. Biol.*, **1996**, 256, 417-422.

[35] Wyatt, J.R.; Vickers, T.A.; Roberson, J.L.; Buckheit, R.W.; Klimkait, T.; DeBaets, E.; Davis, P.W.; Rayner, B.; Imbach, J.L.; Ecker, D.J., Combinatorially selected guanosine-quartet structure is a potent inhibitor of human immunodeficiency virus envelope-mediated cell fusion. *Proc. Natl. Acad. Sci. USA*, **1994**, 91, 1356-1360

[36] Bischoof, G.; Hoffmann, S., DNA-Binding of Drugs Used in Medicinal Therapies, *Curr. Med. Chem*. **2002**, 9, 321-348

[37]Berman, H.M,; Neidel, S., *Nucleic acid geometry and dynamics,* **1980**, Ramaswamy H. Sarma, Ed.; Pergamon Press: New york.

[38] Werner, M.H.; Gronenborn, A.M.; Clore, G.M., Intercalation, DNA kinking, and the control of transcription, *Science, **1996***, 271, 778-784.

[39] Baguley, B.C., Dihydroisoquinolinones: the design and synthesis of a new series of potent inhibitors of poly(ADP-ribose) polymerase, *Anticancer Drug Des.,* **1991**, 6, 1, 107-117.

[40] Geierstanger, B.H.; Wemmer, D.E., Complexes of the minor groove of DNA, *Annu. Rev. Biophys. Biomol. Struct.,* **1995**, 24, 463-493.

[41] Baraldi, P.G.; Bovero, A.; Fruttarolo, F.; Preti, D.; Tabrizi, M.A.; Pavani, M.G.; Romagnoli, R., DNA minor groove binders as potential antitumor and antimicrobial agents, *Med Res Rev*, **2004**, 24, 475-528.

[42] Hiraku Y.; Oikawa S.; Kawanishi S., Distamycin A, a minor groove binder, changes enediyne-induced DNA cleavage sites and enhances apoptosis, *Nucleic Acids symposium series*, **2002**, 1, 95-96.

[43] Arcamone, F.; Penco, S.; Orezzi, P.; Nicolella V.; Pirelli A., Structure and synthesis of distamycin A, *Nature*, **1964**, 203, 1064-1065.

[44] Bejugam, M.; Sewitz, S.; Shirude, P.S.; Rodriguez, R.; Shahid,R.; Balasubramanian, S. Tri-substituted isoalloxazines as a new class of G-quadruplex binding ligands: small molecule regulation of c-kit oncogene expression*., J. Am. Chem. Soc*., **2007**, 129, 12926-12927.

[45] Raymond, E.; Sun, D.; Chen, S.-F.; Windle, B.; Von Hoff, D. D., Agents that target telòmerase and telòmeres, *Curr. Opin. Biotech,* **1996***.* **7,** 583-591.

[46] Zahler, A.M.; Williamson, J.R.; Cech, T.R.; Prescott, D.M., Inhibition of telòmerase by G-quartet DNA structyures, *Nature*, **1991,** 350, 718-720.

[47] Monchaud D.; Teulade-Fichou M.P., A hitchhiker's guide to G-quadruplex ligands, *Org. Biomol. Chem.*, **2008**, 6, 627-636.

[48] Harrison R.J.; Gowan S.M.; Kelland L. R.; Neidle S., Human telòmerase inhibition by substituted acridine derivatives, *Bioorg. Med. Chem. Lett*., **1999**, 9, 2463-2468.

[49] Agbandje M.; Jenkins T. C.; McKenna R.; Reszka A. P.; Neidle S., Anthracene-9,10-diones as potential anticancer agents. Synthesis, DNA-binding, and biological studies on a series of 2,6-disubstituted derivatives, **1992**, 35 (8), 1418-1429.

[50] Leonetti C.; Amodei S.; D'Angelo C.; Rizzo A.; Benassi B.; Antonelli A.; Elli R.; Stevens M. F. G.; D'Incalci M.; Zupi G.; Biroccio A., Biological activity of the G-quadruplex ligand RHPS4 (3,11-difluoro-

6,8,13,trimethyl-8H-quino[4,3,2,kl]acridiniummethosulfate) is associated with telòmere capping alteration, **2004**, Mol. Pharmacol, 66, 1138-1146.

[51] Georgiades S. N.; Karim N. H. A; Suntharalingam K.; Vilar R., Interaction of metal complexes with G-quadruplex DNA, *Angew. Chem.. int. ed.*, **2010**, 49, 4020-4034.

[52] Keating L. R.; Szalai, V. A.,Parallel-stranded guanine quadruplex interactions with a copper cationic porphyrin, *Biochemistry*, **2004**, 43, 15891-15900.

[53] Reed, J. E.; Arnal A. A.; Neidle S.; Vilar R., Stabilization of G-quadruplex DNA and inhibition of telòmerase activity by square-planar Nickel (II) complexes, *J. Am. Chem. Soc.*, **2006**, 128, 5992-5993.

[54] Campbell N. H.; Abd Karim N. H.; Parkison, G. N.; Gunaratnam M.; Petrucci V.; Todd A. K.; Vilar R.; Neidle S., Molecular basis of structure-activity relationships between salphen metal complexes and human telomèric DNA quadruplexes, *J. Med. Chem.*, **2012**, 55, 209-222.

[55]Shin-ya K.; Wierzba K.; Matsuo K. I.; Ohtani T.; Yamada Y.; Furihata K.; Hayakawa Y.; Seto H., Telomestatin, a novel telòmerase inhibitor from Streptomyces anulatus , *J. Am. Chem. Soc.*, **2001**, 123, 1262-1263.

[56] Christopher M. Barbieri C. M.; Srinivasan A. R.; Rzuczek S. G.; Rice J. E.; LaVoie E. J.; Pilch D. S., Defining the mode, energetics and specificity with which a macrocyclic hexaoxazole binds to human telomèric G-quadruplex DNA, *Nucl. Acids Res.,* **2007**, 35 (10), 3272-3286.

[57] Tera M.; Sohtome Y.; Ishizuka H.; Doi T.; Takagi M.; Shin-ya K.; Nagasawa K., Design and Synthesis of Telomestatin Derivatives and Their Inhibitory Activity of Telòmerase, *Heterocycles*, **2006**, 69 (1), 505-514.

[58] Balasubramanian S.; Hurley L. H.; Neidle S., Targeting G-quadruplexes in gene promoters: a novel anticancer strategy?, *Nat. Rev. Drug Discov.,* **2011**, 10(4), 261-275.

[59] Duan W.; Rangan A.; Vankayalapati H.; Kim M.Y.; Zeng Q.; Sun D.; Han H.; Fedoroff O.Y.; Nishioka D.; Rha S.Y.; Izbicka E: Von Hoff D.D.; Hurley L.H., Design and synthesis of fluoroquinophenoxazines that interact with human telomèric G-quadruplexes and their biological effects., *Mol. Cancer Ther.,* **2001**, 1(2), 103-120.

[60] Drygin D.; Siddiqui-Jain A.; O'Brien S.; Schwaebe M.; Lin A.; Bliesath J.; Ho C.B.; Proffitt C.; Trent K.; Whitten J.P., Lim J.K.; Von Hoff D.; Anderes K.; Rice W.G., Anticancer activity of CX-3543: a direct inhibitor of rRNA biogenesis., *Cancer Res.*, **2009**, 69(19), 7653-7661.

1

SÍNTESIS I CARACTERITZACIÓ ESTRUCTURAL DE QUÀDRUPLEX DE GUANINA DE DNA DE GRAN ESTABILITAT UTILITZANT EL FOSFOROAMIDIT TREBLER

SÍNTESIS I CARACTERITZACIÓ ESTRUCTURAL DE QUÀDRUPLEX DE GUANINA DE DNA DE GRAN ESTABILITAT UTILITZANT EL FOSFOROAMIDIT TREBLER.

Synthesis and structural characterization of stable branched DNA G-quadruplexes using the trebler phosphoramidite.

Rubén Ferreira,[a, b] Margarita Alvira,[a, b] Anna Aviñó,[a, b] Irene Gómez-Pinto,[c] Carlos González,[c] Valérie Gabelica,[d] and Ramon Eritja*[a, b]

ChemistryOPEN, 1 (2012) 106-114

[a,b] *Institute for Research in Biomedicine (IRB Barcelona), Institute for Advanced Chemistry of Catalonia (IQAC-CSIC), Networking Centre on Bioengineering, Biomaterials and Nanomedicine (CIBER-BBN), Baldiri Reixac 10, E-08028 Barcelona, Spain.*
[c] *Instituto de Química Física Rocasolano. CSIC. Serrano 119. 28006 Madrid, Spain*
[d] *Mass Spectrometry Laboratory, GIGA-Research, University of Liège, Belgium.*

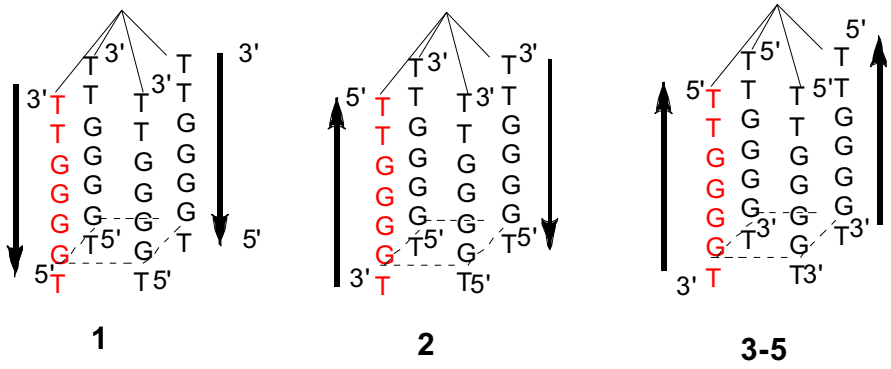

Resum

Les seqüències riques en guanines poden formar estructures no canòniques de quatre cadenes conegudes com a G-quàdruplex. L'interès per la preparació d'estructures de G-quàdruplex és degut a les seves possibles propietats biològiques així com el seu ús potencial en nanociència. Es descriu un mètode per preparar G-quàdruplex molt estables que es basa en la unió de quatre cadenes riques en guanines lligades per un extrem per formar G-quàdruplex unimoleculars. En aquest mètode primer es sintetitza una cadena, després s'afegeix una molècula ramificadora i per finalitzar s'incorporen les altres tres cadenes conjuntament. Aquest mètode permet introduir una modificació específica en una sola cadena. Per exemple, s'ha preparat un G-quàdruplex amb una cadena amb una polaritat inversa respecte les altres cadenes. En una solució d'acetat d'amoni es va observar que formava una estructura híbrida, però en un medi amb ions de sodi o de potassi es formava un G-quàdruplex paral·lel. A més a més dels G-quàdruplex monomoleculars esperats, es va observar la presència d'estructures dimèriques. També s'ha utilitzat aquest mètode per preparar G-quàdruplex amb només una subtitució de 8-aminoguanina, aquest canvi de la base estabilitza l'estructura del G-quàdruplex quan es troba en una posició interna.

ChemistryOPEN

Open Access

DOI: 10.1002/open.201200009

Synthesis and Structural Characterization of Stable Branched DNA G-Quadruplexes Using the Trebler Phosphoramidite

Rubén Ferreira,[a, b] Margarita Alvira,[a, b] Anna Aviñó,[a, b] Irene Gómez-Pinto,[c] Carlos González,[c] Valérie Gabelica,[d] and Ramon Eritja*[a, b]

Guanine (G)-rich sequences can form a noncanonical four-stranded structure known as the G-quadruplex. G-quadruplex structures are interesting because of their potential biological properties and use in nanosciences. Here, we describe a method to prepare highly stable G-quadruplexes by linking four G-rich DNA strands to form a monomolecular G-quadruplex. In this method, one strand is synthesized first, and then a trebler molecule is added to simultaneously assemble the remaining three strands. This approach allows the introduction of specific modifications in only one of the strands. As a proof of concept, we prepared a quadruplex where one of the chains includes a change in polarity. A hybrid quadruplex is observed in ammonium acetate solutions, whereas in the presence of sodium or potassium, a parallel G-quadruplex structure is formed. In addition to the expected monomolecular quadruplexes, we observed the presence of dimeric G-quadruplex structures. We also applied the method to prepare G-quadruplexes containing a single 8-aminoguanine substitution and found that this single base stabilizes the G-quadruplex structure when located at an internal position.

Introduction

Guanine (G)-rich DNA sequences are able to form a noncanonical four-stranded topology called a G-quadruplex. These structures are based on the G-tetrad, also called the G-quartet, which consists of a planar arrangement of four guanine bases associated through a cyclic array of Hoogsteen hydrogen bonds in which each G accepts and donates two hydrogen bonds. G-quadruplexes can be formed in the genome, for example in telomeres[1] but also in other key biological contexts, such as oncogenic promoter elements[2] and RNA 5′-untranslated regions (UTR) in close proximity to translation start sites.[3] Thus, quadruplex motifs could act as topological switches that might regulate gene expression. For all these reasons, structures of biological G-quadruplex DNA are a potential target for drug design.[4] Moreover, G-quadruplexes also have biological interest as therapeutic agents. Aptamers are short DNA- or RNA-based oligonucleotides selected from large combinatorial pools of nucleic acid sequences for their ability to bind to a specific protein.[5] Among several structures, the G-quadruplex motif is present in several aptamers with biological interest, such as the thrombin binding aptamer[6] and the anti-HIV-1 aptamers.[7] Finally, G-quadruplex structures are also receiving increasing attention because of their applications in supramolecular chemistry and nanotechnology. High-order structures, such as G-wires,[8] DNA nanodevices based on quadruplex–duplex interconversion[9] and biosensors[10] have been described in the literature. A quadruplex can be tetramolecular, bimolecular or unimolecular. Within these groups, these structures can be classified on the basis of the relative orientation of the chains (parallel or antiparallel) and the way the loops connect the different strands.[11]

Synthetic branched oligonucleotides have been used for several purposes. Initially, most of the interest in this field focused on the study of branched oligoribonucleotides as splicing intermediates of eukaryotic mRNAs.[12] Moreover, branched oligonucleotides also show high affinity for single-stranded oligonucleotides to form alternated strand triplexes.[13] Recently, branched oligonucleotides have been used as building blocks for the synthesis of new nanostructures.[14] Branched oligonucleotides carrying four G-rich strands linked through their 5′-

[a] R. Ferreira, Dr. M. Alvira, Dr. A. Aviñó, Dr. R. Eritja
Department of Chemical and Biomolecular Nanotechnology
Institute for Advanced Chemistry of Catalonia (IQAC-CSIC)
Networking Centre on Bioengineering, Biomaterials and Nanomedicine (CIBER-BBN)
Jordi Girona 18-26, 08034 Barcelona (Spain)
E-mail: recgma@cid.csic.es

[b] R. Ferreira, Dr. M. Alvira, Dr. A. Aviñó, Dr. R. Eritja
Department of Chemistry and Molecular Pharmacology
Institute for Research in Biomedicine (IRB Barcelona)
Baldiri i Reixac 10, 08028 Barcelona (Spain)

[c] Dr. I. Gómez-Pinto, Dr. C. González
Departmento de Química Física Biológica
Instituto de Química Física 'Rocasolano', CSIC
Serrano 119, 28006 Madrid (Spain)

[d] Dr. V. Gabelica
Department of Chemistry, University of Liège
Allée de la Chimie Building B6c, 4000 Liège (Belgium)

Supporting information for this article is available on the WWW under http://dx.doi.org/10.1002/open.201200009.

© 2012 The Authors. Published by Wiley-VCH Verlag GmbH & Co. KGaA. This is an open access article under the terms of the Creative Commons Attribution Non-Commercial License, which permits use, distribution and reproduction in any medium, provided the original work is properly cited and is not used for commercial purposes.

© 2012 The Authors. Published by Wiley-VCH Verlag GmbH & Co. KGaA, Weinheim

or 3′-end have been synthesized using a clever combination of symmetric and asymmetric doubler phosphoramidites, and the resulting compounds form very stable quadruplexes.[15]

Inspired by these results, we decided to synthesize G-quadruplex branched oligonucleotides carrying modifications on one of the four strands. We used the tetrameric, G/thymidine (T)-containing parallel quadruplex $[d(TG_4T)]_4$ as a model compound to set up our synthetic strategy, since it is well-studied and its structure is well-characterized.[16–18] Moreover, this model compound has been used to assess the effects of substituting guanine for modified guanine derivatives on the stability and kinetics of quadruplex formation.[19] For example, previous work addressed the effect of 8-aminoguanine substitutions on the tetramolecular $[d(TG4T)]_4$ quadruplex.[20] Thermal denaturation studies showed that an 8-aminoguanine replacement is not equally favorable at all positions, but might accelerate parallel quadruplex formation when inserted in the internal region. However, due to the tetrameric nature of the structure, it is not possible to assess the effect of a single substitution in the quadruplex.

Here, we report the preparation of molecules composed of four oligonucleotide strands, whose ends are attached through a tetra-end-linker. This was achieved by first synthesizing one strand, then adding the trebler phosphoramiditethe and synthesizing the other three strands simultaneously (Scheme 1). Using the tetrameric $[d(TG4T)]_4$ parallel quadruplex as a model compound, we synthesized very stable quadruplexes with modifications in only one of the strands (Scheme 1). These results are relevant for the preparation of stable quadruplexes with potential biological activity.

Results and Discussion

Synthesis of oligonucleotides

The synthesis of the branched oligonucleotides designed to form a monomolecular G-quadruplex was performed in an automatic DNA synthesizer (Scheme 1). The sequence of the strands was chosen based on the hexamer $d(TG_4T)$, which is known to form a stable parallel tetramolecular quadruplex that has been well characterized in previous studies.[16–18] In this study, an additional T was inserted to prevent steric hindrance of trebler with the nearest G-quartet. The main structural feature of these oligonucleotides is the attachment of four strand ends through a three-branched linker after the synthetic completion of one of the strands. The branched structure was incorporated into the molecule with commercially available trebler phosphoramidite (Scheme 1). By selecting standard or reversed phosphoramidites at different synthesis steps, three structures with different strand orientations were prepared (Scheme 1). The synthesis of oligonucleotide **1** started with a solid support carrying a T linked via a succinyl linker through its 5′ end (reversed-T). The first TG_4TT strand was assembled using reversed phosphoramidites. Trebler phosphoramidite was then added followed by the assembly of the remaining three strands using standard phosphoramidites. After the assembly of the sequence, the final detritylation was not performed in order to facilitate reversed-phase HPLC purification. Ammonia deprotection generated a major eluted product containing three DMT groups. This product was collected and treated with acetic acid to obtain the desired compound, which was then characterized by MS. Oligonucleotide **1** has all

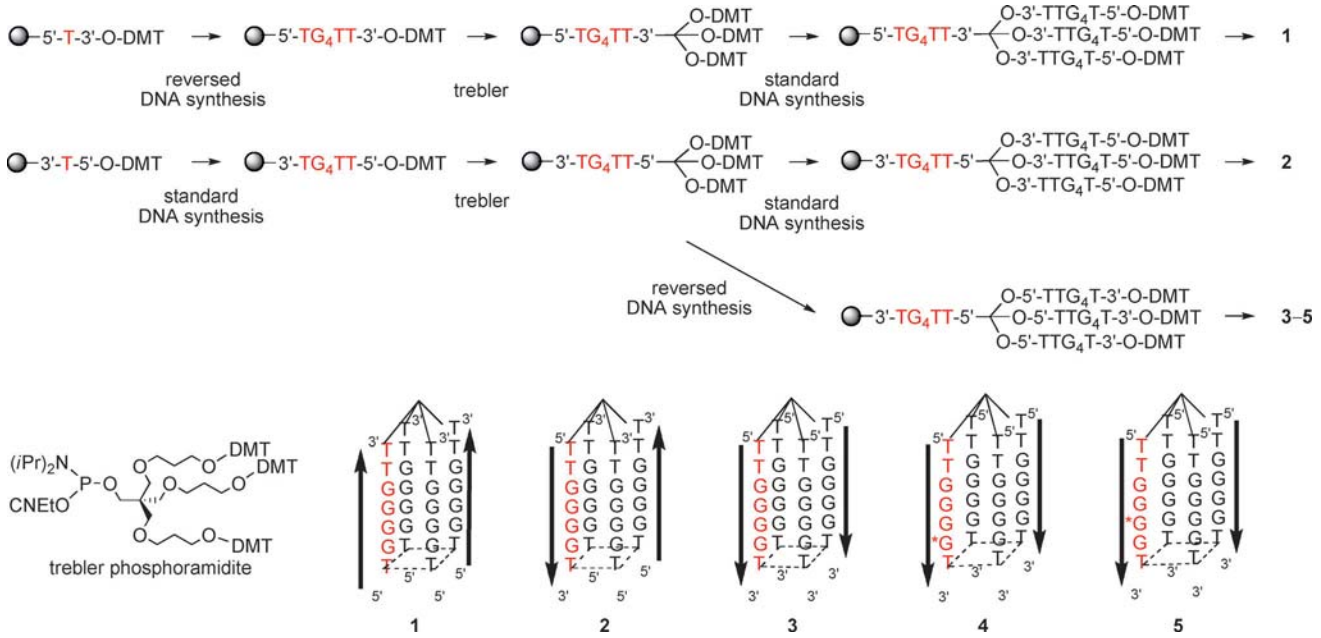

Scheme 1. Outline of the method for the preparation of G-quadruplexes proposed in this study (see Table 2 in the Experimental Section for oligonucleotide sequences). *G denotes the position of 8-aminoguanine residues. For standard DNA synthesis, a cycle for each nucleotide addition consists of the following steps: 1) 3% trichloroacetic acid/dichloromethane; 2) 5′-DMT-nucleoside-3′-phosphoramidite, tetrazole; 3) capping with acetic acid and *N*-methylimidazole; 4) oxidation with 0.01 M iodine solution. The same steps are applied in the reversed DNA synthesis but with the use of 3′-DMT-nucleoside-5′-phosphoramidite as monomers.

 © 2012 The Authors. Published by Wiley-VCH Verlag GmbH & Co. KGaA, Weinheim

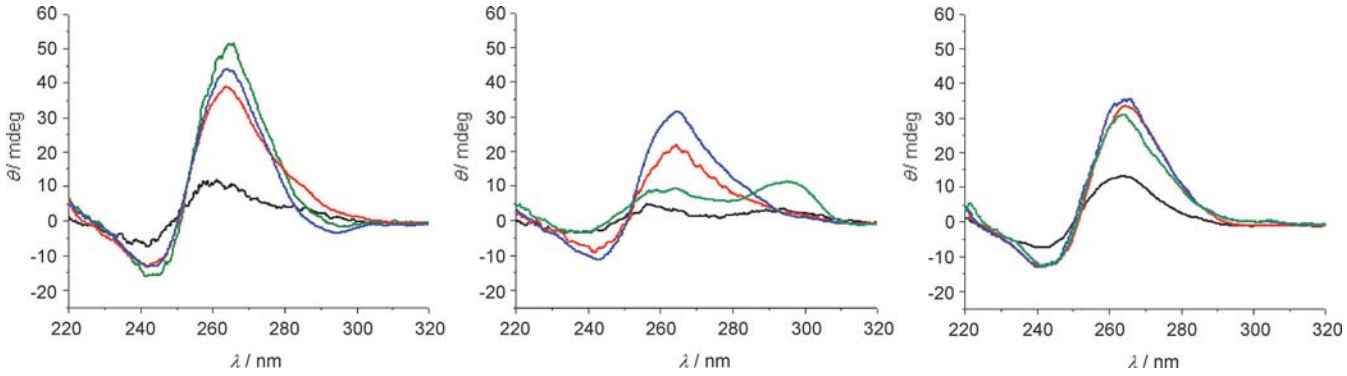

Figure 1. CD spectra of oligonucleotide **1** (left), **2** (middle) and **3** (right) dissolved in water (——), 5 mM KCl (——), 100 mM NaCl (——) and 100 mM NH_4OAc (——).

four strands in the same orientation and was designed to form a monomolecular parallel G-quadruplex structure.

Oligonucleotide **2** was prepared in a similar way. This time, the first strand was assembled using a 3′-end T-linked solid support and standard phosphoramidite. Trebler phosphoramidite was then added, followed by the assembly of the remaining three strands using standard phosphoramidites. Oligonucleotide **2** had one of the strands in antiparallel polarity compared with the other three strands.

Oligonucleotide **3** was prepared using the standard 3′–5′ direction of synthesis as described for oligonucleotide **2**, however, after the addition of the trebler, the assembly of the remaining three strands was performed using reversed phosphoramidites. Thus, oligonucleotide **3** had the four strands in the same orientation as oligonucleotide **1**, but linked through the 5′-end, while in oligonucleotide **1** the strands were linked through the 3′-end. Two additional oligonucleotides carrying one single 8-aminoguanine in each position of the first strand (**4** and **5**) were prepared. Insertion of an 8-aminoguanine residue was performed with 8-amino-dG phosphoramidite protected with a dimethylaminomethylidine group.[21] The synthesis of 8-amino-guanine oligonucleotides is straightforward and requires no changes from regular procedures, with the exception of the addition of 2-mercaptoethanol to the cleavage and deprotection solutions to prevent further oxidative damage.[21] The addition of 8-aminoguanine to the parallel structure was performed to determine the effect of a single substitution in each position of the parallel quadruplex.

It is important to mention that during the synthesis of oligonucleotides **3**–**5**, the removal of the DMT group after DMT-on HPLC purification was very slow. The usual treatment (80% acetic acid, 30 min, RT) was not sufficient to remove the three DMT groups linked to sterically hindered secondary alcohols. Instead an increased temperature was required (80% acetic acid, 30 min, 55 °C).

Analysis of the structure of oligonucleotides 1–3

CD spectra of aqueous solutions of oligonucleotide **1** show a weak positive band with a maximum around 260 nm and a negative band at 240 nm, thereby indicating the presence of residual parallel quadruplex (Figure 1). The addition of K^+ (5 mM), Na^+ (100 mM) and NH_4^+ (100 mM) enhanced the CD signal, indicating a strong stabilization of the parallel quadruplex. CD spectra of aqueous solutions of oligonucleotide **2** in water suggest that the sequence is unstructured. Upon addition of NH_4^+ (100 mM), two positive bands with maxima around 260 and 295 nm were enhanced. This spectrum resembles that expected for a quadruplex with three strands in one direction and one strand in an antiparallel direction (3 + 1 quadruplex).[22] This observation suggests that for oligonucleotide **2** in NH_4^+, the trebler remains on one side of the G-quadruplex and that the four strands keep the 3 + 1 orientation given by the synthesis. In contrast, the positive band around 295 nm disappeared and the 260 nm band increased when K^+ (5 mM) or Na^+ (100 mM) is added instead of NH_4^+. This indicates the formation of a parallel quadruplex in the presence of K^+ and Na^+ ions, and it is consistent with the literature on similar tetra-end-linked quadruplexes.[15a] Our findings show that the branching unit has enough flexibility to allow the antiparallel strand to be antiparallel in water and NH_4^+ solutions or to be in the parallel orientation in the presence of K^+ and Na^+ ions. CD spectra of oligonucleotide **3** were very similar to those of oligonucleotide **1**, thus indicating the formation of a parallel quadruplex under all conditions studied, including water, with strong stabilization by the addition of K^+, Na^+ and NH_4^+ ions.

The thermal denaturation of quadruplexes formed by oligonucleotides **1**–**3** and nonbranched $[TG_4T]_4$ was studied by UV spectroscopy (Table 1). In the presence of KCl (5 mM), all quadruplexes were stable at temperatures up to 80 °C. In the pres-

Table 1. Melting temperatures (T_m).

Oligonucleotide	T_m [°C][a]			
	K^+[b]	Na^+[c]	NH_4^+[d]	H_2O[e]
TG_4T	>80	58	67	–
1	>80	>80	>80	–
2	>80	55	67	–
3	>80	>80	>80	50
4	>80	–	–	52
5	>80	–	–	>80

[a] Measured by UV spectroscopy; [b] 5 mM KCl; [c] 100 mM NaCl, [d] 100 mM NH_4OAc, [e] Measured by CD spectroscopy. In water after HPLC purification and desalting, could contain some residual TEAA.

 © 2012 The Authors. Published by Wiley-VCH Verlag GmbH & Co. KGaA, Weinheim

ence of Na^+ ions (10 mM sodium cacodylate, 100 mM NaCl),[23] tetra-end linked quadruplexes **1** and **3** were stable up to 80 °C. The tetramolecular $[TG_4T]_4$ quadruplex had a melting temperature (T_m) of 58 °C similar to the T_m value of oligonucleotide **2** (55 °C). This result indicates that the quadruplex formed by **2** in the presence of Na^+ ions is the least stable. In the presence of NH_4^+ ions (100 mM NH_4OAc), similar results were obtained. Only parallel tetra-end linked quadruplexes (**1** and **3**) were stable at temperatures up to 80 °C. The tetrameric $[TG_4T]_4$ quadruplexes had a T_m value of 67 °C equal to that of oligonucleotide **2**.

ESI-MS was performed in order to study the stability of these quadruplexes in the gas phase, and hence without the boiling temperature restriction. However, this analysis is possible only with G-quadruplexes produced from ammonium solutions. In the gas phase, the number of trapped ammonium ions indicates the gas phase stability of these branched G-quadruplexes.[19a] Figure 2 (center) shows the bidimensional mass/mobility plots obtained for oligonucleotide **1**. The 2D plot allows the discrimination of monomeric and dimeric structures (the dimer is discussed below). To analyze the monomer, we extracted the mass spectrum corresponding to the *m/z* region 1535–1550. The extracted mass spectra of oligonucleotides **1**–**3** are shown in Figure 2 a–c, and the numbers indicate the number of ammonium ions preserved. Oligonucleotide **2** is the least able to preserve the inner ammonium ions in the gas phase (Figure 2), and hence is the least stable, in agreement with melting experiments in solution. Interestingly, the gas phase data indicate that **1** is more stable than **3**, although both oligonucleotides have solution T_m values above 80 °C. Overall, the relative stability of quadruplexes in the gas phase ranks **1** > **3** > **2**.

The imino proton region of the NMR spectra of oligonucleotides **1**–**3** confirms the formation of a quadruplex structure (Figure 3). NMR spectra were acquired in Na^+ and K^+ buffers. Under both conditions, the spectra of the three oligonucleotides exhibited imino signals at δ values in the range of 10.4–11.5 ppm, characteristic of imino protons involved in the

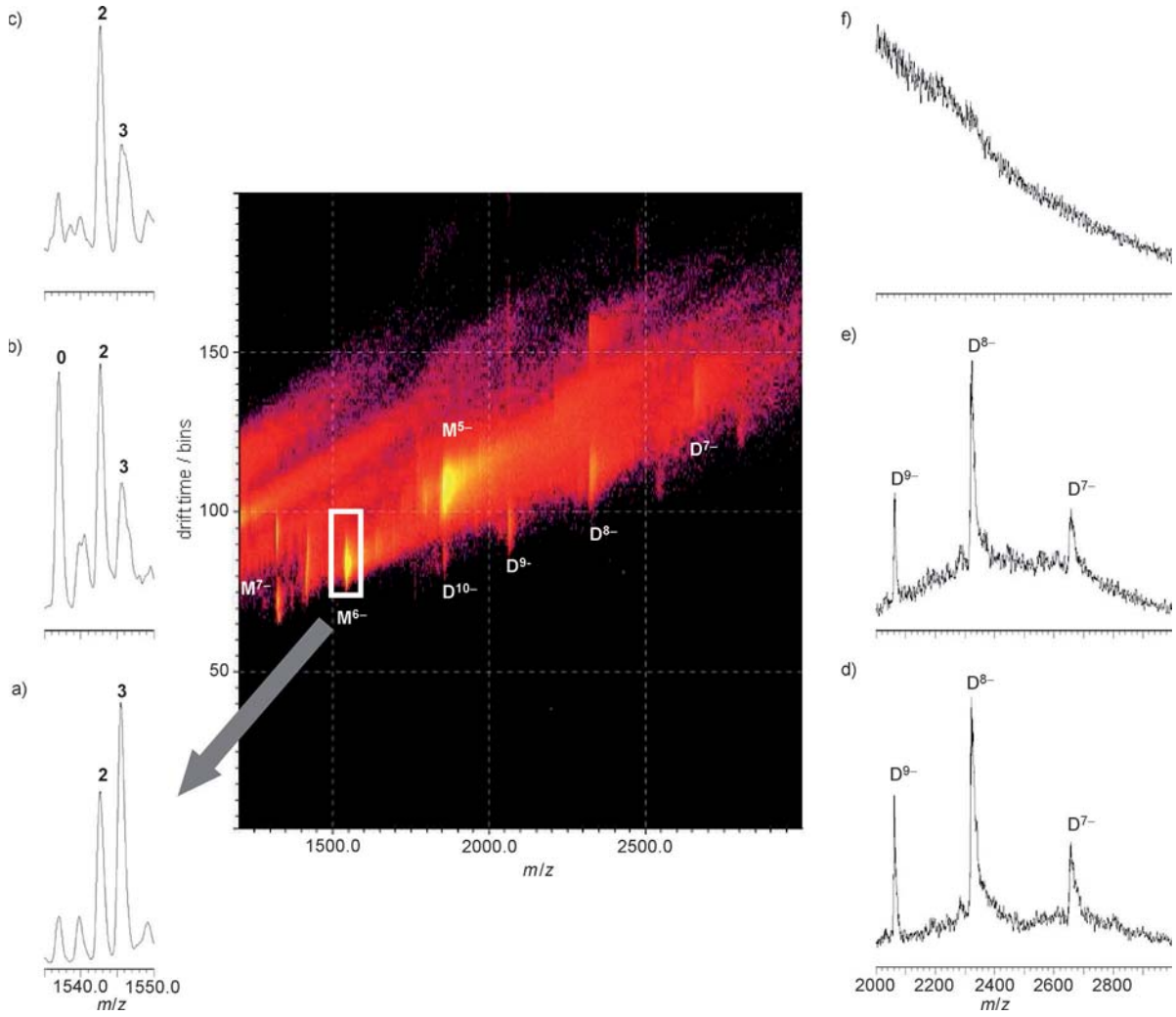

Figure 2. Left: ESI-MS of a quadruplex formed by oligonucleotides **1** (a), **2** (b) and **3** (c) and the distribution of the number of NH_4^+ ions preserved in the G-quadruplex at −6 charge state; the mass spectra were smoothed using a mean function, 2*10 channels, using MassLynx 4.0. Center: 2D ESI-MS and drift time distribution of oligonucleotide **1**. Right: ESI-MS of a dimer formed by oligonucleotides **1** (d), **2** (e) and **3** (f); the mass spectra were smoothed using a mean function, 2*30 channels, using MassLynx 4.0.

 © 2012 The Authors. Published by Wiley-VCH Verlag GmbH & Co. KGaA, Weinheim

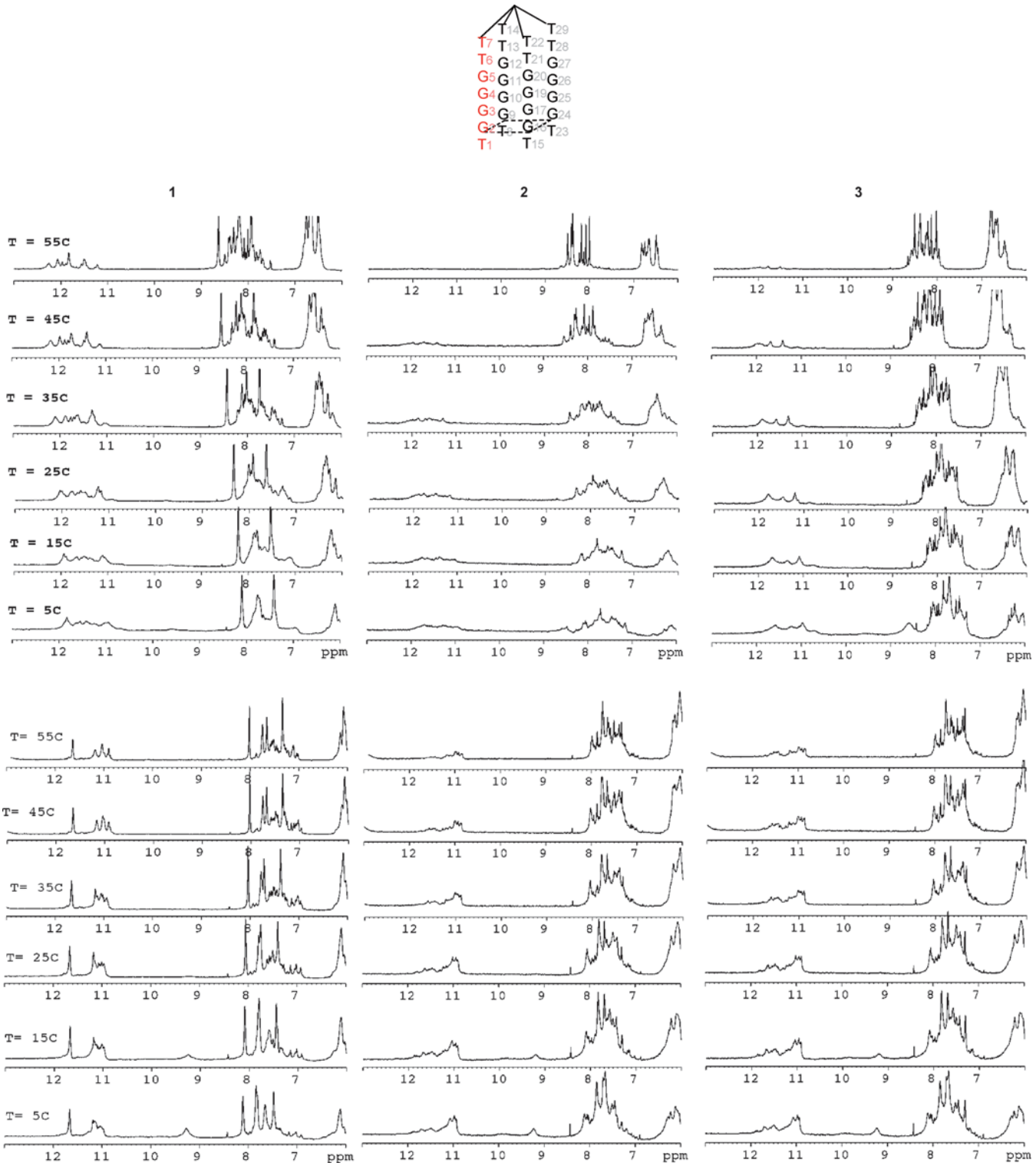

Figure 3. Top: General scheme of a tetra-end-linked quadruplex showing the numeration of the residues as mentioned in the text. Bottom: exchangeable proton region of ^{1}H NMR spectra at different temperatures of oligonucleotides **1**, **2** and **3** in 10 mM sodium phosphate buffer (upper rows) or 10 mM potassium phosphate buffer (lower rows).

Hoogsteen N1H–O6 hydrogen bonds of G-quartets. These imino signals were observed at high temperatures, indicating that the three quadruplexes were very stable, being more stable under K^+ than Na^+ conditions. The relative stability between the three oligonucleotides was in agreement with UV-melting experiments (**1** > **3** > **2**). At low temperatures, NMR signals were broad, suggesting the presence of more than one species in equilibrium. In quadruplex **1**, signals became sharper upon temperature increase. This effect was more pronounced in K^+ buffer and is probably due to the dissociation of multi-

 © 2012 The Authors. Published by Wiley-VCH Verlag GmbH & Co. KGaA, Weinheim

meric species. To determine the oligomerization state of the samples, we performed native gel electrophoreses (see below).

NMR spectra of **1** in K^+ buffer conditions were of sufficient quality to acquire 2D experiments. On the basis of NOESY and TOCSY spectra, four spin systems with relatively sharp signals were clearly identified, and they were sequentially assigned to residues 1–4. NOE cross-peak patterns for these residues indicate that the four chains are equivalent and the guanines adopt an *anti*-conformation. The remaining nucleotides (G5, T6 and T7) presented a broad signal and their NOE cross-peaks were almost invisible at low temperatures (Figure 4). At higher temperatures, these residues exhibited multiple cross-peaks in the NOESY spectra (Figure 4), suggesting the presence of several conformers in this region of the molecule. The presence of these conformers is possibly related to a conformational heterogeneity that affects the nucleotides near the linker. This is consistent with the number of signals and their relative intensities observed in the 1D spectra at this temperature (Figure 3).

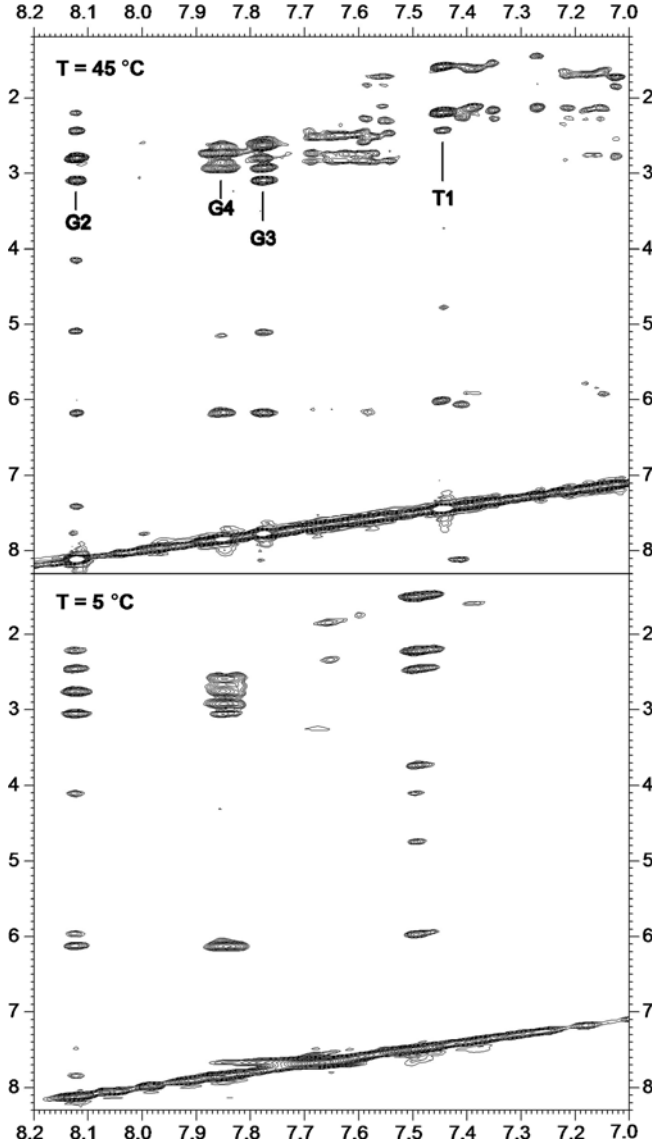

Figure 4. Fragments of NOESY spectra (250 ms mixing time) of oligonucleotide **1** at 5 °C (bottom) and 45 °C (top) in 10 mM potassium phosphate (pH 7).

Methyl-imino cross-peaks in the exchangeable proton region of the NOESY experiment allowed for the assignment of H1 of G2 (Figure S2 in the Supporting Information). Also an imino–imino sequential cross-peak between H1G2 and H1G3 was clearly observed. Other exchangeable protons corresponding to G4 and G5 were also observed, but could not be specifically assigned. The number of exchangeable proton signals and their cross-peak pattern indicated the formation of four guanine tetrads.

In summary, the NMR experiments indicate that at high temperature oligonucleotide **1** forms a symmetrical parallel quadruplex, most probably monomeric, where the four chains are equivalent and all guanines adopt an *anti*-conformation. Although oligonucleotide **1** exhibits a single global fold, some conformational heterogeneity occurs in residues close to the linker. This is probably due to steric constraints provoked by the linker, which impede the interconversion between different conformers. At low temperatures, NMR signals are broader suggesting an equilibrium with other species of higher molecular weight.

Presence of dimeric quadruplex structures

Native polyacrylamide gel electrophoresis (PAGE) has been widely used to detect oligomers and aggregates. Electrophoretic analysis was carried out using the tetramolecular quadruplex $[d(TG_4T)]_4$ as a reference. First, native PAGE was performed to assess the oligomerization state of the quadruplexes studied by NMR (oligonucleotides **1**–**3**). In all cases oligonucleotides resulted in two major bands suggesting that they form not only monomeric species but also dimeric structures (Figure S1 in the Supporting Information). Also, in all cases the band corresponding to the monomer was the major band (60–70%). ESI-MS showed that branched oligonucleotide sequences (**1**–**3**) to some extent form dimers in ammonium acetate (100 mM). The ESI-MS spectra recorded for three sequences are shown in Figure 2 d–f. Quadruplex **3** had a lower signal-to-noise ratio as a result of the presence of residual salts, but in all three cases, the presence of a dimeric quadruplex as a minor component was confirmed by mass spectrometry.

We propose two hypothetical dimeric structures for the dimer formed by these branched oligonucleotides. The association of two molecules allows the formation of two parallel quadruplexes, each containing one strand belonging to the adjacent molecule (e.g., interlocked structure **B** shown in Figure 5). The second model proposed is based on previous observations reported in the literature (structure **A** in Figure 5). Crystallographic studies of $d(TG_4T)$ quadruplexes performed by Cáceres et al.[24] revealed the stacking of T tetrads between neighboring quadruplexes packed in a head-to-head fashion. Recent NMR studies on UG_4U revealed the existence of a dimeric quadruplex structure in the presence of K^+ and NH_4^+ but not Na^+ ions.[25] ESI-MS studies on telomeric sequences performed by Collie et al[26] revealed that telomeric RNA form

 © 2012 The Authors. Published by Wiley-VCH Verlag GmbH & Co. KGaA, Weinheim

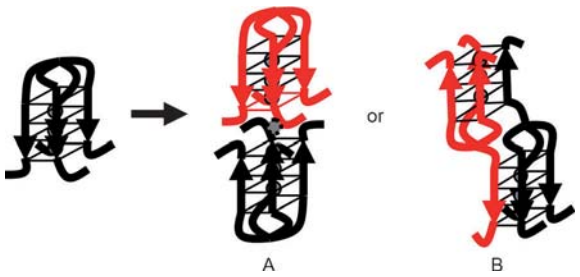

Figure 5. Hypothetical dimerization of the quadruplex-forming structures.

higher-order dimeric assemblies, initiated by cation-mediated stacking of two parallel G-quadruplex subunits.

This dimer, consistent with two G-quadruplex subunits, each with three NH_4^+ ions, plus one NH_4^+ ion stacked between the two subunits was observed by ESI-MS experiments. This result suggests a structural model for the dimer involving the cation-mediated stacking of G-quadruplex subunits (structure **A** in Figure 5).

Analysis of the stability of oligonucleotides carrying 8-aminoguanine

CD studies and thermal denaturation were performed in order to study the effect of 8-aminoguanine substitution on the stability of the quadruplex. As described above, in the presence of K^+ ions (5 mM KCl), all quadruplexes were stable up to 80 °C as no changes in the UV spectra were observed. For this reason, oligonucleotides **3**–**5** were dissolved in water and CD thermal denaturation was performed (see the Supporting Information). Under these conditions, the samples contained some residual triethylammonium acetate (TEAA) from HPLC purification. Even in the absence of K^+ and Na^+ ions, the CD spectra of oligonucleotides **3**–**5** showed the presence of a parallel quadruplex structures: a positive band with a maximum at 260 nm and a negative band with a minimum at 240 nm. In the absence of K^+ and Na^+ ions, unmodified oligonucleotide **3** had a T_m value of 50 °C (Table 1). The introduction of an 8-aminoguanine residue in the external position of the quadruplex (oligonucleotide **4**) produces a quadruplex with similar stability (52 °C). In contrast, the substitution of a single G by 8-aminoguanine in the internal quartet (oligonucleotide **5**) induced the formation of a very stable quadruplex, as only a partial melting was observed at 80 °C.

Conclusion

Here, we have used the trebler branching unit to synthesize molecules containing four G-rich DNA strands linked by one of the ends. These molecules form very stable parallel G-quadruplex structures even in the absence of stabilizing cations. NMR experiments confirmed that oligonucleotide **1** forms a symmetrical parallel quadruplex, where the four chains are equivalent and all guanines adopt an *anti*-conformation. The methodology described here allowed the synthesis of quadruplexes with single modifications in one of the strands. Oligonucleotides with 8-aminoguanine substitutions provide more stable structures when the replacement is carried out in the internal region of the quadruplex. This system has also allowed the synthesis of quadruplexes with a single antiparallel strand. In this case, all-parallel or 3+1 structures are observed depending on the cation present in the solution. Surprisingly, in addition to the monomolecular G-quadruplex, bimolecular structures are also observed. These bimolecular species were not detected in previous studies on branched G-quadruplexes[15] and could be interesting for biomedical applications, as it has been observed that in HIV-binding aptamers these species are relevant for the HIV inhibitory properties.[7] The method described here provides an excellent platform to obtain defined and stable G-quadruplex structures that could provide advantages to the conventional tetramolecular quadruplex in the development of applications, such as convenient functionalization as well as thermodynamic and biological stability.

Experimental Section

Synthesis of oligonucleotides

The oligonucleotide sequences used in this study (Table 2) were prepared on either a 0.2 μmol scale for oligonucleotides **3**–**5** or 1 μmol scale for oligonucleotides **1**, **2** using commercially available phosphoramidites and polystyrene (LV200) or controlled pore glass (CPG) solid supports. The trebler phosphoramidite was obtained from Glen Research (Sterling, VA, USA). 2′-Deoxyguanosine was protected with an isobutyryl group and 2′-deoxycytidine and 2′-deoxyadenosine with a benzoyl group. Reversed phosphoramidites were from Link Technologies (Lanarkshire, UK). The phosphoramidite of 8-amino-2′-deoxyguanosine was protected with two dimethylaminomethylidene groups obtained from Berry Associates (Dexter, MI, USA). Oligonucleotides were purified by HPLC using a Nucleosil C_{18} column (120–10, 250×4 mm, Macherey-Nagel, Düren, Germany). Elution was performed with a mixture of solution A (5% CH_3CN in 0.1 M aq triethylammonium acetate (TEAA)) and solution B (70% CH_3CN in 0.1 M aq TEAA) at a flow rate of 3 mL min^{-1} in 20 min (15–80% B, DMT off conditions).

Table 2. Oligonucleotide sequences used in this study.

Quadruplex	Sequence[a]
1	5′-TGGGGTT-3′-TB-[3′-TTGGGGT-5′]3
2	3′-TGGGGTT-5′-TB-[3′-TTGGGGT-5′]3
3	3′-TGGGGTT-5′-TB-[5′-TTGGGGT-3′]3
4	3′-T**G***GGGTT-5′-TB-[5′-TTGGGGT-3′]3
5	3′-TG**G***GGTT-5′-TB-[5′-TTGGGGT-3′]3

[a] **G***: 8-amino-G nucleotides. TB: trebler linker [–O–phosphate–CH_2–$C(CH_2OCH_2CH_2CH_2O$–phosphate–$)_3$].

The first part of oligonucleotide **1** was prepared using reversed 5′-phosphoramidites. The coupling time for reversed 5′-phosphoramidites was increased to 3 min, while that for the trebler phosphoramidite was increased to 15 min. After trebler phosphoramidite incorporation, the three remaining strands were assembled using standard 3′-phosphoramidites. Oligonucleotide **2** was prepared using standard 3′-phosphoramidites for the entire synthesis. The

 © 2012 The Authors. Published by Wiley-VCH Verlag GmbH & Co. KGaA, Weinheim

first parts of oligonucleotides **3**–**5** were prepared using standard 3′-phosphoramidites. 8-Amino-2′-deoxyguanosine phosphoramidite was used to introduce the 8-aminoguanine residue at the desired positions. The coupling time for 8-aminoguanine phosphoramidite was increased to 5 min. After the incorporation of the trebler phosphoramidite the three remaining strands were assembled using reversed 5′-phosphoramidites. Generally, solid supports were treated with concd aq NH_3 (1 ml) at 55 °C overnight. Supports carrying oligonucleotides **4** and **5** were treated with concd NH_3 (1 ml) containing 2-mercaptoethanol (0.1 M) at 55 °C for 24 h. After filtration, the solid supports were washed with H_2O (3 ml), and the combined solutions were evaporated in vacuo to dryness. The residues were dissolved in H_2O, and the oligonucleotides were purified by HPLC. The purified products were treated with 80% aq AcOH at RT for 30 min, except for oligonucleotides **3**–**5**, which were treated at 55 °C for 30 min because 3′-dimethoxytrityl (3′-DMT) is more resistant to detritylation. AcOH was extracted with Et_2O (3×5 ml), and the resulting compounds were desalted using a NAP-10 column and analyzed using a 4800 Plus MALDI TOF/TOF Analyzer (AB Sciex, Framingham, MA, USA). At 260 nm, yields were around 2 OD units for the 0.2 μmol scale and 15 OD units for the 1 μmol scale.

Oligonucleotide **1**: $[M-H]^-$ calcd: 9227.5, found: 9227; oligonucleotide **2**: $[M-H]^-$ calcd: 9227.5, found 9227; oligonucleotide **3**: $[M-H]^-$ calcd: 9227.5, found: 9227; oligonucleotide **4**: $[M-H]^-$ calcd: 9242.5, found 9236; oligonucleotide **5**: $[M-H]^-$ calcd: 9242.5, found 9233.

Thermal denaturation experiments

UV spectroscopy: The thermal melting curves for oligonucleotides **1**–**5** and $d(TG_4T)_4$ were performed following the UV-absorption change at 240, 260 and 295 nm in a temperature range of 20–95 °C with a linear temperature ramp of 0.5 °C min^{-1} on a JASCO V-650 spectrophotometer equipped with a Peltier temperature control. The measurements were conducted in 5 mM KCl, 100 mM NaCl, 100 mM NH_4OAc or Milli-Q H_2O. Oligonucleotides (5 μM) were annealed by heating to 95 °C and slowly cooling to RT before measurement.

CD spectroscopy: CD spectra were obtained from a spectropolarimeter (Jasco) equipped with a Peltier temperature control. CD spectra were registered between 220 and 320 nm in either Milli-Q H_2O, 5 mM KCl, 100 mM NaCl or 100 mM NH_4OAc. CD thermal denaturation experiments were performed in the temperature range of 10–90 °C using a heating rate of 0.5 °C min^{-1} and monitoring the CD values at 260 nm. Oligonucleotides (5 μM) were annealed by heating the samples to 95 °C and slowly cooling to RT before recording CD spectra and melting profiles.

NMR spectroscopy

Samples for NMR measurements were dissolved in H_2O/D_2O (9:1, 200 μL) containing either NaH_2PO_4/Na_2HPO_4 (10 mM) or KH_2PO_4/K_2HPO_4 (10 mM). Oligonucleotide concentrations were ~300 μM for oligonucleotide **1**, and ~150 μM for **2** and **3**. ^1H NMR spectra were collected at temperatures ranging from 5 to 55 °C on a AV-600 spectrometer (Bruker, Billerica, MA, USA) equipped with a cryoprobe. Water suppression was achieved by including a WATERGATE module in the pulse sequence prior to spectra acquisition.

ESI-MS and Ion mobility spectrometry (IMS)

The ESI-MS experiments described were recorded in ion mobility mode using a SYNAPT G2 HDMS (Waters, Manchester, UK). The capillary voltage was set to −2.2 kV; cone voltage = 30 V; extraction cone = 4 V; source pressure = 3.15 mbar; source and desolvation temperatures = 40 °C; trap and transfer voltages = 4 V. The helium cell is supplied with helium at 180 mL min^{-1}, and the ion mobility cell is supplied with N_2 to reach a pressure of 3.88 mbar in the IMS cell (instrument pirani reading). The wave height was 40 V and the wave speed was 1000 m s^{-1}. The bias voltage for ion introduction into the IMS cell was 35 V. Both instruments were calibrated in collision cross section with oligonucleotides, as described previously.[27] Oligonucleotides **1**, **2** and **3** (200 μM) were folded in NH_4OAc buffer (100 mM) and injected at a final strand concentration of 5 μM and at a rate of 140.0 μL h^{-1} at RT.

Acknowledgements

This work was supported by the Spanish Ministry of Education (grants BFU2007–63287, CTQ2010–20541, CTQ2010–2167-C02–02), the European Cooperation in Science and Technology (COST) (project MP0802, stsm 9145 to RF) and the Generalitat de Catalunya (Spain) (2009/SGR/208). Centro de Investigación Biomédica en Red en Bioingeniería, Biomateriales y Nanomedicina (CIBER-BBN) is an initiative funded by the VI National R&D&i Plan 2008–2011, Iniciativa Ingenio 2010, Consolider Program, CIBER Actions and financed by the Instituto de Salud Carlos III with assistance from the European Regional Development Fund. V.G. acknowledges the support of the Fonds de la Recherche Scientifique (FNRS, France) (research associate position, and grant no. 2.4528.11), and the Groupe Interdisciplinaire de Génoprotéomique Appliquée (GIGA, Belgium) platform for access to the instruments. R.F. is a recipient of an FPI contract from the Spanish Ministry of Science.

Keywords: 8-aminoguanines · branched oligonucleotides · DNA structures · G-quadruplexs · oligonucleotides

[1] a) J. R. Williamson, M. K. Raghuraman, T. R. Cech, *Cell* **1989**, *59*, 871–880; b) E. H. Blackburn, *Cell* **1994**, *77*, 621–623.
[2] a) A. Siddiqui-Jain, C. L. Grand, D. J. Bearss, L. H. Hurley, *Proc. Natl. Acad. Sci. USA* **2002**, *99*, 11593–11598; b) T. S. Dexheimer, D. Sun, L. H. Hurley, *J. Am. Chem. Soc.* **2006**, *128*, 5404–5415.
[3] S. Kumari, A. Bugaut, J. L. Huppert, S. Balasubramanian, *Nat. Chem. Biol.* **2007**, *3*, 218–221.
[4] G. W. Collie, G. N. Parkinson, *Chem. Soc. Rev.* **2011**, *40*, 5867–5892.
[5] K. A. Marshall, A. D. Ellington, *Methods Enzymol.* **2000**, *318*, 193–214.
[6] a) L. C. Bock, L. C. Griffin, J. A. Latham, E. H. Vermaas, J. J. Toole, *Nature* **1992**, *355*, 564–566; b) R. F. Macaya, P. Schultze, F. W. Smith, J. A. Roe, J. Feigon, *Proc. Natl. Acad. Sci. USA* **1993**, *90*, 3745–3749.
[7] a) B. Gatto, M. Palumbo, C. Sissi, *Curr. Med. Chem.* **2009**, *16*, 1248–1265; b) L. Petraccone, G. Barone, C. Giancola, *Curr. Med. Chem.: Anti-Cancer Agents* **2005**, *5*, 463–475; c) E. B. Pedersen, J. T. Nielsen, C. Nielsen, V. V. Filichev, *Nucleic Acids Res.* **2011**, *39*, 2470–2481; d) G. Di Fabio, J. D'Onofrio, M. Chiapparelli, B. Hoorelbeke, D. Montesarchio, J. Balzarini, L. De Napoli, *Chem. Commun.* **2011**, *47*, 2363–2365.
[8] T. C. Marsh, J. Vesenka, E. Henderson, *Nucleic Acids Res.* **1995**, *23*, 696–700.
[9] P. Alberti, A. Bourdoncle, B. Saccà, L. Lacroix, J. L. Mergny, *Org. Biomol. Chem.* **2006**, *4*, 3383–3391.
[10] Y. Xiao, A. A. Lubin, A. J. Heeger, K. W. Plaxco, *Angew. Chem.* **2005**, *117*, 5592–5595; *Angew. Chem. Int. Ed.* **2005**, *44*, 5456–5459.

 © 2012 The Authors. Published by Wiley-VCH Verlag GmbH & Co. KGaA, Weinheim

[11] M. Webba da Silva, M. Trajkosski, Y. Sannohe, N. M. Hessari, H. Sugiyama, J. Plavec, *Angew. Chem.* **2009**, *121*, 9331 – 9334; *Angew. Chem. Int. Ed.* **2009**, *48*, 9167 – 9170.

[12] a) M. J. Damha, K. Geneshan, R. H. E. Hudson, S. V. Zabarylo, *Nucleic Acids Res.* **1992**, *20*, 6565 – 6573; b) S. Carriero, M. J. Damha, *Nucleic Acids Res.* **2003**, *31*, 6157 – 6167; c) M. Grøtli, R. Eritja, B. Sproat, *Tetrahedron* **1997**, *53*, 11317 – 11346.

[13] a) Y. Ueno, M. Takeba, M. Mikawa, A. Matsuda, *J. Org. Chem.* **1999**, *64*, 1211 – 1217; b) M. D. Sørensen, M. Meldgaard, V. K. Rajwanshi, J. Wengel, *Bioorg. Med. Chem. Lett.* **2000**, *10*, 1853 – 1856; c) A. Aviño, M. G. Grimau, M. Frieden, R. Eritja, *Helv. Chim. Acta* **2004**, *87*, 303 – 316.

[14] a) M. S. Shchepinov, K. U. Mir, J. K. Elder, M. D. Frank-Kamenetskii, E. M. Southern, *Nucleic Acids Res.* **1999**, *27*, 3035 – 3041; b) M. G. Grimau, D. Iacopino, A. Aviñó, B. G. de La Torre, A. Ongaro, D. Fitzmaurice, J. Wessels, R. Eritja, *Helv. Chim. Acta* **2003**, *86*, 2814 – 2826; c) S. E. Stanca, A. Ongaro, R. Eritja, D. Fitzmaurice, *Nanotechnology* **2005**, *16*, 1905 – 1911; d) R. Pathak, A. Marx, *Chem. Asian J.* **2011**, *6*, 1450 – 1455.

[15] a) G. Oliviero, J. Amato, N. Borbone, A. Galeone, L. Petraccone, M. Varra, G. Piccialli, L. Mayol, *Bioconjugate Chem.* **2006**, *17*, 889 – 898; b) G. Oliviero, J. Amato, N. Borbone, S. D'Errico, A. Galeone, L. Mayol, S. Haider, O. Olubiyi, B. Hoorelbeke, J. Balzarini, G. Piccialli, *Chem. Commun.* **2010**, *46*, 8971 – 8973; c) L. Petraccone, L. Martino, I. Duro, G. Oliviero, N. Borbone, G. Piccialli, C. Giancola, *Int. J. Biol. Macromol.* **2007**, *40*, 242 – 247; d) G. Oliviero, N. Borbone, J. Amato, S. D'Errico, A. Galeone, G. Piccialli, M. Varra, L. Mayol, *Biopolymers* **2009**, *91*, 466 – 476; e) P. Murat, R. Bonnet, A. Van der Heyden, N. Spinelli, P. Labbé, D. Monchaud, M.-P. Teulade-Fichou, P. Dumy, E. Defrancq, *Chem. Eur. J.* **2010**, *16*, 6106 – 6114.

[16] F. Aboul-ela, A. I. H. Murchie, D. M. J. Lilley, *Nature* **1992**, *360*, 280 – 282.

[17] a) G. Laughlan, A. I. Murchie, D. G. Norman, M. H. Moore, P. C. Moody, D. M. Lilley, B. Luisi, *Science* **1994**, *265*, 520 – 524; b) K. Phillips, Z. Dauter, A. I. H. Murchie, D. M. J. Lilley, B. Luisi, *J. Mol. Biol.* **1997**, *273*, 171 – 182.

[18] F. Aboul-ela, A. I. H. Murchie, D. G. Norman, D. M. J. Lilley, *J. Mol. Biol.* **1994**, *243*, 458 – 471.

[19] a) J. Gros, F. Rosu, S. Amrane, A. De Cian, V. Gabelica, L. Lacroix, J. L. Mergny, *Nucleic Acids Res.* **2007**, *35*, 3064 – 3075; b) P. L. Thao Tran, A. Virgilio, V. Esposito, G. Citarella, J. L. Mergny, A. Galeone, *Biochimie* **2011**, *93*, 399 – 408.

[20] J. Gros, A. Aviñó, J. López de La Osa, C. González, L. Lacroix, A. Pérez, M. Orozco, R. Eritja, J. L. Mergny, *Chem. Commun.* **2008**, 2926 – 2928.

[21] a) R. A. Rieger, C. R. Iden, E. Gonikberg, F. Johnson, *Nucleosides Nucleotides* **1999**, *18*, 73 – 88; b) R. Soliva, R. Güimil García, J. R. Blas, R. Eritja, J. L. Asensio, C. González, F. J. Luque, M. Orozco, *Nucleic Acids Res.* **2000**, *28*, 4531 – 4539.

[22] K. W. Lim, L Lacroix, D. J. E. Yue, J. K. C. Lim, J. M. W. Lim, A. T. Phan, *J. Am. Chem. Soc.* **2010**, *132*, 12331 – 12342.

[23] J. L. Mergny, A. De Cian, A. Ghelab, B. Saccà, L. Lacroix, *Nucleic Acids Res.* **2005**, *33*, 81 – 94.

[24] C. Cáceres, G. Wright, C. Gouyette, G. Parkinson, J. A. Subirana, *Nucleic Acids Res.* **2004**, *32*, 1097 – 1102.

[25] P. Sket, J. Plavec, *J. Am. Chem. Soc.* **2010**, *132*, 12724 – 12732.

[26] G. W. Collie, G. N. Parkinson, S. Neidle, F. Rosu, E. De Pauw, V. Gabelica, *J. Am. Chem. Soc.* **2010**, *132*, 9328 – 9334.

[27] F. Rosu, V. Gabelica, L. Joly, G. Grégoire, E. De Pauw, *Phys. Chem. Chem. Phys.* **2010**, *12*, 13448 – 13454.

Received: March 30, 2012

 © 2012 The Authors. Published by Wiley-VCH Verlag GmbH & Co. KGaA, Weinheim

ChemistryOPEN

Supporting Information

© Copyright Wiley-VCH Verlag GmbH & Co. KGaA, 69451 Weinheim, 2012

Synthesis and Structural Characterization of Stable Branched DNA G-Quadruplexes Using the Trebler Phosphoramidite

Rubén Ferreira,[a, b] Margarita Alvira,[a, b] Anna Aviñó,[a, b] Irene Gómez-Pinto,[c] Carlos González,[c] Valérie Gabelica,[d] and Ramon Eritja*[a, b]

open_201200009_sm_miscellaneous_information.pdf

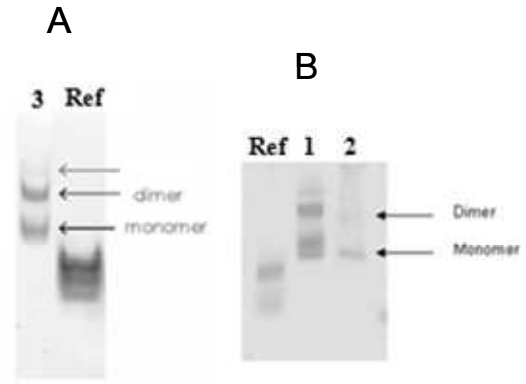

Figure S1. Native gel electrophoresis of A) oligonucleotide **3** and B) oligonucleotides **1** and **2**. In both cases $[d(TGGGGT)]_4$ was used as reference (Ref) for comparison of relative migrations.

Gel electrophoresis experiments were performed on 15% native bis/acrylamide gels at 4ºC. The electrophoresis was run at this temperature at 200 V in a SE-600 Hoefer Scientific apparatus using TAE Mg^{2+} (40 mM Tris, 2mM EDTA, 20 mM AcOH, and 12.5 mM magnesium acetate) as running buffer. The final concentration of oligonucleotides **1**, **2**, **3** and $[d(TGGGGT)]_4$ sample solutions were 25 μM. The samples were annealed in 5 mM K^+ buffer and then dissolved in loading buffer containing 50% glycerol in TAE Mg^{2+} buffer to obtain the final concentration. After the electrophoresis, oligonucleotides were stained by STAINS-ALL (Sigma).

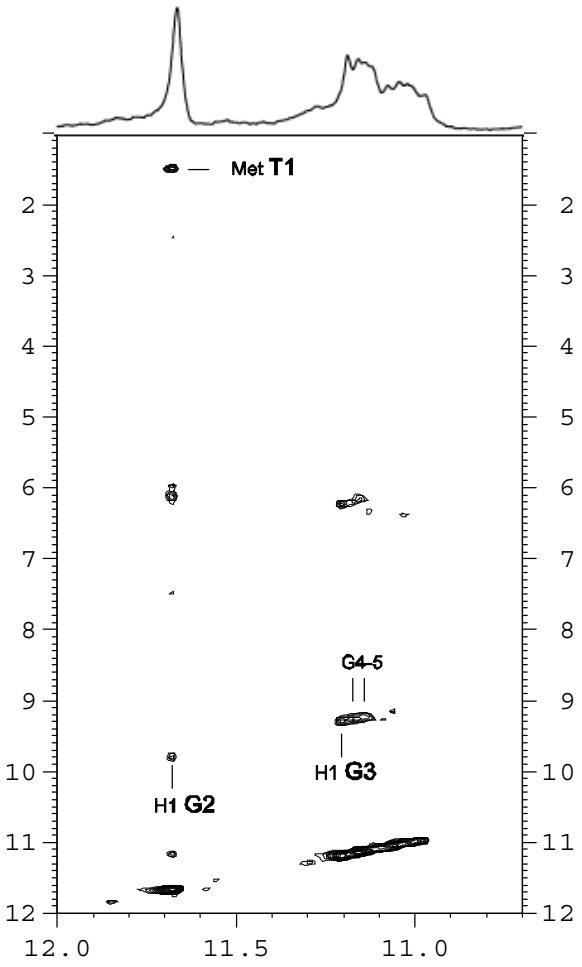

Figure S2. Imino proton region of the NOESY (100ms mixing time) spectra of oligonucleotide **1** in H_2O (5mM K+ concentration, pH 7, T= 5 ºC). The corresponding region of 1D spectrum is shown on the top.

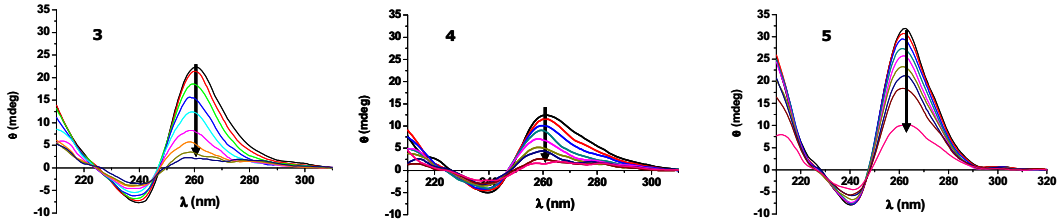

Figure S3. CD spectra of sequences **3-5** registered at different temperatures in the range 10-90 ºC. The spectra show a decrease of the CD signal upon heating.

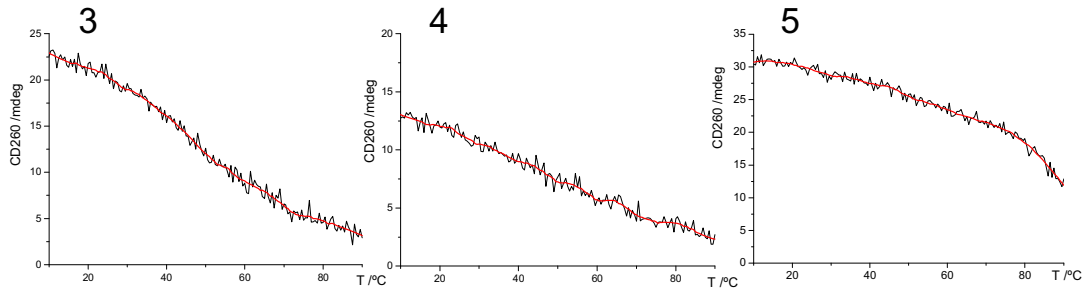

Figure S4. Melting profile of sequences **3-5** monitoring the CD values (mdeg) at 260 nm in the range 10-90 ºC using a heating rate of 0.5 ºC/min.

2

ESPECTROSCÒPIA DE MASSES I ESPECTROSCÒPIA DE MOBILITAT IÒNICA APLICADA ALS QUÀDRUPLEX DE GUANINA. ESTUDI DELS EFECTES DEL DISSOLVENT EN LA FORMACIÓ I EN LES TRANSICIONS ESTRUCTURALS DEL DÍMER EN LA SEQÜÈNCIA TELOMÈRICA dTAGGGTTAGGGT

ESPECTROSCÒPIA DE MASSES I ESPECTROSCÒPIA DE MOBILITAT IÒNICA APLICADA ALS QUÀDRUPLEX DE GUANINA. ESTUDI DELS EFECTES DEL DISSOLVENT EN LA FORMACIÓ I EN LES TRANSICIONS ESTRUCTURALS DEL DÍMER EN LA SEQÜÈNCIA TELOMÈRICA dTAGGGTTAGGGT.

Mass spectrometry and ion mobility spectrometry of G-quadruplex. A study of solvent effects on dimer formation and structural transitions in the telomèric DNA sequence dTAGGGTTAGGGT.

Rubén Ferreira,[1] Adrien Marchand,[2] Valérie Gabelica[*,2]

Methods (2012), Volume 57, Issue 1, May 2012, Pages 56–63

[1] *Department of Chemistry and Molecular Pharmacology, Institute for Research in Biomedicine (IRB Barcelona), IQAC-CSIC, CIBER-BNN,Baldiri i Reixac 10, E-08028 Barcelona (Spain).*
[2] *Department of Chemistry, University of Liège, Allée de la Chimie Building B6C, B-4000 Liège, Belgium.*
** Address correspondence to: v.gabelica@ulg.ac.be*

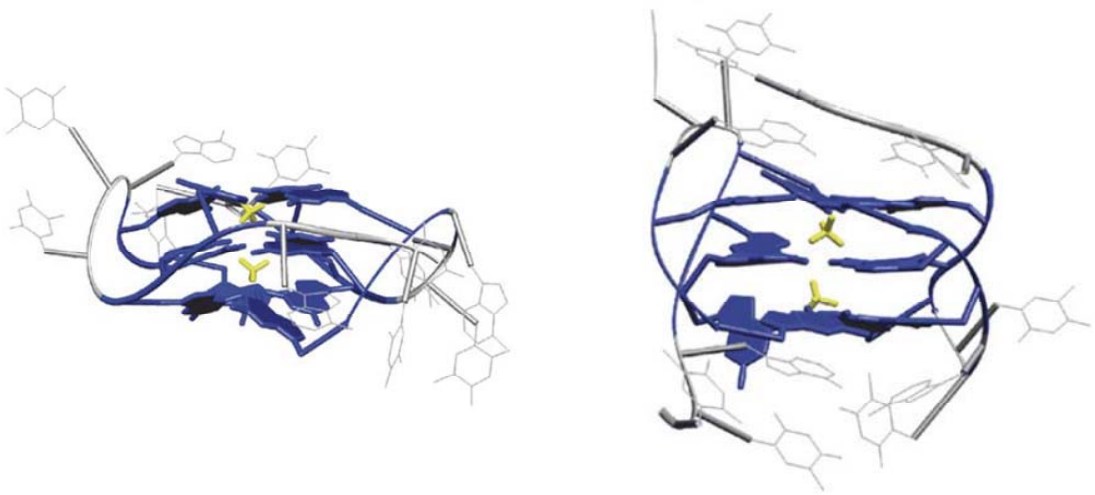

Resum

S'ha examinat la situació actual de les metodologies d'espectroscòpia de masses aplicades als G-quàdruplex i s'ha il·lustrat amb l'estudi d'un model simple: el G-quàdruplex dimèric que forma la seqüència telomèrica 12-mer dTAGGGTTAGGGT, que pot adoptar una estructura paral·lela o antiparal·lela.

S'ha analitzat les limitacions provocades per la solució utilitzada a ESI-MS, la interpretació de la preservació dels ions d'amoni en els complexes en fase gas i l'ús de la mobilitat iònica per resoldre les ambigüitats segons l'estequiometria de les cadenes o per separar i analitzar els diferents isòmers estructurals.

També es descriu, per primer cop, que l'addició de co-dissolvents compatibles amb l'electrosprai (metanol, etanol, isopropanol o acetonitril) a la solució aquosa d'acetat d'amoni augmenta l'estabilitat i la velocitat de formació del G-quàdruplex dimèric i provoca transicions estructurals a estructures paral·leles.

S'ha investigat els canvis estructurals per dicroisme circular i per espectroscòpia de mobilitat iònica i l'excel·lent correlació entre les dues tècniques valida l'ús de la mobilitat iònica per a estudis estructurals de G-quàdruplex. Es va demostrar que les estructures de G-quàdruplex paral·leles es preserven més fàcilment en fase gas que les estructures antiparal·leles.

Methods 57 (2012) 56–63

Contents lists available at SciVerse ScienceDirect

Methods

journal homepage: www.elsevier.com/locate/ymeth

Mass spectrometry and ion mobility spectrometry of G-quadruplexes. A study of solvent effects on dimer formation and structural transitions in the telomeric DNA sequence d(TAGGGTTAGGGT)

Rubén Ferreira [a], Adrien Marchand [b], Valérie Gabelica [b,*]

[a] Department of Chemistry and Molecular Pharmacology, Institute for Research in Biomedicine (IRB Barcelona), IQAC-CSIC, CIBER-BNN, Baldiri i Reixac 10, E-08028 Barcelona, Spain
[b] Department of Chemistry, University of Liège, Allée de la Chimie Building B6C, B-4000 Liège, Belgium

ARTICLE INFO

Article history:
Available online 24 March 2012

Communicated by Stephen Neidle

Keywords:
Mass spectrometry
Ion mobility spectrometry
G-quadruplex
DNA
Solvent
Folding

ABSTRACT

We survey here state of the art mass spectrometry methodologies for investigating G-quadruplexes, and will illustrate them with a new study on a simple model system: the dimeric G-quadruplex of the 12-mer telomeric DNA sequence d(TAGGGTTAGGGT), which can adopt either a parallel or an antiparallel structure. We will discuss the solution conditions compatible with electrospray ionisation, the quantification of complexes using ESI-MS, the interpretation of ammonium ion preservation in the complexes in the gas phase, and the use of ion mobility spectrometry to resolve ambiguities regarding the strand stoichiometry, or separate and characterise different structural isomers. We also describe that adding electrospray-compatible organic co-solvents (methanol, ethanol, isopropanol or acetonitrile) to aqueous ammonium acetate increases the stability and rate of formation of dimeric G-quadruplexes, and causes structural transitions to parallel structures. Structural changes were probed by circular dichroism and ion mobility spectrometry, and the excellent correlation between the two techniques validates the use of ion mobility to investigate G-quadruplex folding. We also demonstrate that parallel G-quadruplex structures are easier to preserve in the gas phase than antiparallel structures.

© 2012 Elsevier Inc. All rights reserved.

1. Introduction

Native electrospray ionisation mass spectrometry (ESI-MS) allows unambiguous determination of the stoichiometry of supramolecular assemblies, either from synthetic or biological origin [1–3]. For biomolecules, "native" mass spectrometry requires that (1) the sample is prepared in solvents and buffers that preserve the native fold, and (2) that the mass spectrometer is tuned so as to just desolvate each complex and then preserve it until it reaches the mass analyser. The second point stems from the fact that mass spectrometry is inherently a destructive technique: the molecule is destroyed to be analysed. Nevertheless, several groups have shown, based on theory and experiments, that many structural elements of proteins and nucleic acids can be conserved in the gas phase sufficiently long to be probed before destruction (for a review, see reference [4]). Fortunately, G-quadruplexes are the nucleic acid structures that are the most prone to be preserved in the gas phase [5–7], thanks to the enhancement of hydrogen bonding (between guanines forming G-quartets) and electrostatic interactions (between the central cations and the G-quartet bases) *in vacuo*.

As a result, native ESI-MS has become widely used to study G-quadruplexes in solution, to determine the number of strands involved in assemblies or to detect and quantify complexes with ligands. A recent review comprehensively covers the literature on mass spectrometry of G-quadruplex DNA until 2009 [8]. Other recent reviews on the characterisation of DNA-ligand interactions by mass spectrometry include extensive discussion of ligand binding to G-quadruplexes [9,10]. In the present contribution, we decided to explain in detail the mass spectrometry-based methodologies we currently apply routinely for G-quadruplex analysis (with no ligand attached). We will also discuss in detail (1) how to quantitate G-quadruplexes using mass spectrometry, (2) how to probe structural transitions using ion mobility spectrometry, and (3) how to interpret ammonium ion preservation in the detected ions. Finally, we also discuss the first criterion of "native" mass spectrometry, namely the structure adopted in electrospray-compatible solution conditions.

All these points will be illustrated with a new mass spectrometric study of dimeric G-quadruplex formation from the 12-mer telomeric DNA sequence $d(TAGGGT)_2$. In potassium solution, this sequence forms a mixture of interconverting antiparallel and parallel dimers (Fig. 1) [11]. A parallel fold was also found by X-ray

* Corresponding author.
E-mail address: v.gabelica@ulg.ac.be (V. Gabelica).

1046-2023/$ - see front matter © 2012 Elsevier Inc. All rights reserved.
http://dx.doi.org/10.1016/j.ymeth.2012.03.021

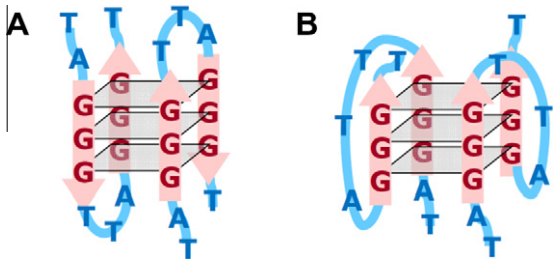

Fig. 1. Schematic structures of the dimer of dTAGGGTTAGGGT in the antiparallel fold (A) and in the parallel fold (B), according to Ref. [11].

diffraction when this sequence was crystallized from K^+ solution [12]. Because ESI-MS cannot be carried out in the presence of millimolar NaCl or KCl concentrations, volatile ammonium salts must be used to ensure a suitable ionic strength for the nucleic acid to fold. This means that for G-quadruplex nucleic acids, these experimental conditions do not satisfy the first criterion for native mass spectrometry, because the structures adopted in NH_4OAc are not necessarily the same as those adopted in KCl. In the particular case of the 12-mer $d(TAGGGT)_2$, only low amounts of dimer form in aqueous ammonium acetate [13], and a previous ion mobility study on the close analogue $d(TTAGGG)_2$ showed that the dimer formed in ammonium acetate was mainly antiparallel [14].

In an effort to render the G-quadruplex structures amenable to investigation by ESI-MS more native-like, we decided to explore how the G-quadruplex structures change in ammonium solutions when electrospray-compatible co-solvents are added. There is indeed increasing evidence that molecular crowding conditions, usually simulated by the addition of co-solutes such as polyethylene glycol, favour parallel structures in the human telomeric sequence [15,16]. The G-quadruplex conformational transitions induced by co-solutes is generally understood as an effect of water activity [17,18]. Ethanol [19,20] or acetonitrile [20,21] were also found to favour the parallel structure in the intramolecular telomeric G-quadruplex. The present article reports dimeric G-quadruplex formation by 12-mer telomeric sequences in ammonium, in the presence of common electrospray co-solvents such as methanol, ethanol, isopropanol or acetonitrile. We found that all co-solvents increased the stability and the rate of dimeric G-quadruplex formation, and caused structural transitions towards parallel structures from ammonium acetate solutions.

2. Materials

2.1. Chemicals

Oligodeoxynucleotides dT_6 and $d(TAGGGT)_2$ were purchased from Eurogentec (Belgium) and used without further purification. For all ESI-MS experiment, the sequence dT_6 (monoisotopic mass 1762.318 Da) was used as an internal standard for normalising peak intensities. Ammonium acetate (BioUltra ~ 5 M, for molecular biology) was provided by Fluka (Sigma–Aldrich NV/SA, Bornem, Belgium), Water was nuclease-free grade from Ambion (Applied Biosystems, Lennik, Belgium). Methanol, ethanol, 2-propanol and acetonitrile were provided by Biosolve, HPLC grade.

2.2. Circular dichroism (CD)

CD spectra were recorded on a JobinYvon CD6 dichrograph using 1-cm path length quartz cells (Hellma, type No. 120-QS, France). The final concentration of oligonucleotides was 5 μM in a solution containing 100 mM ammonium acetate. For each sample, three spectra were recorded from 220 to 350 nm with a scan rate of 0.25 nm/s.

2.3. Electrospray ion mobility mass spectrometry (ESI-IMS-MS)

All mass spectrometry experiments were performed on Waters (Manchester, UK) instruments equipped with electrospray ionisation, a travelling wave ion mobility cell, and a time-of-flight mass analyser. The two instruments (Synapt G1 HDMS and Synapt G2 HDMS) were used in negative electrospray ionisation and ion mobility modes. Each instrument was calibrated in the mobility mode in order to convert drift times into collision cross sections, using oligonucleotides of known collision cross sections, as described previously [22].

On the Synapt G1 HDMS, the capillary voltage was set to −2.2 kV; cone voltage = 30 V; extraction cone = 4 V; source pressure (pirani reading) = 3.15 mbar; source and desolvation temperatures = 40 °C and 60 °C, respectively; trap and transfer voltages = 6 V and 4 V, respectively. The ion mobility cell is filled with N_2 at 0.531 mbar (pirani reading), and an electric field is applied to the cell in the form of waves (wave height = 8 V) that pass through the cell at 300 m/s. The bias voltage for ion introduction into the IMS cell was 15 V, unless otherwise mentioned.

On the Synapt G2 HDMS, the capillary voltage was set to −2.2 kV; cone voltage = 30 V; extraction cone = 4 V; source pressure (pirani reading) = 3.25 mbar; source and desolvation temperatures = 40 °C; trap and transfer voltages = 4 V. The helium cell is supplied with He at 180 mL/min, and the ion mobility cell is supplied with N_2 to reach a pressure of 3.88 mbar in the IMS cell (instrument pirani reading). The wave height was 40 V and the wave speed was 1000 m/s. The bias voltage for ion introduction into the IMS cell was 35 V.

The main difference between the instruments therefore lies in the ion mobility cell. The Synapt G2 HDMS has a higher resolution in ion mobility mode than the Synapt G1 HDMS. However, due to the higher nitrogen pressure and despite the presence of the helium cell at the entrance of the ion mobility cell, the ions undergo more energetic collisions prior to their entrance in the mobility cell of the Synapt G2. We will show in the results and discussion section how this can affect the preservation of the structure of the G-quadruplexes in the gas phase.

The $d(TAGGGT)_2$ stock was single strand concentration of 200 μM in water and annealed by heating to 85 °C and slowly cooling to room temperature before use. To follow the kinetics of dimer formation, the samples were prepared at room temperature (22 ± 1 °C) and injected at a final single strand concentration of 5 μM dT_6 and 5 μM $d(TAGGGT)_2$ at a rate of 140 μL/h. The kinetics of dimerization was tested in 20%, 40%, 60% and 80% volume percentage of co-solvent (methanol, ethanol, 2-propanol and acetonitrile), the rest of the solvent being aqueous ammonium acetate (100 mM). Adequate volumes of aqueous single strand, water, and co-solvents were pre-mixed and allowed to equilibrate 10 min at room temperature. Ammonium acetate (from a 1 M stock solution) was added last, to initiate G-quadruplex formation. The mass spectral recording was started simultaneously with ammonium addition. The sample was thoroughly mixed and loaded into the 250-mL syringe, the spray was initiated as quickly as possible by manually pushing the syringe, and the flow rate was then stabilized at 140 μL/h. The time lapse between ammonium addition and spray stabilization is typically 1 min. The dimer formation can also be triggered either adding the co-solvent, but this is less adequate for accurate kinetics analysis, because the solution temperature transiently changes due to the endothermicity (in the case of ACN) or exothermicity (in the case of alcohols) of solvent mixing. All time-resolved experiments reported here for the determination of the response factors (see Section 4) were therefore triggered by ammonium acetate addition, and performed on the Synapt G1 HDMS spectrometer.

3. Effect of electrospray-compatible organic co-solvents on G-quadruplex assembly in ammonium acetate solution

ESI-MS of nucleic acids from purely aqueous ammonium acetate in the negative mode often gives low ion signals, as compared for example to ESI-MS of proteins in the positive ion mode. This is probably one of the reasons why ESI-MS of nucleic acid complexes is much less widespread than ESI-MS of protein complexes. A typical trick to enhance ion response in ESI-MS is to add to the sample some organic co-solvents more volatile than water in order to aid droplet desolvation and increase the signal-to-noise ratio. Since the early days [23], we took the habit to add 20% or 10% methanol to analyse nucleic acid complexes by ESI-MS, and most mass spectrometrists adopt similar recipes, using for example 10% isopropanol [24,25] or 20–25% methanol [26–30]. Some papers even report fair MS spectra of G-quadruplexes higher-order assembly and ligand binding using up to 50% methanol [31–33]. In contrast, published G-quadruplex MS spectra recorded in purely aqueous ammonium acetate solutions [34–36] often show lower signal-to-noise ratio. Porter and Beck recently mentioned that slight solvent-induced changes in G-quadruplexes were evidenced by ion mobility spectrometry, but the solvent effect was not extensively studied [37]. It is therefore very tempting to systematically add low amounts of organic co-solvents to perform ESI-MS of nucleic acid complexes, and in our past methodological reviews we were also recommending adding 10–20% methanol "just prior to ESI-MS analysis" [10,38].

However, in a recent ESI-MS study of the self-assembly of the tetramolecular $[dTG_5T]_4$ G-quadruplex, we observed that the methanol content had a dramatic influence on the rate of G-quadruplex formation: the higher the methanol percentage, the faster the G-quadruplex assembly [39]. This prompted us to systematically check before publishing results obtained in 20% methanol that similar results were also obtained with 100% aqueous solution. Most often the results agree and the spectra obtained with organic co-solvent show only high signal-to-noise ratio, but sometimes the results are not equivalent, as strikingly demonstrated below.

Here we studied the effect of common electrospray co-solvents like methanol (MeOH), ethanol (EtOH), isopropanol (iPrOH) or acetonitrile (ACN) on the dimeric G-quadruplex formation by a 12-mer. At this point, we cannot conclude that we have a G-quadruplex structure from the sole fact that we detect a dimer. Further evidence that we are indeed in the presence of G-quadruplex structures come from ion mobility spectrometry experiments (see Section 5), from the ammonium ion preservation (see Section 6) and from correlations with other solution-phase methods. The telomeric sequence $(TAGGGT)_2$ does not form significant amounts of dimer when annealed at 5 μM strand concentration in purely aqueous 100 mM NH_4OAc. A dimer forms however when co-solvents are added to this solution, as revealed by the electrospray mass spectra (Fig. 2). The amount of dimer increases with the percentage of organic co-solvent (see Fig. 2 from A to D for EtOH). The spectrum obtained in purely aqueous solution is shown in Fig. 1E for comparison. The other co-solvents, at 60% volume percentage (Fig. 2F (for MeOH), G (for iPrOH), H (for ACN)), also favour the dimer formation. In all cases, the mass-to-charge ratio of the peaks corresponding to the dimer indicate the preferential preservation of two ammonium ions, presumably the two ions trapped in between the three G-quartets. Ammonium ion preservation will be further discussed in Section 6.

Very similar monomer/dimer spectral intensity ratios were obtained after days of reaction or immediately after annealing, showing that the effect of co-solvent is not only a kinetic effect, but also a thermodynamic effect. Structural transitions are also observed within the population of dimer, depending on the solvent and on the reaction time, as will be discussed in detail in Section 5. To conclude the present section, we emphasise that the addition of co-solvents to the electrospray samples prior to analysis should be given greater attention than in the past, now that several studies in solution documented that co-solvents can dramatically affect G-quadruplex structure and self-assembly state [17–21,39]. Addition of co-solvents, actually dehydration [17,18], favours G-quadruplex structures. Therefore, the co-solvents not only increase all ESI-MS signals thanks to better droplet desolvation, but they also increase the G-quadruplex signals simply because more are formed in solution.

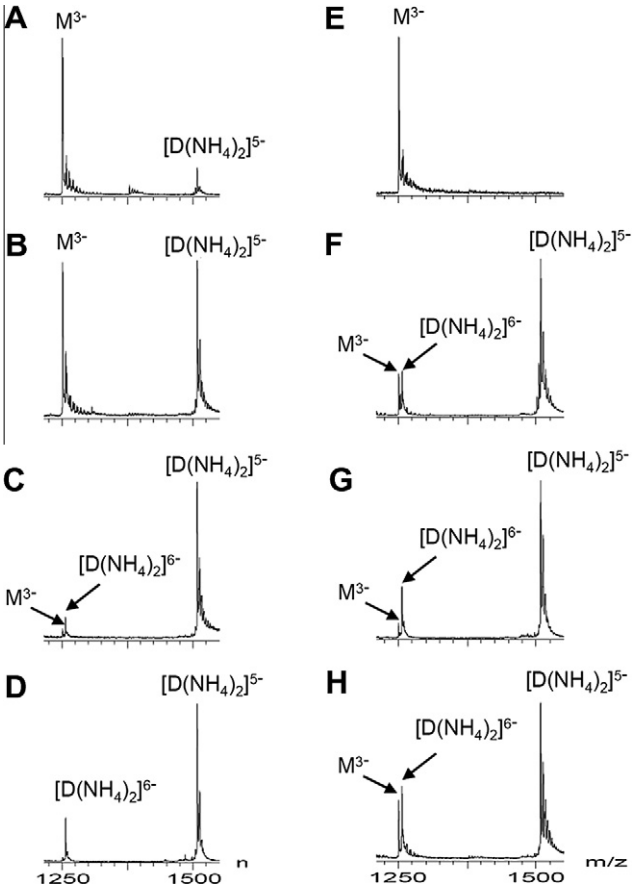

Fig. 2. Electrospray mass spectra of 5 μM telomeric sequence dTAGGGTTAGGGT recorded 1 day at room temperature after preparation in (A) 20/80 (v:v) EtOH/aqueous NH_4OAc 100 mM, (B) 40/60 (v:v) EtOH/aqueous NH_4OAc 100 mM, (C) 60/40 (v:v) EtOH/aqueous NH_4OAc 100 mM, (D) 80/20 (v:v) EtOH/100 mM aqueous NH_4OAc, (E) 100% aqueous NH_4OAc 100 mM, (F) 60/40 (v:v) MeOH/aqueous NH_4OAc 100 mM, (G) 60/40 (v:v) iPrOH/aqueous NH_4OAc 100 mM, (H) 60/40 (v:v) ACN/aqueous NH_4OAc 100 mM. M stands for the monomer, D stands for the dimer, which is observed predominantly with two ammonium ions preserved.

4. Quantitative mass spectrometry: determination of absolute concentrations of monomer and dimer from relative peak intensities

The factor relating the peak intensity of a compound to its concentration is called the response factor [40–46]. In order to determine the absolute concentrations of monomer and dimer from their relative intensities, we therefore need to determine the relative response of the monomer and the dimer. To this aim, we use the internal standard method described in more detail elsewhere [46]. For all nucleic acid response factor determinations, we use a short polythymine oligonucleotide, here dT_6 at 5 μM concentration, as internal standard. To determine the monomer and dimer

relative response with respect to this internal standard, we need a range of conditions where their relative abundances vary and where the total strand concentration (and therefore the mass balance equation) is known. The ideal situation is therefore to follow the dimer and monomer signals with respect to the internal standard in a kinetics experiment: the sample is identical throughout the experiment, except that the monomer is the most abundant at the beginning and the dimer is most abundant at the end of the recording.

In 100 mM ammonium acetate, the 12-mer sequence d(TAGGGT)$_2$ is mainly present as a monomer. The dimer formation can be triggered either by adding the co-solvent, or by adding the ammonium acetate. Both types of experiments were performed, and the relative intensity of dimer formed at the end point was the same, but transient temperature variations of the solution upon water-co-solvent mixing are detrimental to accurate kinetics studies. All kinetics experiments shown here and used to extract rate constants were therefore triggered by ammonium acetate addition. This procedure should be preferred to avoid large temperature changes of the solution shortly after solvent mixing, because the temperature of the solution might affect electrospray response. The relative response factors of the dimer compared with the single strand were determined following a previously described procedure, except that here the additional ion mobility separation further helps to extract the signals of individual species. This step is therefore described in detail below.

The peak areas of each species was extracted as a function of the "retention time" (here the reaction time) using Driftscope 2.0, as illustrated in Fig. 3. The 2D-graph in panel A represents the ion abundance (darkness) as a function of the mass-to-charge (m/z) ratio on the x-axis and the drift time in the ion mobility cell on the y-axis. The projection on the x-axis is the mass spectrum (top of panel A). Driftscope software allows to extract ion signal of a portion of the 2D plot as a function of the "retention time" (here, equal to the reaction time). For example, panel B shows the signal of the internal standard, which is constant over the reaction time. Ion mobility separation is particularly useful to distinguish species that overlap in mass/charge ratio, such as the $[monomer]^{3-}$ from the $[dimer]^{6-}$ (rectangles C and D, respectively) and allows to extract the different signals, even if one of the species is less abundant. The total dimer and monomer signals as a function of reaction time are obtained by additioning all their respective populations.

The response factors were then determined as described previously [46], by solving the matrix expressing the mass balance equation ([M] + 2[D] = 5 μM) at each time point. We determined the ratio between the response of the dimer (sum of peak areas of charge states 6-, 5- and 4-) and the response the single strand (sum of peak areas of charge states 4- and 3-), for the sequence d(TAGGGT)$_2$ discussed in detail here, as well as for the derivative sequences d(TTAGGG)$_2$, d(AGGGTT)$_2$ and d(GGATTT)$_2$ (not shown). We found that the dimer/monomer response ratio was equal to 1.3 ± 0.4 for all sequences, co-solvents, and relative volume percentages. Consequently, the relative response is not very sensitive to the antiparallel/parallel structure (see below) of the G-quadruplex. It also demonstrates that the increased sensitivity when a co-solvent is added to water is due to an increase of signal for both the monomer and dimer, by a similar factor. The response factors above were calculated for the peak *areas* of *all* charge states. We therefore highlight again that, although we find responses of similar order of magnitude for the monomer and the dimer, relative peak heights of the most intense charge states (readily evaluated at the naked eye in the mass spectra) do not necessarily reflect relative abundances in solution. The concentrations of monomer and dimer, respectively, were recalculated using the response factors and are shown in Fig. 3E.

5. Parallel G-quadruplex structures are preserved in the gas phase: comparison between circular dichroism spectroscopy and ion mobility spectrometry

The CD spectrum provides information about the strand orientation (parallel, antiparallel, or hybrid) of G-quadruplexes, because the stacking of consecutive G-quartets is related to the strand orientation and to the syn/anti orientation about glycosilic bonds [47]. Purely parallel-stranded structures exhibit a positive CD peak around 260 nm and a negative peak around 240 nm, whereas purely antiparallel-stranded structures exhibit a positive peak around 295 nm and a negative peak around 260 nm. Fig. 4A and B show the circular dichroism spectra of the structures formed by the sequence d(TAGGGT)$_2$ after 5 min, 1 h, or 1 day at room temperature in ethanol (4A) or methanol (4B). Clearly, a mixture of parallel and antiparallel G-quadruplexes is formed first, and the mixture slowly converts to a parallel structure at longer times. Also, the conversion to a parallel structure in solution is much faster in ethanol than in methanol. Results obtained in acetonitrile and isopropanol (not shown) resemble those obtained in ethanol.

The different folding of this sequence in different solvents constitutes an ideal case to validate whether ion mobility spectrometry can be used to obtain structural information. Mass spectrometry and ion mobility spectrometry should ideally provide snapshots of the solution-phase conformations. The condition is that each structure is preserved in the gas phase. The ion mobility cell separates ions according to their mobility, i.e. the ratio between their velocity in a bath gas and the electric field causing that movement. The ion mobility depends on ion properties such as its charge (the mobility increases, and thereby the drift time decreases when the charge z increases) and its collision cross section (the mobility decreases, and thereby the drift time increases when the collision cross section – noted CCS or Ω – increases). The collision cross section is the orientationally averaged surface of the ion that is exposed to collisions with the bath gas, and is expressed in Å^2. Antiparallel and parallel structures can therefore be differentiated by ion mobility spectrometry provided that (1) these structures have significantly different collision cross sections and that (2) the structures formed in solution are preserved by the multiply charged anions in the gas phase on the time scale of the experiment (several milliseconds).

A previous publication has predicted by theoretical calculations that the dimer of d(TTAGGG)$_2$ would have a CCS of 785 Å^2 in its antiparallel form, and a CCS of 845 Å^2 in its parallel form [14]. Our dimer of d(TAGGGT)$_2$ has the same base composition, and similar CCS values are anticipated. The distribution of CCS were determined for the dimer $[d(TAGGGT)_2]_2^{5-}$ after 5 min, 1 h and 1 day, with two different instruments: the Synapt G1 HDMS (Fig. 4C: ethanol and D: methanol) and the Synapt G2 HDMS (Fig. 4E: ethanol and F: methanol). On both instruments, we see that the contribution corresponding to a parallel G-quadruplex dimer in the gas phase (845 Å^2) increases when the abundance of the parallel structure in solution, as indicated by the CD spectra, increases. However, the contribution of the parallel G-quadruplex is much more clearly seen with the Synapt G2 instruments, thanks to its higher mobility resolution.

In summary, the mass spectra show that a dimer can form both in ethanol and in methanol (Fig. 2C and F in 60% ethanol and methanol, respectively). The ion mobility spectra (Fig. 4) reveal that the structure(s) formed in methanol tend to be less parallel than in ethanol, and these interpretations have been validated by circular dichroism experiments. The dimer structure also changes with the reaction time. In all solvents, antiparallel or mixed structures form first. The population then slowly shifts to a parallel fold, and this conversion is slower in methanol than in the other solvents. Refining the interpretation of the ion mobility peak positions and

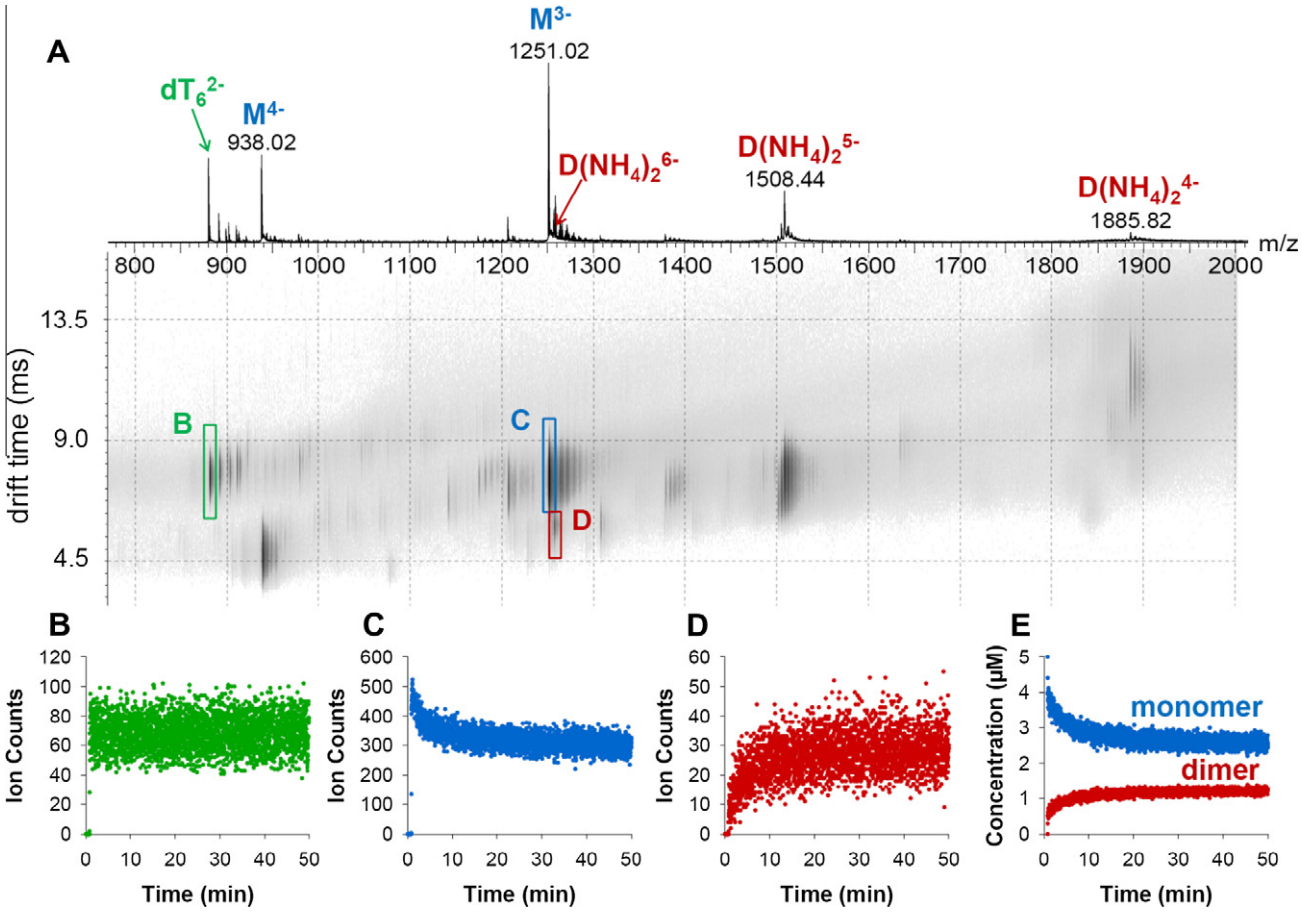

Fig. 3. Illustration of the utility of drift time separation in the ion mobility cell to distinguish single-stranded monomer (M) and G-quadruplex dimer ($D(NH_4)_2$) and extract their respective peak areas. (A) 2D graph showing the total ion abundance (darkness) as a function of the *m*/*z* and of the drift time, obtained in the kinetics experiment, from 0 to 50 min, of 5 μM $d(TAGGGT)_2$ folding in 40/60 (v:v) EtOH/100 mM aqueous ammonium acetate. Note that the mass spectral intensities differ from those of Fig. 1B because the latter were acquired after 1 day of folding. Panels (B–D) shows the extracted ion signals as a function of the reaction times of the internal standard dT_6^{2-}, the monomer M^{3-}, and the dimeric G-quadruplex $D(NH_4)_2^{6-}$, respectively. (E) Time evolution of the concentrations of monomer and dimer, recalculated using the average relative response factor found in EtOH ($R_{monomer(3- \text{ and } 4-)}/R_{dimer(4- \text{ to } 6-)} = 1.25$).

widths would however require additional modelling on the different structures potentially formed by each sequence, and is beyond the scope of the present paper. For example, two ion mobility peaks (830 $Å^2$ and 847 $Å^2$) can be distinguished for $[d(TAGGGT)_2]_2^{5-}$ dimer with the high-resolution instrument, and both arise when the population of parallel structure increases. Molecular modelling would allow proposal of structures compatible to each of these average collision cross sections, but we anticipate that further developments are needed first on the parameterization of collision cross section calculations for nucleic acids.

6. Inner ammonium ions preservation is correlated with the structure: antiparallel structures are more labile in the gas phase than parallel structures

From the ion mobility results, we concluded that the parallel structure was preserved when transferred from the solution to the gas phase, but the results for the antiparallel structure were less clear. The reason is that, in addition to a modification of the collision cross section distribution depending on the solution structures, we also see a modification of the distribution of number of preserved ammonium ions depending on the solution conditions. The insets of panels Fig. 4C–F show the ammonium ion distributions from which the CCS distributions were reconstructed. When the predominant structure in solution is a parallel quadruplex, the ammonium ion distribution becomes more biased towards two ammonium ions. Moreover, quite strikingly, the ammonium ion number distribution varies from instrument to instrument (compare in Fig. 4, C with E and D with F). In this section, we will first discuss, for those not familiar with mass spectrometry instrumentation, what makes the mass spectra appear so different although the samples are the same. Then we will discuss how ammonium ion distributions and collision cross section distributions can be interpreted in terms of structure.

Why do (G-quadruplex) mass spectra look different (in terms of ammonium ion preservation) when recorded on different instruments? The answer to this very general question (read the previous sentence without the parentheses) is that ions can acquire different amounts of internal energy [48] for different amounts of time, depending on the collisions they undergo in the instrument. Inelastic collisions indeed redistribute part of the relative translation energy into vibrational energy of the ion [49]. The relative translation energy depends on ion speed before the collision, and therefore increases when a potential (voltage) difference is increased in a region of the instrument where collisions can occur. Therefore, the distribution of internal energy acquired by the ion population depends both on the hardware configuration of the instrument (pumping system, shape of metal pieces between which voltage differences are applied), and on the experimental parameters (values of voltages and pressures, nature of the collision gas) [50]. When the internal energy distribution of an ion population

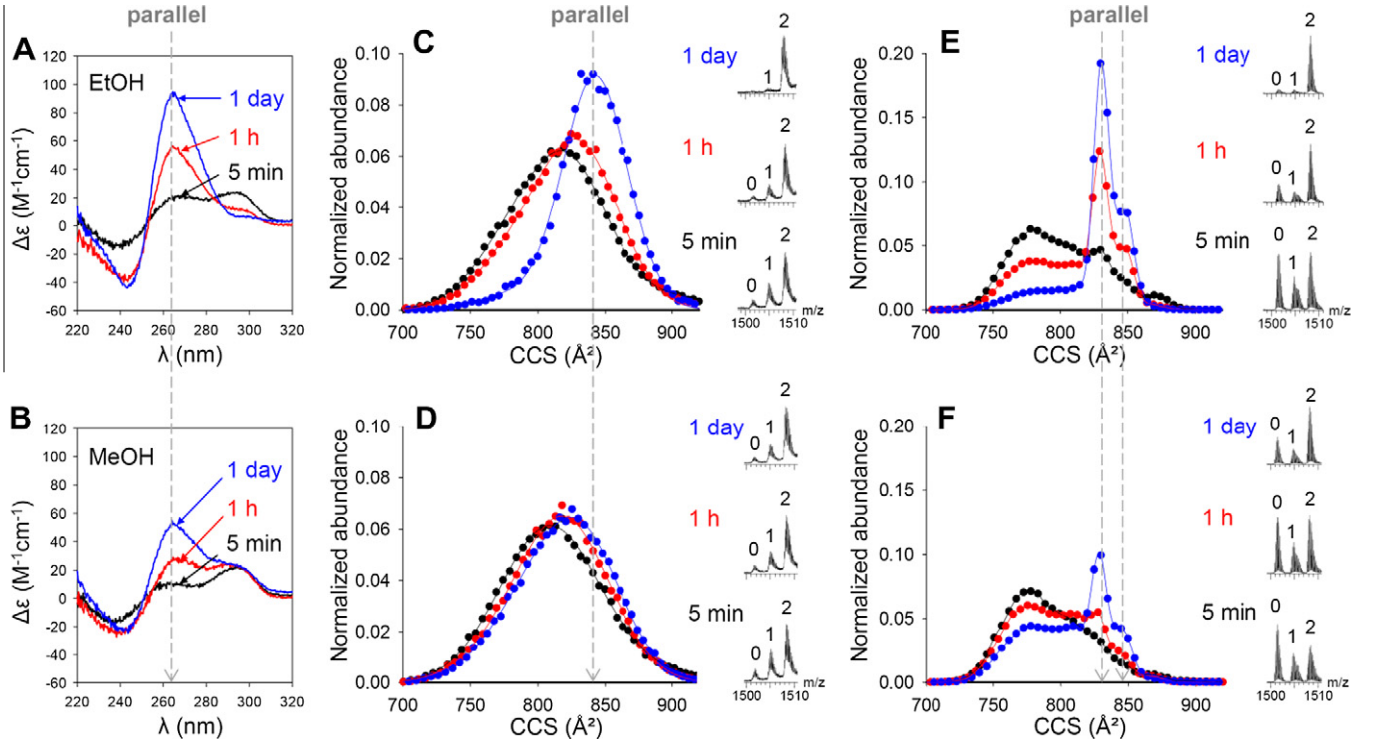

Fig. 4. Comparison between the dimers formed in ethanol and methanol, as a function of folding time. (A and B) Circular dichroism spectra in (A) EtOH and (B) MeOH recorded 5 min (black), 1 h (red) and 24 h (pink) after preparation in 60/40 (v:v) co-solvent/aqueous NH_4OAc 100 mM. The arrows indicate the peaks attributable to parallel (para) and antiparallel (anti) strand arrangement, respectively. (C and D) Collision cross section population obtained with the Synapt G1 HDMS instrument for the $[Dimer]^{5-}$ (total from 0 to 2 ammonium ions preserved) sprayed from the same sample solutions; (C) EtOH; (D) MeOH. The CCS distributions were normalised by their total area. The insets show the distribution of number of preserved ammonium ions in the corresponding mass spectra. (E and F) Same as C and D but obtained with the higher-resolution Synapt G2 HDMS instrument.

increases, in other words the ions get more vibrational energy and start exploring more conformations on their energy landscape, starting with free rotations at low internal energy and more and more energy-costly changes as the energy increases. Ultimately, this can lead to conformational changes, chemical reactions such as proton transfer, and irreversible dissociation [4]. The consequence is that, because of internal energy differences, not only mass spectra, but also ion mobility distributions can look different when recorded on different instruments.

A change in the ion mobility distribution when the internal energy is increased indicates an isomerization in the gas phase involving conformations of sufficiently different collision cross sections. "Ammonium ion" loss when the internal energy is increased actually indicates a proton transfer from the ammonium ion to the DNA strand followed by the irreversible loss of NH_3. Both are consequences of internal energy increase upon voltage increase. Let us now examine whether ammonium ion loss and conformational changes are linked. The dimer $[d(TAGGGT)_2]_2$ provides an excellent model system, because depending on the solvent, either a purely parallel structure (in ethanol) or a mixture of parallel and antiparallel structures (in methanol) can be formed in solution after 1 day. Fig. 5 shows the 2D mass/mobility plots of the $[dimer]^{5-}$ sprayed from methanol (Fig. 5A–D) or from ethanol (Fig. 5E–H), when the IMS bias voltage of the Synapt G1 HDMS instrument is increased. The bias is the voltage difference accelerating the ions towards the ion mobility cell. A non-zero voltage is needed for the ions to enter the mobility cell, which is at higher pressure than the zone upstream. However, the higher the bias voltage, the more energetic the collisions occurring just before the entrance in the mobility cell.

The bidimensional separation allows correlation of ammonium ion loss (differentiated based on the *m/z*; *x*-axis) upon internal energy increase with conformational changes, indicated by changes in the collision cross section (CCS; *y*-axis). At low voltage (low internal energy, Fig. 5A and E), the ion structures are the least likely to have been disturbed. The two ammonium ions are indeed mostly preserved (both from the methanol and the ethanol sample), and the collision cross section distributions indicate a purely parallel structure preserved in ethanol (Fig. 5E) and a mixture of parallel and antiparallel from methanol (Fig. 5A). The latter interpretation is validated by both the fairly good agreement with calculated collision cross sections of parallel and antiparallel structures (845 $Å^2$ and 785 $Å^2$, respectively), and the circular dichroism data of the respective starting solutions (blue spectra in Fig. 4A and B for ethanol and methanol, respectively). When the internal energy is increased, ammonium loss is observed mostly in the case of the methanol sample (in Fig. 5, bias voltage increased from A to D), and much less in the case of the ethanol sample (in Fig. 5, bias voltage increased from E to H). The collision cross section analysis of each mass spectral peak reveals that, independently of the starting solvent, the parallel structure is preserved in the gas phase at high voltage with two ammonium ions. In the methanol sample, the fraction that has lost ammonium ions at moderate voltage had come mostly from the antiparallel structure. At 15 V (Fig. 5B), an intermediate is seen, with 1 ammonium ion and a presumably antiparallel structure. In all cases, the species with zero ammonium ions have always an even smaller collision cross section, presumably indicating a collapse into a globular structure following the ammonia loss.

Now that the influence of the internal energy on the ammonium ion preservation and structure preservation has been explained in detail, we can understand the origin of the differences obtained between the Synapt G1 HDMS instrument (Fig. 4C and D, with a bias

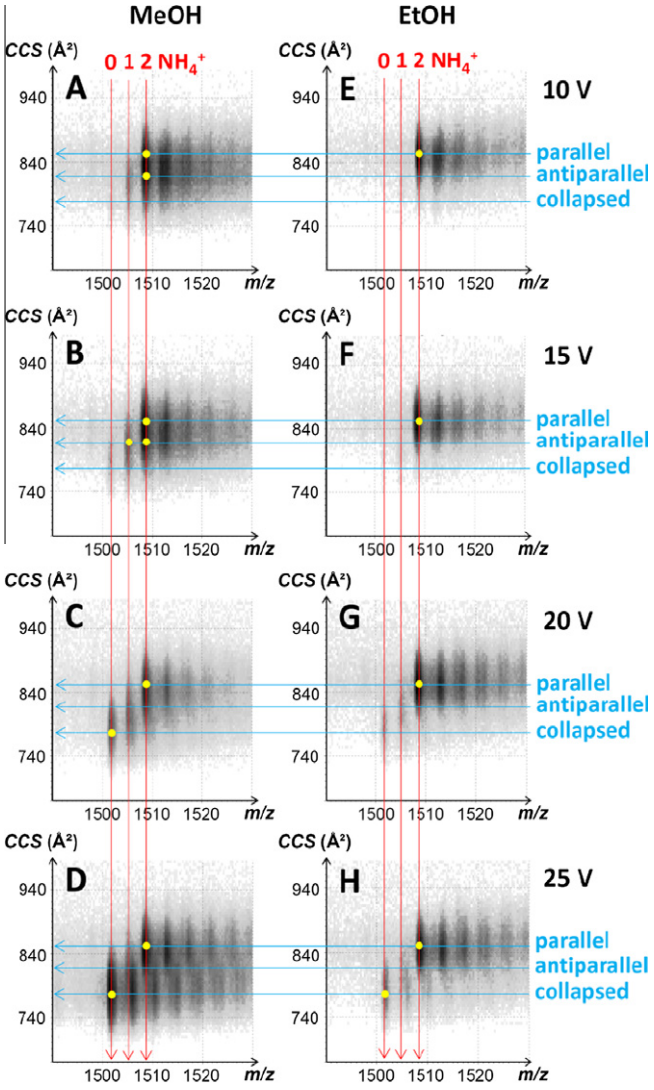

Fig. 5. Influence of the bias voltage of the Synapt G1 HDMS instrument (from 10 V at the top to 25 V at the bottom) on the ammonium ion distribution and on the collision cross section of the dimers formed (A–D) after 1 day in 60% methanol or (E–H) after 1 day in 60% ethanol. The guidelines in red indicate the masses of the dimer with 2, 1 or zero ammonium ions preserved, and the guidelines in blue indicate the interpretation of collision cross sections in terms of dimer structure (see main text).

voltage = 15 V) and the Synapt G2 HDMS instrument (Fig. 4C and D, with a bias voltage = 35 V). The Synapt G2 instrument imparts more internal energy to the ions that the Synapt G1. This is due to the higher pressure in the IMS cell that requires using higher bias voltages to ensure ion transfer. The bias voltage of 35 V is the minimum value to obtain decently intense ion signals. Fig. 6 shows the 2D plots obtained with the Synapt G2, to be compared with those obtained with the Synapt G1 on the same samples (Fig. 5). The minimum internal energy imparted to the $[dimer]^{5-}$ in the Synapt G2 (Fig. 6) is equivalent to that imparted at approximately 25 V on the Synapt G1 (Fig. 5D and H). Hence, the higher mobility resolution attainable in the Synapt G2 HDMS comes at the price of more internal energy imparted to the ions before the analysis, which might disrupt the most fragile structures (here the antiparallel structure). This highlights the importance of instrument choice and of carrying out voltage-dependent experiments to grasp internal energy effects on the mass spectra and the ion mobility spectra.

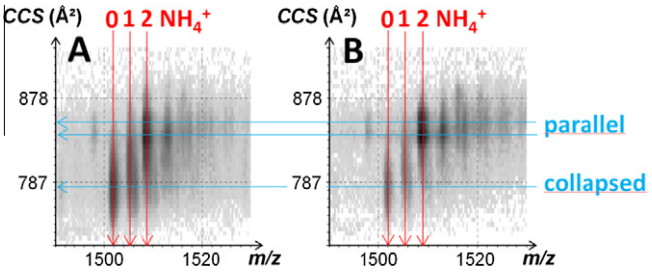

Fig. 6. 2D plot of ammonium ion distribution and collision cross section of the dimers observed on the Synapt G2 HDMS spectrometer (bias = 35 V), formed after 1 day in (A) 60% methanol or (B) 60% ethanol.

In summary:

(1) Only the structures with ammonium ions preserved between their G-quartets are likely to have structural elements preserved from the initial solution.
(2) Ammonia loss is closely linked to, and most likely just precedes the loss of G-quadruplex structure upon internal energy increase. Importantly, because ammonia loss is irreversible, no interconversion from one G-quadruplex structure to another G-quadruplex structure can occur in the gas phase. However, both structures can be disrupted upon ammonia loss.
(3) Parallel structures in the gas phase are more resistant to ammonia loss than antiparallel structures. Although this was suggested in previous works by comparison between different sequences [13], this is now shown unambiguously with two structures formed from the same sequence. Ammonia loss requires proton transfer to the DNA, and the probability of ammonia loss depends on the accessibility proton exchange partners close to the terminal G-quartets. Therefore, faster ammonia loss for antiparallel structures may be due to the presence of more accessible lateral or diagonal loops, and/or to an intrinsically higher degree of conformational fluctuations of antiparallel structures compared to parallel structures in the gas phase.
(4) Ammonium ion preservation depends not only on the structure, but also on the instrument and on experimental parameters such as voltages. Therefore, before concluding on G-quadruplex structure based solely on the preservation of inner ammonium ions, a voltage-dependent analysis must be performed, and ideally ion mobility spectrometry should be used to interpret the results. Conversely, moderately activating conditions can be exploited to intentionally disrupt some structures while preserving others. For example, the ammonium ion distribution obtained with the Synapt G2 instrumental conditions (Fig. 4E and F) actually easily allows to discriminate the parallel dimer (2 ammonium ions preserved) from the antiparallel one (0 or 1 ammonium ions).

7. Conclusions and outlook

In conclusion, the results above demonstrate the strong correlation between ammonium ion preservation and structure preservation in the gas phase. Parallel G-quadruplex structures are generally found to be more stable in the gas phase than antiparallel structures, both in terms of ammonium ion preservation and tridimensional structure preservation as measured by ion mobility spectrometry. However, antiparallel structures are more labile in the gas phase, and one cannot straightforwardly conclude from the absence of preserved ammonium in the gas phase that no G-quadruplex structure was present in solution. Future work will

specifically address the question of antiparallel structure preservation.

The last two sections of the manuscript explained how to interpret bidimensional mass spectrometry/ion mobility spectrometry experiments in terms of structure. The present mixture was fairly simple (one strand forming a monomer and a dimer, plus another strand as internal standard), and only a single peak, the [dimer]$^{5-}$ of the DNA sequence d(TAGGGT)$_2$, was analysed in detail. Similar analysis can in principle be carried out for each peak resolvable in a mass spectrum. The power of mass spectrometry compared to other spectroscopic techniques in solution clearly lies in the possibility of carrying out such structural studies on each species present in a complex mixture, and we hope we have provided some guidelines for mass spectrometry and ion mobility data interpretation.

We have shown that the addition of co-solvents in ammonium acetate can influence G-quadruplex formation and structural transitions. The main result is that electrospray-compatible organic co-solvents can favour the formation of G-quadruplexes, and that the structure obtained depends both on the nature of the solvent and on the reaction time. The temporal evolution of the abundance of dimer of each structure has been studied in detail by ESI-IMS-MS for different sequences and solvents, and the results of this thermodynamic and kinetic analysis as a function of the water activity will be published elsewhere. Organic co-solvent addition is an easy way to generate different folds in solution and make them amenable to mass spectrometry and ion mobility analysis. Future work will also be devoted to study the ligand binding preference for antiparallel versus parallel structures, using ESI-IMS-MS.

Acknowledgements

This work was supported by the Fonds de la Recherche Scientifique-FNRS (research associate position, and FRFC Grant 2.4528.11), the EU COST action (MP0802, STSM 9145 to RF), and the Spanish Ministry of Science (CTQ-2010-20541). The authors acknowledge the GIGA-Proteomics platform for access to the instruments, Hisae Tateishi-Karimata and Daisuke Miyoshi for useful comments on a preliminary version of this manuscript, and Ramon Eritja for proofreading the manuscript.

References

[1] J.A. Loo, Mass Spectrom. Rev. 16 (1997) 1–23.
[2] R.D. Smith, J.E. Bruce, Q. Wu, Q.P. Lei, Chem. Soc. Rev. 26 (1997) 191–202.
[3] A.J.R. Heck, R.H.H. Van Den Heuvel, Mass Spectrom. Rev. 23 (2004) 368–389.
[4] K. Breuker, F.W. McLafferty, Proc. Natl. Acad. Sci. USA 105 (2008) 18145–18152.
[5] M. Rueda, F.J. Luque, M. Orozco, J. Am. Chem. Soc. 128 (2006) 3608–3619.
[6] J. Sponer, N. Spackova, Methods 43 (2007) 278–290.
[7] E. Fadrna, N. Spackova, R. Stefl, J. Koca, T.E. Cheatham III, J. Sponer, Biophys. J. 87 (2004) 227–242.
[8] G. Yuan, Q. Zhang, J. Zhou, H. Li, Mass Spectrom. Rev. 30 (2011) 1121–1142.
[9] J.S. Brodbelt, Annu. Rev. Anal. Chem. 3 (2010) 67–87.
[10] F. Rosu, E. De Pauw, V. Gabelica, Biochimie 90 (2008) 1074–1087.
[11] A.-T. Phan, D.J. Patel, J. Am. Chem. Soc. 125 (2003) 15021–15027.
[12] G.N. Parkinson, M.P.H. Lee, S. Neidle, Nature 417 (2002) 876–880.
[13] G.W. Collie, G.N. Parkinson, S. Neidle, F. Rosu, E. De Pauw, V. Gabelica, J. Am. Chem. Soc. 132 (2010) 9328–9334.
[14] E.S. Baker, S.L. Bernstein, V. Gabelica, E. De Pauw, M.T. Bowers, Int. J. Mass Spectrom. 253 (2006) 225–237.
[15] D. Miyoshi, H. Karimata, N. Sugimoto, Angew. Chem. Int. Ed. 44 (2005) 3740–3744.
[16] Y. Xue, Z.Y. Kan, Q. Wang, Y. Yao, J. Liu, Y.H. Hao, Z. Tan, J. Am. Chem. Soc. 129 (2007) 11185–11191.
[17] D. Miyoshi, K. Nakamura, H. Tateishi-Karimata, T. Ohmichi, N. Sugimoto, J. Am. Chem. Soc. 131 (2009) 3522–3531.
[18] D. Miyoshi, H. Karimata, N. Sugimoto, J. Am. Chem. Soc. 128 (2006) 7957–7963.
[19] M. Vorlickova, K. Bednarova, J. Kypr, Biopolymers 82 (2006) 253–260.
[20] B. Heddi, A.T. Phan, J. Am. Chem. Soc. 133 (2011) 9824–9833.
[21] M.C. Miller, R. Buscaglia, J.B. Chaires, A.N. Lane, J.O. Trent, Hydration is a major determinant of the G-quadruplex stability and conformation of the human telomere 3′ sequence of d(AG(3)(TTAG(3))(3)), J. Am. Chem. Soc. 132 (2010) 17105–17107.
[22] F. Rosu, V. Gabelica, L. Joly, G. Gregoire, E. De Pauw, Phys. Chem. Chem. Phys. 12 (2010) 13448–13454.
[23] V. Gabelica, E. De Pauw, F. Rosu, J. Mass Spectrom. 34 (1999) 1328–1337.
[24] K.B. Turner, S.A. Monti, D. Fabris, J. Am. Chem. Soc. 130 (2008) 13353–13363.
[25] S.E. Evans, M.A. Mendez, K.B. Turner, L.R. Keating, R.T. Grimes, S. Melchoir, V.A. Szalai, J. Biol. Inorg. Chem. 12 (2007) 1235–1249.
[26] W.M. David, J. Brodbelt, S.M. Kerwin, P.W. Thomas, Anal. Chem. 74 (2002) 2029–2033.
[27] Y. Liu, B. Zheng, X. Xu, G. Yuan, Rapid Commun. Mass Spectrom. 24 (2010) 3072–3075.
[28] H. Li, G. Yuan, D. Du, J. Am. Soc. Mass Spectrom. 19 (2008) 550–559.
[29] M. Vairamani, M.L. Gross, J. Am. Chem. Soc. 125 (2003) 42–43.
[30] S.E. Pierce, C.L. Sherman, J. Jayawickramarajah, C.M. Lawrence, J.L. Sessler, J.S. Brodbelt, Anal. Chim. Acta 627 (2008) 129–135.
[31] L.P. Bai, M. Hagihara, Z.H. Jiang, K. Nakatani, Chem. Bio. Chem. 9 (2008) 2583–2587.
[32] B. Datta, M.E. Bier, S. Roy, B. Armitage, J. Am. Chem. Soc. 127 (2005) 4199–4207.
[33] J. Gidden, E.S. Baker, A. Ferzoco, M.T. Bowers, Int. J. Mass Spectrom. 240 (2004) 183–193.
[34] Y. Krishnan-Ghosh, D.S. Liu, S. Balasubramanian, J. Am. Chem. Soc. 126 (2004) 11009–11016.
[35] K.C. Gornall, S. Samosorn, B. Tanwirat, A. Suksamrarn, J.B. Bremner, M.J. Kelso, J.L. Beck, Chem. Commun. 46 (2010) 6602–6604.
[36] W. Li, M. Zhang, J.L. Zhang, H.Q. Li, X.C. Zhang, Q. Sun, C.M. Qiu, FEBS Lett. 580 (2006) 4905–4910.
[37] K.C. Porter, J.L. Beck, Int. J. Mass Spectrom. 304 (2011) 195–203.
[38] V. Gabelica, Methods Mol. Biol. 613 (2010) 89–101.
[39] F. Rosu, V. Gabelica, H. Poncelet, E. De Pauw, Nucleic Acids Res. 38 (2010) 5217–5225.
[40] N.B. Cech, C.G. Enke, Mass Spectrom. Rev. 20 (2001) 362–387.
[41] V. Gabelica, N. Galic, F. Rosu, C. Houssier, E. De Pauw, J. Mass Spectrom. 38 (2003) 491–501.
[42] M.C. Kuprowski, L. Konermann, Anal. Chem. 79 (2007) 2499–2506.
[43] S. Mathur, M. Badertscher, M. Scott, R. Zenobi, Phys. Chem. Chem. Phys. 9 (2007) 6187–6198.
[44] J.M. Wilcox, D.L. Rempel, M.L. Gross, Anal. Chem. 80 (2008) 2365–2371.
[45] M.C. Jecklin, D. Touboul, C. Bovet, A. Wortmann, R. Zenobi, J. Am. Soc. Mass Spectrom. 19 (2008) 332–343.
[46] V. Gabelica, F. Rosu, E. De Pauw, Anal. Chem. 81 (2009) 6708–6715.
[47] S. Masiero, R. Trotta, S. Pieraccini, T.S. De, R. Perone, A. Randazzo, G.P. Spada, Org. Biomol. Chem. 8 (2010) 2683–2692.
[48] K. Vékey, J. Mass Spectrom. 31 (1996) 445–463.
[49] S.A. McLuckey, J. Am. Soc. Mass Spectrom. 3 (1991) 599–614.
[50] V. Gabelica, E. De Pauw, Mass Spectrom. Rev. 24 (2005) 566–587.

3

ESTUDIS ESTRUCTURALS I D'ESTABILITAT DEL QUÀDRUPLEX DE GUANINA PRESENT EN ELS TELÒMERS HUMANS. INTERACCIÓ D'AQUESTS QUÀDRUPLEX AMB 9-AMINO ACRIDINDES EN AVALUACIÓ PRECLÍNICA

ESTUDIS ESTRUCTURALS I D'ESTABILITAT DEL QUÀDRUPLEX DE GUANINA PRESENT EN ELS TELÒMERS HUMANS. INTERACCIÓ D'AQUESTS QUÀDRUPLEX AMB 9-AMINO ACRIDINES EN AVALUACIÓ PRECLÍNICA

Structural and stability of human telomèric G-quadruplex with preclinical 9-amino acridines

Rubén Ferreira[a], Roberto Artali[b], Adam Benoit[c], Raimundo Gargallo[d], Ramon Eritja[a], David M. Ferguson[c], Yuk Y. Sham[e,*], Stefania Mazzini[f,*]

Biochimica et Biophysica Acta, submitted

[a] *Institute for Research in Biomedicine, IQAC-CSIC, CIBER-BBN Networking Center on Bioengineering, Biomaterials and Nanomedicine, Baldiri Reixac 10, E-08028 Barcelona, Spain.*
[b] *Scientia Advice di Roberto Artali, 20851 Lissone (MB), Italy.*
[c] *Department of Medicinal Chemistry, University of Minnesota, Minneapolis, MN 55414, USA*
[d] *Department of Analytical Chemistry, University of Barcelona, Diagonal 645, E-08028 Barcelona, Spain*
[e] *Center for Drug Design, Academic Health Center, University of Minnesota, 516 Delaware St. SE, MMC 204, Minneapolis, MN 55455, USA*
[f] *Department of Agro-Food Molecular Sciences (DISMA), University of Milan, Via Celoria 2, 20133 Milan, Italy; E-Mail: stefania.mazzini@unimi.it*

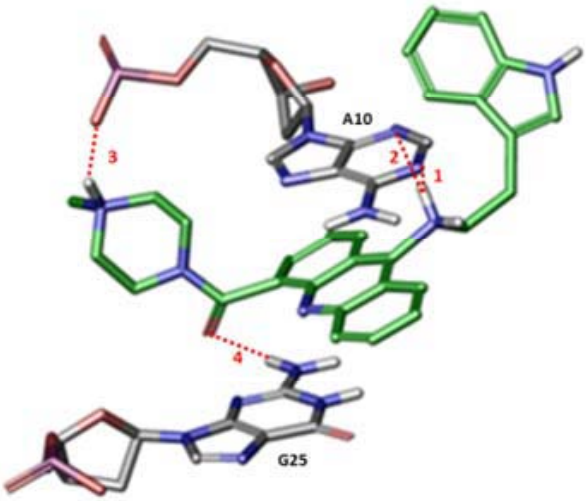

Resum

Les seqüències riques en guanines poden formar estructures no canòniques de quatre cadenes conegudes com a G-quàdruplex. En els últims anys s'han considerat com atractives dianes terapèutiques pel tractament del càncer. Obtenir l'estructura tridimensional del complex format pel G-quàdruplex i les 9-amino acridines i les interaccions específiques que es produeixen en la seva unió selectiva és la clau per entendre el seu mecanisme d'acció.

S'han utilitzat assajos de valoració de fluorescència, diàlisis competitiva i estudis de RMN per estudiar la unió d'aquestes acridines al DNA. S'ha generat un model del complex format amb el G-quàdruplex telomèric humà coherent amb les dades de RMN i posteriorment s'ha analitzat l'estabilitat del model per dinàmica molecular i càlculs energètics.

S'ha observat que les 9-amino acridines s'uneixen selectivament a les seqüències formadores de G-quàdruplex que es troben en regions promotores d'oncogens i en seqüències telomèriques. Aquests compostos s'uneixen entre les tètrades d'A i G, mitjançant interacions π-π i varis enllaços d'hidrogen. S'ha estudiat les interaccions específiques entre les diferents parts que formen els lligands i el DNA i s'ha observat que tenen un paper fonamental en l'estabilitat global del G-quàdruplex induïda pels lligands.

Els resultats obtinguts permeten entendre els paràmetres que influexen sobre les interaccions entre un lligand i un G-quàdruplex, i servirà com a eina pel disseny d'una manera racional de nous compostos.

Structure and stability of human telomeric G-quadruplex with preclinical 9-amino acridines

Rubén Ferreira[a], Roberto Artali[b], Adam Benoit[c], Raimundo Gargallo[d], Ramon Eritja[a], David M. Ferguson[c], Yuk Y. Sham[e,*], Stefania Mazzini[f,*]

[a] Institute for Research in Biomedicine, IQAC-CSIC, CIBER-BBN Networking Center on Bioengineering, Biomaterials and Nanomedicine, Baldiri Reixac 10, E-08028 Barcelona, Spain.

[b] Scientia Advice di Roberto Artali, 20851 Lissone (MB), Italy.

[c] Department of Medicinal Chemistry, University of Minnesota, Minneapolis, MN 55414, USA

[d] Department of Analytical Chemistry, University of Barcelona, Diagonal 645, E-08028 Barcelona, Spain

[e] Center for Drug Design, Academic Health Center, University of Minnesota, 516 Delaware St. SE, MMC 204, Minneapolis, MN 55455, USA

[f] Department of Food, Environmental and Nutritional Sciences (DeFENS), Department of Organic Chemistry, via Celoria 2, 20133 Milano, Italy E-Mail: stefania.mazzini@unimi.it

ABSTRACT

Background: G-quadruplexes are higher-order DNA structures formed from guanine-rich sequences, and have been identified as attractive anticancer drug targets. Elucidating the three-dimensional structure of G-quadruplex with 9-amino acridines and the specific interactions involved in binding selectivity are the key to understanding their mechanism of action.

Methods: Fluorescence titration assays, competitive dialysis and NMR studies have been used to study the binding specificity of 9-amino acridines to DNA. Structural models of the complexes with the telomeric DNA G-quadruplex based on NMR measurements were developed and further examined by molecular dynamics simulations and free energy calculations.

Results and conclusions: Selective binding of 9-amino acridines for G-quadruplex sequences that are found on the promoter regions of oncogenes and the human telomere sequences were observed. These compounds bind between A and G-tetrads, involving significant π-π interactions and several strong hydrogen bonds. The specific interactions between different moieties of the 9-amino acridines to the DNA were examined and shown to play a significant role in governing the overall stabilities of DNA G-quadruplex complexes. Both 9-amino acridines, with similar binding affinities to the G-quadruplex, were shown to induce different level of structural stabilization through intercalation. This unique property of altering structural stability is likely a contributing factor for affecting telomerase function [1, 2] and, subsequently, the observed differences in the anticancer activities between the two 9-amino acridines [2].

General significance: 9-amino acridines bind selectively to G-quadruplex by end-stacking and enhance their overall structural stabilities. These findings will assist in understanding the parameters influencing the G-quadruplex – ligand interaction and will serve as a platform for rational drug design.

Keywords: 9-amino acridine, G-quadruplex, NMR, Molecular Dynamic simulation, DNA-binding drugs, oligonucleotides, anticancer.

1. Introduction

In the last years, tricyclic acridine-containing compounds have been investigated as small molecule chemotherapeutic anticancer agents [3, 4]. Studies on the mechanism of action of acridine drugs have shown these compounds are potent inhibitors of topoisomerase and telomerase function in replicating cells, which ultimately leads to apoptosis and cell death.

Topoisomerase alters DNA topology through the decatenation and relaxation of the supercoiled chromosomal DNA [5]. By unwinding the double-stranded DNA, this essential enzyme enables normal cellular DNA replication and transcription [5]. DNA topoisomerases exist in various eukaryotic and prokaryotic forms [6] and are classified in two large groups, namely type I and type II. Anti-cancer drugs targeting topoisomerase can also be classified as either catalytic inhibitors or "topoisomerase poisons" depending on their mechanism of action [7]. The latter can be further sub-classified into two groups: non-intercalating compounds such as etoposide, and intercalators such amsacrine and doxorubicin [8].

The telomere is a highly repetitive DNA region located at the end of a linear chromosome. Its function is to protect the terminal ends of chromosomes from being recognized as damaged DNA and allows faithful chromosome replication during the cell cycle [9, 10]. Human telomeric DNA contains tandem repeats of the sequence 5'-TTAGGG-3'. This guanine-rich strand can fold into a four-strand G-quadruplex structure involving G-tetrads, which are currently an attractive target for the development of anti-cancer drugs [11, 12].

A wide range of small molecules have been studied as G-quadruplex-binding and stabilizing ligands [13]. Most of these share common structural features, namely: (i) a planar heteroaromatic chromophore, which stacks by π-π interactions onto the G-quartet motif at the terminus of a G-quadruplex; and (ii) short alkyl chain substituents usually terminated by an amino group that is fully cationic at physiological pH. The precise nature of these substituents has been found to influence G-quadruplex affinity and selectivity [14, 15].

Ferguson and coworkers have recently described a series of 9-aminoacridine compounds that inhibit topoisomerase II activity. These compounds have been shown to be active against a variety of cancer cells in vitro and in vivo [16]. Mechanistic studies have shown these compounds bind DNA and block the formation of covalent DNA-Topo II complexes, stalling the cell cycle in the G1->S phase. This, in turn,

induces apoptosis and programmed cell death. Previous studies, however, have shown that acridine compounds are also capable of binding telomeric G-quadruplex structures with high affinity. [17, 18] This is yet another route by which compounds of this type may disrupt DNA replication in rapidly dividing cancer cells. In this study, we examine the binding affinity of several 9-amino acridines to G-quadruplex DNA using competitive dialysis and spectroscopic techniques. High field 2D-NMR experiments are also performed to provide insight to the structural interactions that stabilize the drug-DNA complex. Finally, the NOE data is applied to generate structural models for evaluation using molecular mechanics and dynamics techniques.

2. Materials and methods

2.1. Oligonucleotide synthesis

All the standard phosphoroamidites and reagents for DNA synthesis were purchased from Applied Biosystems and from Link Technologies. The synthesis of the oligonucleotides was performed at 1 µmol scale on an Applied Biosystems' DNA/RNA 3400 synthesizer by solid-phase 2-cyanoethylphosphoroamidite chemistry. The studied sequences are listed in table 1. The resulting oligonucleotides were purified by HPLC and desalted in a Sephadex (NAP-10) G25 column.

2.2. Competitive dialysis studies

A 100 µl of a 50 µM oligonucleotide in potassium phosphate buffer was introduced into a separated dialysis unit and a blank sample containing only buffer. All dialysis units were allowed to equilibrate during 24h at room temperature in a beaker containing the 1 µM solution of the appropriate acridine derivative. At the end of the dialysis experiment, the amount of ligand bound to the DNA was quantified by fluorescence after the digestion of the oligonucleotide (λ_{ex} and λ_{em} were set to 265 nm and 435 nm, respectively) [19].

2.3. NMR Spectroscopy

The NMR spectra were recorded by Bruker AV-600 spectrometer operating at a frequency of 600.10 MHz for ^{1}H and 242.94 MHz for ^{31}P nuclei, equipped with a *z*-gradient triple resonance TXI and 5mm BB probe. ^{1}H and ^{31}P spectra (broad-band ^{1}H decoupled mode) were recorded at variable temperature ranging from 5°C to 75°C. Chemical shifts (δ) were measured in ppm. ^{1}H and ^{31}P NMR spectra were referenced respectively to external DSS (2,2-dimethyl-2-silapentane-5-sulfonate sodium salt) set at 0.00 ppm and MDA (methylenedisphosphonic acid) set at 16.8 ppm. Estimated accuracy for protons is within 0.01 ppm, for phosphorous is within 0.03 ppm.

Standard homonuclear 2D-NMR experiments were performed to assign the resonances of the complexes, including DQF-COSY, TOCSY and NOESY [20, 21]. The mixing times were set at 150 ms and 300 ms for NOESY and 60 ms for TOCSY. For samples in H_2O, the excitation sculpting sequences from standard Bruker pulse program libraries were employed. Typically, 2048 x 1024 data points were acquired using TPPI and transformed to a final 4K×4K real data matrix after apodisation with a 90° and

90°-shifted sine-bell squared function in f2- and f1-domain, respectively. Baseline correction was achieved by a 5th-degree polynomial function. ^{1}H assignments for ligands were performed by using ROESY (spin lock 300ms) and TOCSY experiments. The sequential assignments in free and bound oligonucleotides were performed by applying well established procedures for the analysis of double stranded and quadruplex structures. The program Sparky [22] was used to assign the NOESY cross-peaks. The G-quadruplex Htel and duplexes ds6, ds8 and ds32 were previously assigned [23, 24]

The samples for NMR measurements were dissolved in 500 μl H_2O/D_2O (9:1) containing 25 mM KH_2PO_4, KCl 150 mM and EDTA 1 mM (pH 6.7) for the G-quadruplex Htel and containing 10 mM KH_2PO_4, KCl 70 mM and EDTA 0.2 mM (pH 7.0) for the double helix ds6, ds8, ds26 and ds24. The final concentration of the oligonucleotides was ranging between 0.2-0.7 mM. A stock solution of **1** and **2** was prepared in DMSO-d6 at the concentration of 20 mM.

NMR titration was performed by adding increasing amounts of **1** and **2** to the oligonucleotides solution at R= [Ligand]/[DNA] ratio equal to 0, 0.25, 0.5, 0.75, 1, 2 and 3 and in inverse order, by adding increasing amounts of DNA to a solution of **1** from R = 40 to R = 1.0.

2.4. Fluorescence assays

The study of the interaction equilibrium of **1** and **2** and the G-quadruplex Htel or the duplex ds6 consists of recording the fluorescence spectra of a 1 μM solution of the drug after the addition of increasing amounts of oligonucleotide (from 0 to 25 μM) in potassium phosphate buffer (185 mM NaCl, 185 mM KCl, 6mM Na_2HPO_4, 2mM NaH_2PO_4, 1mM Na_2EDTA at pH7).

The emission spectra of the resulting solutions were recorded from 300 to 500 nm at 265 nm excitation wavelength at 25C. The macroscopic binding constant corresponding to complex formation was calculated from the multivariate analysis of fluorescence data recorded in the range 300-425 nm using the hard modeling program Equispec [25].

2.5. Molecular Modeling

The model was built based on a G-quadruplex NMR structure 5'-TTAGGGT-3' HtelT, in complex with a quinacridine-based ligand (N,N'-(dibenzo[b,j][1,7]phenanthroline-2,10-diyldimethanediyl)dipropan-1-amine) (PDB code 2JWQ) [26]. After the separation of the coordinates of ligands and DNA, polar hydrogens were added with the GROMACS package [27] using the GROMOS 53a6 force field [28].The structures of **1** and **2** were refined using a systematic conformer, search followed by geometry optimization of the lowest energy structure with MOPAC (PM3 Methods, RMS gradient 0.0100) [29].

Molecular docking experiments were performed with Autodock 4.0, which uses an empirical scoring function based on the free energy of binding [30, 31]. The 9-aminoacridines (**1** and **2**) and the DNA G-quadruplex were further processed using the Autodock Tool Kit (ADT) [32]: Gasteiger-Marsili charges [33] were assigned to **1** and **2** and Cornell parameters were used for the phosphorous atoms in the DNA. Solvation parameters were added to the final docked structure using Addsol utility. Structures with less than 1.0 Å root-mean-square deviation (rmsd) were clustered together and representative model of

each cluster was selected based on the most favorable free energy of binding. Visual inspection was carried out to select the final structure with the expected mode of intercalation, minor groove binding, or others (major groove binding, interaction with phosphate groups, etc.).

In the current study, we used the pseudo-bond *ab-initio* QM/MM approach as implemented in Gaussian-03 [34]. For the QM/MM calculations, the DNA-ligand system resulting from the docking study was first partitioned into a QM subsystem and an MM subsystem. The reaction system used a smaller QM subsystem consisting of the ligand and bases within 3.5 Å, whereas the rest of the system (the MM subsystem) was treated using the AMBER force field, together with a low memory convergence algorithm. The boundary problem between the QM and MM subsystems was treated using the pseudo-bond approach. With this G-quadruplex-substrate QM/MM system, an iterative optimization procedure was applied to the QM/MM system, using B3LYP/3-21G* QM/MM calculations, leading to an optimized structure for the reactants. The convergence criterion used was set to obtain an energy gradient of $<10^{-4}$, using the twin-range cutoff method for nonbonded interactions, with a long-range cutoff of 14 Å and a short-range cutoff of 8 Å.

2.6. MD simulation

All simulations were carried out using IMPACT (New York, NY) with the OPLS2005 force field [35] and the TIP3P water model [36] at 298, 400 and 500K. Two potassium ions were manually overlayed into the central channel between the G-quartet planes in the complex models. Each DNA complex was solvated in a rectangular box with a 10 Å water buffer from the DNA. Na^+ and Cl^- counterions were added at 5 Å from the box boundary to neutralize the total charge of the system.

Each system was initialized by a 1000-step conjugate gradient energy minimization. The simulations were carried out under the periodic boundary condition using particle mesh Ewald [37]. The SHAKE method [38] was employed to restrain all hydrogen bonds. Atoms involved in NOE's bonds were restrained to their experimental value at (500 kcal/mol Å). Snapshots of the simulated trajectories were collected at 1 ps time intervals.

3. Results and discussion

3.1. Competitive dialysis studies

In order to evaluate the selectivity of the compounds for DNA structures or sequences, a competitive dialysis experiment was performed using 11 oligonucleotides representing several nucleic acid structures [39-41] We used T20 and the C-rich complementary strand of bcl-2 as model compounds for single stranded DNA sequences. As duplexes we used the self-complementary sequences *Dickerson-Drew* dodecamer and a 26 mer (ds26). A parallel and an antiparallel triplex were also selected. Finally several DNA sequences known to form G-quadruplex were selected: TG4T [42] is a tetramolecular parallel G-quadruplex, the TBA [43] is the antiparallel thrombin-binding aptamer, the HT24 [44] is the human telomerase sequence, the cmyc and bcl-2 [45] are promoter sequences of *c-myc* and *bcl-2* protooncogenes.

Competitive dialysis experiments show clear differences on the affinity of ligands to a different DNA structures (figure 1). Higher affinities are found in G-quadruplex sequences present on the promoter regions of *c-myc* and *bcl-2* oncogenes and the human telomere sequence. Ligand **2** has a clear selectivity for G-quadruplex-forming DNA sequences while compound **1** has also an affinity for duplex ds26 as show in figure 1.

3.2. NMR 9-amino acridines-DNA experiments

NMR studies were performed to confirm and elucidate the structure of the complexes formed between compounds **1** and **2** and DNA. The oligomers ds6, ds8, ds24, ds26 and Htel were used as models for double stranded DNA and G-quadruplex parallel structures respectively. ^{31}P and ^{1}H resonance experiments were performed to derive both the mode of binding and the details of the molecular structure. Assignment of the phosphorous, of the exchangeable and non-exchangeable protons for all oligonucleotides was carried out on the basis of previously reported assignments [23, 24].

The sequential assignments in free and bound oligonucleotides were performed by applying well established procedures for the analysis of double stranded and G-quadruplex structures. ^{1}H assignments for **1** and **2** in absence of DNA were performed by using ROESY, NOESY, TOCSY and COSY experiments. Complete assignments are reported in Table 2 and 3.

3.2.1. NMR 9-amino acridines and G-quadruplex experiments

Titration experiments performed with **1** and **2** on the solution of Htel show that the proton resonances of the drug become broad and move up-field with respect to the free drug, just after the addition of a small quantity, *i.e.* with *R* = [drug]/[DNA] = 0.25. Increasing the *R* value from 0.25 to 3, the shielding of the drug protons carries on and it spread over the whole drug molecule. In order to better identify the drug protons in the complex, the inverse titration experiment was performed, by adding increasing amounts of DNA, from R = 20 to 2.0, to a solution of **1** at constant concentration (0.2 mM). Figure 2 depicts the chemical shift variation observed for protons and of **1** during the titration experiment. The chemical shift at higher R values must be related to the free drug in solution, the addition of the oligonucleotide induces a shielding of the drug protons. When an excess of oligonucleotide is reached (low values of R), the drug is found predominantly in a bound state. Actually, the chemical shift variation of a ligand is due to the sum of different processes, involving both specific and non-specific interactions with DNA (intercalation or groove binding and outside binding) and drug self-aggregation phenomena.

On the other hand, our experience suggests that shift variations of oligonucleotide proton signals arise when a ligand intercalates between the base-pairs or binds to the minor groove [23, 46, 47]. The addition of the **1** to oligonucleotide solution induced progressively changes in the chemical shift of the DNA but only selected resonances are changed: *i.e.* NH imino and the aromatic proton of G4 (Δδ= -0.12 ppm and -0.11 ppm respectively), H1' and H3' of T2 (Δδ=-0.22 ppm and -0.19 ppm respectively). Moreover methyl of T1 (Δδ=+0.13 ppm), H3' of T1 (Δδ=+0.17 ppm) experience a down field shift as well as aromatic protons of A3 and T2 (Δδ=+0.1 ppm). The other protons are almost unchanged and a very small up-field shift ($\Delta\delta \leq 0.1$ ppm) was observed. In addition the oligonucleotide protons, specially, H8 of A3 became broad due to the complex formation (Figure 3). No separate signals were observed for the

free and bound species, because an intermediate exchange, with respect to the NMR time scale, of the drug with the possible sites of binding of the oligonucleotide.

The same experiments were performed with **2** (Figure 4). The results are the same even if, due to the extensive overlapping of **2** and oligonucleotide protons, the analysis was quite difficult. All the aromatic protons of ligand collapsed at 8.46 ppm, 7.88 ppm, 7.80 ppm and 7.38 ppm. Even in these case the addition of **2** to the oligonucleotide solution causes notable chemical shift variation on drug resonances, whereas the protons of TTAGGG are almost unchanged a part from an up-field shift of NH imino G4 and the aromatic proton of G4 (Δδ= -0.10 ppm), a down-filed shift of aromatic protons of T1, T2 and A3 (Δδ= +0.14 ppm, +0.11 ppm+0.12 ppm respectively) , methyl of T1 and T2 (Δδ= +0.2 ppm and 0.12 ppm, respectively).

The chemical shift variations of ligands resonances and the chemical shift values of Htel in the complexes are reported in Table 2 and Table 3 respectively. All these findings give a first indication of a probable intercalation binding mode of **1** and **2** near the $T_2A_3G_4$ residues adjacent to the G-quadruplex quartets.

The ^{1}H NOE experiments, allowing the detection of specific interactions between protons of the ligand and protons of the DNA, were performed in order to recognize possible preferred interaction sites. NOESY spectra were acquired with *R* = [drug]/[DNA] = 0.5 and 3. The results are reported in Table 4.

The sequential NH imino cross peaks between G4, G5 and G6 are still observed in 2D NOESY of the complexes and it proves the position of the **1** between A3 and G4 without disrupting the G quartets. The presence of NOEs interactions, characteristic of the presence of G tetrads (*i.e.* imino protons with aromatic protons of own residue and with the 5' neighboring), together with the weakness of H8A3/H8G4, H8A3/H6T2, H8A3/H1'A3, H8A3/H2"T2 and of H8A3/MeT2 (Figure 5(a) and (b)) (total lack in the case of **1** complex) in comparison with the oligonucleotide alone, confirms a slight distortion at these level in the sequence.

A certain number of NOE interactions between **1** and the DNA was extracted despite of some overlapping between the signals of TTAGGG and the **1** (Table 4). Examples are reported in Figure 5(a). The NOEs observed between the drug and the oligonucleotide protons provide information regarding the sequence of the binding sites and confirm that **1** prefers the A3G4 step of TTAGGG G-quadruplex as intercalation site with the indole positioned at A3T2 step. Specific intermolecular contacts were found, involving aromatic protons of indole moiety with the ribose protons of A3 and methyl of T2. For the acridine moiety, we detected NOE contacts with aromatic protons and H3' of G4 and A3 residues. Following these few experimental NOEs, a model of the complex was built.

In the case of Htel and **2** complex it was very hard to unambiguously identify intermolecular interactions between **2** and DNA, due to the extensive overlapping, but a low number of NOE interactions was extracted from the 2D-NOESY and allowed to identify the **2** position inside the G-quadruplex structure. An aromatic proton (7.88 ppm) is close to the methyl, H2' and H3' of T2 unit and another aromatic protons (8.46 ppm) is close to H1' and H2'A3 and G4. As for **1**, the interaction site for **2** is at the level of T2 A3 and G4 residues.

3.2.2. NMR 9-amino acridines-duplex experiments

The dialysis experiments gave an evidence that only the **1** interacts with the oligonucleotide double helix ds26. In order to better understand the specific interaction involved, we performed different NMR titration experiments. To this end, we used a short oligonucleotide duplex 5'-CGATCG-3', ds6. This oligonucleotide was used in a previous studies with intercalating agents [23, 48, 49] and it is stable as a double helix even at room temperature and all the phosphate resonances, already assigned, are well separated.

The titration experiment performed with **1** was fruitless: the addition of **1** to the double helix did not induce shielding and did not induce line broadening of the oligonucleotide resonances similar to those observed with "classical" intercalating agents. (Figure 1S). For instance, the intercalation of daunomycins between the CG base-pairs of 5'-CGTACG-3', induces a significant up-field shift of the resonances at the level of the intercalation sites, *i.e.* imino NH of G2:C5 base pairs $\Delta\delta$ 0.6–0.7 ppm, 5-H (C1) and 5-H (C5) $\Delta\delta$ 0.5 ppm. Nevertheless it is the shift variation of the ^{31}P resonances that can give exclusive indication of an intercalation process [50]. The intercalating molecule induces a deformation of the phosphodiester chain, which usually assumes a *gauche–trans* conformation with angles of -60° and 180°; this is associated with a low-field shift of 1.0–1.5 ppm The addition of **1** to the oligonucleotide did not induce significant chemical shift variations of the phosphate signals in the ^{31}P NMR spectra ($\Delta\delta$ < 0.2 ppm). Figure 9 shows the ^{31}P NMR spectrum of the oligonucleotide ds6 in absence (a) and in presence of **1** (b). These findings do not support the intercalation of **1** into the double helix as previously described and its mechanism of action targets specifically the DNA G-quadruplexes.

The self-complementary oligomers ds8 and ds24 were used as models for CG- and AT-rich sequences respectively. These sequences are longer than the previous one and are partially contained into the ds26 sequence. In both cases NOESY experiments performed on the **1**/DNA complexes did not show intermolecular interactions. Interestingly, the addition of **1** to a solution of the double helix fragments induces a line broadening of the resonances (Figure 2S and 3S) of the oligomers. In particular the imino protons, that present almost unchanged chemical shift ($\Delta\delta$ <0.*1* ppm) were observed to become very broad. The inverse titration experiment was performed with ds24 and with ds26 oligonucleotides (Figure 4S and Figure 10) (Table 1S), by adding increasing amounts of DNA to a solution of **1** at constant concentration. No relevant chemical shift variations were detected, but a selective line broadening occurs for NH indole, aromatic 4A and 2A protons of **1** with ds26. These findings suggest a specific outside binding of the **1** that can not happen with a shorter oligonucleotide as ds6 because of the hindrance of the side chains.

3.2.3. Stability of 9-amino acridines-Htel complexes

The imino proton region of the NMR spectra of both complexes clearly indicates the presence of G-quadruplex structure. Three imino signals are observed between 10.0 and 11.5 ppm (Figure 6 (a), (b), (c)). These spectra are consistent with a single G-quadruplex parallel structure similar to that of the Htel. In the case of Htel/**2** complex the exceeding number of imino signals in the NMR spectra of at 5°C

suggests the presence of several species in equilibrium in slow exchange with respect to NMR time scale.

We performed melting experiments in order to see whether **1** and **2** stabilize or not the G-quadruplex structure. The imino protons signals are diagnostic for the G-quadruplex formation and the melting of the structure causes their disappearance due to the break of the G quartet hydrogen bonds. The NH signals of Htel without drugs disappeared between 45°C and 55°C (Figure 6(a)) whereas in the presence of **1** and **2** they can still be observed at 55°C and disappear up to 55°C (Figure 6 (b,c)). These findings clearly indicate a significant stabilization of the G-quadruplex structure by the interaction with ligands. The slight higher stabilization induced by **2** compared with **1** are in agreement with more favorable specific interactions between different moieties of the ligand **2** to the DNA obtained by per residue energy free studies and discussed below.

Finally, the stability of the interaction complex formed by ligand **1** and **2** with G-quadruplex Htel and duplex ds6 was quantified by recording the fluorescence spectra of a solution of the ligand after the addition of increasing amounts of oligonucleotide. Changes in the fluorescence spectra upon the addition of G-qaudruplex were observed in **1** and **2**. No significant changes in the fluorescence spectra were observed upon the addition of duplex. The increase of the fluorescence emission of these compounds reflects their interaction with the G-quadruplex Htel (Figure 5S).

Table 5 shows the logarithm of the binding constants calculated using Equispec program assuming a 1:1 stoichiometry DNA:ligand for the interaction complex. The calculated values are not very high, around 10^5 M^{-1} which, according to literature, could be related to intercalating species [51]. Groove-binding compounds are expected to show larger association constants.

3.4. Model generation

3.4.1. 9-amino acridines-HtelT G-quadruplex complexes

The 5'-TTAGGGT-3' sequence, HtelT, was used as model for telomeric parallel G-quadruplex for the molecular docking of the ligands. In both cases, Autodock placed the ligand in an intercalated binding mode within the G-quadruplex. Docking experiments show that **1** fit in the original gap region, located between the virtual planes made by the four A and G bases, with the tryptophan group adjacent to A10 and T16, and the acridine moiety placed just under the A10 base, to give a π-π stacking interaction. It should be noted that the best docked orientation obtained for **1** has proven to be in agreement with experimental data of the inter-molecular NOE interactions previously discussed (as shown by the values of the distances reported in Table 4), thus, supporting the proposed binding model. On the contrary, compound **2** was unable to intercalate so efficiently, thus giving rise to a less stable orientation. The differences observed with respect to **1** could be due to the shift of the acridine moiety away from the center of the G-quadruplex, probably because of the greater steric hindrance produced by the presence of the piperidine group.

The above described systems were further optimized using the QM/MM mixed approach. This technique allowed us to obtain a better and more complete description of the interactions with the G-

quadruplex, as well as an estimate of the structural changes induced in the G-quadruplex by the binding of both ligands, **1** and **2**. In both cases, major differences were observed at the level of the acridine substituents, while the acridine ring maintained its position inside the G-quadruplex, together with the π-π interactions previously described (Figure 7 A and B).

The position of compound **1** is stabilized by four strong hydrogen bonds: two between the 9-amino acridine hydrogen and N1A10 and N3A10 of 1.8 and 2.6 Å, other between the methyl piperazine hydrogen and OPA10 of 1.95 Å and other between the carbonyl oxygen and HN2G25 of 2.12 Å (Figure 8A). Considering the structure of the G-quadruplex, the presence of **1** has influenced mainly the A10 position. Indeed due to the presence of the ligand, A10 undergoes a small clockwise rotation (about 6°) with respect to the original structure. This rotation of A10 leads to the formation of an additional hydrogen bond with T9, while keeping the two original hydrogen bonds with A24 and A17.

In the case of **2** an orientation close to that of **1** was obtained. This position is stabilized by six hydrogen bonds: three between the 9-amino acridine hydrogen and N1A10, N2G11 and N7A17 of 3.1, 2.3 and 2.8 Å; other between the methyl piperazine hydrogen and OPA10 3.3 Å; other between the carbonyl oxygen and HN2G25 of 3.3 Å and other between the acridine nitrogen and HN6A10 of 3.5 Å (Figure 8C and D).

However, the biggest difference between **1** and **2** was found to be at the level of their interaction with the G-quadruplex. Differently from **1**, the interaction of **2** resulted in a clockwise rotation of G11 (about 9°) with respect to the original structure. This rotation allowed G11 to form two new hydrogen bonds with G26, while losing two of the four hydrogen bonds with G18 and G25.

3.5. MD simulation

Computational methods are widely used to investigate biomolecules and complexes, and have been shown to provide valuable deeper understanding of the structural, dynamic and energetic properties [26, 52, 53].

To assess the overall structural stability of the 9-amino acridines – G-quadruplex complex, we evaluated the root mean square deviation (rmsd) of the whole structure over the course of the MD simulation. G-quadruplex structures without potassium between the G-tetrads were structurally less stable than K^+ saturation complexes and significant disorder was observer during the MD simulation (results not shown). The rmsd values of the whole complex remain < 4 Å (Figure 6S) reflecting the fluctuations of the terminal T residues, as they are not held tightly by hydrogen bonds and, hence, are free to move during simulation. To consistently examine the stability of the complex without the interference of the terminal residues, the rmsd values for the A and G-quartets core, with bound ligand **1** and **2**, were examined and their structural integrity were conserved in both cases with less than 2.5 Å rmsd (Figure 11). To examine how 9-amino acridines occupies within the A and G tetrad, we evaluated the rmsd values for the ligands **1** and **2** within the G-quadruplex, showing that acridine scaffolds are free to move within the gap region between the virtual planes made by the four A and G bases, but remains within the G-quadruplex (Figure 11).

To examine the overall stability of the structural complex, MD simulations at elevated temperature were also performed. The goal was to identify the specific interactions observed in our NMR studies that can play an important role in maintaining the G-quadruplex structure. We expect transient interactions will be subsided at elevated temperature allowing us to identify the stable contacts essential for retaining the overall G-quadruplex structure. The rmsd values for these studies are shown in Figure 7S-8S. The MD simulation at 400K indicates that the rmsd values for the A and G-quartets core with bound ligand **2** is similar to value obtained at 298K. In the case of ligand **1**, the higher value of rmsd indicates that interactions established between ligand and HtelT were not maintained at high temperature (Figure 7S). Significant disorder was observed during the simulation at 500K, only G-quadruplex with bound ligand **2** keep the G-quadruplex structure as indicated the rmsd value for the A and G-quartets core (Figure 8S). This suggests that ligand **2** has a more stabilizing effect on the quadruplex structure as compared to **1**.

We also examined the essential hydrogen bonding for 9-amino acridines binding. An interaction was considered to be a hydrogen bond if the distance between the hydrogen donor and acceptor was less than 3.5 A. As mentioned above four hydrogen bounds are formed with ligand **1**, only the bond between the methyl piperazine hydrogen and OPA10 was not kept during the dynamic simulation due to the rotation of the N-Me-Piperazine ring. Moreover, during the simulation the rotation of the indole group has allowed the formation of two additional hydrogen bonds between NH and OA17 and OPA17 from 6.4 and 5.0 A to 2.7 and 1.9 A (Figure 8 B). In the case of ligand **2**, six hydrogen bounds are observed, but weaker compared with hydrogen bonds formed with ligand **1**. The hydrogen bond between 9-amino acridine hydrogen and N2G11 and N7A17 and between N-Me piperazine hydrogen and OPA10 were kept during the simulation (Figure 8 C and D).The N-Bz-piperidine group acts as the indole in **1** but, probably due to the bulkiness of the phenyl group, in this case the quaternary nitrogen fails to approach the phosphate group of A17 enough to form hydrogen bonds.

Finally, the per residue interaction energy between compound **1** and **2** to individual nucleotide residues of HtelT G-quadruplex are shown in Figure 12. Examination of the interactions revealed a slight variation in the signature of binding between compounds **1** and **2** with the G-quadruplex DNA (Figure 12A). The main difference is found in the G25. Figure 12 B-C show the per residue interaction energy between moieties that form compound **1** and **2**. While as piperazine moiety in compound **2** has an energetic favorable contribution, in compound **1** this interaction is not favorable. The slight higher HtelT stabilization induced by compound **2** observed during NMR melting experiments may be due the most favorable interactions between the different moieties of **2** to the G-quadruplex.

4. Conclusions

In summary we have used fluorescence titration assays, competitive dialysis, NMR studies and molecular dynamics simulations in order to determine the binding properties of preclinical 9-amino acridines to DNA. A selectivity of acridine derivatives for G-quadruplex structures, commonly present on the promoter regions of oncogenes and the human telomere sequence, was observed. Slightly higher stabilization of the structural complex induced by the interaction of compound **2** as compared to **1** was observed by NMR melting experiments. Detailed structural studies by NMR and molecular dynamic simulation on G-quadruplex telomeric complex showed the core of both 9-amino acridines intercalates

directly between the virtual planes made by the four A and G bases via π- π interactions, but do not exactly overlap. The indole moiety in ligand **1** does not fit as closely to the G-quadruplex groove as the N-Bz-piperidine group in ligand **2**. Structurally, ligand **1** establishes only four strong hydrogen bonds with telomeric G-quadruplex while ligand **2** established six. The most significant interaction observed involved the carbonyl oxygen with G25 for both ligands and the 9-amino acridine hydrogen with A10 for ligand **1** and with A17 and G11 for ligand **2**. Per residue interaction free energy profiles of each compounds showed the substituents of ligand **1** exhibit two distinctly unfavorable interactions between the piperazine group to G25 and the piperidine group to A10 (Fig 13b). The strength of these interactions was further examined by MD simulations at elevated temperatures showing the interactions between ligand **2** and the G-quadruplex are tighter than that of ligand **1**. Rmsd analysis over the course of simulation further support the slight enhanced structural stabilization by compound **2** over compound **1** with relative lower rmsd among the unbound and bound complexes. The slightly stronger interactions between ligand **2** to the G-quadruplex over ligand **1** could explain the experimental differences in structural stabilities between the two 9-amino acridines. The ability of 9-amino acridines to exhibit similar binding affinity to the G-quadruplex while inducing different level of structural stabilization through intercalation could be a unique strategy for altering the overall biological function of telomerase and their subsequent anticancer activity. These findings will assist in the understanding the parameters influencing the G-quadruplex – ligand interaction and will serve as an enhanced platform for rational drug design.

Acknowledgments

This work was partially supported by grants from Spanish Ministerio de Ciencia e Innovación MICINN (CTQ2008-00177, CTQ2010-20541), Generalitat de Catalunya, (2009/SGR/208), CIBER-BBN, Networking Centre on Bioengineering, Biomaterials and Nanomedicine, Institute for Research in Biomedicine, and the Barcelona Science Park. CIBER-BBN is an initiative funded by the VI National R&D&i Plan 2008–2011, Iniciativa Ingenio 2010, Consolider Program, CIBER Actions and financed by the Instituto de Salud Carlos III with assistance from the European Regional Development Fund. This work was supported by the University of Milan (PUR09) and by MIUR (Funds PRIN09). The University of Minnesota Supercomputing Institute provided all the computational resources for the MD simulation.

Appendix A. supplementary data

References

[1] A.M. Zahler, J.R. Williamson, T.R. Cech, D.M. Prescott, Inhibition of telomerase by G-quartet DNA structures, Nature, 350 (1991) 718-720.
[2] M.K. Cheng, C. Modi, J.C. Cookson, I. Hutchinson, R.A. Heald, A.J. McCarroll, S. Missailidis, F. Tanious, W.D. Wilson, J.L. Mergny, C.A. Laughton, M.F.G. Stevens, Antitumor polycyclic acridines. 20. search for DNA quadruplex binding selectivity in a series of 8,13-dimethylquino 4,3,2-kl acridinium salts: Telomere-targeted agents, J. Med. Chem., 51 (2008) 963-975.
[3] W.A. Denny, Acridine derivatives as chemotherapeutic agents, Curr. Med. Chem., 9 (2002) 1655-1665.
[4] P. Belmont, J. Bosson, T. Godet, M. Tiano, Acridine and acridone derivatives, anticancer properties and synthetic methods: Where are we now?, Anti-Cancer Agents Med. Chem., 7 (2007) 139-169.
[5] A.K. Larsen, A.E. Eseargueil, A. Skladanowski, Catalytic topoisomerase II inhibitors in cancer therapy, Pharmacol. Ther., 99 (2003) 167-181.
[6] K.D. Corbett, J.M. Berger, Structure, molecular mechanisms, and evolutionary relationships in DNA topoisomerases, Annu. Rev. Biophys. Biomolec. Struct., 33 (2004) 95-118.
[7] Z. Topcu, DNA topoisomerases as targets for anticancer drugs, J. Clin. Pharm. Ther., 26 (2001) 405-416.
[8] P.B. Arimondo, C. Helene, Design of new anti-cancer agents based on topoisomerase poisons targeted to specific DNA sequences, Current medicinal chemistry. Anti-cancer agents, 1 (2001) 219-235.
[9] E.H. Blackburn, Telomere states and cell fates, Nature, 408 (2000) 53-56.
[10] E.H. Blackburn, Switching and signaling at the telomere, Cell, 106 (2001) 661-673.
[11] S. Neidle, G. Parkinson, Telomere maintenance as a target for anticancer drug discovery, Nat. Rev. Drug Discov., 1 (2002) 383-393.
[12] J.L. Mergny, C. Helene, G-quadruplex DNA: A target for drug design, Nat. Med., 4 (1998) 1366-1367.
[13] D. Monchaud, M.P. Teulade-Fichou, A hitchhiker's guide to G-quadruplex ligands, Org. Biomol. Chem., 6 (2008) 627-636.
[14] T.M. Ou, Y.J. Lu, J.H. Tan, Z.S. Huang, K.Y. Wong, L.Q. Gu, G-quadruplexes: Targets in anticancer drug design, ChemMedChem, 3 (2008) 690-713.
[15] N.H. Campbell, M. Patel, A.B. Tofa, R. Ghosh, G.N. Parkinson, S. Neidle, Selectivity in Ligand Recognition of G-Quadruplex Loops, Biochemistry, 48 (2009) 1675-1680.
[16] J.R. Goodell, A.V. Ougolkov, H. Hiasa, H. Kaur, R. Remmel, D.D. Billadeau, D.M. Ferguson, Acridine-based agents with topoisomerase II activity inhibit pancreatic cancer cell proliferation and induce apoptosis, J. Med. Chem., 51 (2008) 179-182.
[17] I. Naasani, H. Seimiya, T. Yamori, T. Tsuruo, FJ5002: A potent telomerase inhibitor identified by exploiting the disease-oriented screening program with COMPARE analysis, Cancer Res., 59 (1999) 4004-4011.
[18] M. Franceschin, L. Rossetti, A. D'Ambrosio, S. Schirripa, A. Bianco, G. Ortaggi, M. Savino, C. Schultes, S. Neidle, Natural and synthetic G-quadruplex interactive berberine derivatives, Bioorg. Med. Chem. Lett., 16 (2006) 1707-1711.
[19] R. Ferreira, A. Avino, R. Perez-Tomas, R. Gargallo, R. Eritja, Synthesis and g-quadruplex-binding properties of defined acridine oligomers, Journal of nucleic acids, 2010 (2010).
[20] A. Kumar, R.R. Ernst, K. Wuthrich, A two-dimensional nuclear overhauser enhancement (2D NOE) experiment for the elucidation of complete proton-proton cross-relaxation network in biologial macromolecules, Biochem. Biophys. Res. Commun., 95 (1980) 1-6.
[21] L. Braunschweiler, R.R. Ernst, Coherence transfer by isotropic mixing - pplication to proton correlation spectroscoyp, J. Magn. Reson., 53 (1983) 521-528.
[22] D.G.K. T.D. Goddard, SPARKY 3, University of California, San Francisco, USA, (2004).

[23] S. Mazzini, R. Mondelli, E. Ragg, Structure and dynamics of intercalation complexes of anthracyclines with d(CGATCG)(2) and d(CGTACG)(2). 2D-H-1 and P-31 NMR investigations, J. Chem. Soc.-Perkin Trans. 2, (1998) 1983-1991.
[24] Y. Wang, D.J. Patel, Guanine residues in d(T2AG3) and d(T2G4) form parallel-stranded potassium cation stabilized G-quadruplexes with antiglycosidic torsion angles in solution, Biochemistry, 31 (1992) 8112-8119.
[25] R.M. Dyson, S. Kaderli, G.A. Lawrance, M. Maeder, A.D. Zunderbuhler, Second order global analysis: the evaluation of series of spectrophotometric titrations for improved determination of equilibrium constants, Anal. Chim. Acta, 353 (1997) 381-393.
[26] C. Hounsou, L. Guittat, D. Monchaud, M. Jourdan, N. Saettel, J.L. Mergny, M.P. Teulade-Fichou, G-quadruplex recognition by quinacridines: a SAR, NMR, and biological study, ChemMedChem, 2 (2007) 655-666.
[27] E. Lindahl, B. Hess, D. van der Spoel, GROMACS 3.0: a package for molecular simulation and trajectory analysis, J. Mol. Model., 7 (2001) 306-317.
[28] C. Oostenbrink, T.A. Soares, N.F.A. van der Vegt, W.F. van Gunsteren, Validation of the 53A6 GROMOS force field, Eur. Biophys. J. Biophys. Lett., 34 (2005) 273-284.
[29] J.P. Stewart, Optimization of parameters for semiempirical methods V: Modification of NDDO approximations and application to 70 elements, J. Mol. Model., 13 (2007) 1173-1213.
[30] G.M. Morris, D.S. Goodsell, R.S. Halliday, R. Huey, W.E. Hart, R.K. Belew, A.J. Olson, Automated docking using a Lamarckian genetic algorithm and an empirical binding free energy function, J. Comput. Chem., 19 (1998) 1639-1662.
[31] R. Huey, G.M. Morris, A.J. Olson, D.S. Goodsell, A semiempirical free energy force field with charge-based desolvation, J. Comput. Chem., 28 (2007) 1145-1152.
[32] M.F. Sanner, Python: A programming language for software integration and development, J. Mol. Graph., 17 (1999) 57-61.
[33] J. Gasteiger, M. Marsili, Iterative partial equalization of orbital electonegativity - a rapid access to atomic charges, Tetrahedron, 36 (1980) 3219-3228.
[34] G.W.T. M. J. Frisch, H. B. Schlegel, G. E. Scuseria, M. A. Robb, J. R. Cheeseman, J. A. Montgomery, Jr., T. Vreven, K. N. Kudin, J. C. Burant, J. M. Millam, S. S. Iyengar, J. Tomasi, V. Barone, B. Mennucci, M. Cossi, G. Scalmani, N. Rega, G. A. Petersson, H. Nakatsuji, M. Hada, M. Ehara, K. Toyota, R. Fukuda, J. Hasegawa, M. Ishida, T. Nakajima, Y. Honda, O. Kitao, H. Nakai, M. Klene, X. Li, J. E. Knox, H. P. Hratchian, J. B. Cross, V. Bakken, C. Adamo, J. Jaramillo, R. Gomperts, R. E. Stratmann, O. Yazyev, A. J. Austin, R. Cammi, C. Pomelli, J. W. Ochterski, P. Y. Ayala, K. Morokuma, G. A. Voth, P. Salvador, J. J. Dannenberg, V. G. Zakrzewski, S. Dapprich, A. D. Daniels, M. C. Strain, O. Farkas, D. K. Malick, A. D. Rabuck, K. Raghavachari, J. B. Foresman, J. V. Ortiz, Q. Cui, A. G. Baboul, S. Clifford, J. Cioslowski, B. B. Stefanov, G. Liu, A. Liashenko, P. Piskorz, I. Komaromi, R. L. Martin, D. J. Fox, T. Keith, M. A. Al-Laham, C. Y. Peng, A. Nanayakkara, M. Challacombe, P. M. W. Gill, B. Johnson, W. Chen, M. W. Wong, C. Gonzalez, and J. A. Pople, Gaussian 03, Revision C.02, Gaussian, Inc., Wallingford CT, (2004).
[35] W.L. Jorgensen, D.S. Maxwell, J. TiradoRives, Development and testing of the OPLS all-atom force field on conformational energetics and properties of organic liquids, J. Am. Chem. Soc., 118 (1996) 11225-11236.
[36] W.L. Jorgensen, J. Chandrasekhar, J.D. Madura, R.W. Impey, M.L. Klein, Comparison of simple potential function for simulating liquid water J. Chem. Phys., 79 (1983) 926-935.
[37] U. Essmann, L. Perera, M.L. Berkowitz, T. Darden, H. Lee, L.G. Pedersen, A smooth particle mesh ewald method, J. Chem. Phys., 103 (1995) 8577-8593.
[38] J.P. Ryckaert, G. Ciccotti, H.J.C. Berendsen, Numerical-integration of cartesian equations of motion of a system with constraints - molecular-dynamics of N-alkanes, J. Comput. Phys., 23 (1977) 327-341.

[39] C. Granotier, G. Pennarun, L. Riou, F. Hoffschir, L.R. Gauthier, A. De Cian, D. Gomez, E. Mandine, J.F. Riou, J.L. Mergny, P. Mailliet, B. Dutrillaux, F.D. Boussin, Preferential binding of a G-quadruplex ligand to human chromosome ends, Nucleic Acids Res., 33 (2005) 4182-4190.
[40] J.S. Ren, J.B. Chaires, Sequence and structural selectivity of nucleic acid binding ligands, Biochemistry, 38 (1999) 16067-16075.
[41] P. Ragazzon, J.B. Chaires, Use of competition dialysis in the discovery of G-quadruplex selective ligands, Methods, 43 (2007) 313-323.
[42] J. Gros, F. Rosu, S. Amrane, A. De Cian, V. Gabelica, L. Lacroix, J.L. Mergny, Guanines are a quartet's best friend: impact of base substitutions on the kinetics and stability of tetramolecular quadruplexes, Nucleic Acids Res., 35 (2007) 3064-3075.
[43] L.C. Bock, L.C. Griffin, J.A. Latham, E.H. Vermaas, J.J. Toole, Selection of single-stranded-DNA molecules that bind and inhibit human thrombin Nature, 355 (1992) 564-566.
[44] Y. Wang, D.J. Patel, Solution structure of a parallel-stranded G-quadruplex DNA J. Mol. Biol., 234 (1993) 1171-1183.
[45] J.X. Dai, T.S. Dexheimer, D. Chen, M. Carver, A. Ambrus, R.A. Jones, D.Z. Yang, An intramolecular G-quadruplex structure with mixed parallel/antiparallel G-strands formed in the human BCL-2 promoter region in solution, J. Am. Chem. Soc., 128 (2006) 1096-1098.
[46] E. Ragg, S. Mazzini, R. Bortolini, N. Mongelli, R. D'Alessio, H-1 NMR investigations on the solution structure of the oligonucleotide 5 '-d(ACCT(5)GATGT)-3 '/5 '-d(ACATCA(5)GGT)-3 ' and its interaction with tallimustine, J. Chem. Soc.-Perkin Trans. 2, (1998) 149-158.
[47] S. Mazzini, M.C. Bellucci, S. Dallavalle, F. Fraternali, R. Mondelli, Mode of binding of camptothecins to double helix oligonucleotides, Org. Biomol. Chem., 2 (2004) 505-513.
[48] R. Bortolini, S. Mazzini, R. Mondelli, E. Ragg, C. Ulbricht, S. Vioglio, S. Penco, P-31 NMR-Studies on the interaction of morpholinyl anthracyclines and relade-compound with d(CGTACG)2 - thermodynamic and kinetic-parameters, Appl. Magn. Reson., 7 (1994) 71-87.
[49] S. Mazzini, L. Scaglioni, F. Animati, R. Mondelli, Interaction between double helix DNA fragments and the new antitumor agent sabarubicin, Men10755, Bioorg. Med. Chem., 18 (2010) 1497-1506.
[50] D.G. Gorenstein, Conformation and dynamics of DNA and protein-DNA complexes by P-31 NMR, Chem. Rev., 94 (1994) 1315-1338.
[51] R. Palchaudhuri, P.J. Hergenrother, DNA as a target for anticancer compounds: methods to determine the mode of binding and the mechanism of action, Curr. Opin. Biotechnol., 18 (2007) 497-503.
[52] L. Rao, J.D. Dworkin, W.E. Nell, U. Bierbach, Interactions of a Platinum-Modified Perylene Derivative with the Human Telomeric G-Quadruplex, J. Phys. Chem. B, 115 (2011) 13701-13712.
[53] J. Šponer, X. Cang, T.E. Cheatham Iii, Molecular dynamics simulations of G-DNA and perspectives on the simulation of nucleic acid structures, Methods.

Table 1. Oligonucleotides sequences used in this study

DNA code	5'-sequence-3'
T20	TTT TTT TTT TTT TTT TTT TT
24bclc	CCC GCC CCC TTC CTC CCG CGC CCG
Dickerson	CGC GAA TTC GCG
ds26	CAA TCGGAT CGA ATT CGA TCC GAT TG
GA triplex	GAA AGA GAGGAG GCC TTT TTG GAG GAG AAG + CCT CCT CTC TTT C
TC triplex	CCT CCT CTC TTT CCC TTT TTC TTT CTC TCC TCC + GAA AGA GAG GAG G
TG_4T	TGG GGT
TBA	GGT TGG TGT GGT TGG
HT24	TAG GGT TAG GGT TAG GGT TAGGGT
Htel	TTA GGG
HtelT	TTA GGG T
24bcl	CGG GCG CGG GAGGAA GGG GGC GGG
cmyc	GGG GAG GGT GGG GAG GGT GGG GAA GGT GGG G
ds6	CGA TCG
ds8	GCG ATC GC
ds24	AAG AAT TCT TAA GAA TTC TTA ATT

Table 2. [1]H chemical shift assignments for **1** and **2** (δ) and shift variation of **1** (Δδ) in the presence of Htel[a]

1	**δ free**	**δ bound Htel**	**Δδ** (*δ***bound**–*δ***free**)	**2** [b]	**δ free**
4A	8.36	8.10	-0.26	1B	8.31
1B	8.28	8.10	-0.18	3A	8.22
3B	7.92	7.74	-0.18	4B	7.92
4B	7.87	7.74	-0.13	1A	7.90
2A	7.80	7.66	-0.14	2B	7.80
2B	7.55	7.48	-0.07	3B	7.49
3A	7.55	7.20	-0.35	2A	7.30
H1	7.27	7.00	-0.27	H Phe	7.26-7.40
H4	7.25	7.00	-0.25	CH_2 ring1	4.00, 3.75, 3.49, 2.60, 2.45
H2	7.10	6.61	-0.49	CH_2 ring2	2.85, 2.15, 2.05, 1.86
H3	6.76	6.42	-0.34	CH_2 benz	3.55
Hind	6.94	6.60	-0.34	CH	2.62
NH ind	9.75	9.60	-0.15	NCH_3	2.27
CH_2-NHind	3.45	n.d.	-	-	-
CH_2-NH	4.60	n.d.	-	-	-
NCH_3	2.20	n.d.	-	-	-
CH_2 ring	2.8,2.9	2.27	-0.53, -0.63	-	-
	3.4,3.9	2.82, 4.10	-0.58, 0.20	-	-

[a] Measured in ppm at 25°C, *R* = [drug]/[DNA] = 3; [b] Tentatively the chemical shift variations are within -0.08 ppm and -0.5 ppm.

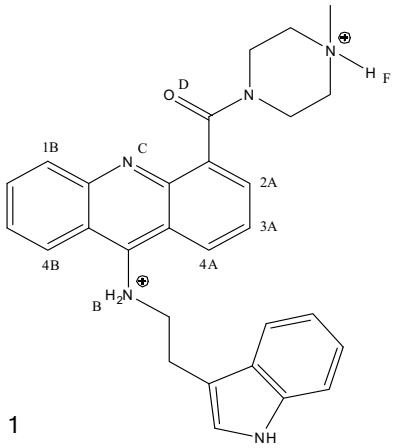

1

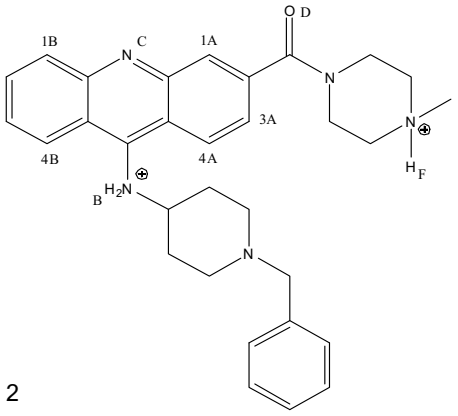

2

Table 3. ^{1}H chemical shift assignments for Htel (δ) in the presence of **1** and **2**[a]

TTAGGG/1	NH	H2/H8/H6	H1'	H2',H2''	H3'	H4'	CH_3
T1	-	7.43	6.05	2.42, 2.11	4.86	4.11	1.86
T2	-	7.43	6.05	2.42, 2.18	4.86	4.24	1.86
A3	-	8.10, 8.51	6.38	2.98, 2.98	5.19	4.57	-
G4	11.23	7.72	6.07	2.93, 2.60	5.04	4.32	-
G5	10.89	7.48	6.07	2.91, 2.68	5.03	4.39	-
G6	10.53	7.37	6.12	2.87, 2.66	4.88	4.53	-
TTAGGG/2	**NH**	**H2/H8/H6**	**H1'**	**H2',H2''**	**H3'**	**H4'**	**CH_3**
T1	-	7.60	6.06	2.48,2.28	4.85	3.96	1.93
T2	-	7.46	6.23	2.49, 2.25	4.93	4.28	1.93
A3	-	8.10, 8.54	6.42	3.02, 3.02	5.22	4.61	-
G4	11.35	7.88	6.11	3.02, 2.76	5.03	4.43	-
G5	10.96	7.59	6.20	3.02,2.83	5.17	4.46	-
G6	10.61	7.46	6.23	3.00, 2.77	4.96	4.62	-

[a] Measured in ppm at 25°C, *R* = [drug]/[DNA] = 3.0

Table 4. Inter-molecular NOE interactions between protons of the **1** with protons of Htel[a]. The distances are calculated on the basis of the **1** best docked conformation.

TTAGGG	1	Theoretical distances(Å)
CH_3 T2	H1 or H4	4.31 (H4)
H2' A3	H1 or H4	4.37 (H4)
H2' A3	H2 or H3	4.33 (H3)
H1' A3	H2 or H3	1.68 (H3)
H3', G4 or A3	H3A	3.96 (A3)

[a] Acquired at 25°C, *R* = [drug]/[DNA] = 3. 2' H and 2" H stand for low field and up field proton respectively.

Table 5. Logarithm of the binding constants calculated using Equispec program. n.d. not determinded due to lack of changes in the fluorescence spectra.

DNA	1	2
Htel	4.9 ± 0.1	4.4 ± 0.1
ds6	n.d.	n.d.

Figure 1. Results obtained by the competitive dialysis assays. The amount of ligand bound to each DNA structure is shown as a bar graph.

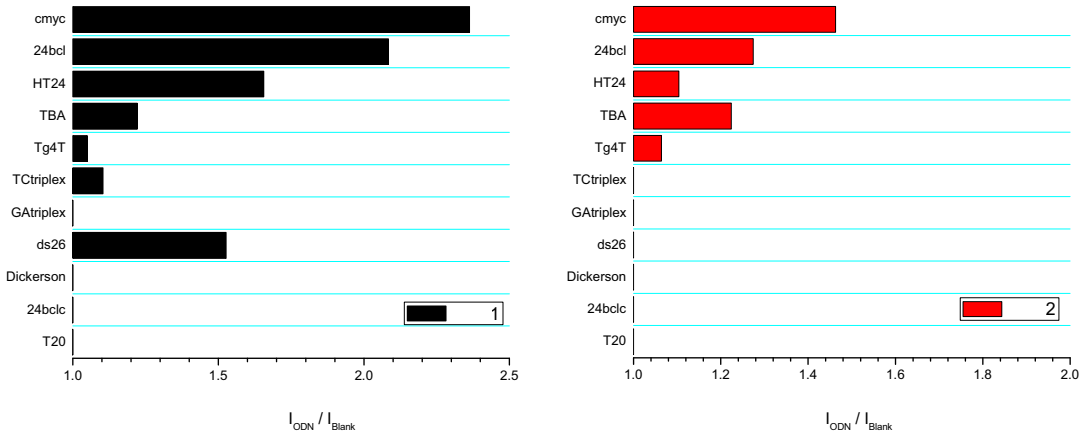

Figure 2. ^{1}H NMR spectra showing NH of indole moiety and aromatic protons of **1** in the free state (R = Htel/$[\mathbf{1}]_4$=0) and at different R. High and low R values must be related to the free and bound state of **1** in solution respectively.

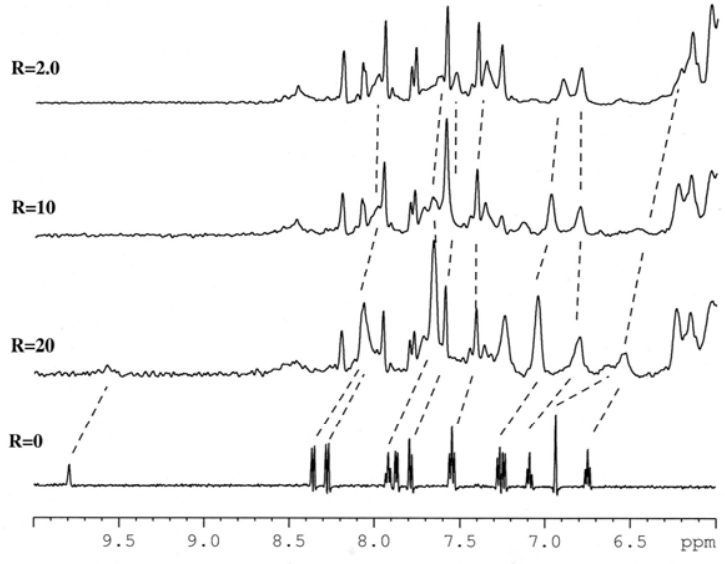

Figure 3. ^{1}H NMR spectra (11.5-10.2 ppm and 9.0-7.0 ppm), acquired at T=25°C in H_2O, containing 25 mM KH_2PO_4, KCl 150 mM and EDTA 1 mM (pH 6.7), showing resonance of imino protons G4, G5 and G6 as well as the aromatic protons at different R = [**1**]/Htel.

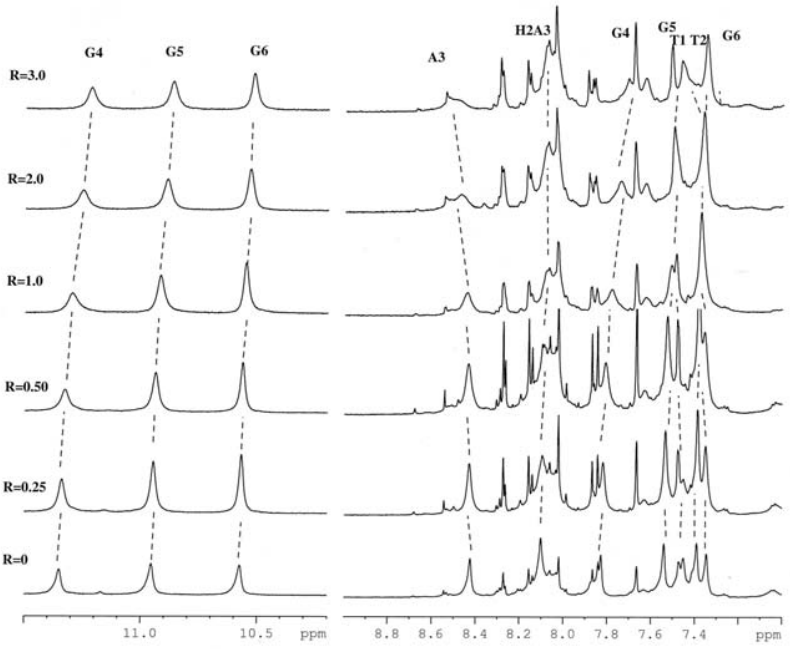

Figure 4. ^{1}H NMR spectra (11.5-10.2 ppm and 9.0-7.0 ppm) showing resonance of imino protons G4, G5 and G6 as well as the aromatic protons at different R = [**2**]/Htel.

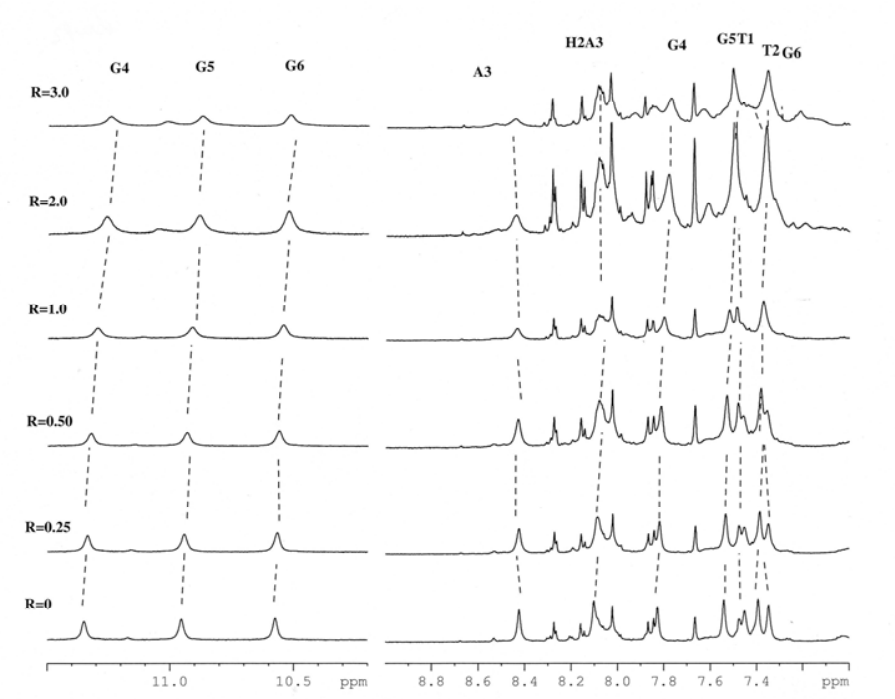

Figure 5. Selected region of 2D NOESY spectra of Htel/**1** (a) and Htel/**2** (b) complexes at 25°C in H_2O, containing 25 mM KH_2PO_4, KCl 150 mM and EDTA 1 mM (pH 6.7). The weakness of H8A3/H2"T2 and of H8A3/MeT2 (total lack in the case of Htel/**1**) confirms a slight distortion at these level in the sequence. The peaks A, B and C are intermolecular NOEs, (A) H1 or H4 with CH_3T2, (B) H1 or H4 with H2', H2" A3, (C) H3 with H2',H2" A3, (D) Ar with MeT2 (E) Ar with H2',H2"T2 (F) Ar with H2',H2"A3.

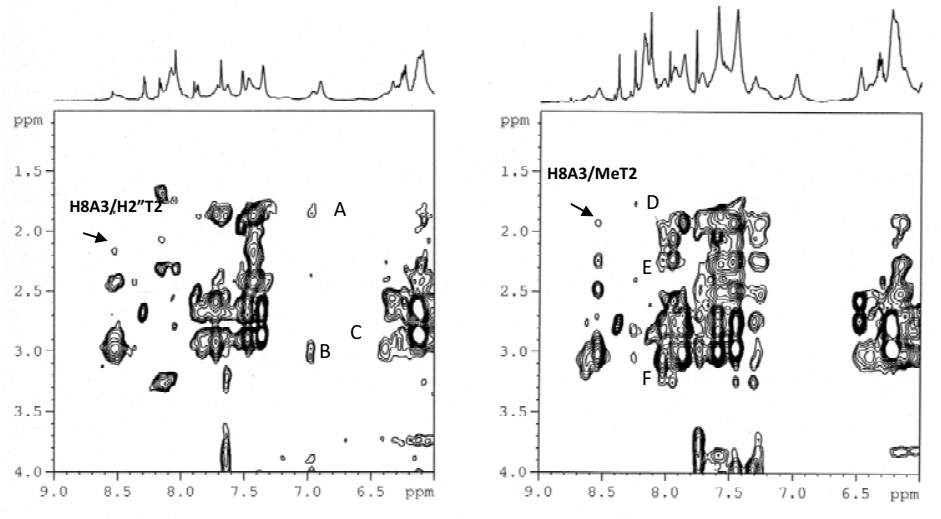

(a) (b)

Figure 6. Imino protons regions of the NMR spectra of Htel (a) Htel/**1**(b) and Htel/**2** (c) at different temperatures.

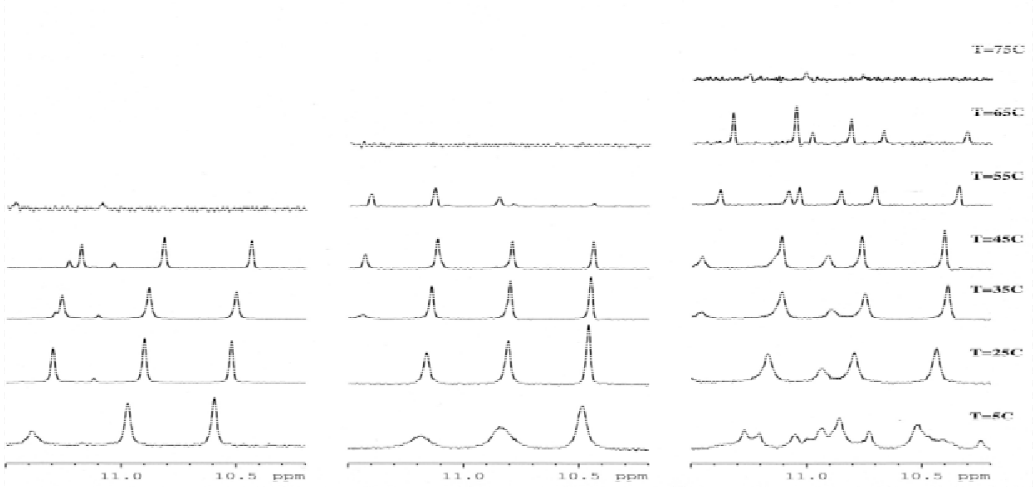

(a) (b) (c)

Figure 7. Lateral (A) and upper (B) views of the best docked conformations for **1** and **2**. **1** is shown in green stick and **2** in yellow stick. In DNA, the base pairs are shown using the ladder representation, with the backbones displayed as arrows.

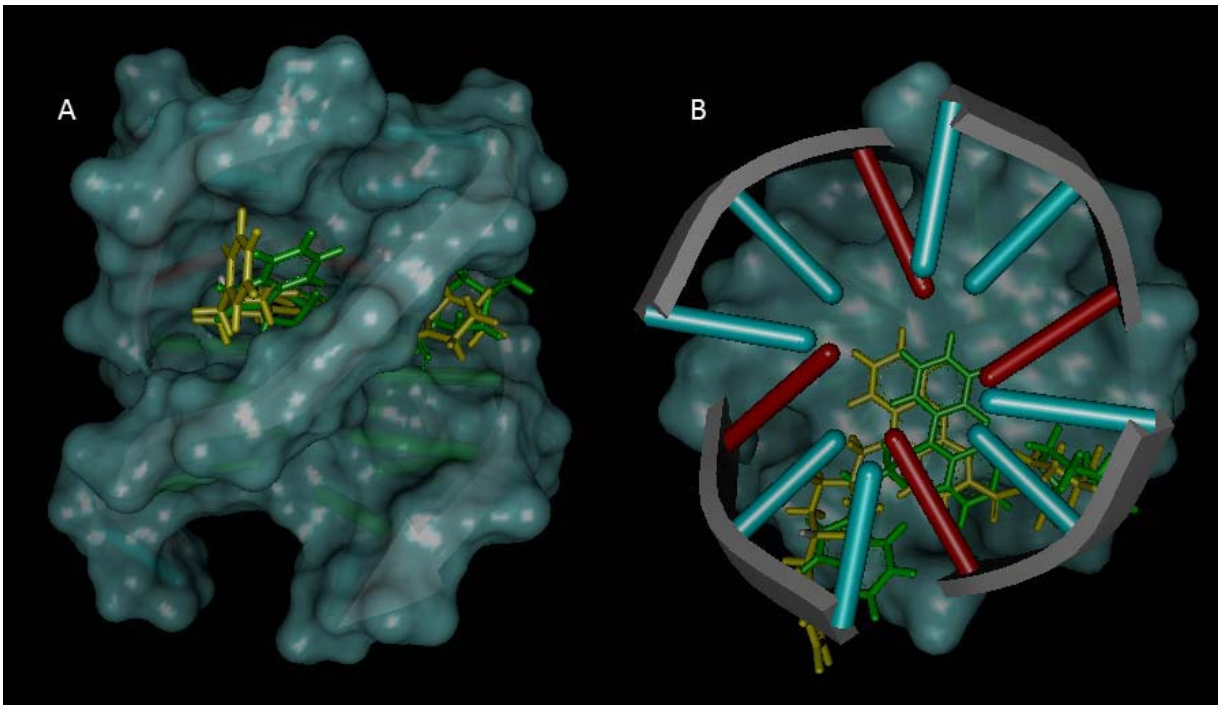

Figure 8. Time dependence of hydrogen bond distances observed between G-quadruplex and ligand **1** (A and B) and **2** (C and D). A)1. Hb and N1A10 (cyan) 2. Hb and N3A10 (green) 3. Hf and OPA10 (blue) 4. Od and HN2G25 (red). B) 1. Hi and OaA17 (blue) 2. Hi and OPA17 (red). C) 1. Hb and N1A10 (blue) 2. Nc and HN6A10 (red) 3. Hf and OPA10 (green) D) 1. Hb and N2G11 (blue) 2. Hb and N7A17 (red) 3. Od and HN2G25 (green).

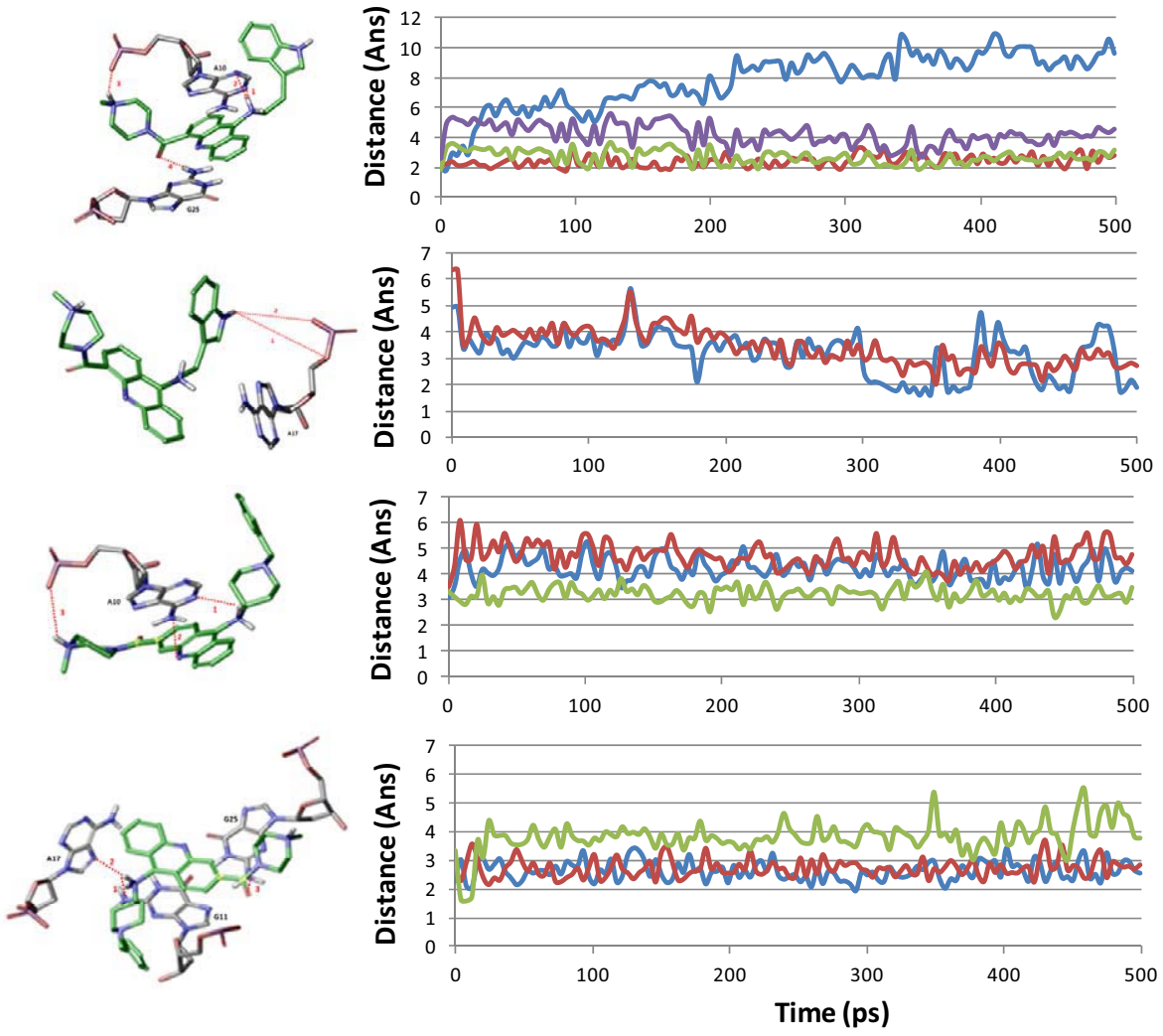

Figure 9. ^{1}H decoupled ^{31}P NMR spectra of (a) ds6 at T = 25°C, (b) R = [**1**]/[DNA]= 3.0

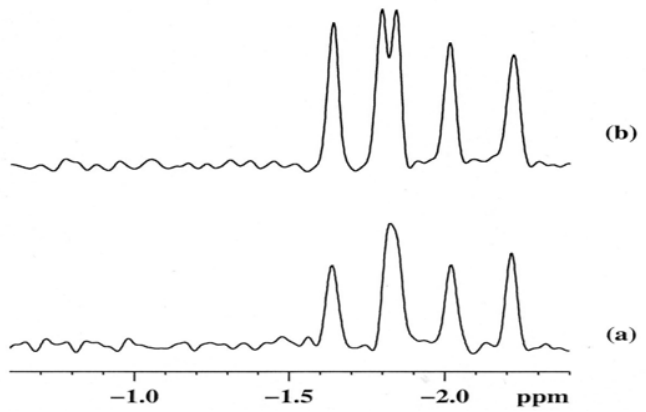

Figure 10. ^{1}H NMR spectra showing NH of indole moiety and aromatic protons of **1** in the free state (R = [ds26] /[**1**]=0) and at different R. High and low R values must be related to the free and bound state of **1** in solution respectively.

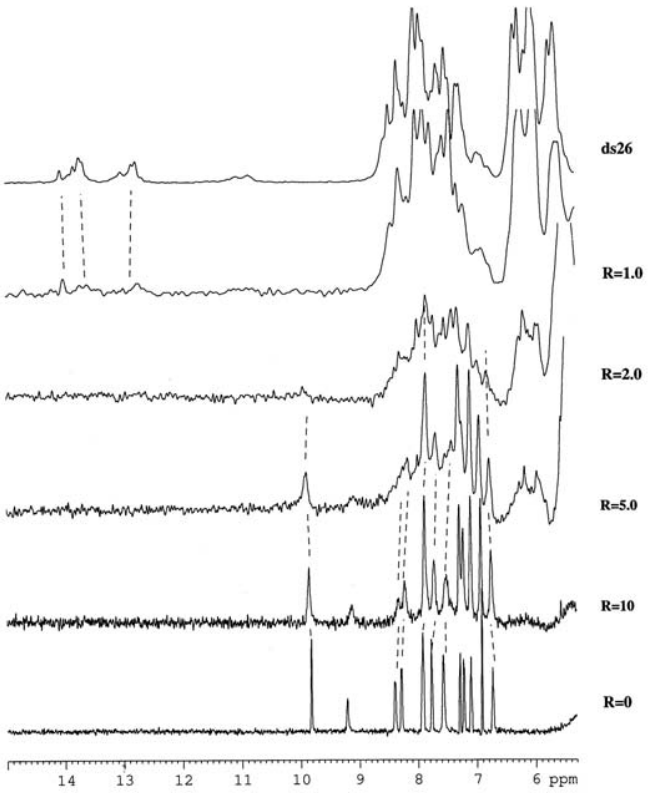

Figure 11. Time dependence of the RMSD of ligand **1** and **2** on the complex (cyan and yellow, respectively) and A and G-quartet heavy atoms (blue) with ligand atoms (**1** and **2** are shown in red and green, respectively) at 298K.

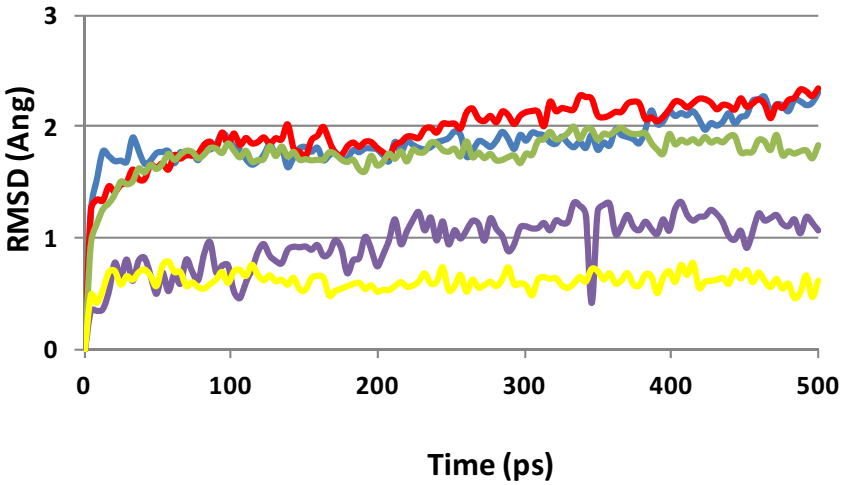

Figure 12. Per residue interaction energy in Kcal/mol between compound **1** and **2** (A), between acridine (blue), piperazine (red) and tryptophan (green) moiety in compound **1** (B) and between acridine (blue), piperazine (red) and piperidine (green) in compound **2** (C).

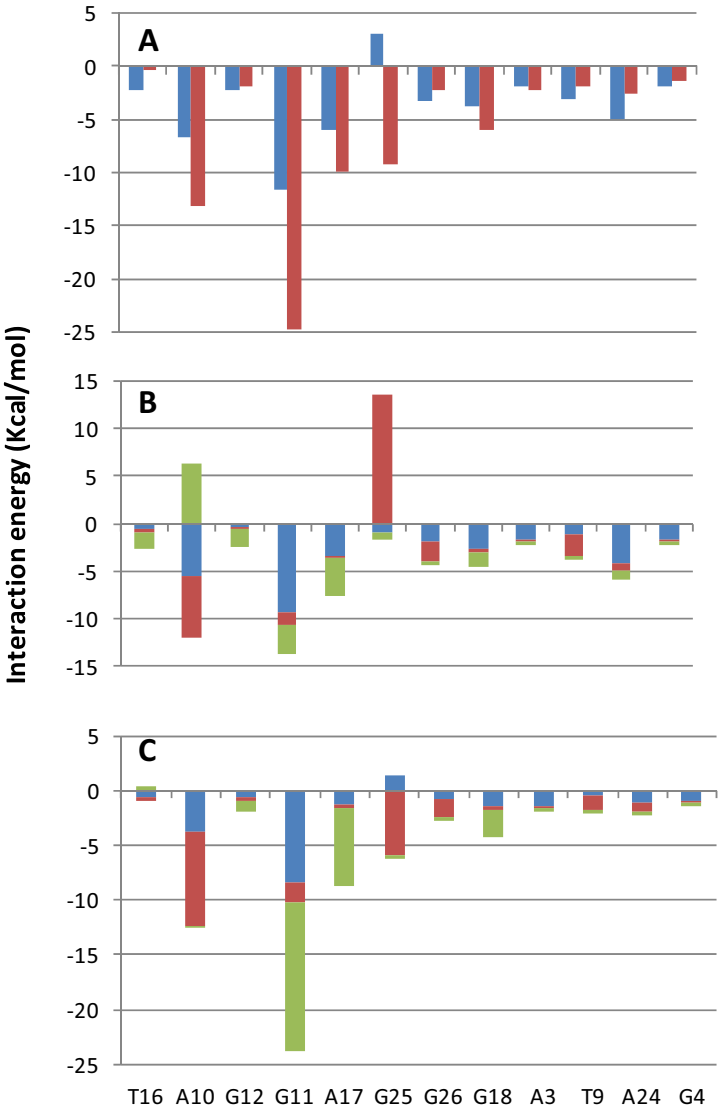

Structure and stability of human telomeric G-quadruplex with preclinical 9-amino acridines

Supporting Information

Figure 1S. ^{1}H NMR spectra (15-12 ppm and 9.0-5.5 ppm) showing resonance of imino and aromatic and ribose H1' protons region at different R = [**1**]/[d(CGATCG)]$_2$.

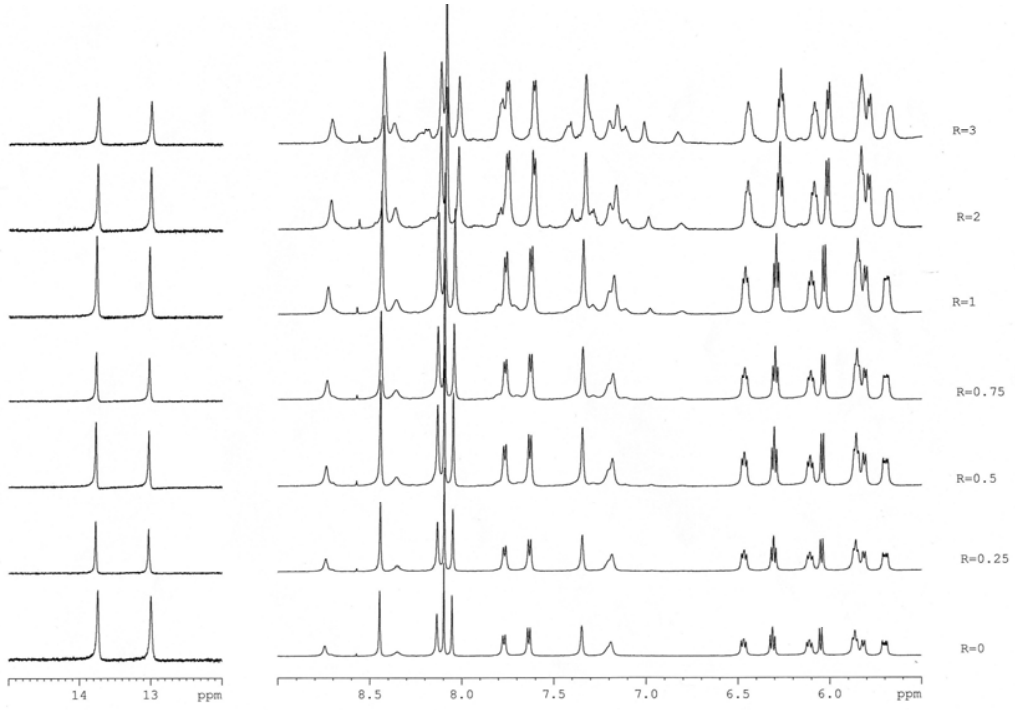

Figure 2S. ^{1}H NMR spectra (15-12 ppm and 10-5.5 ppm) showing resonance of imino and aromatic and ribose H1' protons region at different R = [**1**]/[d(GCGATCGC)]$_2$

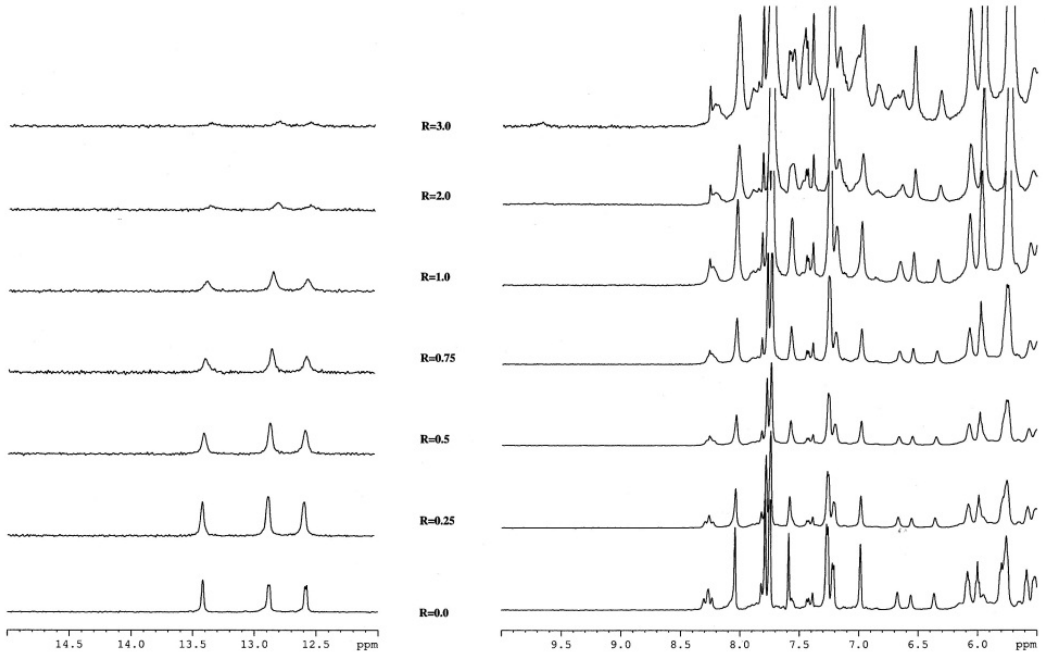

Figure 3S. ^{1}H NMR spectra (15-12 ppm and 10-5.5 ppm) showing resonance of imino and aromatic and ribose H1' protons region at different R = [**1**]/[d(AAGAATTCTT)$_2$]

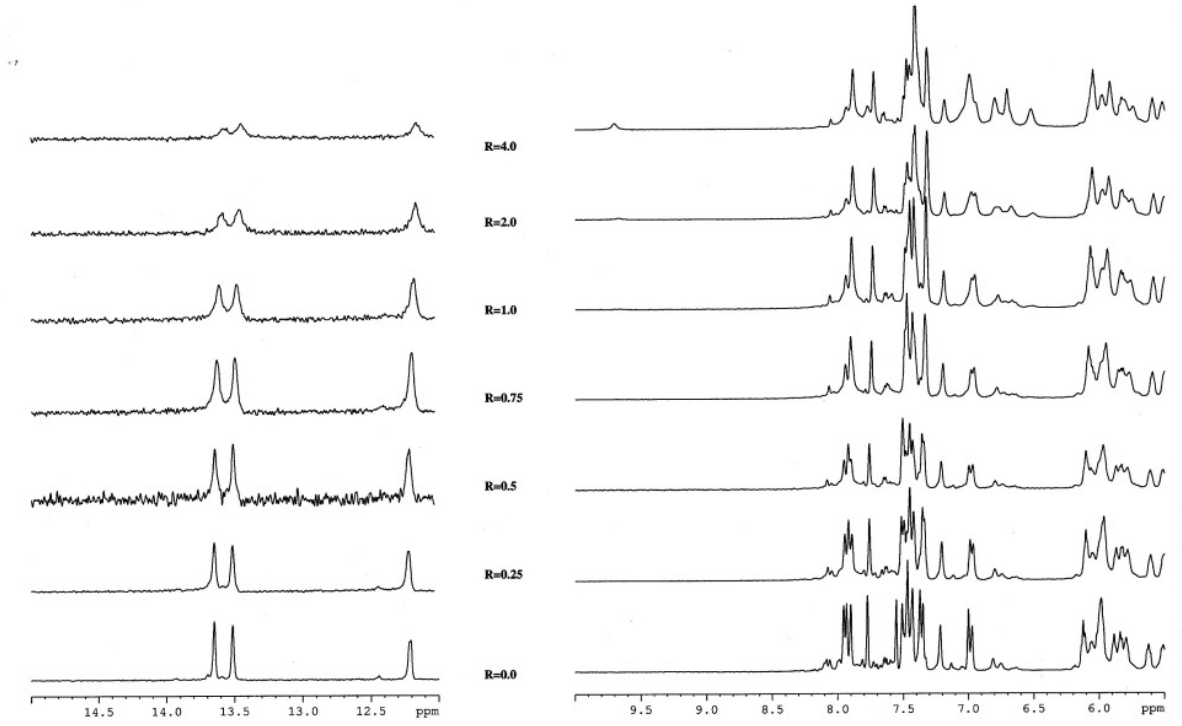

Figure 4S. ^{1}H NMR spectra showing NH of indole moiety and aromatic protons of **1** in the free state (R = [d(AAGAATTCTT)$_2$] /[**1**]=0) and at different R. High and low R values must be related to the free and bound state of DMF1 in solution respectively.

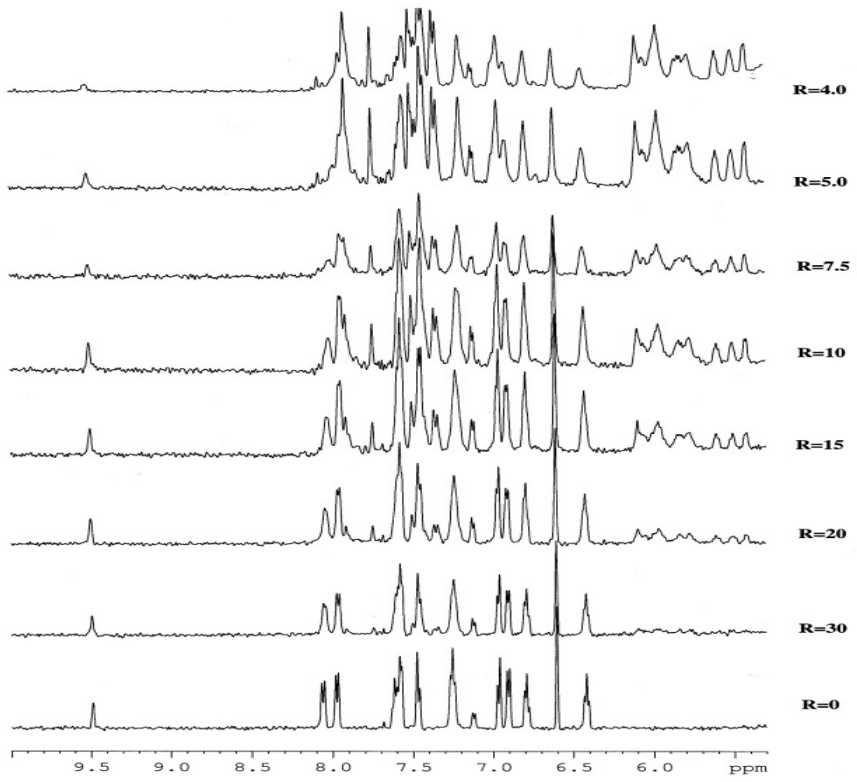

Figure 5S. Fluorescence titration spectra. Fluorescence spectra of a 1 M solution of 1 (left) and 2 (right) after the addition of increasing amounts of Htel (from 0 to 25 μM) in potassium phosphate buffer. Excitation wavelength is 265 nm.

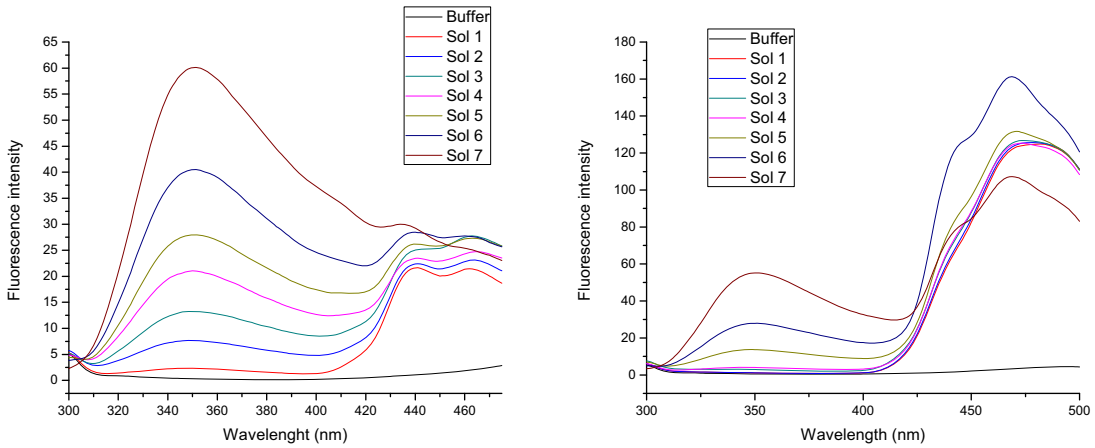

Figure 6S. Time dependence of the RMSD of heavy atoms of complete G-quadruplex (blue) with ligand atoms (**1** and **2** are shown in red and green, respectively) at 298 K.

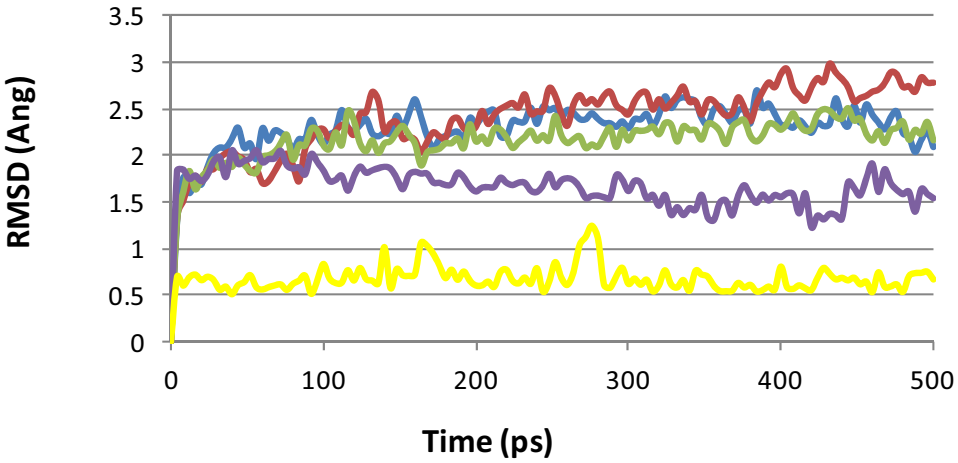

Figure 7S. Time dependence of the RMSD of ligand **1** and **2** on the complex (cyan and yellow, respectively) and A and G-quartet heavy atoms (blue) with ligand atoms (**1** and **2** are shown in red and green, respectively) at 400K.

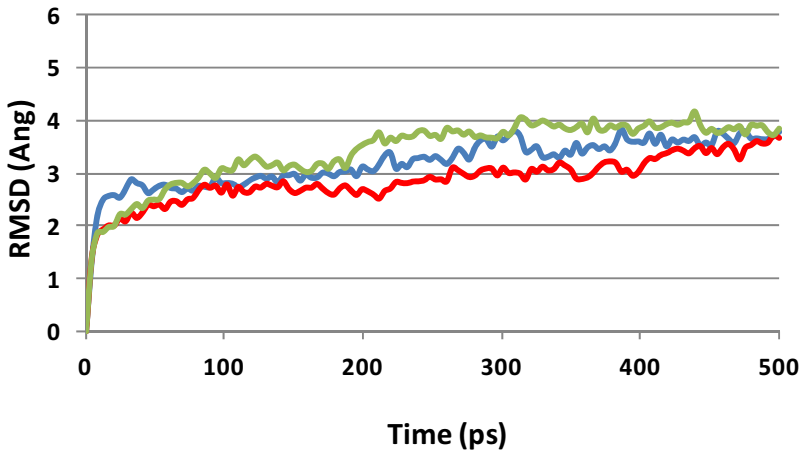

Figure 8S. Time dependence of the RMSD of ligand **1** and **2** on the complex (cyan and yellow, respectively) and A and G-quartet heavy atoms (blue) with ligand atoms (**1** and **2** are shown in red and green, respectively) at 500K.

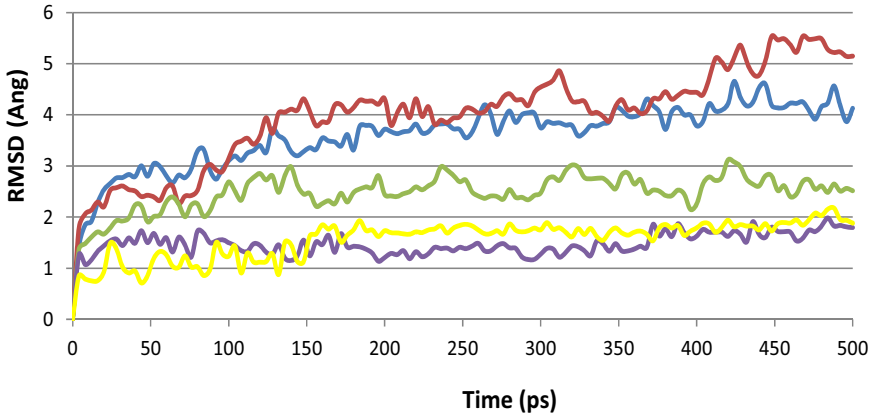

Table 1S. Selected ^{1}H chemical shift assignments for ds24 (δ) in the presence of **1**[a]

ds24/1	H2/H8/H6	H1'	NH/H5/CH_3
A1	7.74,	5.60	-
A2	7.89,	5.52	-
G3	7.50	5.16	-
A4	7.88,	5.79	-
A5	7.94,	5.97	-
T6	6.96	5.96	1.07
T7	7.20	5.73	1.33
C8	7.38	5.82	5.39
T9	7.31	5.93	1.54
T10	7.34	6.05	1.54
G3C8			12.13
A4T7			13.58
A5T6			13.42

[a] Measured in ppm at 15°C, *R* = [drug]/[DNA] = 4.0

4

SÍNTESIS D'OLIGÒMERS D'ACRIDINA I LES SEVES PROPIETATS D'UNIÓ A QUÀDRUPLEX DE GUANINA

SÍNTESIS D'OLIGÒMERS D'ACRIDINA I LES SEVES PROPIETATS D'UNIÓ A QUÀDRUPLEX DE GUANINA

Synthesis and G-Quadruplex-binding properties of defined acridine oligomers.

Rubén Ferreira,[1] Anna Aviñó,[1] Ricardo Pérez-Tomás,[2] Raimundo Gargallo,[3] and Ramon Eritja[1]

Journal of Nucleic Acids, volume 2010, article ID 489060, 10 pages

[1] *Institute for Research in Biomedicine, IQAC-CSIC, CIBER-BBN Networking Centre on Bioengineering, Biomaterials and Nanomedicine, Edifici Helix, Baldiri Reixac 15, 08028 Barcelona, Spain*
[2] *Cancer Cell Biology Research Group, Department of Pathology and Experimental Therapeutics, Faculty of Medicine, University of Barcelona Campus Bellvitge, Feixa Llarga, L'Hospitalet de Llobregat, 08907 Barcelona, Spain*
[3]*Department of Analytical Chemistry, University of Barcelona, Diagonal 647, 08028 Barcelona, Spain*

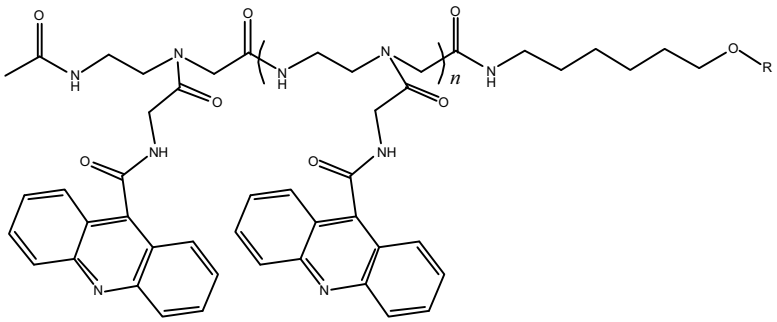

Resum

Es descriu la síntesis d'oligòmers amb dos o tres unitats d'acridina unides mitjançant la 2-aminoetiglicina, utilitzant una metodologia en fase sòlida. Estudis de viabilitat cel·lular mostren que aquests compostos no són citotòxics. S'ha estudiat la unió a diferents estructures de DNA per diàlisi competitiva i s'observa una clara afinitat per seqüències de DNA que formen G-quàdruplex i tríplex paral·lel. Els espectres de fluorescència d'aquests oligòmers d'acridina es veuen fortament afectats quan s'uneixen amb el DNA. Aquests canvis en l'espectre es van utilitzar per calcular les constants d'afinitat (K). Els logaritmes d'aquestes constants estan en el rang de 4-6.

SAGE-Hindawi Access to Research
Journal of Nucleic Acids
Volume 2010, Article ID 489060, 10 pages
doi:10.4061/2010/489060

Research Article

Synthesis and G-Quadruplex-Binding Properties of Defined Acridine Oligomers

Rubén Ferreira,[1] Anna Aviñó,[1] Ricardo Pérez-Tomás,[2] Raimundo Gargallo,[3] and Ramon Eritja[1]

[1] *Institute for Research in Biomedicine, IQAC-CSIC, CIBER-BBN Networking Centre on Bioengineering, Biomaterials and Nanomedicine, Edifici Helix, Baldiri Reixac 15, 08028 Barcelona, Spain*
[2] *Cancer Cell Biology Research Group, Department of Pathology and Experimental Therapeutics, Faculty of Medicine, University of Barcelona Campus Bellvitge, Feixa Llarga, L'Hospitalet de Llobregat, 08907 Barcelona, Spain*
[3] *Department of Analytical Chemistry, University of Barcelona, Diagonal 647, 08028 Barcelona, Spain*

Correspondence should be addressed to Ramon Eritja, recgma@cid.csic.es

Received 14 January 2010; Revised 22 March 2010; Accepted 13 April 2010

Academic Editor: Daniela Montesarchio

Copyright © 2010 Rubén Ferreira et al. This is an open access article distributed under the Creative Commons Attribution License, which permits unrestricted use, distribution, and reproduction in any medium, provided the original work is properly cited.

The synthesis of oligomers containing two or three acridine units linked through 2-aminoethylglycine using solid-phase methodology is described. Subsequent studies on cell viability showed that these compounds are not cytotoxic. Binding to several DNA structures was studied by competitive dialysis, which showed a clear affinity for DNA sequences that form G-quadruplexes and parallel triplexes. The fluorescence spectra of acridine oligomers were affected strongly upon binding to DNA. These spectral changes were used to calculate the binding constants (K). Log K were found to be in the order of 4–6.

1. Introduction

Small organic molecules with specific interactions with DNA have become antitumor, antiviral, and antibiotic drugs [1, 2]. Duplex DNA-binding drugs interact in two main ways, through groove binding and through intercalation. Medicinal chemistry has made a considerable effort in searching for and testing of a large number of drugs with increased selectivity to a range of DNA sequences or structures. More recently, some of this interest has moved to the search of new ligands for G-quadruplexes [3]. This structure motif is formed by the planar association of four guanines in a cyclic Hoogsteen hydrogen bonding tetrad.

Guanine-rich sequences form G-quadruplex structures and have been found in telomeres [4] and in transcriptional regulatory regions of critical oncogenes such as *c-myc* and *c-kit* [5, 6]. Ligands that selectively bind and stabilize these structures have become anticancer drugs of interest [7].

The G-quadruplex stabilization occurs in most cases by π-π stacking and electrostatic interaction. G-quadruplex ligands are normally planar aromatic molecules that are prone to stacking with G-tetrads. Some of them are also positively charged or have hydrophilic groups to favor electrostatic interaction [8].

Although there is a long way to go in the development of potent drugs that target G-quadruplexes, some promising lead compounds have been achieved [9]. Several ligand structures have been studied, such as anthraquinones, cationic porphyrins, perylene derivatives, and a large number of compounds [9]. Among the acridine compounds, 3,6,9-trisubstituted acridines have inhibitory activity in the nanomolar range and they have entered preclinical studies [8, 10, 11].

In previous studies we described the preparation of sequence specific oligomers of DNA-intercalating drugs using protocols based on solid-phase synthesis in an attempt to facilitate the preparation of compounds with improved DNA-binding selectivity [12, 13]. It has been proposed that bis- and tris-intercalating drugs show promising activity and selectivity [14, 15]. Here we described solid-phase synthesis protocols for the preparation of several acridine oligomers linked through 2-aminoethylglycine units as well as their DNA-binding properties. Although the acridine derivatives described in this study are not cytotoxic, they show a clear

Table 1: Sequences of oligonucleotides.

No.	Name	Sequence (5′–3′)
1	T20	TTT TTT TTT TTT TTT TTT TT
2	24bclc	CCC GCC CCC TTC CTC CCG CGC CCG
3	Dickerson	CGC GAA TTC GCG
4	Ds26	CAA TCG GAT CGA ATT CGA TCC GAT TG
5	GA triplex	GAA AGA GAG GAG GCC TTT TTG GAG GAG AGA AAG + CCT CCT CTC TTT C
6	TC triplex	CCT CCT CTC TTT CCC TTT TTC TTT CTC TCC TCC + GAA AGA GAG GAG G
7	TG4T	TGG GGT
8	TBA	GGT TGG TGT GGT TGG
9	HT24	TAG GGT TAG GGT TAG GGT TAG GGT
10	24bcl	CGG GCG CGG GAG GAA GGG GGC GGG
11	cmyc	GGG GAG GGT GGG GAG GGT GGG GAA GGT GGG G

affinity for several DNA G-quadruplex structures, especially those sequences found in the promoter regions of *c-myc* [16] and *bcl*-2 [17, 18] oncogenes.

2. Materials and Methods

2.1. Chemicals. The phosphoramidites and ancillary reagents used during oligonucleotide synthesis were obtained from Applied Biosystems (USA) and Link Technologies Ltd. (Scotland). The rest of the chemicals were purchased from commercial sources. The Slide-A-Lyzer Mini Dialysis Units 3500 MWCO were purchased from Pierce. Acridine-9-carboxylic acid was obtained from Aldrich. 2-(Acridine-9-carboxamide)acetic acid was prepared by reaction of acridine-9-carboxylic acid with glycine methyl ester and subsequent saponification of the methyl ester as described [10]. Boc-(2-aminoethyl)glycine(Fmoc) (Boc-Aeg(Fmoc)-OH) was obtained from Iris Biotech and Fmoc-glycine (Fmoc-Gly-OH) was obtained from Bachem. Boc-6-aminohexyl hemisuccinate was prepared by reaction of Boc-6-aminohexanol with succinic anhydride.

2.2. Oligonucleotide Synthesis. Oligonucleotide sequences (Table 1) were prepared on an automatic Applied Biosystems 3400 DNA synthesizer on 1 μmoL (CPG resin) scale using commercially available 2-cyanoethyl phosphoromidites. After the assembly of the sequences, oligonucleotide-supports were deprotected using 32% aqueous ammonia at 55°C for 16 h. Ammonia solutions were concentrated to dryness and the residue was desalted by a NAP-10 (*Sephadex G-25*) column.

2.3. Solid-Phase Synthesis of Acridine Oligomers. Acridine dimers and trimers (**1–4**, Figure 1) were prepared with the 2-aminoethylglycine scaffold, which allows the growth of a polyamide skeleton on solid-phase and the following incorporation of acridine unit.

The assembly of 2-aminoethylglycine derivatives was carried out on methylbenzhydrylamine (MBHA) polystyrene-1%-divinylbenzene solid support applying an Fmoc/Boc hybrid strategy using Boc-Aeg(Fmoc)-OH, Fmoc-Gly-OH, and acridine-9-carboxylic acid as building blocks (Figure 2).

Fmoc-Sarcosine-OH (5 eq) was coupled to the resin using standard coupling conditions (5 eq. PyBOP and 10 eq. DIEA, 1 h), then the Fmoc group was removed (20% of piperidine in DMF, 30 min), and Boc-6-aminohexyl hemisuccinate (Boc–NH–$(CH_2)_6$–$OCOCH_2CH_2COOH$) was coupled (5 eq R-COOH, 5 eq. PyBOP and 10 eq. DIEA, 1 h) to the support. The residual unreacted amino groups were acetylated with 5 eq. of acetic anhydride and 5 eq. of DIEA.

Next, the Boc group was removed (40% trifluoroacetic acid in dichloromethane) and the 2-aminoethylglycine skeleton was synthesized by repetitive couplings of Boc-Aeg(Fmoc)-OH until reaching the desired dimer or trimer compound. The last Boc group of the sequence was removed and the resulting amino group was acetylated (5 eq. acetic anhydride and 5 eq. DIEA).

Once the aminoethylglycine backbone was built, the Fmoc-protecting groups of the side chains were removed (20% of piperidine in DMF, 30 min), and Fmoc-Gly-OH followed by 9-acridine carboxyl acid was coupled to the support. The progress of the coupling reactions was followed by ninhydrine test and by UV monitoring of the 9-methylene-9H-fluorene released during deprotection, which allowed optimization of the coupling conditions.

The acridine dimer **1** and trimer **3** were obtained by treatment of the appropriate solid supports with HF anhydrous at 0°C. Finally the acridine dimer **2** and trimer **4** were obtained by treatment of dimer **1** and trimer **3** respectively with 32% aqueous ammonia (1 h, 55°C).

Good yields and purities were obtained for the products (around 85% for **1** and **2,** 75% for **3** and **4**). HPLC and MALDI-TOF spectra are shown in Supplementary Material available onlie at doi: 10.4061/2010/489060.

The compounds were analyzed by MALDI-TOF, **1** $[M+Na^+]$ = 1080.3 (expected 1054.2), **2** [M] = 885.2 (expected 884.0), **3** [M] = 1418.9 (expected 1416.5), and **4** [M] = 1247.4 (expected 1246.4). MALDI-TOF spectra were obtained using a *Perseptive* Voyager DETMRP mass spectrometer, equipped with nitrogen laser at 337 nm using a 3 ns pulse. The matrix used contained 2,5-dihydroxybenzoic acid (DHB, 10 mg/mL in water).

Analytical HPLC was performed using XBridge OST C_{18} (*Waters*), 2.5 μm, 4.6 × 50 mm column using a 10-minute

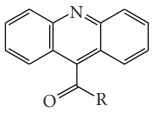

R = OH, acridine-9-carboxylic acid
R = $NHCH_2COOH$, 2-(acridine-9-carboxamide) acetic acid

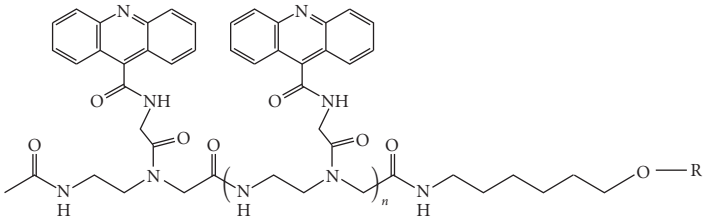

Dimer **1** R = $CO–CH_2CH_2CONH(CH_3)CH_2CONH_2$, $n = 1$
Dimer **2** R = H, $n = 1$
Trimer **3** R = $CO–CH_2CH_2CONH(CH_3)CH_2CONH_2$, $n = 2$
Trimer **4** R = H, $n = 2$

Figure 1: Structure of the acridine derivatives prepared.

linear gradient from 9% to 45% B, flow rate 1 mL/min; solution A was 5% ACN in 0,1 M aqueous TEAA, and B 70% ACN in 0.1M aqueous TEAA. HPLC chromatograms and MS spectra can be found in Supplementary Material.

Fluorescence spectra were recorded using a Jasco FP-6200 spectrofluorometer equipped with a Peltier temperature controller, $\lambda_{em} = 435$ nm ($\lambda_{exc} = 252$ nm).

UV spectra were recorded using a Jasco spectrophotometer V-650, $\lambda_{max} = 252$ nm, 360 nm.

2.4. Cell Viability Assays. The *in vitro* cytotoxicity of the compounds (Figure 1) was evaluated by colorimetric assays with tetrazole salts (MTT) on Jurkat clone E6-1 (human leukemia), GLC-4 clone (human lung carcinoma) cell lines, and one mouse fibroblast cell line (NIHT-3T3).

GLC4 and Jurkat cell lines were cultured in RPMI and NIH3T3 in DMEM and supplemented with 10% fetal calf serum, 10000 u/mL penicillin, 10 μg/mL streptomycin and 200 mM L-glutamine. Cells were grown in a humidified atmosphere of air containing 5% CO_2 at 37°. Cells were plated in triplicate wells ($1.5 \cdot 10^4$ cells well) in 100 μL of growth medium in 96-well plates and proliferate for 24 h and then treated with increasing concentrations of acridine oligomers. After 72 h of incubation, 10 μM of MTT (5 mg/mL in Phosphate buffer saline 10%) was added for an additional 4 h. The absorbance at 570 nm was measured on a multiwell plate reader after addition of 100 μl of isopropanol : 1N HCl (24 : 1). Cell viability was expressed as a percentage of control and IC_{50} was determined as the concentration of drug that produced a 50% reduction of absorbance at 570 nm.

2.5. Competitive Dialysis Assays. 100 μL of a 50 μM oligonucleotide (Table 1) in potassium phosphate buffer (185 mM NaCl, 185 mM KCl, 2 mM NaH_2PO4, 1 mM Na_2EDTA, 6 mM Na_2HPO_4 at pH 7) was introduced into a separated dialysis unit. A blank sample containing only buffer without oligonucleotide was also prepared. All 12 dialysis units were then placed in the beaker containing the 1 μM solution of the appropriate acridine derivative. The samples were allowed to equilibrate with continuous stirring at room temperature overnight. After the equilibration period, DNA samples were removed to an Eppendorf tube. SDS is usually added to denature the DNA sample and release the acridine oligomer, but in our case the presence of K^+ ions induced the formation of a white precipitate, which interfered with the measurement of the fluorescence spectra of the samples.

In order to measure the compound retained in the dialysis unit, samples were treated with snake-venom phosphodiesterase to degrade the DNA and release the acridine oligomer. 350 μL of potassium phosphate buffer (without EDTA), buffer at pH 8.5, 50 μL of 100 mM $MgCl_2$, and 1 μm of snake venom phosphodiesterase solution were added for an additional overnight incubation at 37°C. Finally, the fluorescence of each sample was measured (λ_{ex} and λ_{em} were set to 252 and 435 nm, resp.).

2.6. Fluorescence Assays. The study of the interaction equilibrium of acridine derivatives and oligonucleotides consists of recording the fluorescence spectra of a 0.2 μM solution of the acridine derivative after the addition of increasing amounts of oligonucleotide (from 0 to 10 μM) in potassium phosphate buffer (185 mM NaCl, 185 mM KCl, sodium phosphate, 1 mM EDTA, pH 7). These experiments were carried out by adding small volumes of an oligonucleotide stock solution to the 0.2 μM solution of the acridine derivative. After 24 h the emission spectra of the resulting solutions were recorded from 300 to 500 nm at 252 nm excitation wavelength at 25°C.

The macroscopic binding constant (K) corresponding to the reaction

$$\text{DNA} + \text{ligand} \rightleftharpoons \text{Interaction complex} \quad (1)$$

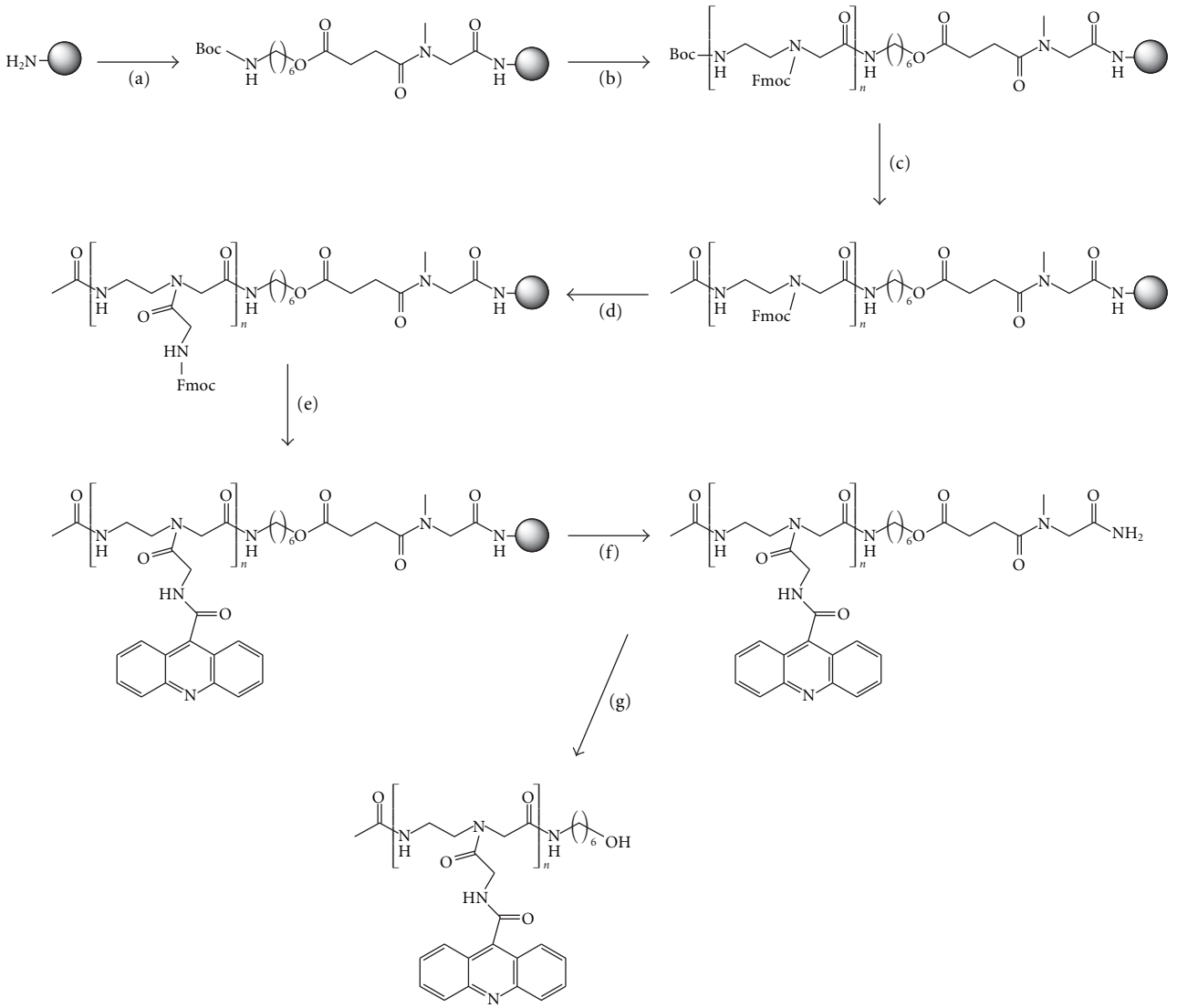

Figure 2: Solid-phase synthesis of dimer and trimer acridine derivatives. (a) (i) Fmoc-Sar-OH, PyBOP, DIEA; (ii) 20% piperidine, DMF; (iii) Boc–NH–$(CH_2)_6$–OCH_2CH_2COOH, PyBOP, DIEA; (b) (i) 40% TFA, DCM; (ii) Fmoc-Aeg(Boc)-OH, PyBOP, DIEA; (iii) Repeat steps (i) and (ii) *n* times; (c) (i) 40% TFA, DCM; (ii) Ac_2O, DIEA, DMF; (d) (i) 20% piperidine, DMF; (ii) Fmoc-Gly-OH, PyBOP, DIEA; (e) (i) 20% piperidine, DMF; (ii) acridine-9-carboxylic acid, PyBOP, DIEA; (f) anhydrous HF (0°); (g) 32% aqueous NH_3.

was calculated from the multivariate analysis of fluorescence data recorded in the range 300–390 nm using the hard-modeling program Equispec [19]. This program performs a nonlinear least squares optimization of K and of the pure fluorescence spectra corresponding to each of the species considered (DNA, ligand, and interaction complex). A 1 : 1 stoichiometry DNA : ligand for the interaction complex was assumed. The logarithms of the binding constants calculated are given as their weighted means with twice their standard errors (units of the least significant digit). Results are shown in Table 2.

2.7. Circular Dichroism. An increasing amount of **1** (from 0 to 8 μM) in potassium phosphate buffer (185 mM NaCl, 185 mM KCl, sodium phosphate, 1 mM EDTA, pH 7) was added to a 1 μM solution of the oligonucleotide. The CD spectra were recorded after 24 h on a Jasco J-810 spectropolarimeter attached to a Julabo F/25HD circulating water bath in 1 cm path-length quartz cylindrical cells, using a 50 nm/min scan rate, a spectral band width of 1 nm, and a time constant of 4 s. All the spectra were corrected with the buffer blank, normalized to facilitate comparisons and noise-reduced using Matlab software. CD spectra are shown as supplementary data.

3. Results and Discussion

3.1. Synthesis of Acridine Oligomers. The synthesis of acridine dimer and trimers has been described previously [13] using a Boc-(2-aminoethyl)glycine derivative carrying the

Table 2: Logarithm of the binding constants (log K) calculated from data recorded throughout fluorescence titrations using Equispec program assuming a 1 : 1 stoichiometry DNA : ligand for the interaction complex (details in materials and methods). Compounds 1–4 correspond to the acridine dimers and trimers prepared in this study. HT24, 24bcl, cmyc, and Dickerson correspond to oligonucleotide sequences shown in Table 1.

	1	**2**	**3**	**4**
HT24	4.9 ± 0.4	4.6 ± 0.5	5.3 ± 0.3	n.d.
24bcl	6.8 ± 0.5	5.1 ± 0.1	5.3 ± 0.2	n.d.
cmyc	5.5 ± 0.3	4.9 ± 0.2	4.8 ± 0.5	5.3 ± 0.2
Dickerson	n.d.	n.d.	n.d.	n.d.

n.d. not determined.

2-(acridine-9-carboxamide)acetyl residue. The synthesis of this monomer was long and yields were low.

An alternative method developed is to first assemble the Boc-(2-aminoethyl)glycine backbone on solid-phase, and then the intercalating agent is added. This strategy is more convenient for rapid synthesis, as it is unnecessary to construct each intercalating monomer.

Thus, acridine oligomers were assembled using the methylbenzhydrylamine (MBHA) resin by applying an Fmoc/Boc hybrid strategy and using Boc-(2-aminoethyl)-(Fmoc)glycine [Boc-Aeg(Fmoc)-OH] as building block (Figure 2). The Boc group was used to protect the aminoethyl group of each unit, which thus facilitated elongation of the backbone. Fmoc was the semipermanent protecting group for the amino group of glycine through which the intercalating compound was introduced. The succinyl linker was selected to connect the solid support and the oligomer. This linker is used in oligonucleotide synthesis and it is labile to ammonia. Unfortunately, the linker is not compatible with Fmoc chemistry. It has been described that an intramolecular side reaction can lead to premature loss of the oligomers during the base treatment used to remove the Fmoc group [20]. Thus, *N*-methylglycine (sarcosine) was incorporated between the amino-support and the succinyl linker. The presence of the *N*-methyl group prevents the potential side reaction [20]. 6-Aminohexanol was used to connect the succinyl linker and the oligomer backbone, as described for the synthesis of peptide nucleic acid (PNA) oligomers [21].

The (2-aminoethyl)glycine backbone was assembled by consecutive additions of Boc-Aeg(Fmoc)-OH to obtain the dimer and trimer sequence. Acetylation of the *N*-terminal position was carried out using acetic anhydride and a base.

Next, the removal of the Fmoc group allowed the addition of a Fmoc-glycine unit as a spacer, which was followed by the addition of acridine-9-carboxylic acid. The acridine dimer and trimer were synthesized in this way (Figure 2).

After assembly of the oligomers, the resulting supports were treated with ammonia. The desired oligomers were not released from the support even after prolonged time and high temperatures. We therefore treated the supports with anhydrous HF to yield the acridine oligomers **1** and **3**, which contain the sarcosyl succinyl linker. At this point HPLC spectra showed a major peak that had the expected molecular weight for the oligomers **1** and **3** carrying the sarcosyl succinyl linker (see supplementary data). This observation indicates that the simultaneous incorporation of all acridines proceeded with excellent yields. Ammonia treatment of acridines **1** and **3** in solution now yielded the desired acridine dimer **2** and trimer **4** in excellent yields and purity (see supplementary data). Compounds **1–4** were fully characterized and their properties were analyzed.

The pKa of the acridine ring of acridine-9-carboxylic acid and 2-(acridine-9-carboxamide)acetic acid was measured by UV titration. pKa of acridine-9-carboxylic acid was 5.5 ± 0.1 and 2-(acridine-9-carboxamide)acetic acid 4.1 ± 0.2. We therefore estimated that the acridine rings of compounds **1–4** are mainly unprotonated at pH 7.0.

3.2. Cell Viability Assay. The *in vitro* cytotoxicity of the compounds was evaluated by colorimetric assays with tetrazole salts (MTT). This assay is based on the capacity of living cells to incorporate and reduce MTT. This reaction can be followed by the change of absorbance of the reduced and oxidized forms. This reaction is done by the action of the mitochondrial enzyme succinatehydrogenase, which is active only in living cells. The intensity of color is directly correlated with the number of living cells in the sample. No cytotoxicity activity was observed in compounds **1–4** at concentrations up to 50 μM.

3.3. Competitive Dialysis Studies. In order to evaluate the selectivity of the compounds for DNA structures, a competitive dialysis experiment was performed using 11 oligonucleotides (Table 1) representing several nucleic acid structures [22]. The more acridine accumulated in the dialysis unit indicates a higher binding affinity to the oligonucleotide present in the dialysis unit. As model for single stranded structures we used T_{20} and the C-rich complementary strand of *bcl-2* (24bclc). This last oligonucleotide folds in an *i*-form quadruplex structure at acidic pH but has no structure in the conditions used in the dialysis (pH 7) [18]. As duplexes we used the self-complementary sequences *Dickerson-Drew* dodecamer (Dickerson) and a 26 mer (ds26). A parallel triplex (TC triplex) and an antiparallel triplex (GA triplex) were also prepared by mixing a hairpin Watson-Crick sequence and the corresponding triplex-forming sequence. Finally, the following G-quadruplex sequences were prepared: the tetramolecular parallel G-quadruplex TG_4T [23], the antiparallel thrombin-binding aptamer (TBA) [24], the human telomere sequence (HT24) [25], and the promoter sequences of *c-myc* (cmyc) [16] and *bcl*-2 (24bcl) [17, 18].

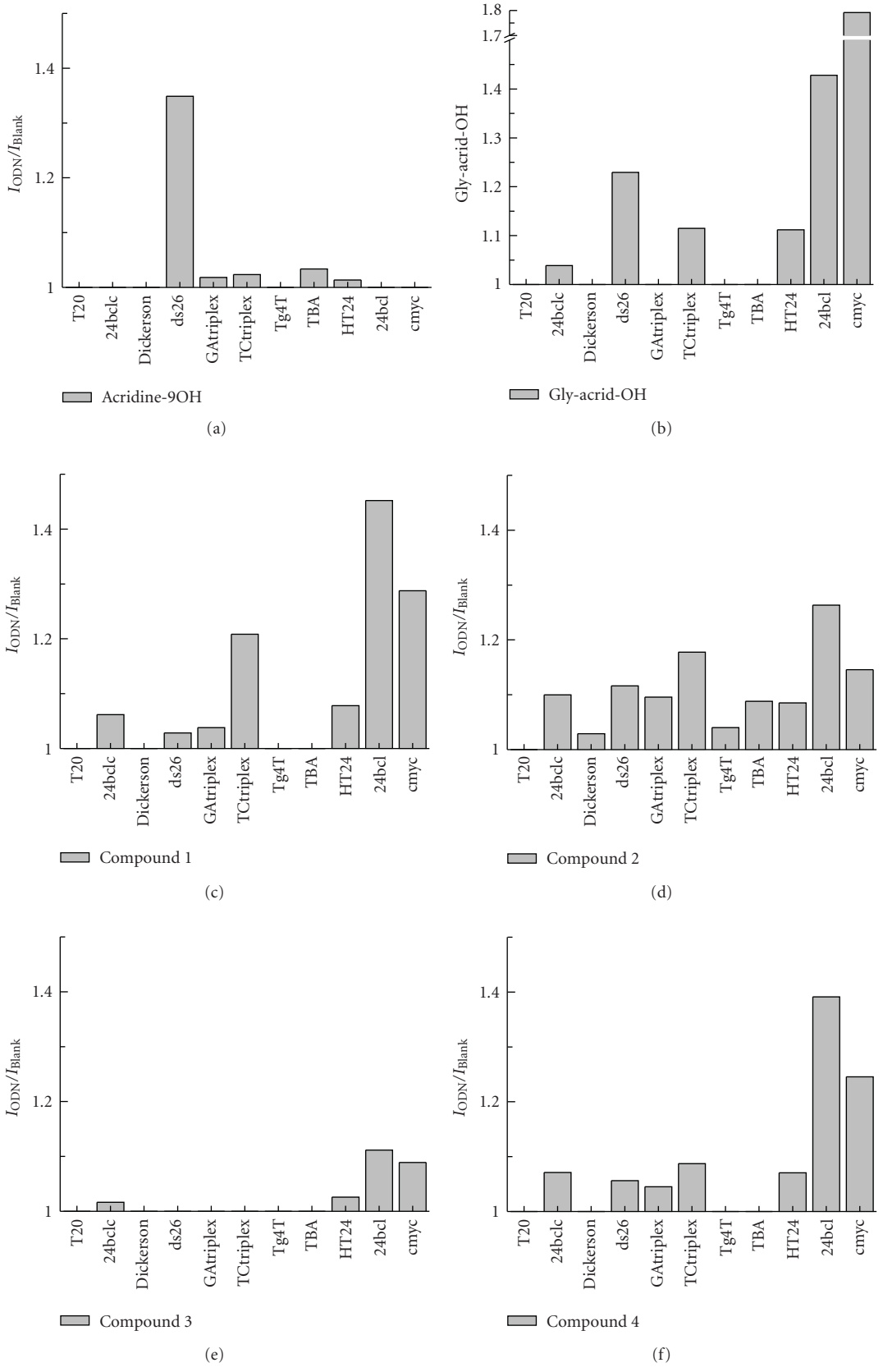

Figure 3: Results obtained by the competitive dialysis assay. The amount of ligand bound to each DNA structure is shown as a bar graph. The fluorescence of each sample was measured using an excitation wavelength of 252 nm and an emission wavelength of 435 nm, respectively.

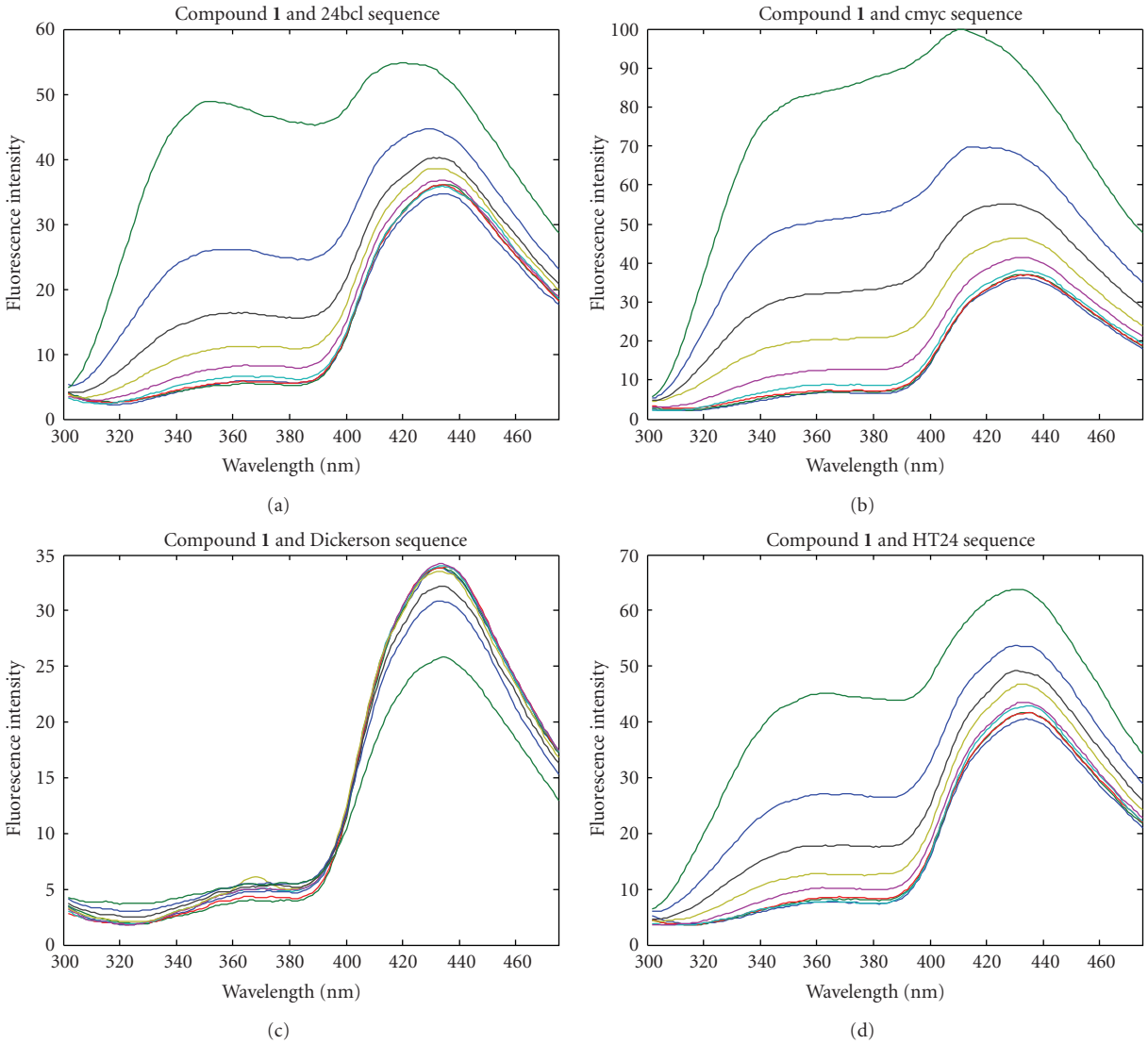

FIGURE 4: Fluorescence titration spectra. Fluorescence spectra of a 0.2 μM solution of the acridine derivative after the addition of increasing amounts of oligonucleotide (from 0 to 10 μM) in potassium phosphate buffer. Excitation wavelength is 252 nm.

We used the protocol described by Ren and Chaires [26] with a few modifications. The buffer solution was similar to that described in [26] but K^+ was included (185 mM) to ensure the formation of the most stable G-quadruplex structures. At the end of the dialysis experiment, the amount of acridine derivative bound to the DNA was analyzed by fluorescence measurement of the acridine compound. After dialysis, we observed that the spectra of the acridine derivatives of some samples (especially those from G-quadruplexes) differed greatly from the fluorescence spectra of the initial compounds. This difference is attributed to the interaction of the acridine derivatives with the G-quadruplex. In order to release the acridine oligomer, the addition of SDS is recommended [26, 27]. Using SDS, the presence of K^+ ions resulted in the formation of a white precipitate with SDS which did not allow the measurements of the fluorescence spectra [27]. In order to solve this problem, the oligonucleotide was digested with snake venom phosphodiesterase at the end of the dialysis experiment. Thus, the fluorescence spectra of the acridine derivatives were recorded with high accuracy without the interference of DNA and without the use of SDS.

We measured the binding preferences of compounds **1–4** and the acridine monomers acridine-9-carboxylic acid and 2-(acridine-9-carboxamide)acetic acid (Figure 1). Acridine-9-carboxylic acid showed affinity only for duplex ds26 (Figure 3). Unexpectedly, the addition of the glycine residue, used as spacer, induced a change in the affinity. 2-(Acridine-9-carboxamide)acetic acid showed the highest affinity for the G-quadruplex sequences cmyc and 24bcl and less affinity for duplex ds26.

Dimer **1** (dimer with the sarcosylsuccinyl linker) has a similar profile as 2-(acridine-9-carboxamide)acetic acid. In this case, the G-quadruplex 24bcl is preferred to the cmyc

sequence. Some affinity for the TC triplex is observed but no affinity for duplex ds26. Surprisingly, dimer **2** (without the sarcosylsuccinyl linker) lost most of the selectivity although some residual higher affinity for G-quadruplex 24bcl was observed.

In contrast, trimer **3** (trimer with the sarcosylsuccinyl linker) presented lower binding affinity than the other compounds. However, trimer **4** (without the sarcosylsuccinyl linker) recovered most of the affinity for 24bcl and cmyc showing a similar profile to that observed for dimer **1**.

3.4. Measurement of G-Quadruplex-Affinity Constants by Fluorescence Spectroscopy. Dialysis experiments suggest that some of the acridine derivatives prepared have special affinity for 24bcl and cmyc G-quadruplexes. In order to confirm this observation, binding constants were estimated using mole-ratio experiments monitored with fluorescence spectroscopy. Hence, increasing amounts of oligonucleotides 24bcl, HT24, cmyc, and Dickerson were added to a solution with a fixed concentration of the acridine derivatives, and the fluorescence spectra were recorded at excitation wavelengths 252 and 360 nm.

At both wavelengths, changes in the fluorescence spectra upon the addition of oligonucleotides were observed. Figure 4 shows the changes in the fluorescence spectra of acridine dimer **1** at excitation wavelengths 252 nm when oligonucleotides 24bcl, HT24, cmyc, and Dickerson were added. A dramatic increase in fluorescence intensity was observed around 360 nm upon addition of G-quadruplex DNA sequences (24bcl, HT24, and cmyc). The greatest changes were seen with 24bcl and cmyc. Similar results were found with compounds **2**, **3**, and **4** as well as 2-(acridine-9-carboxamide)acetic acid (see supplementary data). Interestingly, when the Dickerson dodecamer was added, no changes in the fluorescence spectra were detected. The progressive modification of the fluorescence spectrum of these compounds reflects their interaction with the G-quadruplex.

Fluorescence data obtained at an excitation wavelength of 252 nm were analyzed with the hard-modelling EQUISPEC program in order to calculate the corresponding binding constants (Table 2). The values of the logarithm of the binding constant ($\log K$) obtained lie in the range 4–6, suggesting a weak interaction with DNA. Of all the compounds, dimer **1** showed the highest binding constants, thereby suggesting a stronger interaction with DNA than the other compounds studied. However these values were slightly lower than the binding constants calculated for other similar ligands, such as the acridine monomers BRACO-19 ($\log K = 7.4$) and BSU6048 ($\log K = 6.5$) [28] or a hemicyanine-peptide ligand ($\log K = 7.1$ [29]), when interacting with human telomere quadruplex.

Changes in the fluorescence spectra at an excitation wavelength of 360 nm were also recorded. Fluorescent emission at this wavelength 360 nm was much lower than that recorded at 252 nm; so the fluorescent signal was low. Upon addition of the oligonucleotide to a solution of compounds **1**–**4**, the formation of a new maximum at 442 nm was observed (see supplementary data). Although the fluorescent intensity was low, we could estimate the binding constant of the stronger interactions of compound **1** with 24bcl (7.2 ± 0.4) and cmyc (5.5 ± 0.2) sequences (see supplementary data). These values are in agreement with those recorded at an excitation wavelength of 252 nm (Table 1).

Finally, CD spectra of the DNA : ligand mixtures showed no significant differences in relation to those of DNA (see supplementary data). This observation suggests that the DNA G-quadruplex structure is not altered significantly upon binding of the acridine derivatives.

4. Conclusions

In summary, here we have described a new optimized protocol for the synthesis of acridine oligomers with a (2-aminoethyl)glycine backbone. In this method, the Boc-(2-aminoethyl)glycine backbone is first assembled on solid-phase, and then the intercalating agent is assembled on the backbone. This strategy is faster and more efficient than the one described previously [13] and yields the desired oligomers with good yields. A succinyl linker was used to connect the oligomers to the solid support. The succinyl linker attached to sarcosine was unexpectedly too stable and oligomers could not be directly released from the support by a single ammonia treatment. Instead a two-step protocol was used obtaining the desired compounds and an intermediate oligomer carrying a long succinyl sarcosine chain at the C-terminal position.

Competitive dialysis experiments have shown differences on the affinity of acridine oligomers to G-quadruplexes. Higher affinities are found in G-quadruplex sequences present on the promoter regions of *c-myc* and *bcl*-2 oncogenes. This affinity is modulated by the number of acridines and the presence of the succinyl sarcosine chain at the C-terminal position, dimer **1** and trimer **4** being the more relevant compounds for G-quadruplex binding. The monomer 2-(acridine-9-carboxamide)acetic acid also shows binding properties of interest and it is the simplest compound to be prepared. Unfortunately, the compounds synthesized in this study did not have antiproliferative activity in spite of their affinity to quadruplex. This observation contrasts with other reported quadruplex-binding acridine derivatives, such as BRACO-19 [11, 30] which shows anticancer activity. The lower affinity to telomere G-quadruplex sequence and the larger size of the acridine derivatives described in the present study may hinder cellular uptake and may explain the absence of antiproliferative activity.

The acridine nucleus is described to interact to G-quadruplex. Depending on the substituents, the acridine nitrogen can be charged when bound to DNA, and with the ring stacked on a G-tetrad, the charge will occupy a position similar to that of the potassium cation that stabilizes the G-quadruplex [28]. The introduction of protonable side chains on the acridine ligand enhances binding by electrostatic interactions [28]. In our case the acridines had no protonable substituents and the acridine nitrogen was not charged when bound to DNA. For this reason, the affinity of oligomeric acridines to G-quadruplexes is due to the multimeric nature of the compounds as well as the addition of a glycine

to acridine-9-carboxylic acid. An interesting possibility for future development is the introduction of protonable sites at the oligomeric acridines, which may increase solubility in water, affinity to target, and cellular uptake. The method described here will contribute to accelerating the preparation of potential active oligomeric compounds.

Abbreviations

ACN:	Acetonitrile
Ac_2O:	acetic anhydride
Aeg:	(2-aminoethyl)glycine
Boc:	*t*-butoxycarbonyl
CPG:	controlled pore glass
DIEA:	diisopropylethylamine
DCM:	dichloromethane
DMEM:	Dulbecco's Modified Eagle's Medium
DMF:	*N*,*N*-dimethylformamide
EDTA:	Ethylenediaminetetraacetic acid
Fmoc:	(9-fluorenyl)methoxycarbonyl
MALDI-TOF:	Matrix-assisted laser desorption ionization time-of-flight
MBHA:	methylbenzhydrylamine
MTT:	Thiazolyl blue tetrazolium bromide
PNA:	peptide nucleic acid
PyBOP:	(benzotriazol-1-yloxy) trispyrrolidino-phosphonium hexafluorophosphate
Sar:	sarcosine
SDS:	sodium dodecasulphate
TEAA:	Triethylammonium acetate
TFA:	trifluoroacetic acid
UV:	Ultraviolet.

Acknowledgments

This study was supported by the Dirección General de Investigación Científica y Técnica (Grant BFU2007-63287) and the Generalitat de Catalunya (2009/SGR/208). R. Ferreira acknowledges a predoctoral fellowship from the Spanish Ministry of Science.

References

[1] R. Palchaudhuri and P. J. Hergenrother, "DNA as a target for anticancer compounds: methods to determine the mode of binding and the mechanism of action," *Current Opinion in Biotechnology*, vol. 18, no. 6, pp. 497–503, 2007.

[2] B. A. D. Neto and A. A. M. Lapis, "Recent developments in the chemistry of deoxyribonucleic acid (DNA) intercalators: principles, design, synthesis, applications and trends," *Molecules*, vol. 14, no. 5, pp. 1725–1746, 2009.

[3] D. J. Patel, A. T. Phan, and V. Kuryavyi, "Human telomere, oncogenic promoter and 5′-UTR G-quadruplexes: diverse higher order DNA and RNA targets for cancer therapeutics," *Nucleic Acids Research*, vol. 35, no. 22, pp. 7429–7455, 2007.

[4] G. N. Parkinson, M. P. H. Lee, and S. Neidle, "Crystal structure of parallel quadruplexes from human telomeric DNA," *Nature*, vol. 417, no. 6891, pp. 876–880, 2002.

[5] J. L. Huppert, "Hunting G-quadruplexes," *Biochimie*, vol. 90, no. 8, pp. 1140–1148, 2008.

[6] L. H. Hurley, "Secondary DNA structures as molecular targets for cancer therapeutics," *Biochemical Society Transactions*, vol. 29, no. 6, pp. 692–696, 2001.

[7] H. Han and L. H. Hurley, "G-quadruplex DNA: a potential target for anti-cancer drug design," *Trends in Pharmacological Sciences*, vol. 21, no. 4, pp. 136–142, 2000.

[8] N. H. Campbell, G. N. Parkinson, A. P. Reszka, and S. Neidle, "Structural basis of DNA quadruplex recognition by an acridine drug," *Journal of the American Chemical Society*, vol. 130, no. 21, pp. 6722–6724, 2008.

[9] D. Monchaud and M.-P. Teulade-Fichou, "A hitchhiker's guide to G-quadruplex ligands," *Organic and Biomolecular Chemistry*, vol. 6, no. 4, pp. 627–636, 2008.

[10] S. M. Haider, G. N. Parkinson, and S. Neidle, "Structure of a G-quadruplex-ligand complex," *Journal of Molecular Biology*, vol. 326, no. 1, pp. 117–125, 2003.

[11] M. J. B. Moore, C. M. Schultes, J. Cuesta, et al., "Trisubstituted acridines as G-quadruplex telomere targeting agents. Effects of extensions of the 3,6- and 9-side chains on quadruplex binding, telomerase activity, and cell proliferation," *Journal of Medicinal Chemistry*, vol. 49, no. 2, pp. 582–599, 2006.

[12] A. Aviñó, I. Navarro, J. Farrera-Sinfreu, et al., "Solid-phase synthesis of oligomers carrying several chromophore units linked by phosphodiester backbones," *Bioorganic and Medicinal Chemistry Letters*, vol. 18, no. 7, pp. 2306–2310, 2008.

[13] J. Farrera-Sinfreu, A. Aviñó, I. Navarro, et al., "Design, synthesis and antiproliferative properties of oligomers with chromophore units linked by amide backbones," *Bioorganic and Medicinal Chemistry Letters*, vol. 18, no. 7, pp. 2440–2444, 2008.

[14] D. P. Arya and B. Willis, "Reaching into the major groove of B-DNA: synthesis and nucleic acid binding of a neomycin-Hoechst 33258 conjugate," *Journal of the American Chemical Society*, vol. 125, no. 41, pp. 12398–12399, 2003.

[15] E. J. Fechter, B. Olenyuk, and P. B. Dervan, "Design of a sequence-specific DNA bisintercalator," *Angewandte Chemie—International Edition*, vol. 43, no. 27, pp. 3591–3594, 2004.

[16] A. Siddiqui-Jain, C. L. Grand, D. J. Bearss, and L. H. Hurley, "Direct evidence for a G-quadruplex in a promoter region and its targeting with a small molecule to repress c-MYC transcription," *Proceedings of the National Academy of Sciences of the United States of America*, vol. 99, no. 18, pp. 11593–11598, 2002.

[17] J. Dai, T. S. Dexheimer, D. Chen, et al., "An intramolecular G-quadruplex structure with mixed parallel/antiparallel G-strands formed in the human BCL-2 promoter region in solution," *Journal of the American Chemical Society*, vol. 128, no. 4, pp. 1096–1098, 2006.

[18] M. del Toro, P. Bucek, A. Aviñó, et al., "Targeting the G-quadruplex-forming region near the P1 promoter in the human BCL-2 gene with the cationic porphyrin TMPyP4 and with the complementary C-rich strand," *Biochimie*, vol. 91, no. 7, pp. 894–902, 2009.

[19] R. M. Dyson, S. Kaderli, G. A. Lawrance, and M. Maeder, "Second order global analysis: the evaluation of series of spectrophotometric titrations for improved determination of equilibrium constants," *Analytica Chimica Acta*, vol. 353, no. 2-3, pp. 381–393, 1997.

[20] K.-P. Stengele and W. Pfleiderer, "Improved synthesis of oligodeoxyribonucleotides," *Tetrahedron Letters*, vol. 31, no. 18, pp. 2549–2552, 1990.

[21] D. W. Will, G. Breipohl, D. Langner, J. Knolle, and E. Uhlmann, "The synthesis of polyamide nucleic acids using

a novel monomethoxytrityl protecting-group strategy," *Tetrahedron*, vol. 51, no. 44, pp. 12069–12082, 1995.

[22] C. Granotier, G. Pennarun, L. Riou, et al., "Preferential binding of a G-quadruplex ligand to human chromosome ends," *Nucleic Acids Research*, vol. 33, no. 13, pp. 4182–4190, 2005.

[23] J. Gros, F. Rosu, S. Amrane, et al., "Guanines are a quartet's best friend: iImpact of base substitutions on the kinetics and stability of tetramolecular quadruplexes," *Nucleic Acids Research*, vol. 35, no. 9, pp. 3064–3075, 2007.

[24] L. C. Bock, L. C. Griffin, J. A. Latham, E. H. Vermaas, and J. J. Toole, "Selection of single-stranded DNA molecules that bind and inhibit human thrombin," *Nature*, vol. 355, no. 6360, pp. 564–566, 1992.

[25] Y. Wang and D. J. Patel, "Solution structure of the human telomeric repeat d[AG3(T2AG3)3] G-tetraplex," *Structure*, vol. 1, no. 4, pp. 263–282, 1993.

[26] J. Ren and J. B. Chaires, "Sequence and structural selectivity of nucleic acid binding ligands," *Biochemistry*, vol. 38, no. 49, pp. 16067–16075, 1999.

[27] P. Ragazzon and J. B. Chaires, "Use of competition dialysis in the discovery of G-quadruplex selective ligands," *Methods*, vol. 43, no. 4, pp. 313–323, 2007.

[28] E. W. White, F. Tanious, M. A. Ismail, et al., "Structure-specific recognition of quadruplex DNA by organic cations: influence of shape, substituents and charge," *Biophysical Chemistry*, vol. 126, no. 1–3, pp. 140–153, 2007.

[29] J. J. Green, S. Ladame, L. Ying, D. Klenerman, and S. Balasubramanian, "Investigating a quadruplex—ligand interaction by unfolding kinetics," *Journal of the American Chemical Society*, vol. 128, no. 30, pp. 9809–9812, 2006.

[30] A. M. Burger, F. Dai, C. M. Schultes, et al., "The G-quadruplex-interactive molecule BRACO-19 inhibits tumor growth, consistent with telomere targeting and interference with telomerase function," *Cancer Research*, vol. 65, no. 4, pp. 1489–1496, 2005.

Supplementary data

Synthesis and G-quadruplex binding properties of defined acridine oligomers.

Rubén Ferreira, Anna Aviñó, Ricardo Pérez-Tomás, Raimundo Gargallo, Ramon Eritja*

CONTENTS:

Figure S1. HPLC and MALDI-TOF spectra. See conditions in Material and Methods section.

Compound 1

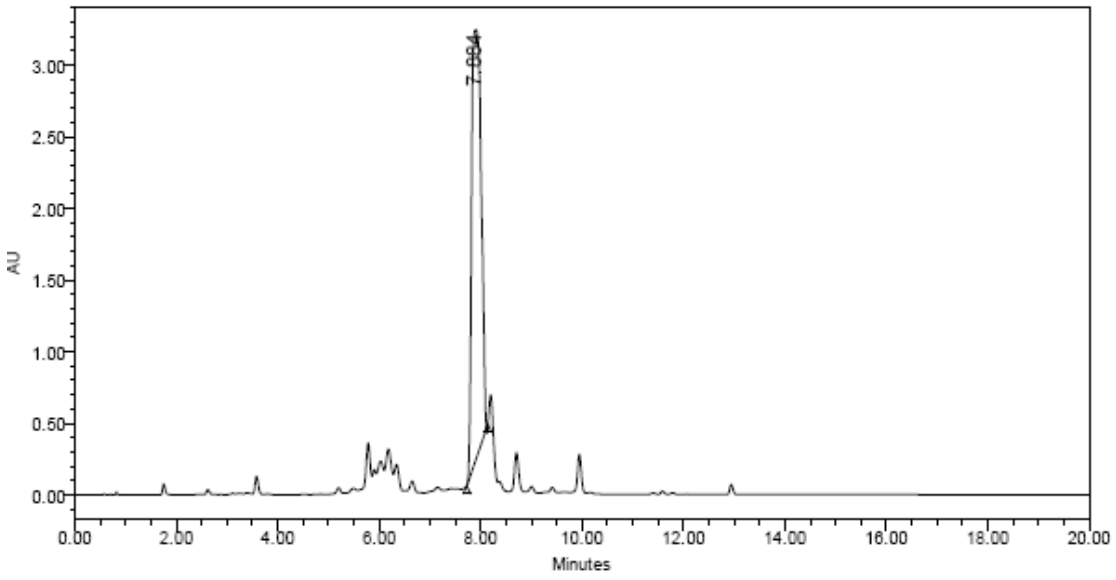

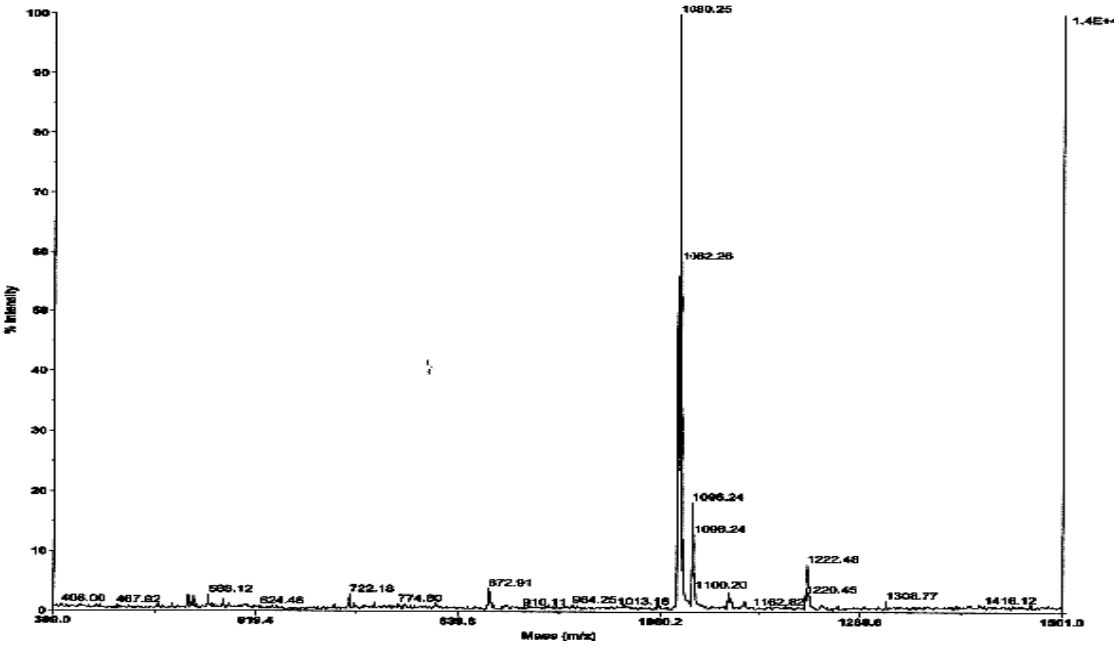

Compound 2

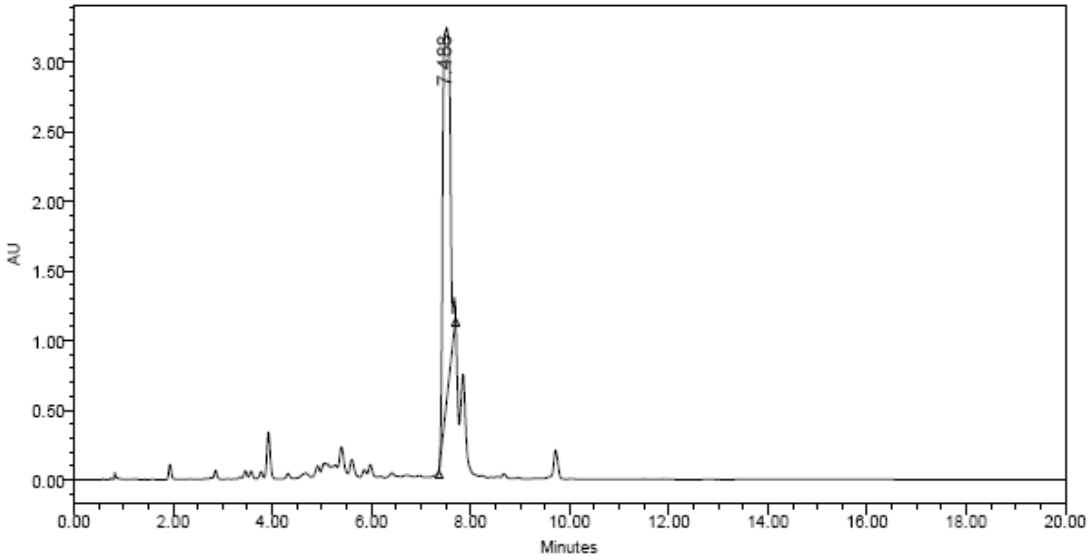
7.488
AU
3.00
2.50
2.00
1.50
1.00
0.50
0.00
0.00
2.00
4.00
6.00
8.00
10.00
12.00
14.00
16.00
18.00
20.00
Minutes

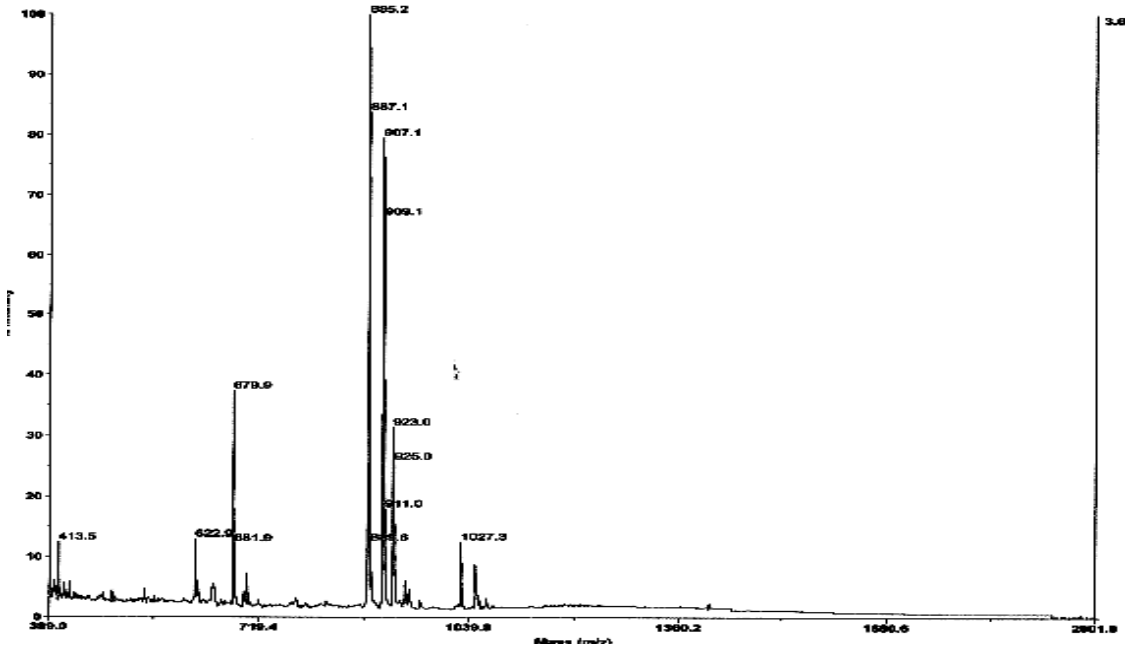
885.2
887.1
907.1
909.1
679.9
923.0
925.0
911.0
413.5
622.9
881.9
1027.3

Compound 3

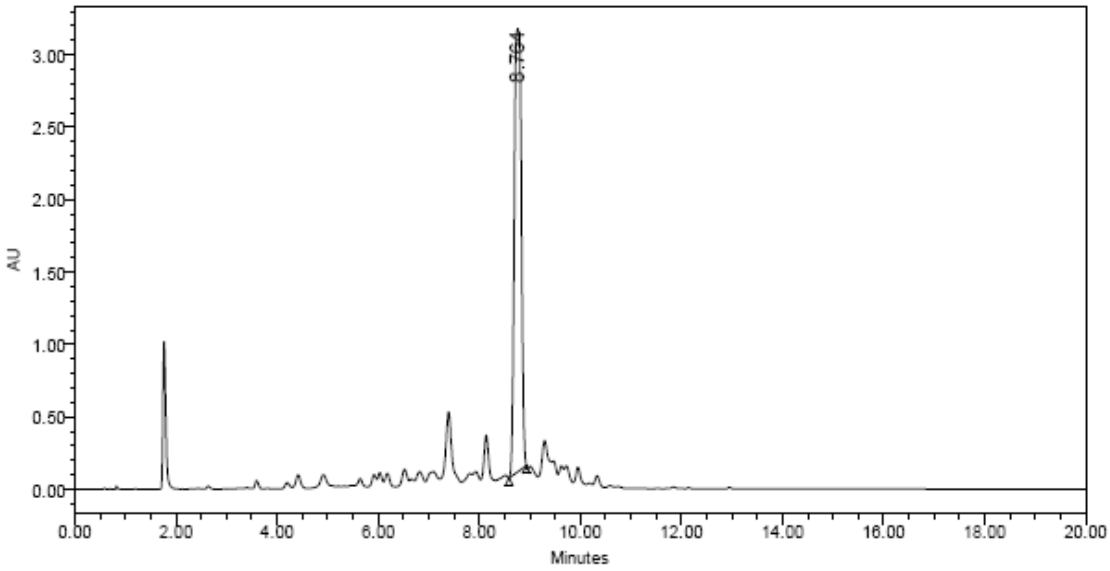
AU
Minutes
8.764

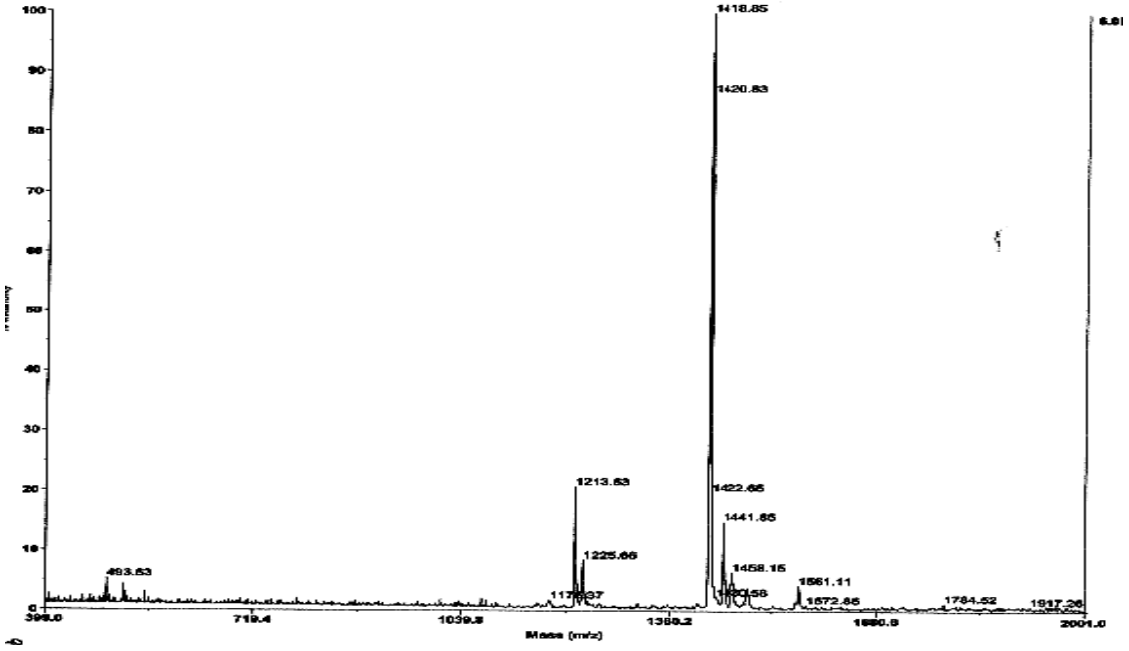
1418.85
1420.83
1213.63
1422.65
1441.65
1225.66
1458.15
1561.11
1572.65
1784.52
1917.26
493.63
719.4
1039.3
1359.2
1680.9
2001.0
Mass (m/z)

Compound 4

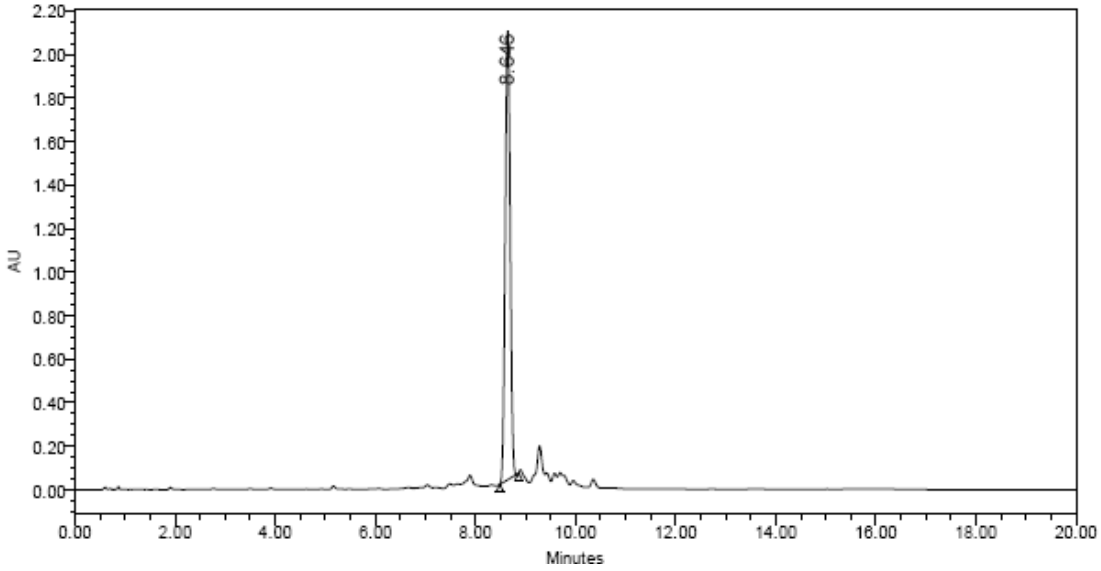
8.646
AU
Minutes

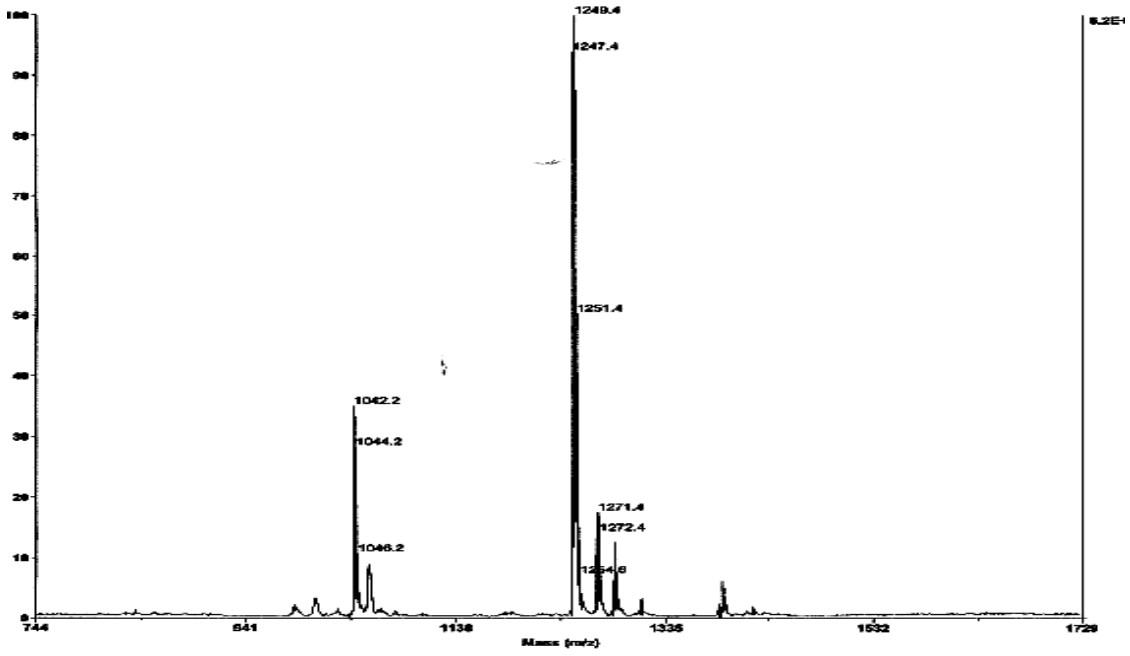
1249.4
1247.4
1251.4
1042.2
1044.2
1046.2
1271.4
1272.4
744
941
1138
1335
1532
1729
Mass (m/z)

Figure S2. Fluorescence titrations spectra of compounds **2-4** with oligonucleotide sequences 24bcl, cmyc, Dickerson and HT24. See conditions in Material and Methods section**.**

Compound 2 and 24bcl sequence

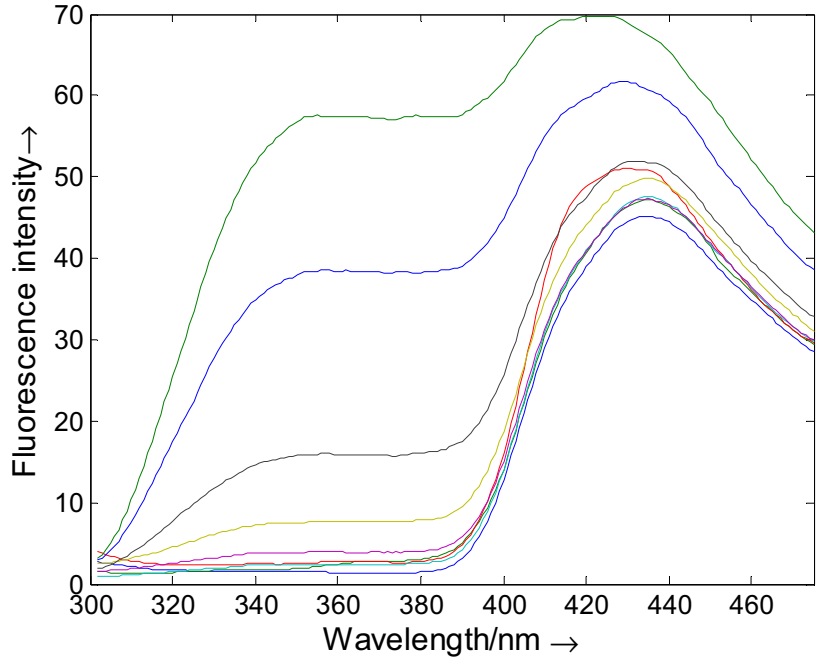

Compound 2 and cmyc sequence

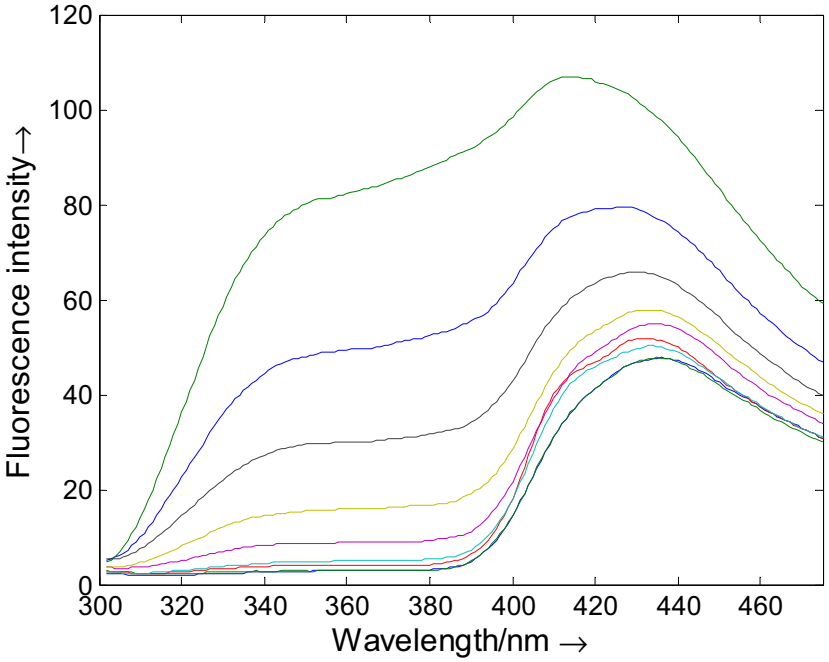

Compound 2 and Dickerson sequence

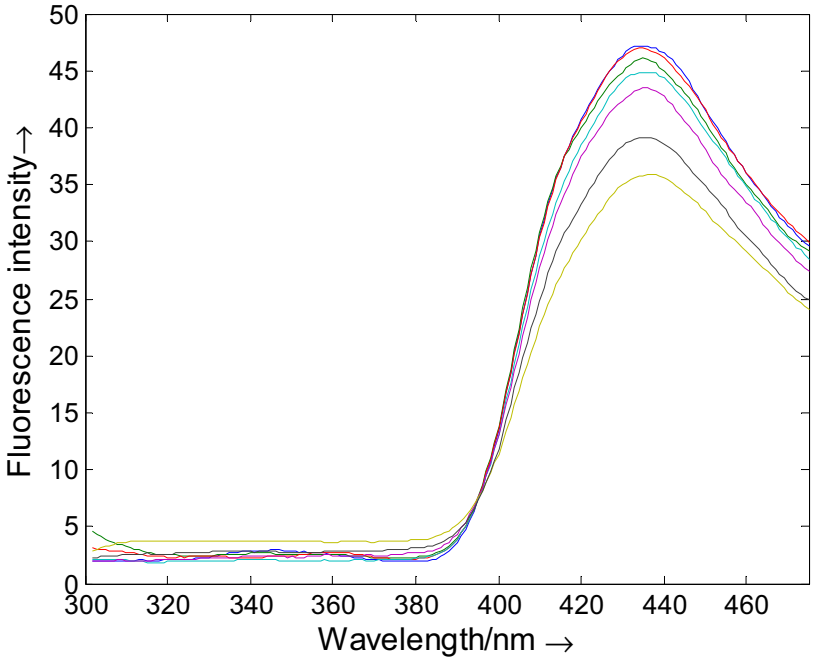

Compound 2 and HT24 sequence

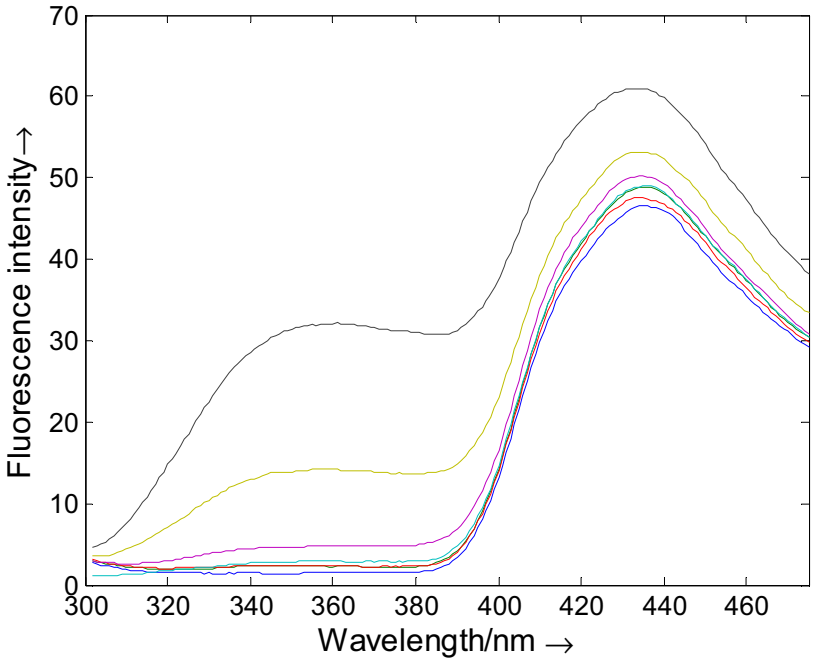

Compound 3 and 24bcl sequence

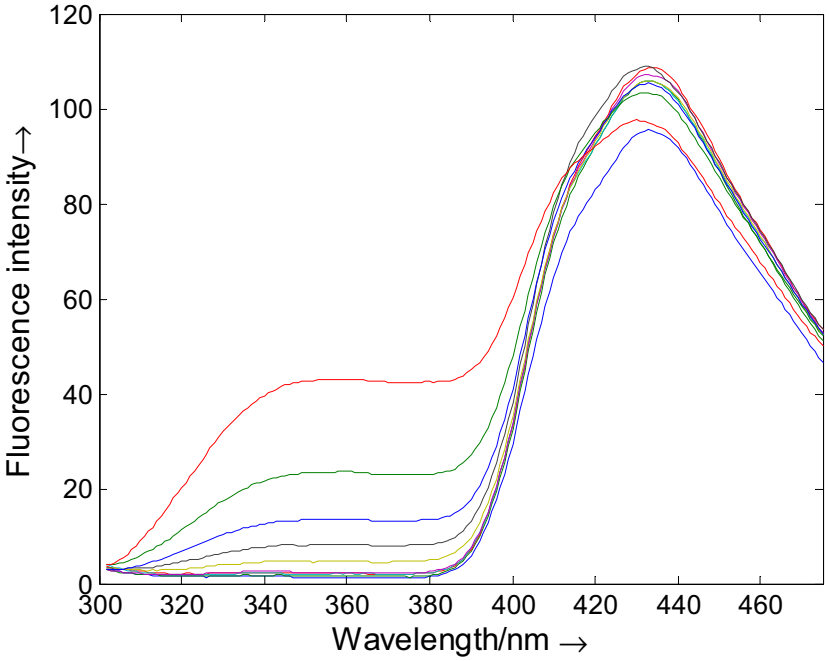

Compound 3 and cmyc sequence

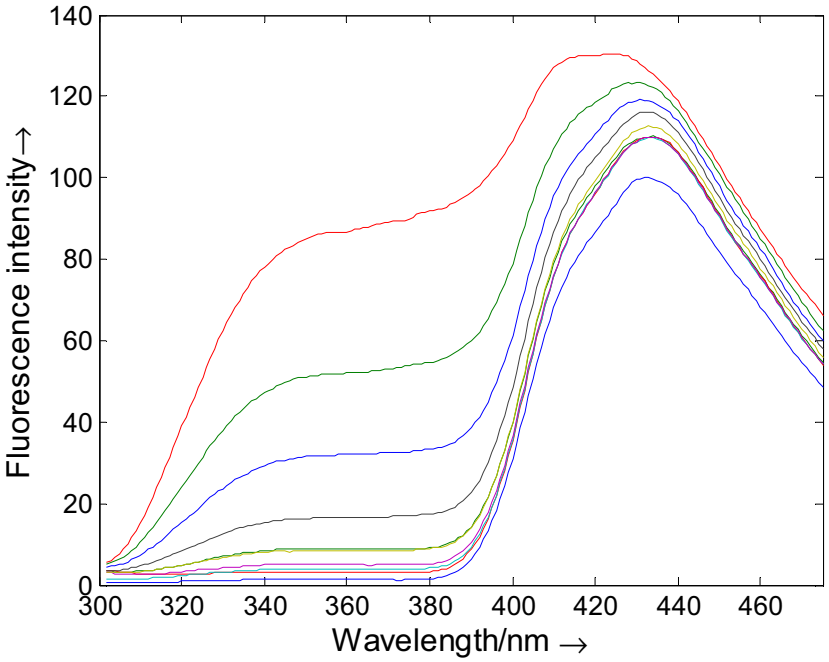

Compound 3 and Dickerson sequence

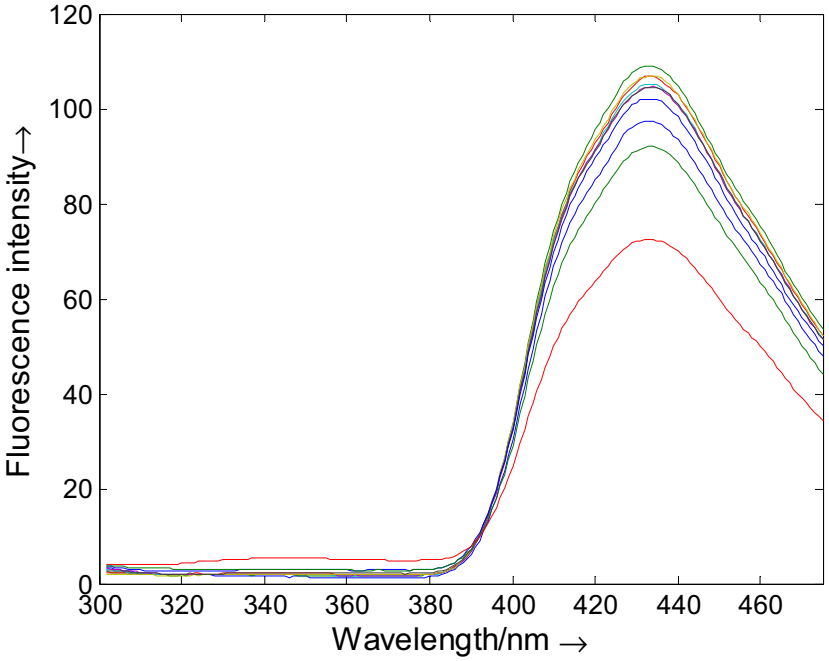

Compound 3 and HT24 sequence

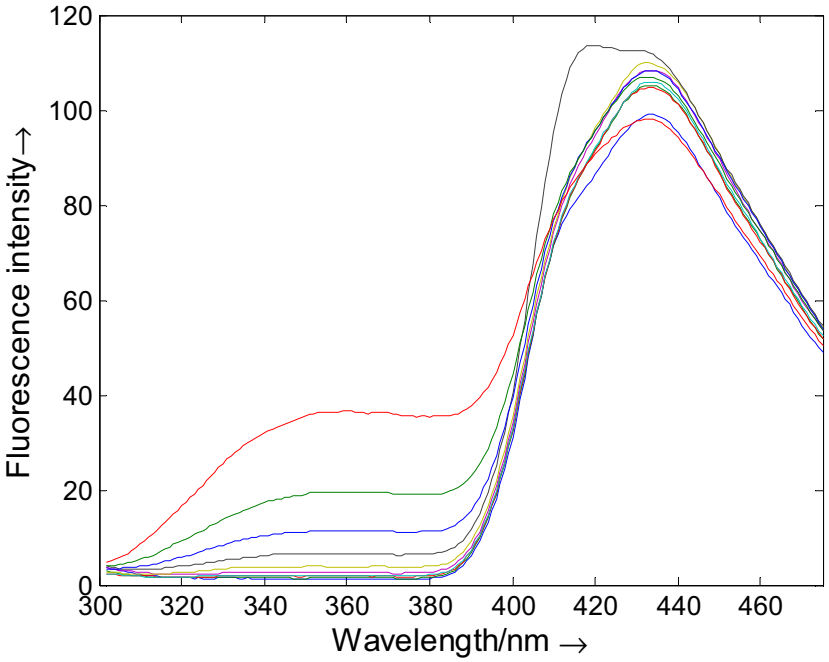

Compound 4 and 24bcl sequence

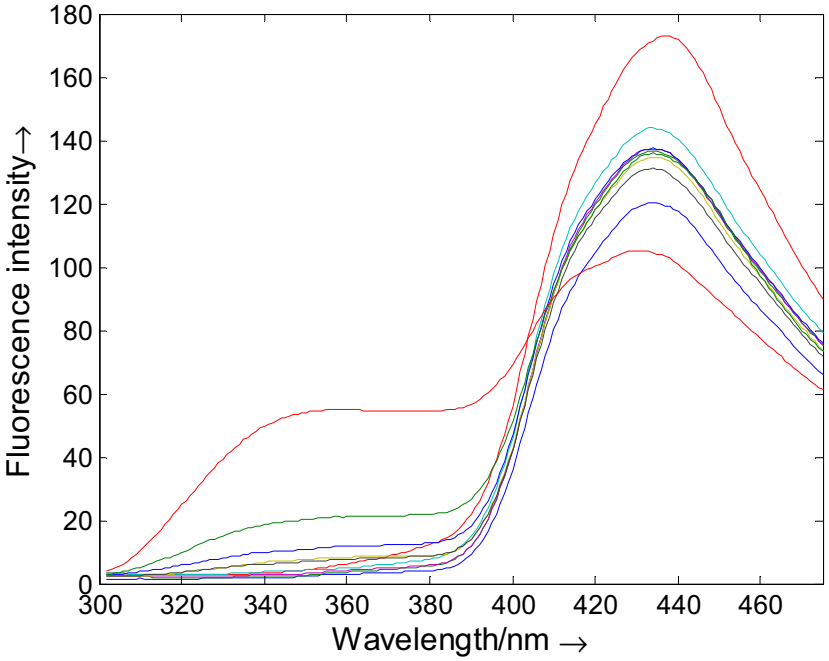

Compound 4 and cmyc sequence

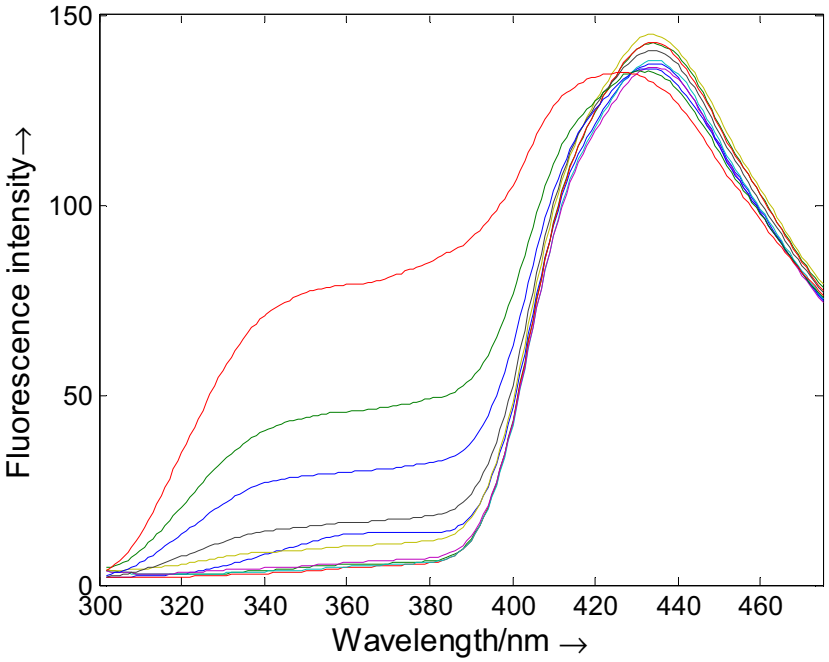

Compound 4 and Dickerson sequence

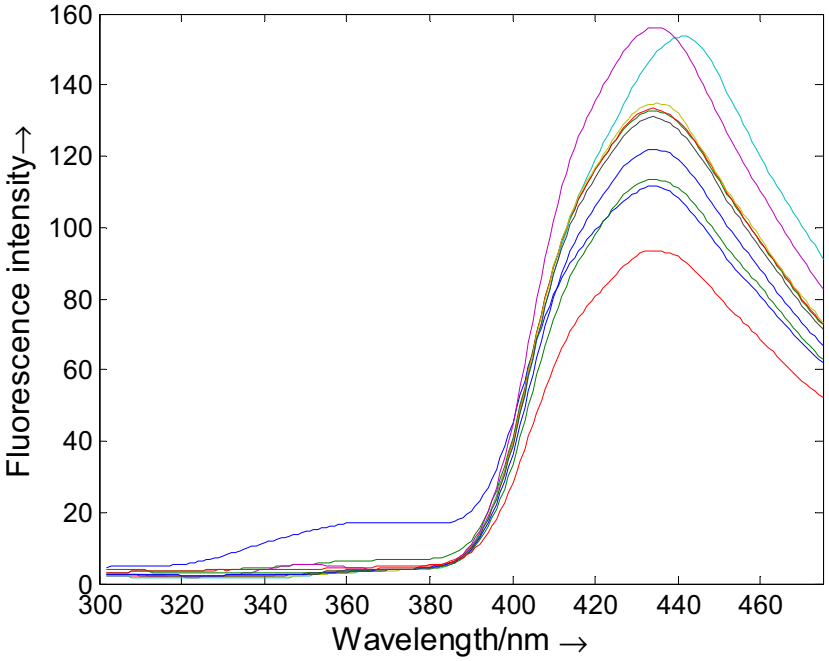

Compound 4 and HT24 sequence

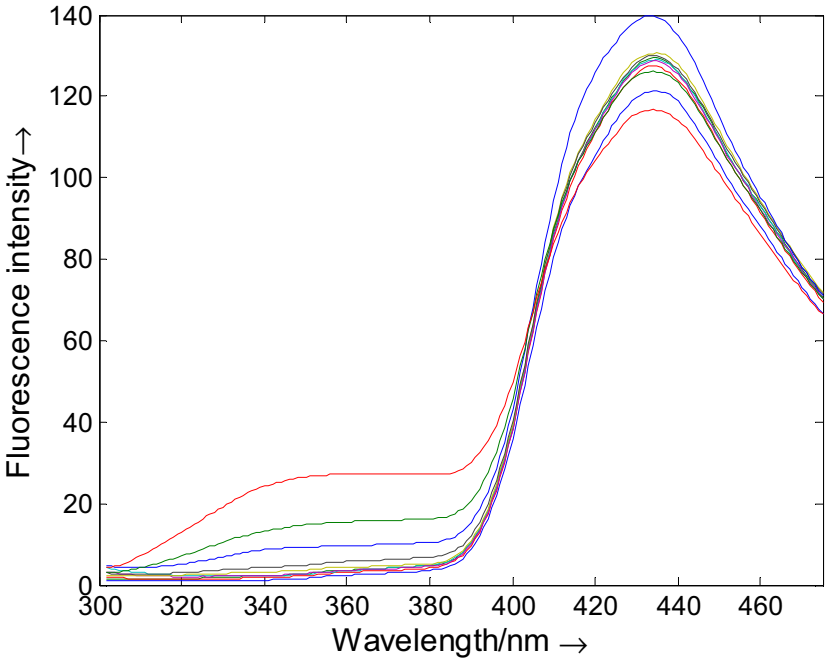

Figure S3. Circular dichroism spectra of cmyc sequence in the presence of compound **1**. To a 1 μM solution of the oligonucleotide were added an increasing amount of **1** (from 0 to 8 μM) in potassium phosphate buffer (185 mM NaCl, 185 mM KCl, sodium phosphate, 1 mM EDTA, pH 7). The CD spectra were recorded after 24 hours.

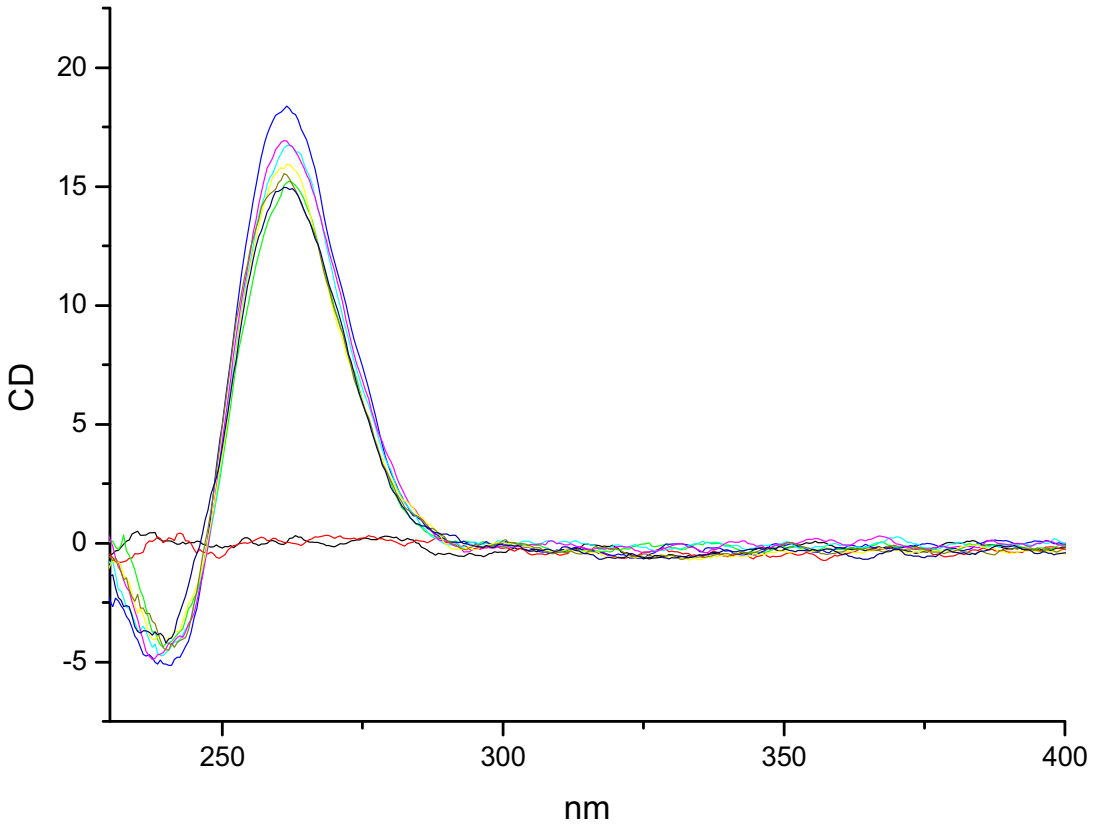

5

ELS OLIGÒMERS D'ACRIDINA I QUINDOLINA UNITS MITJANÇANT LA 4-AMINOPROLINA PREFEREIXEN LES ESTRUCTURES DE QUÀDRUPLEX DE GUANINA

ELS OLIGÒMERS D'ACRIDINA I QUINDOLINA UNITS MITJANÇANT LA 4-AMINOPROLINA PREFEREIXEN LES ESTRUCTURES DE QUÀDRUPLEX DE GUANINA.

Acridine and quindoline oligomers linked through a 4-aminoproline backbone prefer G-quadruplex structures.

Rubén Ferreira[a], Roberto Artali[b], Josep Farrera-Sinfreu[c], Fernando Albericio[d,e], Miriam Royo[c], Ramon Eritja[a,*], Stefania Mazzini[f,**]

Biochimica et Biophysica Acta, 1810 (2011) 769-776

[a] *Institute for Research in Biomedicine, IQAC-CSIC, CIBER-BBN Networking Centre on Bioengineering, Biomaterials and Nanomedicine, Baldiri Reixac 10, E-08028 Barcelona, Spain*
[b] *Faculty of Pharmacy, Dipartimento di Scienze Farmaceutiche "P. Pratesi", Università degli Studi di Milano, Via Mangiagalli, 25I-20133, Milano, Italy*
[c] *Combinatorial Chemistry Unit, Barcelona Science Park, CIBER-BBN Networking Centre on Bioengineering, Biomaterials and Nanomedicine, Baldiri Reixac 10, E-08028 Barcelona, Spain*
[d] *Institute for Research in Biomedicine, University of Barcelona, CIBER-BBN Networking Centre on Bioengineering, Biomaterials and Nanomedicine, Baldiri Reixac 10, E-08028 Barcelona, Spain*
[e] *Department of Organic Chemistry, University of Barcelona, Martí i Franqués 1-11, E-08028 Barcelona, Spain*
[f] *Dipartimento di Scienze Molecolari Agroalimentari, Università degli Studi di Milano, via Celoria 2, 20133 Milano, Italy*

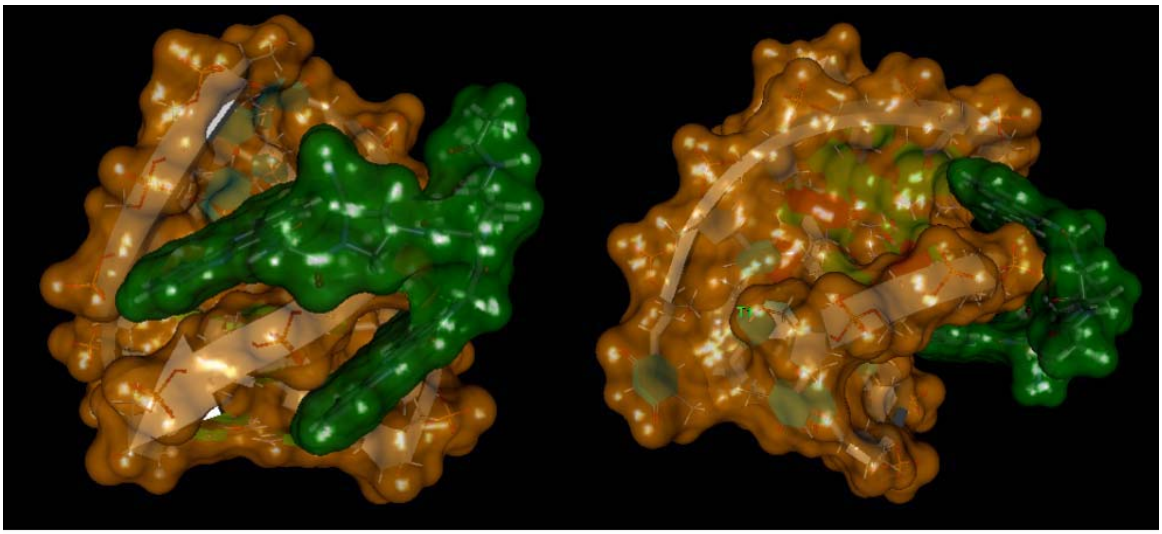

Resum

Els compostos que s'intercalen al DNA acostumen a ser molècules planes amb diversos anells aromàtics fusionats que s'apilen entre els parells de bases del DNA, reduint l'obertura i el desenrotllament de la doble hèlix.

S'ha analitzat per diàlisis competitiva les propietats d'unió amb el DNA dels oligòmers de la 4-aminoprolina funcionalitzats amb una, dos i tres unitats d'acridina i/o quindolina. S'ha observat una selectivitat dels oligòmers de la 4-aminoprolina amb la quindolina per estructures formadores de G-quàdruplex i tríplex, especialment per les seqüències de G-quàdruplex que es troben en els telòmers i en les regions promotores dels oncogens *c-myc* i *bcl-2*. Posteriorment, es van realitzar estudis de Ressonància Magnètica Nuclear i de dinàmica molecular en seqüències telomèriques formadores de G-quàdruplex amb el dímer de la 4-aminoprolina amb dues unitats de quindolina. Es descriu un model del complex format amb el G-quàdruplex de DNA telomèric, on el dímer de la quindolina s'estabilitza per apilament, formant-se interaccions π-π entre els anells aromàtics del lligand i les nucleobases de la seqüència telomèrica que estan localitzades a la part superior i inferior de la molècula.

El resultat d'aquest treball pot ser el punt de partida pel disseny de noves molècules amb una gran afinitat pels telòmers que podrien presentar propietats anticancerígenes.

Biochimica et Biophysica Acta 1810 (2011) 769–776

Contents lists available at ScienceDirect

Biochimica et Biophysica Acta

journal homepage: www.elsevier.com/locate/bbagen

Acridine and quindoline oligomers linked through a 4-aminoproline backbone prefer G-quadruplex structures

Rubén Ferreira [a], Roberto Artali [b], Josep Farrera-Sinfreu [c], Fernando Albericio [d,e], Miriam Royo [c], Ramon Eritja [a,*], Stefania Mazzini [f,**]

[a] Institute for Research in Biomedicine, IQAC-CSIC, CIBER-BBN Networking Centre on Bioengineering, Biomaterials and Nanomedicine, Baldiri Reixac 10, E-08028 Barcelona, Spain
[b] Faculty of Pharmacy, Dipartimento di Scienze Farmaceutiche "P. Pratesi", Università degli Studi di Milano, Via Mangiagalli, 25I-20133, Milano, Italy
[c] Combinatorial Chemistry Unit, Barcelona Science Park, CIBER-BBN Networking Centre on Bioengineering, Biomaterials and Nanomedicine, Baldiri Reixac 10, E-08028 Barcelona, Spain
[d] Institute for Research in Biomedicine, University of Barcelona, CIBER-BBN Networking Centre on Bioengineering, Biomaterials and Nanomedicine, Baldiri Reixac 10, E-08028 Barcelona, Spain
[e] Department of Organic Chemistry, University of Barcelona, Martí i Franqués 1-11, E-08028 Barcelona, Spain
[f] Dipartimento di Scienze Molecolari Agroalimentari, Università degli Studi di Milano, via Celoria 2, 20133 Milano, Italy

ARTICLE INFO

Article history:
Received 13 January 2011
Received in revised form 7 April 2011
Accepted 27 April 2011
Available online 5 May 2011

Keywords:
Oligonucleotides
Acridine
Quindoline
G-quadruplex
NMR
DNA-binding drugs

ABSTRACT

Background: DNA-intercalating drugs are planar molecules with several fused aromatic rings that form stacks between DNA base pairs, reducing the opening and unwinding of the double helix. Recently, interest on intercalating agents has moved in the search for new ligands to G-quadruplex structures.
Methods: The DNA binding properties of 4-aminoproline oligomers functionalized with one, two or three units of acridine and/or quindoline have been analyzed by competitive dialysis. A NMR/molecular dynamics study was performed on G-quadruplex telomeric sequence and the 4-aminoproline dimer carrying two quindolines. A model of the complex with the telomeric DNA quadruplex is described.
Results and conclusions: A selectivity of quindoline 4-aminoproline oligomers for G-quadruplex and triplex structures was observed, especially for those quadruplex sequences found in telomeres and in the promoter regions of *c-myc* and *bcl*-2 oncogenes. In this model the quindoline dimer is stabilized by π–π stacking interactions between the aromatic rings of the ligand and the nucleobases of the telomeric sequence that are located above and below the molecule.
General significance: The results of this work can be used for the design of new molecules with high affinity to telomeres which may have anticancer properties.

© 2011 Elsevier B.V. All rights reserved.

1. Introduction

DNA-intercalating drugs are planar molecules formed by several fused aromatic rings that form stacks between DNA base pairs, thus reducing the opening and unwinding of the double helix. Each intercalating drug binds strongly to particular base pairs due to several interactions, ranging from van der Waals interactions to the formation of hydrogen bonds with adjacent nucleobases [1,2]. The selectivity of intercalating drugs may be improved by linking several intercalating units. Various authors have described the synthesis of bis- or tris-intercalating drugs with promising activity and selectivity [3,4].

Recently, interest on intercalating agents has moved in the search for new ligands to G-quadruplex structures [5]. This structure motif is formed by the planar association of four guanines in a cyclic Hoosgsteen hydrogen bonding tetrad. Guanine rich sequences are able to form G-quadruplex structures which have been found in telomeres [6] and in transcriptional regulatory regions of important oncogenes such as *c-myc*, and *c-kit*, [7,8]. Ligands that selectively bind and stabilize these structures have become interesting anticancer drugs [9]. G-quadruplex stabilization occurs in most of the cases by π–π stacking and electrostatic interaction. G-quadruplex ligands are normally planar aromatic molecules that are prone to stacking with G-tetrads [10]. Some of them are also positively charged or have hydrophilic groups to favor electrostatic interaction [11].

In previous papers we have described the preparation of sequence specific oligomers of DNA-intercalating drugs using protocols based on solid-phase synthesis in an attempt to facilitate the preparation of compounds with improved DNA-binding selectivity [12,13]. The preparation of several acridine oligomers linked through 2-aminoethylglycine units by solid-phase synthesis protocols was also

* Corresponding author.
** Corresponding author. Tel.: +39 02 50316824; fax: +39 02 50316801.
E-mail addresses: ruben.ferreira@irbbarcelona.org (R. Ferreira), roberto.artali@unimi.it (R. Artali), albericio@irbbarcelona.org (F. Albericio), mroyo@pcb.ub.cat (M. Royo), recgma@cid.csic.es (R. Eritja), stefania.mazzini@unimi.it (S. Mazzini).

0304-4165/$ – see front matter © 2011 Elsevier B.V. All rights reserved.
doi:10.1016/j.bbagen.2011.04.013

described [14]. These compounds show a clear affinity for several DNA G-quadruplex structures. Here we describe the DNA-binding properties of a complete series of 4-aminoproline oligomers carrying up to three units of acridine and quindoline molecules. Competitive dialysis experiments show a very high affinity of quindoline 4-aminoproline oligomers for G-quadruplex especially those quadruplex sequences found in the promoter regions of *c-myc*[15] and *bcl*-2 [16,17] oncogenes. A detailed NMR/molecular dynamics study was performed on G-quadruplex telomeric sequence and the dimer quindoline-quindoline which is the oligomer with higher affinity for quadruplexes. A model of the complex that explains the affinity of the quindoline dimer with the DNA quadruplex is described.

2. Materials and methods

2.1. Compounds

(1) Acridine-9-carboxylic acid, **(2)** 2-(acridine-9-carboxamide) acetic acid, **(3)** 10H-Indolo[3,2b]quinoline-11-carboxylic acid, **(4)** 2-(10H-Indolo[3,2b]quinoline-11-carboxamide) acetic acid and **(5–18)** acridine

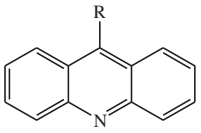

1: R= COOH
2: R= $CONHCH_2COOH$

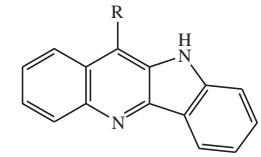

3: R= COOH
4: R= $CONHCH_2COOH$

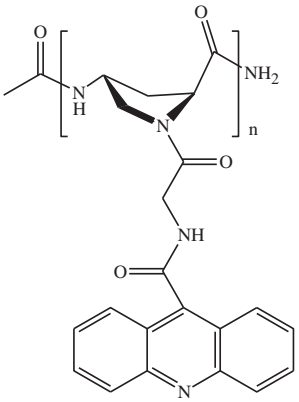

5, 6 and 7: n=1, 2 and 3

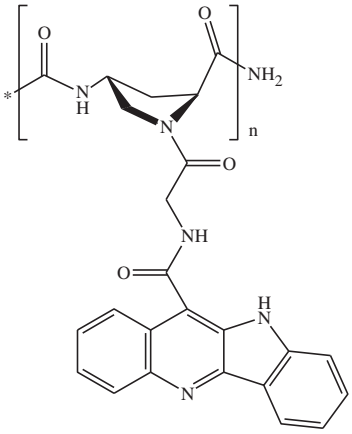

8, 9 and 10 : n=1, 2 and 3

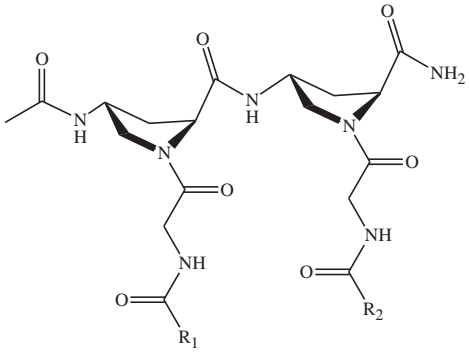

11: R_1= Acridine, R_2= Quindoline
12: R_1= Quindoline, R_2= Acridine

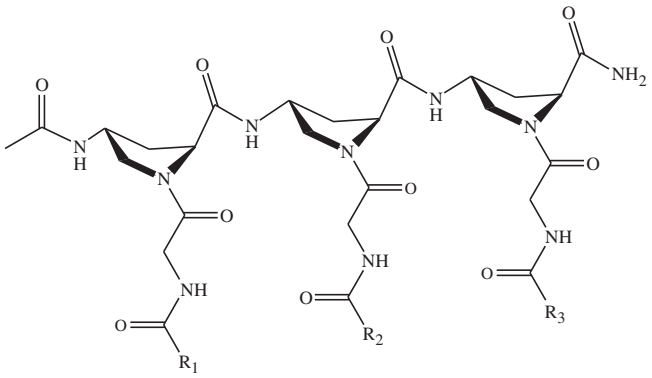

13: R_1= Acridine, R_2= Acridine, R_3= Quindoline
14: R_1= Acridine, R_2= Quindoline, R_3=Acridine
15: R_1= Quindoline, R_2= Acridine, R_3= Acridine
16:R_1= Acridine, R_2= Quindoline, R_3= Quindoline
17:R_1= Quindoline, R_2= Quindoline, R_3= Acridine
18:R_1= Quindoline, R_2= Acridina, R_3= Quindoline

Fig. 1. Structure of the acridine and quindoline derivates.

and quindoline 4-aminoproline backbone oligomers were synthesized according to published procedures [13]. Their formulas are shown in Fig. 1.

2.2. Oligonucleotide synthesis

All the standard phosphoroamidites and reagents for DNA synthesis were purchased from Applied Biosystems and from Link Technologies. The synthesis of the oligonucleotides was performed at 1 μmol scale on an Applied Biosystem DNA/RNA 3400 synthesizer by solid-phase 2-cyanoethylphosphoroamidite chemistry. The following sequences were prepared: T20: d(5′-TTT TTT TTT TTT TTT TTT TT-3′), 24bclc: d(5′-CCC GCC CCC TTC CTC CCG CGC CCG-3′), 6-mer: d(5′-CGA TGC-3′), Dickerson: d(5′-CGC GAA TTC GCG-3′), ds26: d(5′-CAA TCG GAT CGA ATT CGA TCC GAT TG-3′), GA triplex : d(5′-GAA AGA GAG GAG GCC TTT TTG GAG GAG AAG-3′) + d(5′-CCT CCT CTC TTT C-3′), TC triplex: d(5′-CCT CCT CTC TTT CCC TTT TTC TTT CTC TCC TCC-3′) + d (5′-GAA AGA GAG GAG G-3′), TG4T: d(5′-TGG GGT-3′), TBA: d(5′-GGT TGG TGT GGT TGG-3′), HT24: d(5′-TAG GGT TAG GGT TAG GGT TAG GGT-3′), T2AG3: d(5′-TTA GGG-3′), 24bcl: d(5′-CGG GCG CGG GAG GAA GGG GGC GGG-3′), cmyc: d(5′-GGG GAG GGT GGG GAG GGT GGG GAA GGT GGG G-3′). The resulting oligonucleotides were purified by HPLC and desalted in a Sephadex (NAP-10) G25 column.

2.3. Competitive dialysis assays

A total 200 mL of the dialysate solution containing 1 μM compound was used for each competition dialysis assay. A volume of 100 1vμL at 50 μM monomeric unit of each of oligonucleotide sequence was placed in dialysis unit. Potassium phosphate buffer containing 185 mM NaCl, 185 mM KCl, 2 mM NaH_2PO4, 1 mM Na_2EDTA and 6 mM Na_2HPO_4 at pH 7 was used for all experiments.

The samples were allowed to equilibrate with continuous stirring at room temperature overnight. Dialysis samples were removed to an Eppendorf tube. In order to measure the compound entered in the dialysis unit, dialysis samples were degraded to liberate the derivate as described previously [14].

Finally, the fluorescence of each samples was measured (λ_{ex} and λ_{em} were set to 252 and 435 nm in acridine derivates and 276 and 500 nm in quindoline derivates) and normalized for each compound.

2.4. NMR spectroscopy

The NMR spectra were recorded by Bruker AV-600 spectrometer operating at a frequency of 600.10 MHz for ^1H. ^1H spectra were recorded at variable temperature ranging from 5 °C to 75 °C. ^1H chemical shifts (δ) were measured in ppm and referenced to external DSS (2,2-dimethyl-2-silapentane-5-sulfonate sodium salt) set at 0.00 ppm. Estimated accuracy for protons is within 0.02 ppm.

The samples for NMR measurements were dissolved in 500 μl H_2O/D_2O (9:1) containing 25 mM KH_2PO_4, 150 mM KCl and 1 mM EDTA (pH 6.7) for the quadruplex d(5′-TTA GGG-3′)$_4$ and containing 10 mM KH_2PO_4, 70 mM KCl and 0.2 mM EDTA (pH 7.0) for the double helix d(5′-CGA TCG-3′)$_2$. The final concentration of the oligonucleotide solutions ranged between 0.6 and 0.7 mM. A stock solution of **9** and **3** was prepared in DMSO-d_6 at the concentration of 6 and 12.5 mM, respectively.

NMR titration was performed by adding increasing amounts of drugs to the oligonucleotides solution at R = [ligand]/[DNA] ratio from 0 to 0.75 (after this value the drug precipitates) for **9** and from 0 to 3.0 for **3**.). In order to better identify the drug protons in the complex, the inverse titration experiment was performed, by adding increasing amounts of DNA, from R = 20 to R = 1.5, to a solution of **9** at constant concentration (0.2 mM).

Standard homonuclear 2D-NMR experiments were performed to assign the resonances of the complexes, including DQF-COSY, TOCSY and NOESY [18,19]. The mixing times were set at 150 ms and 300 ms for NOESY and 60 ms for TOCSY. For samples in H_2O, the excitation sculpting sequences from standard Bruker pulse program libraries were employed.

Typically, 2048 × 1024 data points were acquired using TPPI and transformed to a final 4 K × 4 K real data matrix after apodisation with a 90° and 90°-shifted sine-bell squared function in f2- and f1-domain, respectively. Baseline correction was achieved by a 5th-degree polynomial function.

The sequential assignments in free and bound oligonucleotides were performed by applying well established procedures for the analysis of double stranded and quadruplex structures.

The program Sparky [20] was used to assign the NOESY cross-peaks. The d(5′-TTA GGG-3′)$_4$ and d(5′-CGAT CG-3′)$_2$ NMR spectra were previously assigned [21,22].

2.5. Molecular modelling

The structure of compound **9** was built using a Silicon Graphics 4D35GT workstation running the Insight II and Discover software and was generated using standard bond lengths and angles. Molecular mechanics (MM) and molecular dynamics (MD) was carried out using both CVFF and AMBER forcefield. Molecular docking experiments were performed on an Apple® QuadXeon MacPro workstation with Autodock 4.0. This software uses an empirical scoring function based on the free energy of binding [23,24]. Among the stochastic search algorithms offered by the Autodock suite, we chose the Lamarckian Genetic Algorithm (LGA) which combines global search (Genetic Algorithm alone) to local search (Solis and Wets algorithm [25]). Genetic algorithms are based on the evolutionary concept in which the solution to an adaptive problem is spread among a genetic pool. In molecular docking, the “solution” corresponds to the best binding position for the ligand, and it is represented by a “chromosome” file containing translation, orientation, and torsion “genes.” Basically, a genetic algorithm creates a randomly placed population of individuals (ligands) and then applies cycles of genetic operators (mutation and crossover) giving rise to new generations until a suitable solution is achieved. The “solutions” are evaluated through their free energy of binding and (for **9**) looking at their agreement with the NOE data. The small molecule compounds (**3** and **9**) and the quadruplex (obtained from Protein Data Bank [http://www.rcsb.org], PDB ID: 1NP9) were processed using the Autodock Tool Kit (ADT) [26]. Gasteiger–Marsili charges [27] were loaded on the small molecules in ADT and Cornell parameters were used for the phosphorous atoms in the DNA. Solvation parameters were added to the final macromolecule structure using Addsol utility of Autodock. Each docking consisted of an initial population of 50 randomly placed individuals, a maximum number of 200 energy evaluations, a mutation rate of 0.02, a crossover rate of 0.80, and an elitism value of 1. For the local search, the so-called pseudo-Solis and Wets algorithm was applied using a maximum of 250 iterations per local search. The probability of performing local search on an individual in the population was 0.06 and the maximum number of consecutive failures before doubling or halving the local step size was 4. Fifty independent docking runs were carried out for each ligand. The grid maps representing the system in the actual docking process were calculated with Autogrid. The grids (one for each atom type in the ligand, plus one for electrostatic interactions) were chosen to be sufficiently large to include the entire width of the DNA fragment in which the original inhibitor was posed, together with a portion of minor and major grooves. The simpler intermolecular energy function based on the Weiner force field in Autodock was used to score the docking results. Results differing by less than 1.0 Å in positional root-mean-square deviation (rmsd) were clustered together and represented by the result with the most favorable free energy of binding. Since we could not use rmsd as the only accuracy criterion, we opted for a more subjective yet more representative criterion, which was to classify the resulting binding

mode by consistence with the NOE results and visual inspection as intercalation, minor groove binding, or others (major groove binding, interaction with phosphate groups and so on).

3. Results and discussion

3.1. Competitive dialysis studies

To evaluate the selectivity and the affinity of acridine and quindoline derivates for different DNA structures, we performed a competitive dialysis experiment using 11 nucleic acid structures [14].

As models for single stranded structures we used T20 and 24bclc. As duplexes we used the self-complementary sequences Dickerson–Drew dodecamer (Dickerson) and a 26 mer (ds26). A parallel triplex (TC triplex) and an antiparallel triplex (GA triplex) were also prepared by mixing a hairpin Watson–Crick sequence and the corresponding triplex-forming sequence. Finally, the following G-quadruplex sequences were prepared: the tetramolecular parallel G-quadruplex TG_4T [28], the antiparallel thrombin-binding aptamer (TBA) [29], the human telomere sequence (HT24) [30], and the promoter sequences of c-myc (cmyc) [15] and bcl-2 (24bcl) [16,17]. The amount of the bound ligand was directly proportional to the binding constant for each DNA structure [31,32].

Fig. 2 displays the oligonucleotide affinity for each compound. Fig. 2A showed the results for acridine derivates **1**, **2**, **5**, **6** and **7**. Acridine-9-carboxylic **1** interacts only with duplex ds26, the derivate **2** with a glycine residue, induced a change in the affinity showing a slight quadruplex preference, in particular for cmyc and 24bcl. On the

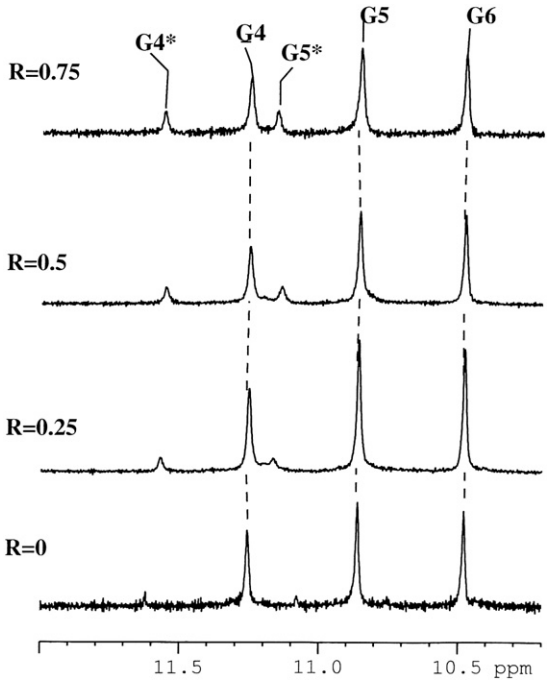

Fig. 3. Low field region of ^{1}H NMR spectra of $(T2AG3)_4$/**9** complex in H_2O, 25 mM KH_2PO_4, 150 mM KCl, 1 mM EDTA (pH 6.7), 25°C at different $R = [9]/[(T2AG3)_4]$. The resonances belonging to the bound species are indicated by an asterisk.

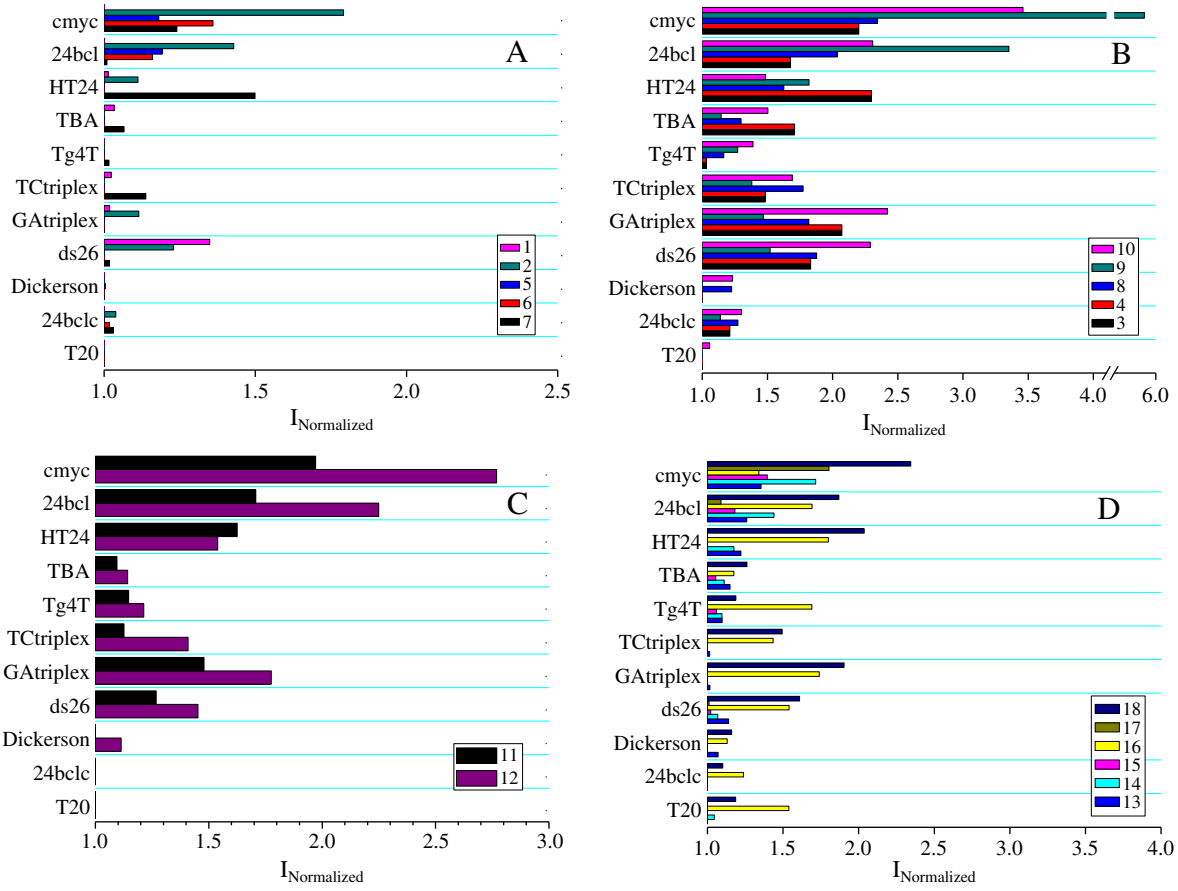

Fig. 2. Results obtained by the competitive dialysis assay. The amount of ligand (Fig. 1) bound to each DNA structure is shown as a bar graph. The nucleic acid names are given on the left, and structures are described in Materials and methods. The values are normalized for each compound. A) Acridine derivatives: monomers **1**, **2**, **5**, acridine dimer **6** and acridine trimer **7**. B) Quindoline derivatives: monomers **3**, **4**, **8**, quindoline dimer **9** and quindoline trimer **10**. C) Dimers carrying acridine and quindoline **11**, **12**. D) Trimers carrying acridine and quindoline **13**–**18**.

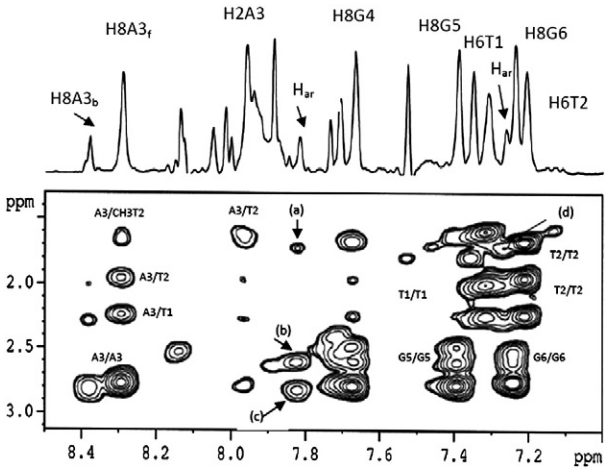

Fig. 4. 2D NOESY spectrum of $(T2AG3)_4$/**9** complex at $R = [\mathbf{9}]/[(T2AG3)_4] = 0.75$, 25 mM KH_2PO_4, 150 mM KCl and 1 mM EDTA (pH 6.7) at 25°C. Intra and inter residues interactions were shown. Extra aromatic protons of **9** and $(T2AG3)_4$ contacts were observed with: (a) CH_3T2, (b) H2′G5, (c) H2′G4 (d) CH_3T2.

contrary, the acridine 4-aminoproline oligomers **5**, **6** and **7** only interacts with quadruplex structures.

Fig. 2B shows that quindoline-11-carboxylic acid **3**, quindoline-11-carboxamide acetic acid **4** monomer **8** and trimer **10** derivatives do not present any selectivity. The affinity and selectivity for the quadruplex structures increases up in the dimer **9**. The oligonucleotide affinity and selectivity drop down in the mixed dimers **11** and **12** (Fig. 2C). No selectivity and affinity improvement are observed for the mixed trimers **13**–**18** (Fig. 2D) compared with the mixed dimers.

3.2. *^{1}H NMR experiments and molecular modeling on the [**9**]/[(T2AG3)$_4$] complex*

On the basis of dialysis studies compound **9** demonstrated the higher affinity and selectivity for the quadruplex structures studied in this work. In order to study in depth this binding, compound **9**, which had the higher affinity for quadruplex structures, was titrated into a solution of quadruplex model $(T2AG3)_4$ contained in the human telomere sequence and the resulting mixtures were analyzed by ^{1}H-NMR. T2AG3 is short model sequence contained in HT24 oligonucleotide. This oligonucleotide has been used previously for NMR characterization of drug binding on telomeric DNA sequences [33]. The short oligonucleotide has a more simple NMR spectrum than HT24 sequence facilitating the study of the interactions of the drug with the DNA sequence.

We performed competitive dialysis experiments with compound **9** including the T2AG3 oligonucleotide (Fig. 1S supplementary section). The affinity of compound **9** for HT24 is slightly higher than T2AG3 but it is in the range of the high affinity group that includes quadruplex forming oligonucleotide: HT24, cmyc and 24bcl sequences.

Moreover, the buffer conditions used in the competitive dialysis experiments are not appropriate for NMR studies as the salt concentration is too high. NMR experiments were performed in 25 mM KH_2PO_4, 150 mM KCl and 1 mM EDTA. Competitive dialysis experiments for quindoline dimer, **9**, in both (dialysis and NMR) buffer conditions are included in the supplementary section (Fig. 1S). There are small changes but essentially the relative affinities are similar in both buffer conditions.

The spectra in H_2O showed three signals, in the region of 11–12 ppm, belonging to Hoogsteen-bound guanine imino proton of the G quartets (Fig. 3). The addition of **9** to the quadruplex solution till a ratio $R = [9]/[(T2AG3)_4] = 0.75$ basically did not change the imino proton resonances but causes the appearance of two new down field signals (+0.3 ppm) belonging to a bound species in low chemical exchange. Unfortunately the very low solubility of **9** in water

Table 1
Intermolecular NOE interactions and inter-proton distances (Å) for the complex of **9** with $(T2AG3)_4$[a].

9	**d(TTAGGG)$_4$**	d[b]
H (7.80 ppm)	1′-H A_3	4.60 I
	8-H G_4	5.06 II
	2′-H G_4	5.20 II
	2″-H G_5	4.38 II
	3′-H G_5	5.61 II
	4′-H G_5	3.58 I
	4′-H G_6	4.95 II
	CH_3 T_2	2.86 I
H (7.26 ppm)	1′-H A_3	3.92 II
	1′-H A_3	5.18 I
	CH3 T_2	3.75 I
Distance violations (>0.3 Å)		

[a] Acquired at 25 °C, H_2O-D_2O (90:10 v/v), pH 6.7, 25 mM KH_2PO_4, 150 mM KCl and 1 mM EDTA. 2′-H and 2″-H stand for low field and up field proton, respectively.
[b] Obtained from the best structures of the complex resulting from the molecular docking studies. The distances are referred to the T_1–G_6 also in different strands (I and II).

Table 2
^{1}H chemical shift values for the complexes d(5′-TTA GGG-3′)$_4$[a] and d(5′-CGA TCG-3′)$_2$[b] with **9**.

Protons	$(TTAGGG)_4$/9	Protons	$(CGATCG)_2$/9
NH G4	11.60	NHC_1G_6	n.d.
NH G5	11.20	NHG_2C_5	12.92
NH G6	10.51	NHA_3T_4	13.66
6H T1	7.40	NH_2 C_1	8.28, 7.07
6H T2	7.29	NH_2 C_5	8.63, 7.07
8H A3	8.42	6H C_1	7.67
2H A_3	8.05	8H G_2	8.03
8H G4	7.76	8H A_3	8.34
8H G5	7.48	2H A_3	7.93
8H G6	7.34	8H G_6	8.00
CH_3 T_1	1.67	6H T_4	7.25
CH_3 T_2	1.75	6H C_5	7.53
1′H T1	5.99	5H C_1	6.00
1′H T2	6.22	5H C_5	5.70
1′H A3	6.24	CH_3 T_4	1.45
1′H G4	6.00	1′H C_1	5.76
1′H G5	6.00	1′H G_2	5.91
1′H G6	6.09	1′H A_3	6.36
2′2″H T_1	2.33, 2.08	1′H T_4	6.00
2′2″H T_2	2.33, 2.03	1′H C_5	5.77
2′2″H A_3	2.85, 2.85	1′H G_6	6.20
2′2″H G_4	2.80, 2.56	2′2″H C_1	2.45, 1.93
2′2″H G_5	2.86, 2.69	2′2″H G_2	2.89, 2.78
2′2″H G_6	2.83, 2.60	2′2″H A_3	3.02, 2.75
3′H T_1	4.65	2′2″H T_4	2.48, 2.07
3′H T_2	4.72	2′2″H C_5	2.40, 2.08
3′H A_3	5.08	2′2″H G_6	2.68, 2.41
3′H G_4	4.98	3′H C_1	4.63
3′H G_5	5.02	3′H G_2	5.04
3′H G_6	4.85	3′H A_3	5.07
4′H T_1	3.98	3′H T_4	5.08
4′H T_2	4.05	3′H C_5	4.86
4′H A_3	4.44	3′H G_6	4.72
4′H G_4	4.49	4′H C_1	4.17
4′H G_5	4.30	4′H G_2	n.d.
4′H G_6	4.47	4′H A_3	4.53
		5′5″H C1	4.02
		5′5″H G_2	4.02, 4.02
		5′5″H C_5	4.20, 4.17
		5′5″H G_6	4.12, 4.06
		5′5″H A_3	4.28, 4.14
		5′5″H T_4	4.34, 4.22

[a] Measured at 25°C in ppm (δ) and referenced from external DSS, H_2O- D_2O (90:10 v/v), pH 6.7, 25 mM KH_2PO_4, 150 mM KCl and 1 mM EDTA.
[b] Measured at 15°C in ppm (δ) and referenced from external DSS. Solvent H_2O-D_2O (90:10 v/v); pH 6.7, $R = [\mathbf{9}]/[DNA] = 1$.

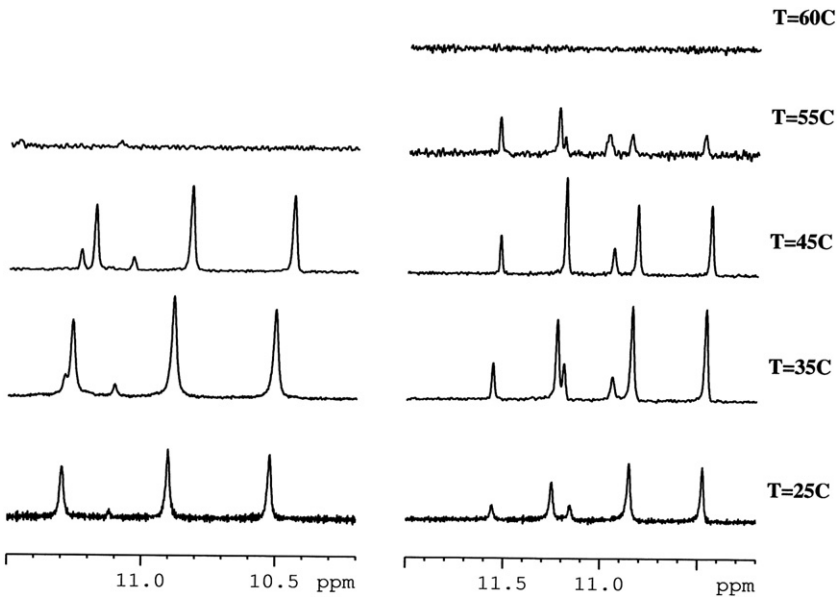

Fig. 5. Thermal denaturation of the parallel $(T2AG3)_4$ quadruplex structure (25 mM KH_2PO_4, 150 mM KCl and 1 mM EDTA, pH 6.7). On the left the spectrum of DNA alone is shown and on the right the spectrum of the complex with **9**.

precluded to continue the titration experiment. The non-exchangeable protons of the oligonucleotide showed the appearance of two new signals at 7.80 and 7.26 ppm, belonging to the drug, together with a signal at 8.40 ppm attributed to H8A3 in the bound species (Fig. 2S). The spectrum of the **9** without oligonucleotide, because of the high symmetry of the molecule showed only 4 signals on the aromatic protons region (Fig. 3S). In order to better identify the drug protons in the complex, the inverse titration experiment was performed, by adding increasing amounts of DNA, from $R = 20$ to $R = 1.5$, to a solution of **9** at constant concentration (0.2 mM) (Fig. 4S). The results are the same of the direct titration (Fig. 2S).

Despite this, NOESY spectra were acquired at $R = [\mathbf{9}]/[(T2AG3)_4] =$ 0.5 and 0.75 that revealed few but significant contacts of **9** with T2, A3, G4, G5 and G6 protons indicating a binding to the quadruplex. Some examples are reported in Fig. 4 and Table 1 lists the NOE data and the distances values of the final structure obtained by MD. All the protons of the bound species were attributed and the assignments are reported in Table 2.

A slight stabilization of the complex was proved by a melting experiment that resulted in an increase of the melting temperature (T_m) in comparison with the free oligonucleotide (Fig. 5)

The dimer structure of **9** was built using the fragment library in Insight II and Discover. Each fragment was optimized by conjugate algorithm and the resulting monomer was also optimized. The dimer was built by joining two monomers and the final structure was optimized once more. Analysis of the resulting geometries revealed that the energetically most favorable conformation was that in which the two aromatic rings adopt a folded structure (Fig. 6) with an angle between aromatic systems around 60°, showing a π stack arrangement.

The so-derived structure was then used as a starting point to study its interaction with the quadruplex by using a molecular docking experiment. Because of the interaction between the dimer structure of **9** and the quadruplex, all the conformation of the dimer obtained by molecular docking were found to be different than the structure previously optimized and used as a starting point in the calculation. Moreover, none of **9**-quadruplex complexes resulting from the calculation has shown the ability of the **9** molecule to intercalate within the quadruplex, probably due to steric hindrance caused by the large size of the dimer.

The analysis of the best solution obtained from molecular docking shows that the dimer molecule binds externally on the two opposite sides of the same strand, stabilized by π–π stacking interactions between the two aromatic rings of the dimer and the aromatic systems of the nucleotides, clamping one strand of the quadruplex (see Fig. 7). By adopting this conformation, the ligand is able to interact with T2, A3, G4 and G5 of various strands, a situation which leads to a significant stabilization of the complex in according the melting experiment. The complex is further stabilized by the presence of a strong hydrogen bond between the ligand amide nitrogen and the OP2 oxygen belonging to G4, at a distance of 2.25Å.

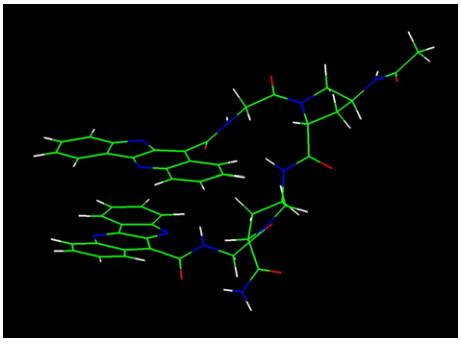

Fig. 6. Energy minimized structure of **9**.

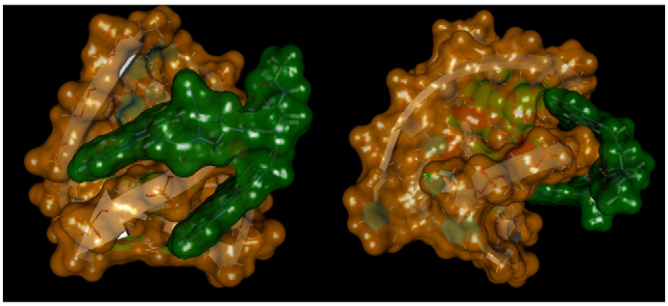

Fig. 7. Lateral (left) and upper (right) views of the **9**-quadruplex best-solution obtained from molecular docking calculations. Both molecules are represented by their solvent accessible surfaces (SAS), green for the **9** molecule and yellow for the quadruplex (PDB ID:1NP9).

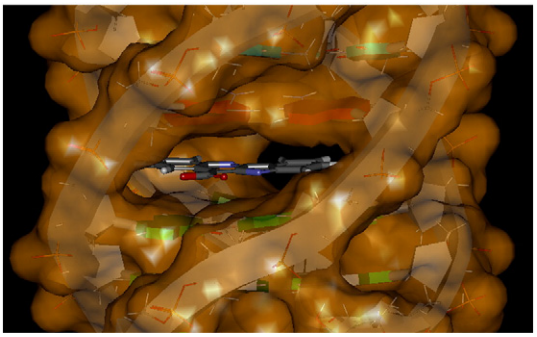

Fig. 8. Schematic drawing of the lowest energy intercalation complex **3**-quadruplex obtained from molecular docking calculation. The ligand is represented in stick, while quadruplex is in rings style, surrounded by the solvent accessible surface.

The goodness of this conformation was confirmed by NOE data with the distance calculated on the basis of the modeling obtained (Table 1).

We built the model of compound **3** and the quadruplex. It was energy-minimized and subjected to a restrained molecular dynamics calculations (MD). The resulting structure was used to obtain a prediction for the complex with the quadruplex structure, using again a molecular docking experiment. Unlike the previous case, the compound **3** behaves as a true intercalating agent, fitting completely within the quadruplex, in the pocket between the A3 and G4 units belonging to the four strands (Fig. 8). These results agree with the interaction between 5-N-Methyl quindoline derivatives and the same quadruplex structure already described in the literature [33,34].

The resulting complex is only stabilized by π–π stacking interactions between the aromatic ring of the ligand and the rings of bases that are located above and below the molecule. The ability of the **3** to fit within the quadruplex, and then to behave as a true intercalating agent, indirectly proves what has been stated before, namely that in the case of the dimer **9**, this possibility is precluded only by steric factors and not by structural and/or electronic characteristics of the molecule.

3.3. *^{1}H NMR experiments on the [**9**]/[d(5′-CGA TCG-3′)$_2$] complex*

The increase in the line broadening of the resonances of NHG_2C_5, NHA3T4 imino, aromatic and anomeric protons can easily be followed during the titration experiments with **9**, as shown in Fig. 9. The imino proton NHC_1G_6 is difficult to monitor because of the fraying which involve the base pairs terminal ends. A slight shielding at maximum of 0.09 ppm was shown for the aromatic protons. The protons were attributed and the assignments are reported in Table 2. The addition of **9** into double stranded oligonucleotide produces a generalized line broadening. The ^{1}H NOESY spectra of the complex with **9** suggest, even with few number of NOEs interactions, the binding at the level of G2, C5 bases (H8G2/Har, H5and H6C5/Har).

The same titration experiment performed with **3** shows no line broadening of imino proton resonances and no chemical shift variations (Fig. 5S Supporting Information) even at high [**3**]/[d(5′-CGA TCG-3′)$_2$] ratio. These observations suggest that compound **3** does not interact with short double helix oligonucleotides as it was also confirmed by 2D NOESY experiments which do not show any contact points between drug and oligonucleotide.

4. Conclusions

In summary we have used competitive dialysis experiments in order to determine the DNA binding properties of a complete series of 4-aminoproline oligomers carrying up to three units of acridine and quindoline molecule. A high selectivity of quindoline 4-aminoproline oligomers for G-quadruplex and triplex structures was observed. Selectivity for quadruplex was also found for some acridine oligomers but the affinity was lower compared with quindoline oligomers. The affinity of acridine 4-aminoproline oligomers was similar to the affinity described for acridine oligomers built on the 2-aminoethylglycine backbone [14] indicating that both backbones provide similar DNA-binding properties to the resulting oligomers.

A detailed NMR/molecular dynamics study on G-quadruplex telomeric sequence and the 4-aminoproline dimer carrying two quindolines shows the reasons of the affinity of the quindoline dimer with the telomeric DNA quadruplex. First the most stable conformation of the quindoline dimer alone adopts a structure in which the two aromatic rings stack with an angle around 60°. This structure fits on the quadruplex clamping one strands and the complex is stabilized by π–π stacking interactions between the aromatic rings of the ligand and the nucleobases of the telomeric sequence that are located above and below the molecule. The results of this work and specially the model of the complex can be used for the design of new molecules with high affinity to telomeres which may have anticancer properties.

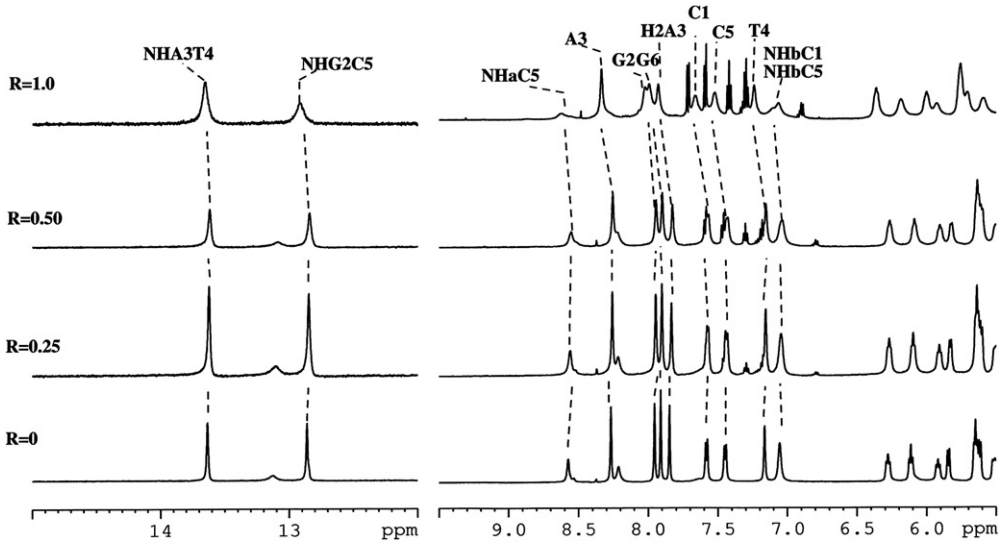

Fig. 9. Imino and aromatic protons region of ^{1}H NMR spectra of d(5′-CGA TCG-3′)$_2$/**9** complex in H_2O, 10 mM KH_2PO_4, 70 mM KCl and 0.2 mM EDTA (pH 7.0), 15 °C at different R = [**9**]/[d(5′-CGA TCG-3′)$_2$].

Acknowledgments

This work was partially supported by grants from Spanish Ministerio de Ciencia e Innovación MICINN (CTQ2005-00315/BQU, CTQ2008-00177, BFU2007-63287, CTQ2009-20541), *Generalitat de Catalunya*, (2009/SGR/208), CIBER-BBN, Networking Centre on Bioengineering, Biomaterials and Nanomedicine, Institute for Research in Biomedicine, and the Barcelona Science Park. CIBER-BBN is an initiative funded by the VI National R&D&i Plan 2008–2011, *Iniciativa Ingenio 2010*, *Consolider Program*, *CIBER Actions* and financed by the Instituto de Salud Carlos III with assistance from the *European Regional Development Fund*.

Appendix A. Supplementary data

Supplementary data to this article can be found online at doi:10.1016/j.bbagen.2011.04.013.

References

[1] R. Palchaudhuri, P.J. Hergerother, DNA as a target for anticancer compounds: methods to determine the mode of binding and the mechanism of action, Curr. Opin. Biotechnol. 18 (2007) 497–503.
[2] B.A. Neto, A.A. Lapis, Recent developments in the chemistry of deoxyribonucleic acid (DNA) intercalators: principles, design, synthesis, applications and trends, Molecules 14 (2009) 1725–1746.
[3] D.P. Arya, B. Willis, Reaching into the major groove of B-DNA: synthesis and nucleic acid binding of a neomycin-Hoechst 33258 conjugate, J. Am. Chem. Soc. 125 (2003) 12398–12399.
[4] E. Fechter, B. Olenyuk, P.B. Dervan, Design of a sequence specific DNA bis-intercalator, Angew. Chem. Int. Ed. 43 (2004) 3591–3594.
[5] D.J. Patel, A.T. Phan, V. Kuryavyi, Human telomere, oncogenic promoter and 5′-UTR G-quadruplexes: diverse higher order DNA and RNA targets for cancer therapeutics, Nucleic Acids Res. 35 (2007) 7429–7455.
[6] G.N. Parkinson, M.P.H. Lee, S. Neidle, Crystal structure of parallel quadruplexes from human telomeric DNA, Nature 417 (2002) 876–880.
[7] J.L. Huppert, Hunting G-quadruplexes, Biochimie 90 (2008) 1140–1148.
[8] L.H. Hurley, Secondary DNA structures as molecular targets for cancer therapeutics, Biochem. Soc. Trans. 29 (2001) 692–696.
[9] H. Han, L.H. Hurley, G-quadruplex DNA: a potential target for anti-cancer drug design, Trends in Pharm. Sci. 21 (2000) 136–142.
[10] D. Monchaud, M.P. Teulade-Fichou, A hitchhiker's guide to G-quadruplex ligands, Org. Biomol. Chem. 6 (2008) 627–636.
[11] N.H. Campbell, G.N. Parkinson, A.P. Reszka, S. Neidle, Structural basis of DNA quadruplex recognition by an acridine drug, J. Am. Chem. Soc. 130 (2008) 6722–6724.
[12] A. Aviñó, I. Navarro, J. Farrera-Sinfreu, M. Royo, J. Aymamí, A. Delgado, A. Llebaria, F. Albericio, R. Eritja, Solid-phase synthesis of oligomers carrying several chromophore units linked by phosphodiester backbones, Bioorg. Med. Chem. Lett. 18 (2008) 2306–2310.
[13] J. Farrera-Sinfreu, A. Aviñó, I. Navarro, J. Aymamí, N.G. Beteta, S. Varón, R. Pérez-Tomás, W. Castillo-Avila, R. Eritja, F. Albericio, M. Royo, Design, synthesis and antiproliferative properties of oligomers with chromophore units linked by amide backbones, Bioorg. Med. Chem. Lett. 18 (2008) 2440–2444.
[14] R. Ferreira, A. Aviñó, R. Pérez-Tomás, R. Gargallo, R. Eritja, Synthesis and G-quadruplex-binding properties of defined acridine oligomers, J. Nucleic Acids (2010), doi:10.4061/2010/489060 article ID 489060 10 pages.
[15] A. Siddiqui-Jain, C.L. Grand, D.J. Bearss, L.H. Hurley, Direct evidence for a G-quadruplex in a promoter region and its targeting with a small molecule to repress *c-myc* transcription, Proc. Natl. Acad. Sci. USA 99 (2002) 11593–11598.
[16] J. Dai, T.S. Dexheimer, D. Chen, M. Carver, A. Ambrus, R.A. Jones, D. Yang, An intermolecular G-quadruplex structure with mixed parallel/antiparallel G-strands formed in the BCL-2 promoter region in solution, J. Am. Chem. Soc. 128 (2006) 1096–1098.
[17] M. Del Toro, P. Puceck, A. Aviñó, J. Jaumot, C. González, R. Eritja, R. Gargallo, Targeting the G-quadruplex-forming region near the P1 promoter in the human BCL-2 gene with the cation porphyrin TMPyP4 and with the complementary C-rich strand, Biochimie 91 (2009) 894–902.
[18] A. Kumar, R.R. Ernst, K. Wüthrich, A two-dimensional nuclear Overhauser enhancement (2D NOE) experiment for the elucidation of complete proton-proton cross-relaxation networks in biological macromolecules, Biochem. Biophys. Res. Comm. 95 (1980) 1–6.
[19] L. Braunschweiler, R.R. Ernst, Coherence transfer by isotropic mixing. Application to proton correlation spectroscopy, J. Magn. Reson. 53 (1983) 521–528.
[20] T.D. Goddard, D.G. Kneller, SPARKY 3, University of California, San Francisco, USA, 2004.
[21] Y. Wang, D.J. Patel, Guanine residues in d(T2AG3) and d(T2G4) form parallel-stranded potassium cation stabilized G-quadruplexes with anti glycosidic torsion angles in solution, Biochemistry 31 (1992) 8112–8119.
[22] S. Mazzini, R. Mondelli, E. Ragg, Structure and dynamics of intercalation complexes of anthracyclines with d(CGATCG)(2) and d(CGTACG)(2). 2D-H-1 and P-31 NMR investigations, J. Chem. Soc., Perkin Trans 2 (1998) 1983–1991.
[23] G.M. Morris, D.S. Goodsell, R.S. Halliday, R. Huey, W.E. Hart, R.K. Belew, A.J. Olson, Automated docking using Lamarckian Genetic Algorithm and an empirical binding free energy function, J. Comput. Chem. 19 (1998) 1639–1662.
[24] R. Huey, G.M. Morris, A.J. Olson, D.S. Goodsell, A semiempirical free energy force field with charge-based desolvation, J. Comput. Chem. 28 (2007) 1145–1152.
[25] F.J. Solis, J.-B. Wets, Minimization by random search techniques, Math. Oper. Res. 6 (1981) 19–30.
[26] M.F. Sanner, Python: a programming language for software integration and development, J. Mol. Graphics Modell. 17 (1999) 57–61.
[27] J. Gasteiger, M. Marsili, Iterative partial equalization of orbital electronegativity—a rapid access to atomic charges, Tetrahedron 36 (1980) 3219–3228.
[28] J. Gros, F. Rosu, S. Amrane, A. De Cian, V. Gabelica, L. Lacroix, J.L. Mergny, Guanines are a quartet's best friends: impact of base substitutions on the kinetics and stability of tetramolecular quadruplexes, Nucleic Acids Res. 35 (2007) 3064–3075.
[29] L.C. Bock, L.C. Griffin, J.A. Latham, E.H. Vermaas, J.J. Toole, Selection of single-stranded DNA molecules that bind and inhibit human thrombin, Nature 355 (1992) 564–566.
[30] Y. Wang, D.J. Patel, Solution structure of the human telomeric repeat d[AG_3 (T_2AG_3)$_3$] G-tetraplex, Structure 1 (1993) 263–282.
[31] J. Ren, J.B. Chaires, Sequence and structural selectivity of nucleic acid binding ligands, Biochemistry 38 (1999) 16067–16075.
[32] P. Ragazzon, J.B. Chaires, Use of competition dialysis in the discovery of G-quadruplex selective ligands, Methods 43 (2007) 313–323.
[33] Y.J. Lu, T.M. Ou, J.H. Tan, J.Q. Hou, W.Y. Shao, D. Peng, N. Sun, X.D. Wang, W.B. Wu, X.Z. Bu, Z.S. Huang, D.L. Ma, K.Y. Wong, L.Q. Gu, 5-*N*-methylated quindoline derivatives as telomeric G-quadruplex stabilizing ligands: effects of 5-*N* positive charge on quadruplex binding affinity and cell proliferation, J. Med. Chem. 51 (2008) 6381–6392.
[34] O.Y. Fedoroff, M. Salazar, H. Han, V.V. Chemeris, S.M. Kerwin, L.H. Hurley, NMR-based model of a telomerase-inhibiting compound bound to G-quadruplex DNA, Biochemistry 37 (1998) 12367–12374.

Supporting Information

Acridine and quindoline oligomers linked through a 4-aminoproline backbone prefer G-quadruplex structures

Rubén Ferreira, Roberto Artali, Josep Farrera-Sinfreu, Fernando Albericio, Miriam Royo, Ramon Eritja, Stefania Mazzini

INDEX

A

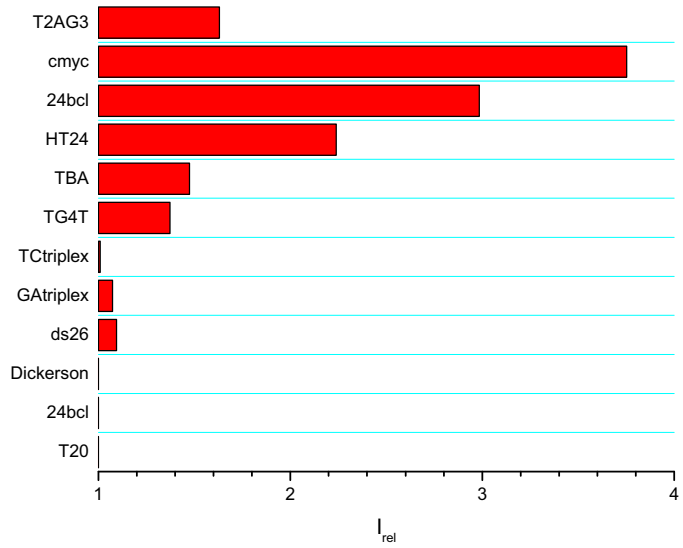

B

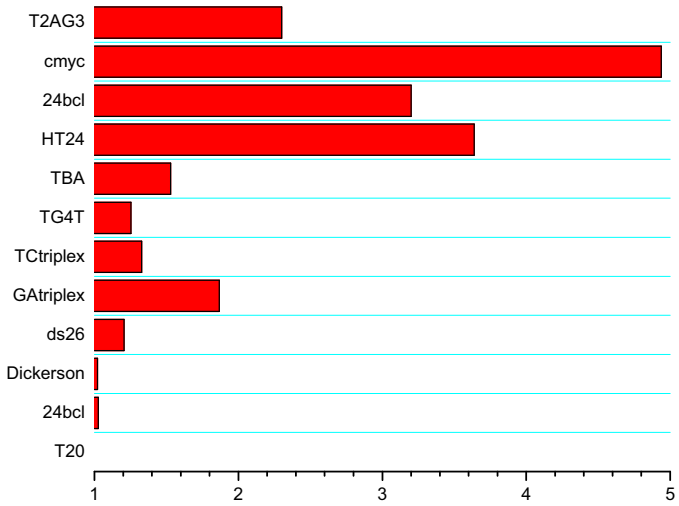

Figure 1S. Competitive dialysis assay for compound **9. A**) 185 mM NaCl, 185 mM KCl, 2 mM NaH_2PO_4, 1 mM EDTA and 6mM Na_2HPO_4 (same conditions than competitive dialysis experiments shown in Figure2). **B**) 25 mM KH_2PO_4, 150 mM KCl and 1 mM EDTA (same conditions than NMR studies). The oligonucleotide sequence T_2AG_3 used in NMR studies is included in addition to the oligonucleotides shown in Figure 2.

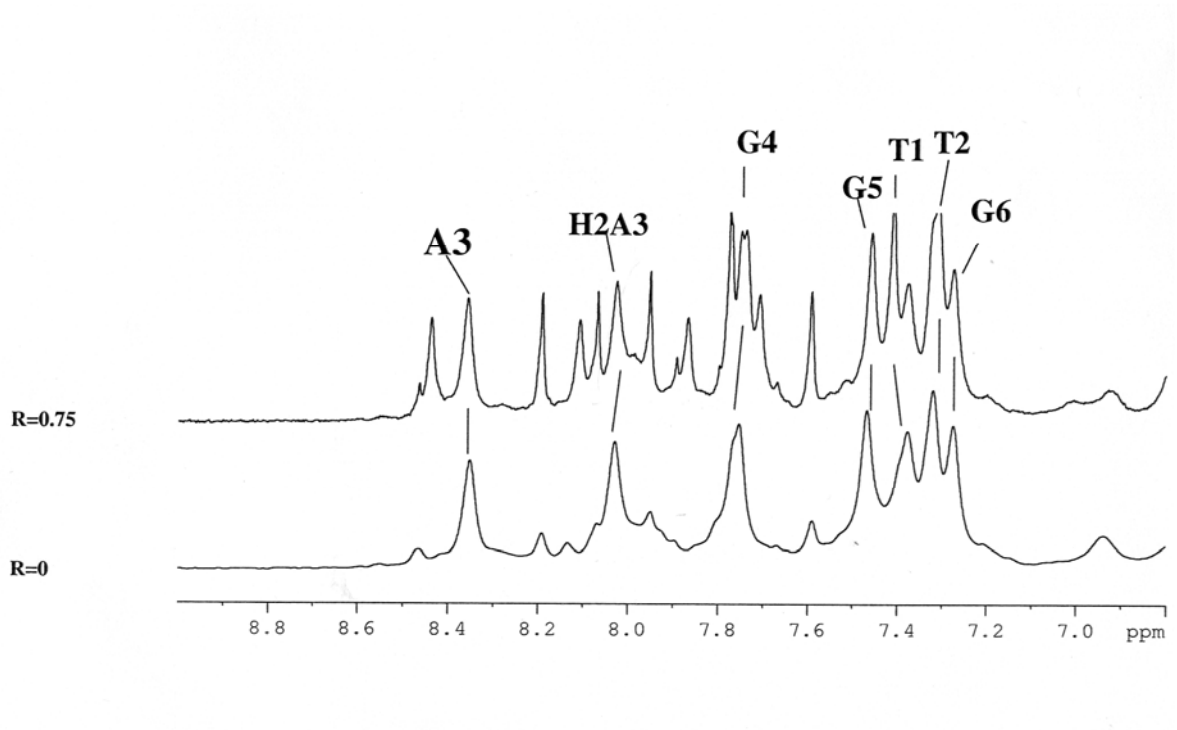

Figure 2S. Aromatic protons region of ^{1}H NMR spectra of $(T2AG3)_4$/ **9** complex in H_2O, 25 mM KH_2PO_4, 150 mM KCl and 1 mM EDTA, pH 6.7, 25°C at R = [**9**]/[$(T2AG3)_4$]=0 and R=0.75. The addition of the **9** causes the loss of the original symmetry of T2AG3.

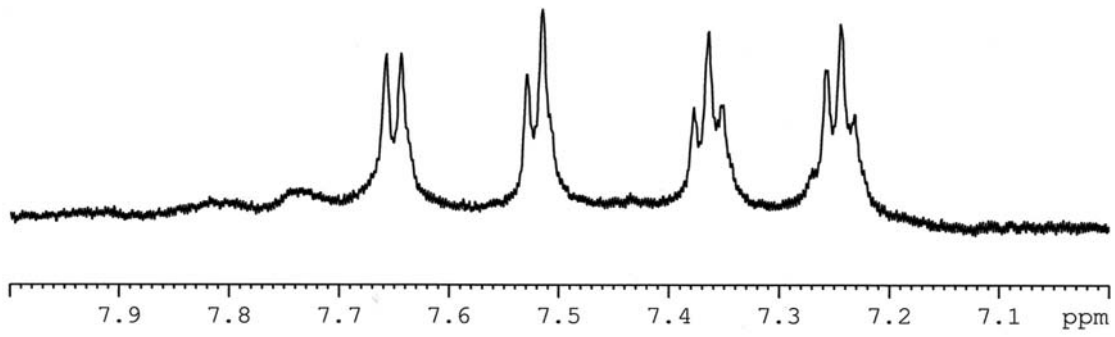

Figure 3S. Aromatic protons region of ^{1}H NMR spectrum of **9** in D_2O, 25 mM KH_2PO_4, 150 mM KCl and 1 mM EDTA, pH 6.7, 25°C.

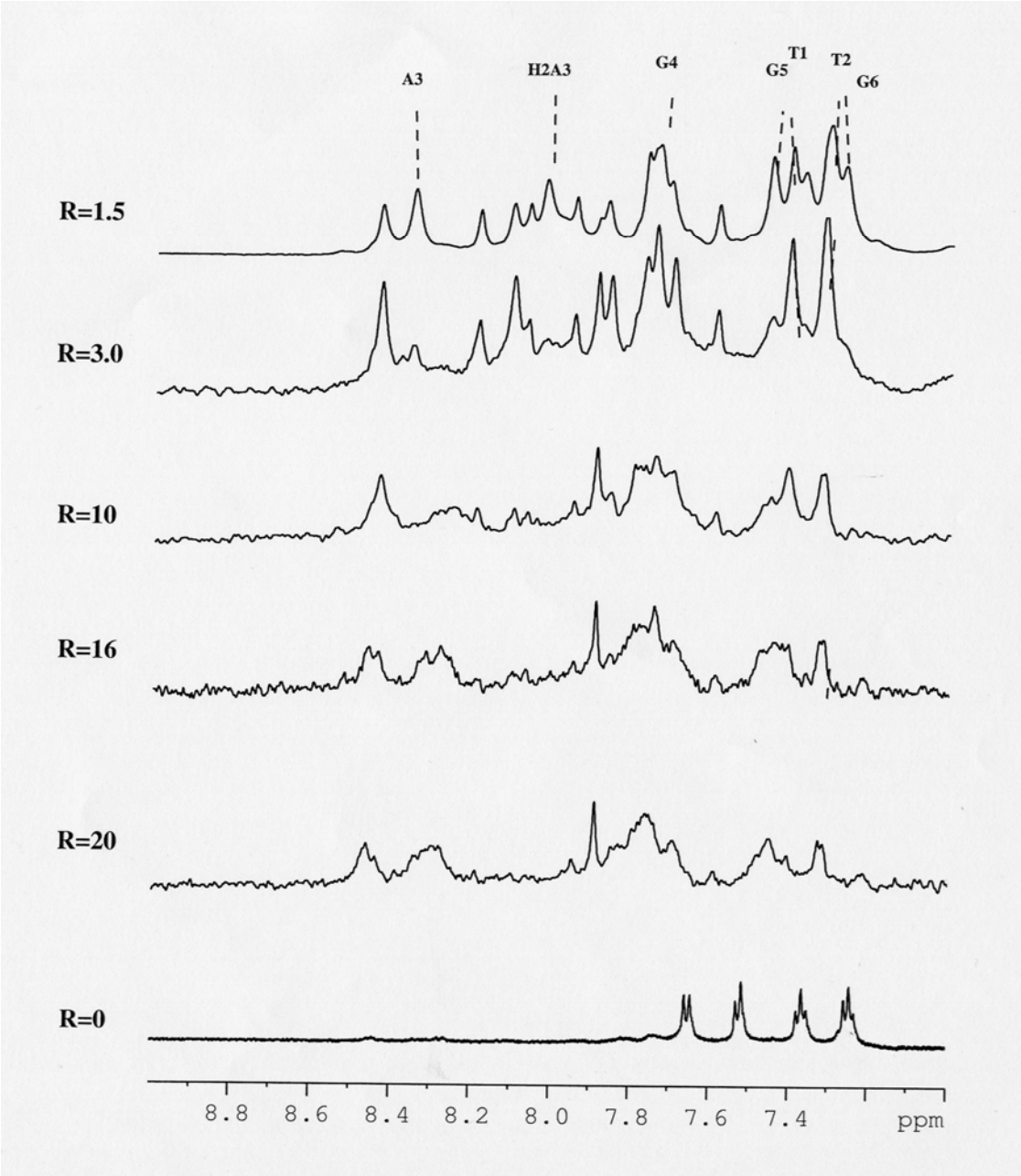

Figure 4S. Aromatic protons region of ^{1}H NMR spectra of $(T2AG3)_4$/ **9** complex in H_2O, 25 mM KH_2PO_4, 150 mM KCl and 1 mM EDTA, pH 6.7, 25°C at different R = [$(T2AG3)_4$]/ [**9].**

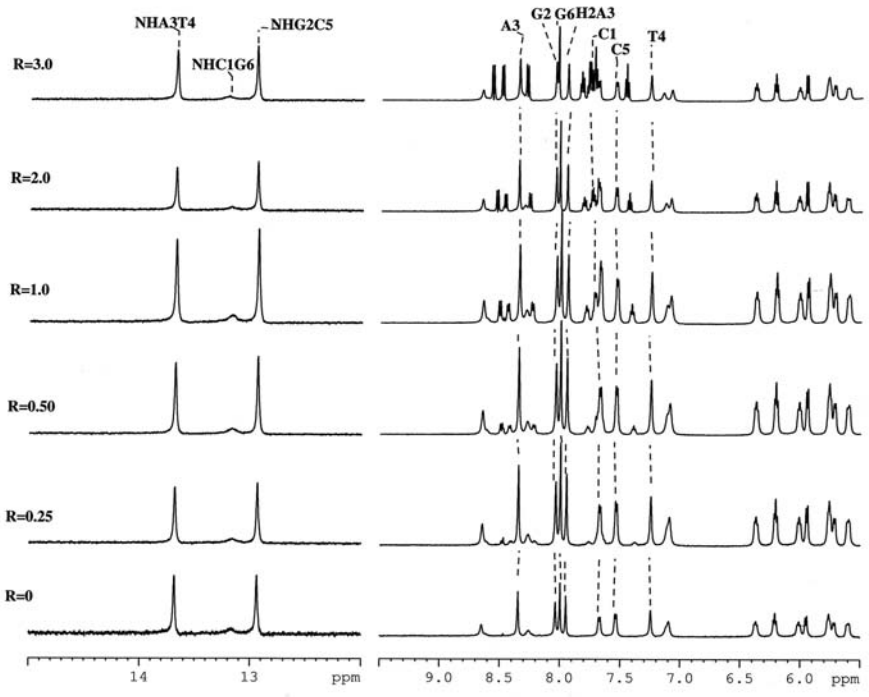

Figure 5S. Imino and aromatic protons region of ^{1}H NMR spectra of $(CGATCG)_2$/ **3** complex in H_2O, 10 mM KH_2PO_4, 70 mM KCl and 0.2 mM EDTA (pH 7.0), 15°C at different R = [**3**]/[$(CGATCG)_2$].

6

SÍNTESIS, PROPIETATS D'UNIÓ AL DNA I ACTIVITAT ANTIPROLIFERATIVA DE DERIVATS DE L'ACRIDINA I DE LA 5-METILACRIDINA

SÍNTESIS, PROPIETATS D'UNIÓ AL DNA I ACTIVITAT ANTIPROLIFERATIVA DE DERIVATS DE L'ACRIDINA I DE LA 5-METILACRIDINA.

Synthesis, DNA-binding and anti-proliferative properties of acridine and 5-methylacridine derivatives

Rubén Ferreira[a], Anna Aviñó[a], Stefania Mazzini[c,*], Ramon Eritja[a,*],

Molecules, 17 (2012) 7067-7082.

[a]*Institute for Research in Biomedicine, IQAC-CSIC, CIBER-BBN Networking Centre on Bioengineering, Biomaterials and Nanomedicine, Baldiri Reixac 10, E-08028 Barcelona, Spain. (Email: ruben.ferreira@irbbarcelona.org, aaagma@cid.csic.es, recgma@cid.csic.es)*

[b]*Dipartimento di Scienze Molecolari Agroalimentari, Università degli Studi di Milano, via Celoria 2, 20133 Milano, Italy, (Email: stefania.mazzini@unimi.it)*

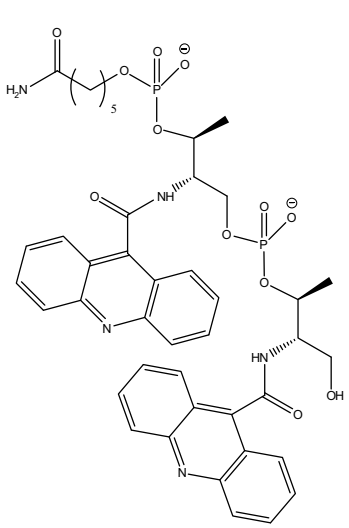

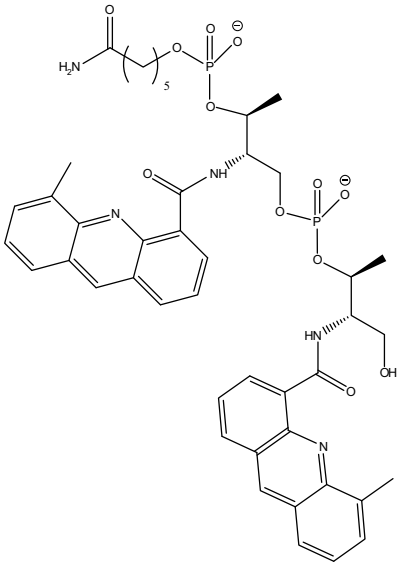

Resum

S'ha sintetitzat diversos derivats d'acridina i s'ha determinat les seves propietats antiproliferatives. Les molècules més actives són els derivats de l'àcid 5-metilacridina-4-carboxilic. S'ha analitzat les propietats d'unió al DNA de les acridines sintetitzades per diàlisis competitiva i es van comparar amb les activitats antiproliferatives. Així doncs, mentre que els derivats de l'acridina inactius mostren una gran selectivitat per estructures formadores de G-quàdruplex, el derivat més actiu de la 5-metilacridina-4-carboxamida té una gran afinitat pel DNA però mostra poca especificitat. Es van realitzar estudis de RMN amb una seqüència de DNA telomèrica formadora de G-quàdruplex i amb una de dúplex amb el compost més actiu de la 5-metilacridina-4-carboxamida. Les valoracions per RMN confirmen la gran afinitat del compost més actiu pel DNA dúplex i pel G-quàdruplex.

Molecules **2012**, *17*, 7067-7082; doi:10.3390/molecules17067067

OPEN ACCESS

molecules

ISSN 1420-3049

www.mdpi.com/journal/molecules

Article

Synthesis, DNA-Binding and Antiproliferative Properties of Acridine and 5-Methylacridine Derivatives

Rubén Ferreira [1,2], Anna Aviñó [1,2], Stefania Mazzini [3] and Ramon Eritja [1,2,*]

[1] Institute for Research in Biomedicine (IRB Barcelona), Baldiri Reixac 10, E-08028 Barcelona, Spain; E-Mails: ruben.ferreira@irbbarcelona.org (R.F.); anna.avinyo@irbbarcelona.org (A.A.)

[2] Institute for Advanced Chemistry of Catalonia (IQAC), CSIC, CIBER-BBN Networking Centre on Bioengineering, Biomaterials and Nanomedicine, Jordi Girona 18, E-08034 Barcelona, Spain

[3] Department of Agro-Food Molecular Sciences (DISMA), University of Milan, Via Celoria 2, 20133 Milan, Italy; E-Mail: stefania.mazzini@unimi.it

* Author to whom correspondence should be addressed; E-Mails: recgma@cid.csic.es or ramon.eritja@irbbarcelona.org; Tel.: +34-93-403-9942; Fax: +34-93-204-5904.

Received: 8 May 2012; in revised form: 24 May 2012 / Accepted: 4 June 2012 / Published: 8 June 2012

Abstract: Several acridine derivatives were synthesized and their anti-proliferative activity was determined. The most active molecules were derivatives of 5-methylacridine-4-carboxylic acid. The DNA binding properties of the synthesized acridines were analyzed by competitive dialysis and compared with the anti-proliferative activities. While inactive acridine derivatives showed high selectivity for G-quadruplex structures, the most active 5-methylacridine-4-carboxamide derivatives had high affinity for DNA but showed poor specificity. An NMR titration study was performed with the most active 5-methylacridine-4-carboxamide, confirming the high affinity of this compound for both duplex and quadruplex DNAs.

Keywords: acridine; DNA-binding drugs; solid-phase synthesis; G-quadruplex; NMR

1. Introduction

DNA-intercalating drugs are planar molecules composed by several fused aromatic rings that form stacks between DNA base pairs, thus reducing the opening and unwinding of the double helix. Each

intercalating drug binds strongly to particular base pairs as a result of several interactions, ranging from van der Waals forces to the formation of hydrogen bonds with adjacent nucleobases [1,2].

Telomeres are specialized DNA-protein structures at the termini of chromosomes crucial for chromosomal stability and accurate replication. Human telomeric DNA contains tandem repeats of the sequence TTAGGG. The guanine-rich strand can fold into four-stranded G-quadruplex structures involving G-tetrads, which are currently an attractive target for the development of anti-cancer drugs [3,4]. Acridine derivatives inhibit telomerase, presumably through their interaction with the G-quadruplex structures found in telomeric DNA [5,6]. A wide range of small molecules have been studied as quadruplex-binding and stabilizing ligands [7]. Most of these share common structural features, namely: (i) a planar heteroaromatic chromophore, which stacks by π-π interactions onto the G-quartet motif at the terminus of a quadruplex; and (ii) short alkyl chain substituents usually terminated by an amino group that is fully cationic at physiological pH. The precise nature of these substituents has been found to influence quadruplex affinity and selectivity [8,9].

Topoisomerase alters DNA topology through the decatenation and relaxation of supercoiled DNA [10]. By unwinding double-stranded DNA, this essential enzyme allows for normal cellular functions, such as replication and transcription [10]. DNA topoisomerases exist in various eukaryotic and prokaryotic forms [11] and are classified in two large groups named type I and type II. Topoisomerase-targeting anti-cancer drugs can be divided into two broad classes depending on their mechanism of action, either catalytic inhibitors or "topoisomerase poisons" [12]. The latter can be further subclassified into two groups: non-intercalating compounds, such as etoposide, and intercalators, like amsacrine and doxorubicin [13]. Intercalators act by forming ternary complexes with topoisomerases and DNA to inhibit re-ligation. However, the selectivity of intercalators for a particular DNA sequence is very low. Most often, selectivity is obtained from interactions of side-chain substitution in the major and minor grooves [14]. Another strategy to improve the selectivity of intercalating drugs is by linking several intercalating units. Various authors have described the synthesis of bis- or tris-intercalating drugs that show promising activity and selectivity [15–18].

The consensus is that acridine analogs target DNA through intercalation and disrupt enzyme recognition and/or association [19]. Acridine-4-carboxamides are a series of DNA intercalating topoisomerase poisons that show anti-tumor activity [20]. Among these, *N*-[2-(dimethylamino)ethyl]acridine-4-carboxamide (DACA) is a DNA-intercalating agent that inhibits both topoisomerase I and II [21] and is currently in phase II clinical trials. There are tight correlations between ligand structure, cytotoxicity and DNA-binding kinetics [22].

In the present study, we designed, synthesized and studied acridine and 5-methylacridine derivatives as potential anti-tumoral agents. During the selection of the acridine derivatives, we considered solid-phase methods for the preparation of the target compounds. Recently, we used peptide [23] and oligonucleotide chemistry [24] to prepare DNA-intercalating oligomers with several backbones for the assembly of a number of intercalating units. The modular character of solid-phase methods allows the rapid preparation of larger molecules that have G-quadruplex specific affinity [25,26]. The cytotoxicity of the acridine and 5-methylacridine derivatives to a tumoral cell line was assessed in MTT cell viability assays, thus identifying compounds exerting anti-tumoral activity. The DNA binding properties of the synthesized acridines were studied by competitive dialysis experiments. The affinity of the most active 5-methylacridine-4-carboxamide derivative to G-quadruplex telomeric and

duplex DNA sequences was further analyzed by NMR. This analysis confirmed the binding of this compound to both quadruplex and duplex DNA sequences.

2. Results and Discussion

2.1. Synthesis of the Acridine Derivatives

We selected acridine-9-carboxylic acid (**1**) and 5-methylacridine-4-carboxylic acid (**2**) as starting compounds for the preparation of the new derivatives (Figure 1). Compound **1** is commercially available and has no anti-proliferative properties [24]. Compound **2** has been described as an intermediate in the synthesis of the bis-acridine derivatives of DACA [18]. Thus, in this study, we undertook the synthesis of compounds with this unit. Two types of derivatives were prepared. First, the replacement of the dimethylamino group of DACA for two residues of lysine (**3**) or arginine (**4**) was studied (Figure 2). These derivatives were prepared to check whether the protonable dimethylamino group can be replaced by amino acids with amino (Lys) or guanidino (Arg) groups. The synthesis of compounds **3** and **4** was performed by a standard solid-phase peptide approach using Fmoc-amino acids. After assembly of the dipeptide carboxylic acid **2** was coupled to the α-amino group of the dipeptides. Next we studied the possibility to generate compounds holding two units of the 5-methylacridine ring present in the 5-methyl derivative of DACA [18]. To join the units, we chose the L-threoninol backbone connected by phosphodiester links [27] for several reasons. The length of the threoninol linker is compatible with DNA structure and can be obtained in an enantiomerically pure form.

Figure 1. Chemical structures of *N*-[2-(dimethylamino)ethyl]acridine-4-carboxamide (DACA) and starting compounds **1** and **2**.

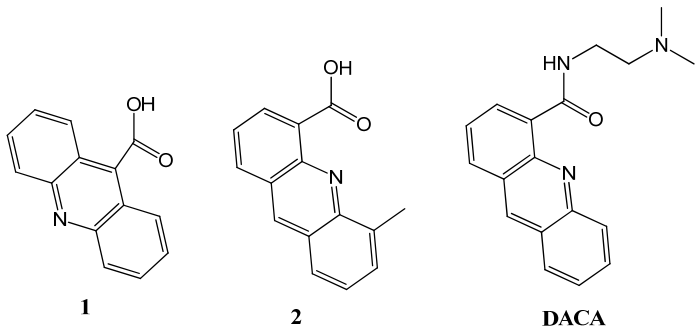

Figure 2. The acridine and 5-methylacridine derivatives synthesized in this study.

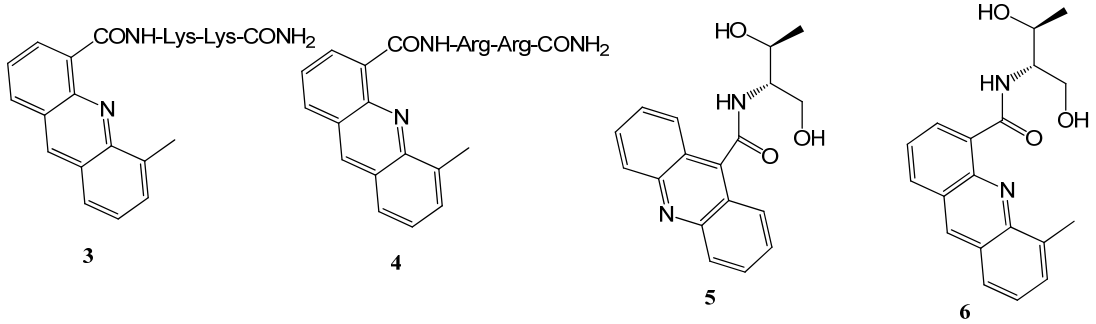

Figure 2. *Cont.*

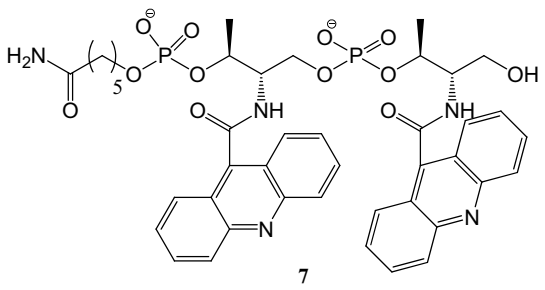

7

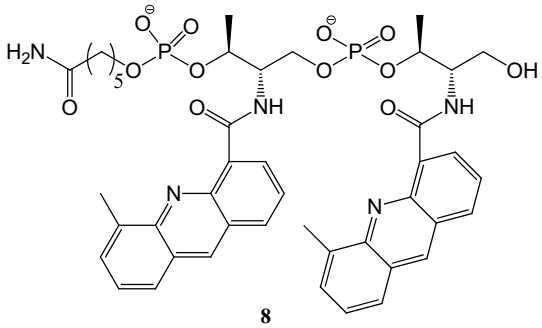

8

Threoninol has two distinct hydroxyl groups and one amino group. The intercalating agent can be attached at the amino group position, thus leaving the hydroxyl groups to build the backbone using standard solid-phase oligonucleotide methods [23,27]. To this end, the primary hydroxyl group of threoninol was protected by the 4,4′-*O*-dimethoxytrityl (DMT) group and the secondary alcohol was used to prepare the phosphoramidite derivative (Scheme 1).

Scheme 1. Synthesis of the threoninol phosphoramidite derivative.

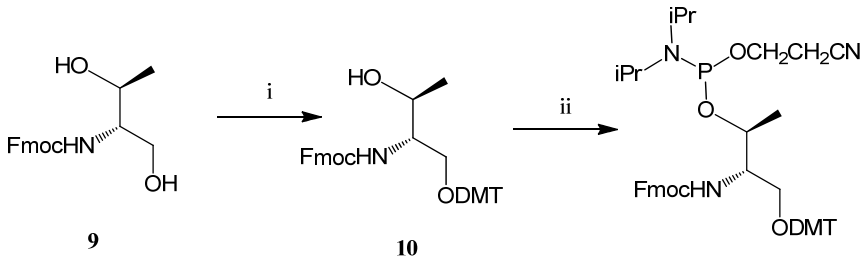

9 **10** **11**

Reagents and Conditions: i. Dimethoxytrityl chloride, DMAP, Pyr, o.n.; ii. *O*-2-cyanoethyl-*N*,*N*-diisopropyl chlorophosphoramidite, DCM, DIEA, 0 °C then 25 °C for 1 h.

For the synthesis of intercalating oligomers **7** and **8**, the threoninol backbone was grown on solid-phase, and then the intercalating agent was assembled on solid support. This strategy is more convenient for rapid synthesis, as it is unnecessary to construct each monomer with its intercalating agent, as described previously [23]. Here we report a hybrid synthesis. First, the phosphoramidite described above was assembled into a dimer (Scheme 2).

Modified standard phosphoramidite chemistry was used. This consists of cycles of 3 chemical reactions: (1) removal of the DMT group with 3% trichloroacetic acid in dichloromethane; (2) phosphoramidite coupling using 10-fold excess of phosphoramidite and 40-fold excess of tetrazole and (3) oxidation of phosphite to phosphate with hydroperoxide solution in acetonitrile. The use of iodine for the oxidation of phosphites was avoided as we have previously observed some side products attributable to the premature removal of the Fmoc group. Also a capping reaction with acetic anhydride and *N*-methylimidazole was omitted in order to avoid the acetylation of the amino group observed in the synthesis of oligonucleotide-peptide conjugates using Fmoc-amino acids [28]. To guarantee a high coupling yield, two consecutive phosphoramidite coupling reactions were systematically performed. Finally, Fmoc groups of threoninol were removed to allow coupling of

carboxylic acids **1** or **2**, thereby providing the desired dimers **7** and **8** in satisfactory yields. Monomeric threoninol derivatives **5** and **6** were prepared as described [23].

Scheme 2. Solid-phase synthesis of acridine oligomers.

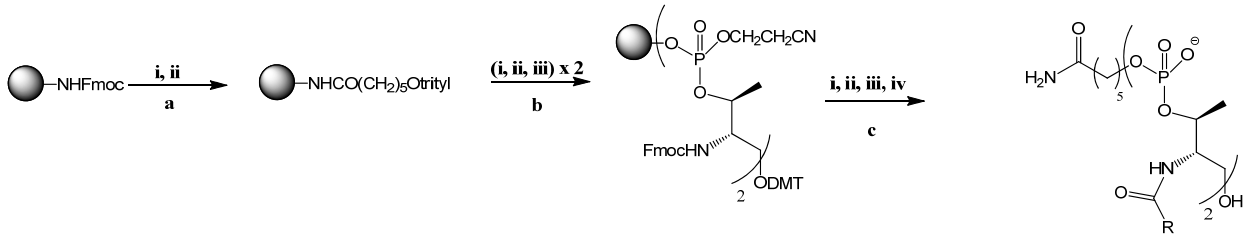

Reagents and Conditions: (a) i. 20% piperidine, DMF, 30 min; ii. 5 eq. Trityl-O-$(CH_2)_5$COOH, 5 eq. PyBOP, 10 eq. DIEA in DMF, 1 h; (b) i. 3% trichloroacetic acid in DCM, 10 min; ii. 10 eq. compound **11**, 40 eq. tetrazole in acetonitrile, 10 min × 2; iii. 70% aq. *tert*-butylhydroperoxide/acetonitrile (14:84 v/v), 10 min; (c) i. 20% piperidine, DMF, 30 min; ii. 5 eq. compound **1** or **2**, 5 eq. PyBOP, 10 eq. DIEA in DMF, 1 h; iii. 3% trichloroacetic acid in DCM, 10 min; iv. TFA 95%, 2 h. R = acridine (**7**) or 5-methylacridine (**8**).

2.2. Cell Viability Assay

The *in vitro* cytotoxicity of the compounds **1**–**8** was evaluated by colorimetric assays with a tetrazole salt (MTT) on the human colon carcinoma HBT38 cells. This assay is based on the capacity of living cells to incorporate and reduce the tetrazole salt. This reaction can be followed by the absorbance change of the reduced and oxidized forms. The reduction is observed only in living cells and the color intensity is directly correlated with the number of viable cells. The IC_{50} values for compounds **1**–**8** are given in Table 1.

Table 1. Anti-proliferative activity: n.a. not active.

Compound	IC_{50} (μM) HBT38
1	n.a.
2	75
3	n.a.
4	n.a.
5	n.a.
6	60
7	n.a.
8	25

The acridine derivatives **1**, **5** and **7** did not show anti-tumoral activity. These results were expected as acridine-9-carboxylic acid [24] as well as 2-aminoethylglycine and aminoprolyl oligomers have no antiproliferative activity [24,25]. On the other hand, the 5-methylacridine-4-carboxylic acid derivatives **2**, **6** and **8** had moderate activity, dimer **8** being the most active compound. In contrast, the peptide derivatives **3** and **4** lost this activity. This is partially in agreement with the antiproliferative properties assigned to 5-methylacridine-4-carboxylic acid derivatives [17,18,20–22]. We expected some activity for peptide derivatives **3** and **4** because these compounds have a positively charged residue linked to

the carboxylic acid function as in the case of 5-methyl-*N*-[2-(dimethylamino)ethyl]acridine-4-carboxamide that have potent antitumor activity [21]. But in our study the addition of lysine and arginine residues instead of the *N*-dimethylaminoethyl group were detrimental for the antiproliferative activity. Also, literature reports that 5-substituted bis(acridine-4-carboxamide) derivatives have good anticancer activities [18]. In this work we observed the best antiproliferative activity for the dimer carrying two 5-methylacridine-4-carboxamide units linked through threoninol phosphate backbone confirming the increase of activity by linking two DNA intercalating units. To our knowledge this is the first bisintercalating molecule linked by phosphate bonds with increased activity. In order to confirm that the activity may be mediated by DNA binding, competitive dialysis experiments were performed.

2.3. Competitive Dialysis Studies

To evaluate the selectivity and the affinity of intercalating derivates for DNA structures, we performed a competitive dialysis experiment using 11 nucleic acid structures [25]. The DNA sequences were selected to represent all the potential DNA structures that may be present at physiological pH: single-stranded, duplex, parallel and antiparallel triplexes and quadruplexes. As models for single-stranded structures, we used T20 and 24bclc. As duplexes, we used a self-complementary sequences Dickerson–Drew dodecamer (Dickerson) and a 26 mer (ds26). A parallel triplex (TC triplex) and an antiparallel triplex (GA triplex) were also prepared by mixing a hairpin Watson–Crick sequence and the corresponding triplex-forming sequence. Finally, the following G-quadruplex sequences were prepared: the tetramolecular parallel G-quadruplex TG_4T [29]; the antiparallel thrombin-binding aptamer (TBA) [30]; the human telomere sequence (HT24) [31]; and the promoter sequences of *c-myc* (cmyc) [32] and *bcl-2* (24bcl) [33]. The amount of bound ligand was directly proportional to the binding constant for each DNA structure [34,35]. Figure 3 shows the oligonucleotide affinity for each compound and Figure 3A the results for acridine and 5-methyl acridine carboxylic acids **1** and **2**. Acridine-9-carboxylic acid **1** interacts only with duplex ds26, the methyl derivative **2** induced a change in the affinity showing also a triplex preference. While acridine derivatives **5** and **7** showed quadruplex selectivity, the methyl analogs **6** and **8** lost most of the selectivity, although they presented a higher affinity for most DNA sequences (Figures 3C,D). In contrast, the peptide derivatives **3** and **4** presented lower binding affinity for DNA (Figure 3B). Comparing the competitive dialysis results with the antiproliferative activity we can observe that the peptide derivatives **3** and **4** have both low affinity for any DNA molecule and no antiproliferative activity. Acridine derivatives **5** and **7** have interesting binding affinities for DNA quadruplex sequences but this affinity does not trigger inhibition of cell grown of HBT38 cancer cell lines. This is agreement with previous work on 2-aminoethylglycine and aminoprolyl acridine oligomers [24,25]. Finally, the most antiproliferative compounds **6** and **8** have a strong affinity for all type of DNA sequences. Although we cannot discard the hypothesis that the antiproliferative activity of these compounds is due to direct binding to proteins, we can hypothesize that the antiproliferative activity of these compounds may be mediated by DNA binding. This is in agreement with the inhibition of DNA topoisomerases described for this family of compounds [12,17,18,20–22].

Figure 3. Competitive dialysis assay: The amount of ligand bound to each DNA structure is shown as a bar graph.

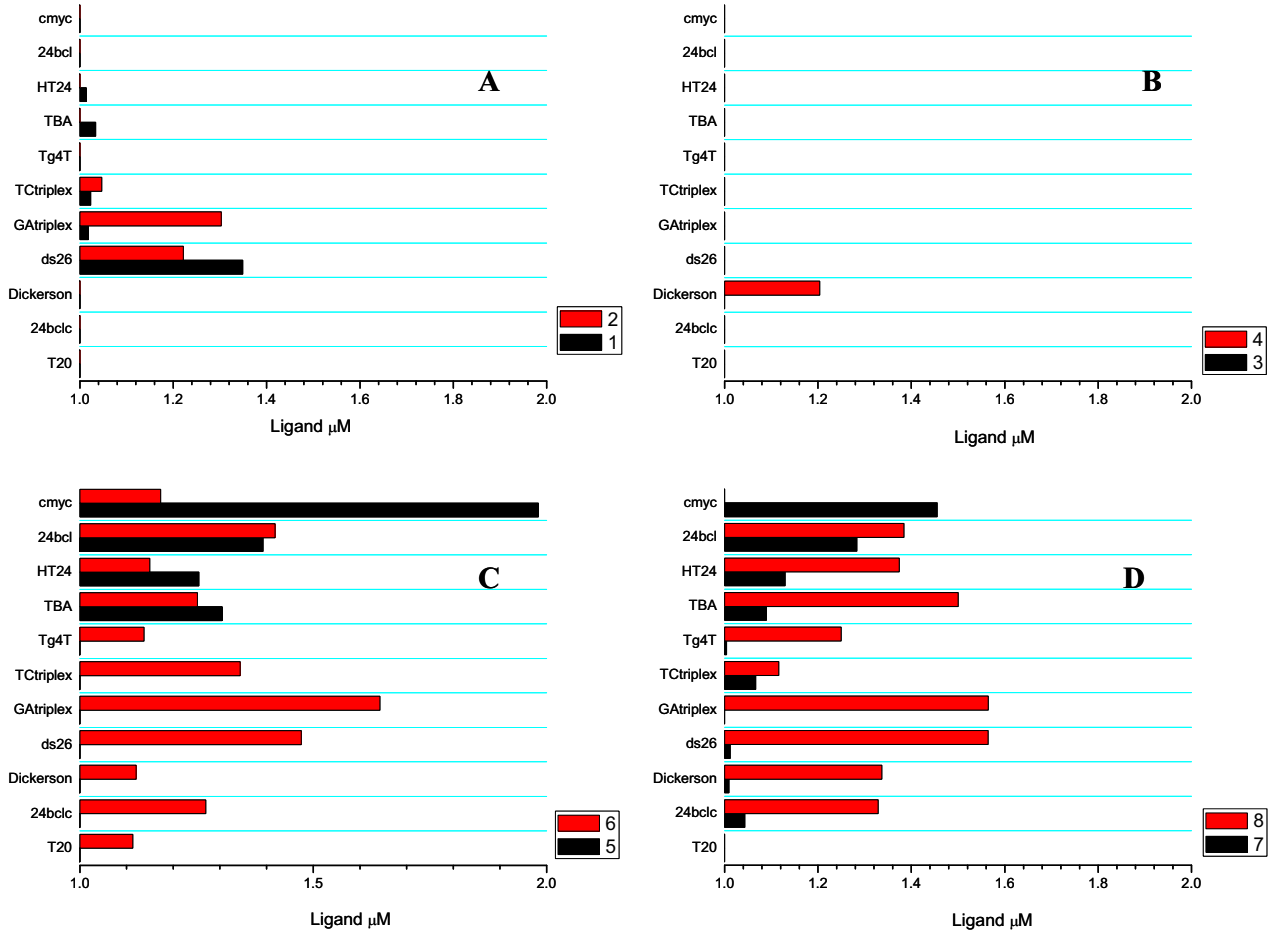

2.4. NMR Spectroscopy

On the basis of cell viability studies the compound **8** demonstrated the highest anti-tumoral activity. Competitive dialysis experiments also show that compound **8** has affinity to all types of DNA sequences in spite of the presence of a negative phosphate backbone that may hinder binding with the DNA polyanionic molecule. As it is the first time that a bisintercalating molecule having a negatively charged phosphate backbone is shown to have DNA binding properties we confirmed that compound **8** is able to bind to both duplex and quadruplex DNA molecules. First we tried the classical methods such UV- and fluorescence-based melting assays [36], fluorescence intercalator displacement assay [37], and mass spectrometry [38]. But any of these methods provide conclusive results and some of these methods were not compatible with the fluorescence properties of the acridine derivatives. For these reasons and in order to confirm the interaction with DNA, **8** was titrated into a solution of the quadruplex model $(T_2AG_3)_4$ of the human telomere sequence and the resulting mixtures were analyzed by ^{1}H-NMR. Similar experiments were performed with the starting carboxylic acid **2**. T_2AG_3 is a short model sequence contained in the HT24 oligonucleotide. This oligonucleotide has been used previously for NMR characterization of drug binding on telomeric DNA sequences [39]. The short oligonucleotide has a more simple NMR spectrum than HT24 sequence, thus facilitating the study of the interactions of the drug with the DNA sequence.

The NMR spectra for the quadruplex showed three signals in the region of 10–12 ppm, belonging to Hoogsteen-bound guanine imino proton of the G quartets (Figure 4). During the addition of **8** to the quadruplex solution until reaching a ratio R = [**8**]/[$(T_2AG_3)_4$] = 3, the imino proton signals caused by G4, G5 and G6 splits in the downfield-shifted region were related to the bound quadruplex form. This result confirms an **8** quadruplex interaction complex associated with drug toxicity. The imino protons signals were broad and disappeared at high R indicating that more than one species in equilibrium were present in solution (Figure 4).

Figure 4. Imino proton region of $(TTAGGG)_4$ resulting from the titration of the quadruplex with compounds **2** and **8**.

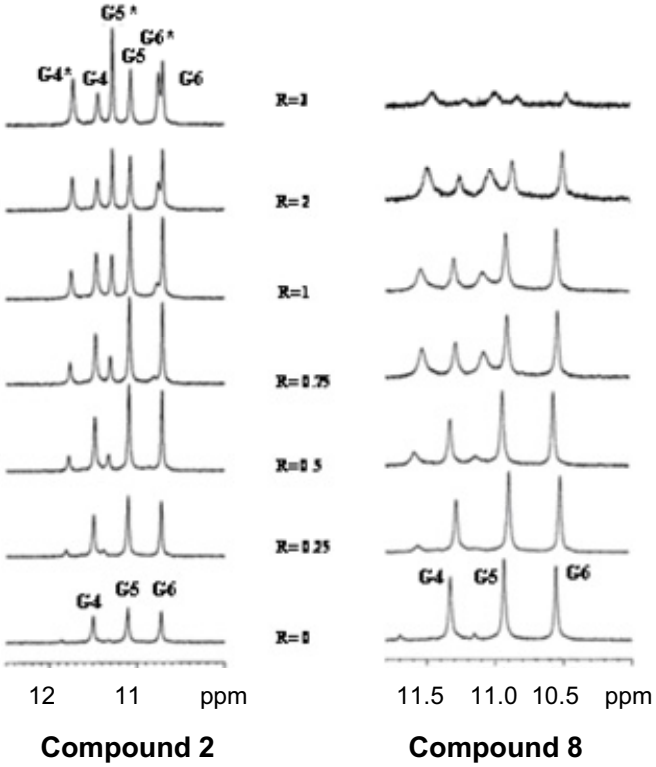

The oligonucleotide sequence 5′-CGATCG-3′ was used as model for a DNA duplex. In the region of 13–14 ppm, the NMR spectra of the duplex showed two signals, these belonging to imino proton of A3T4 and G2C5 (Figure 5).

During the addition of **8** to the duplex solution until reaching the ratio R = [**8**]/[$(CGATCG)_2$] = 1, the imino proton signals caused by G2 decreased the intensity of the signal, thereby indicating a preferred site of interaction at this level. The equivalent experiments with compound **2** showed slight differences. During the addition of **2** to the quadruplex solution until reaching the ratio R = [**2**]/[$(T_2AG_3)_4$] = 3, the imino proton signals caused by G4, G5 and G6 split in the downfield-shifted region, thus indicating a binding interaction. In this case the imino proton signals were not broad at high R (Figure 4), indicating that only one bound species was present in the solution. Free quadruplex species structure was still present at this ratio.

During the addition of **2** to the duplex solution until reaching the ratio R = [**2**]/[$(CGATCG)_2$] = 1, the imino proton signal decreased in the intensity and was broad, suggesting the presence of multiple binding sites and complex equilibria (Figure 5).

Figure 5. Imino proton region of $(CGATCG)_2$ resulting from the titration of the duplex with compounds **2** and **8**.

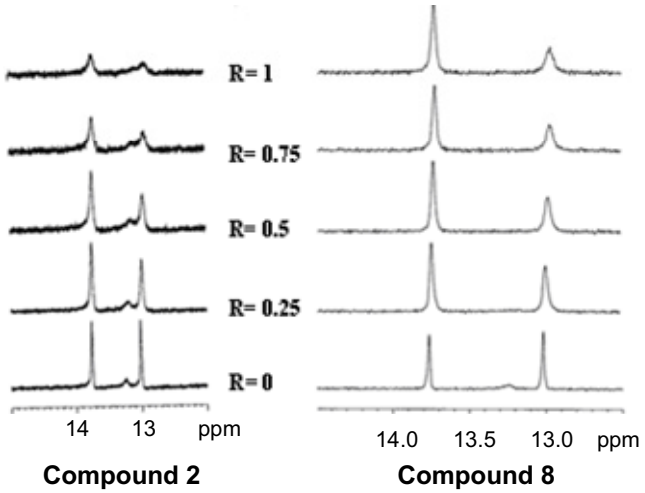

In summary, NMR titration experiments confirm the interaction of compound **8** with both duplex and quadruplex DNA sequences, even when the quadruplex complex equilibria in solution were involved, whereas the interaction was more specific with the double helix, compound **2** showing the opposite behavior.

3. Experimental

3.1. Oligonucleotides and General Information

Standard phosphoroamidites and reagents for DNA synthesis were purchased from Applied Biosystems and from Link Technologies. The synthesis of the oligonucleotides was performed at a scale of 1 μmol on an Applied Biosystem DNA/RNA 3400 synthesizer by solid-phase 2-cyanoethylphosphoroamidite chemistry. The following sequences were prepared: T20: d(5′-TTT TTT TTT TTT TTT TTT TT-3′), 24bclc: d(5′-CCC GCC CCC TTC CTC CCG CGC CCG-3′), Dickerson: d(5′-CGC GAA TTC GCG-3′), ds26: d(5′-CAA TCG GAT CGA ATT CGA TCC GAT TG-3′), GA triplex : d(5′-GAA AGA GAG GAG GCC TTT TTG GAG GAG AGA AAG-3′) + d(5′-CCT CCT CTC TTT C-3′), TC triplex: d(5′-CCT CCT CTC TTT CCC TTT TTC TTT CTC TCC TCC-3′) + d(5′-GAA AGA GAG GAG G-3′), TG4T: d(5′-TGG GGT-3′), TBA: d(5′-GGT TGG TGT GGT TGG-3′), HT24: d(5′-TAG GGT TAG GGT TAG GGT TAG GGT-3′), 24bcl: d(5′-CGG GCG CGG GAG GAA GGG GGC GGG-3′) and cmyc: d(5′-GGG GAG GGT GGG GAG GGT GGG GAA GGT GGG G-3′). The resulting oligonucleotides were purified by HPLC and desalted in a Sephadex (NAP-10) G25 column. Acridine-9-carboxylic acid (**1**) was obtained from Aldrich and 5-methylacridine-4-carboxylic acid (**2**) (Figure 1) was prepared following the strategy described previously [40]. Threoninol derivative (**5**) (Figure 2) was prepared following the literature [23]. NMR spectra were recorded on a Varian Mercury 400 (small compounds) or a Bruker AV-600 (oligo-nucleotides) spectrometers.

3.2. Solid-Phase Synthesis of Peptide Derivatives **3** *and* **4**

Peptide derivatives **3**, **4** were synthesized using Fmoc solid phase peptide synthesis. Fmoc-protected amino acids were obtained from Nova Biochem. The side chain of lysine was protected with the *t*-butoxycarbonyl (Boc) group and the arginine side chain was protected with the 2,2,4,6,7-pentamethyldihydrobenzofuran-5-sulfonyl (Pbf) group. Amino acids were assembled on 4-(2',4'-dimethoxyphenyl-Fmoc-aminomethyl)-phenoxy resin (Rink amide resin) solid support which allowed the cleavage in a single step treatment with 95% TFA, providing peptide amides in high yields and purities. Synthesis of amino acids derivatives: a cycle for each amino acid addition consisted of the following steps: (1) 20% piperidine in DMF; (2) 5% DIPEA in DCM; and (3) Fmoc-protected amino acid coupling with TBTU, HOBT and DIPEA catalysis then (1) 20% piperidine in DMF; (2) either compound **1** or compound **2** coupling with PyBOP, HOBT and DIPEA catalyst; and (3) cleavage with 95% TFA. The compounds were analyzed by MALDI-TOF: **3** [M^+] = 493.3 (expected 493.3) and **4** [M^+] = 549.3 (expected 549.3), and by HPLC obtaining a single peak of retention time 7.9 and 8.2 min, respectively. Analytical HPLC was performed using an XBridge OST C18 (Waters) column (2.5 μM, 4.6 × 5.5 mm) using a 10-min linear gradient from 9% to 45% B, and a flow rate of 1 mL/min; solution A was 5% ACN in 0.1 M aqueous TEAA, and B 70% ACN in 0.1 M aqueous TEAA. MALDI-TOF spectra were obtained using a *Perseptive Voyager DETMRP* mass spectrometer, equipped with a nitrogen laser at 337 nm using a 3 ns pulse. The matrix used contained 2,5-dihydroxybenzoic acid (DHB, 10 mg/mL in water).

3.3. N-((2S,3S)-1,3-Dihydroxybutan-2-yl)-5-methylacridine-4-carboxamide (**6**)

5-Methylacridine-4-carboxylic acid (**2**, 100 mg, 0.42 mmol) was reacted with EDCI (121 mg, 0.63 mmol), HOBt (85 mg, 0.63 mmol), L-threoninol (44 mg, 0.42 mmol) and 100 μL DIEA in DMF. Purification by chromatography on silica gel (10% methanol over AcOEt) yielded the compound **6** (50 mg, 35%) as a foam. UV (λ_{max}): 249, 343, 359 and 385 nm. Fluorescence spectra: exc: 385 nm, em: 433 nm. HPLC: a single peak of retention time 9.0 min. ^{1}H-NMR, δ_H (400 MHz, $CDCl_3$): 8.99 (dd, 1H, J = 7.1 and 1.6 Hz), 8.87 (s, 1H), 8.15 (dd, 1H, J = 8.4 and 1.1 Hz), 7.90 (d, 1H, J = 8.4 Hz), 7.65 (dd, 1H, J = 8.4 and 7.1 Hz), 7.50 (dd, 1H, J = 8. 4 and 7.0 Hz), 4.39–4.35 (m, 1H), 4.34–4.29 (m, 1H), 4.16–4.08 (m, 2H), 2.96 (s, 3H), 1.35 (d, 3H, J = 6.4). [M^+] = 324.8 (expected for $C_{42}H_{48}N_5O_{12}P_2$ 324.4).

3.4. Solid-Phase Synthesis of Acridine Oligomers **7** *and* **8**

The assembly of L-threoninol derivatives (**7**, **8**) was carried out on Rink amide polystyrene solid support. An optimized oligonucleotide synthesis was used to build the main chain and then the intercalating agent was introduced (Scheme 2). Oligomer synthesis: a cycle for each L-threoninol backbone addition consisted of the following steps: (1) 3% trichloroacetic acid/dichlorometane; (2) coupling of compound **11** with tetrazole activation, 2 times; and (3) oxidation with 70% aq. *tert*-butyl hydroperoxide/acetonitrile (14:84 v/v) then (1) 20% piperidine in DMF; (2) either compound **1** or compound **2** coupling with PyBOP, HOBT and DIPEA catalyst; (3) 3% trichloroacetic acid/dichlorometane; and (4) cleavage with 95% TFA. The compounds were analyzed by

MALDI-TOF: **7** [M^+] = 876.8 (expected for $C_{42}H_{48}N_5O_{12}P_2$ 876.8), **8** [M^+] = 905.4 (expected for $C_{44}H_{52}N_5O_{12}P_2$ 904.9) and by HPLC obtaining a peak of retention time 4.1 and 13.2 min, respectively.

3.5. (9H-Fluoren-9-yl)methyl (2R,3R)-1-(bis(4-methoxyphenyl)(phenyl)methoxy)-3-hydroxybutan-2-ylcarbamate (**10**)

N-[(9*H*-Fluoren-9-yl)methyloxycarbonyl]-L-threoninol (compound **9**, 500 mg, 1.53 mmol) was dissolved in anhydrous pyridine (10 mL) and reacted with 4,4′-*O*-dimethoxytriphenylmethyl chloride (1.84 mmol) and 4-dimethylaminopyridine (0.20 mmol, DMAP). The mixture was stirred at room temperature overnight. The reaction was quenched with methanol (0.5 mL) and the solvents were removed under reduced pressure. The residue was dissolved in dichloromethane (100 mL) and the organic phase was washed with saturated aqueous NaCl (50 mL). The solvent was evaporated and the residue was purified by chromatography on neutral aluminum oxide. The product was eluted with dichloromethane and 1% of methanol. The pure compound was obtained as an oil (733 mg, 76%). ^{1}H-NMR, δ_H (400 MHz, $CDCl_3$): 8.55–6.77 (m, 21H), 4.45–4.33 (m, 3H), 4.22 (t, 1H, J = 7.0 Hz), 4.08 (m, 1H), 3.76 (s, 6H), 3.43 (dd, 1H, J = 9.8 and 5.0), 3.25 (dd, 1H, J = 9.8 and 3.8 Hz), 1.16 (d, 3H, J = 6.3 Hz). ^{13}C-NMR, δ_C (100 MHz, $CDCl_3$): 158.6; 158.5; 1475; 145.0; 144.1; 144.0; 139.6; 130.1; 129.2; 128.3; 127.9; 127.7; 127.1; 125.2; 119.9; 113.2; 69.2; 68.9; 66.7; 58.4; 20.2; 19.5.

3.6. (9H-Fluoren-9-yl)methyl (4R,5R)-7-(2-cyanoethoxy)-8-isopropyl-1,1-bis(4-methoxyphenyl)-5,9-dimethyl-1-phenyl-2,6-dioxa-8-aza-7-phosphadecan-4-ylcarbamate (**11**)

Compound **10** (1.1 mmol) was dried by evaporation with anhydrous ACN. The residue was dissolved in anhydrous DCM (20 mL) and diisopropylethylamine (DIEA) (4.6 mmol) was added under argon atmosphere. The solution was cooled to 0 °C in a ice bath and 2-cyanoethoxy-*N,N*-diisopropyl-aminochlorophosphine (2.2 mmol) was added dropwise with a syringe. After the completion of the reaction, DCM (50 mL) was added and the organic layer was washed with saturated aqueous NaCl (100 mL). The solvent was evaporated under reduced pressure and the residue was purified by column chromatography on neutral aluminum oxide. The product was eluted with hexane/ethyl acetate 2:3. The desired compound was obtained (556 mg, 61%). ^{1}H-NMR, δ_H (400 MHz, $CDCl_3$): 7.77–6.80 (m, 21H), 5.09 and 4.99 (d, 1H, J = 9.6 and 9.5 Hz, respectively, two isomers), 4.41–4.38 (m, 3H), 4.36–4.29 (m, 2H), 4.22 (t, 1H, J = 7.0 Hz), 3.93–3.79 (m, 1H), 3.79 (s, 6H), 3.55–3.34 (m, 4H), 2.36 (t, 2H, J = 6.3 Hz), 1.27–1.11 (m, 15H). ^{31}P-NMR, δ_P (81 MHz, $CDCl_3$): 148.88, 148.63 (phosphoric acid as external reference). ^{13}C NMR, δ_C (100 MHz, $CDCl_3$): 158.6; 158.4; 144.8; 144.9; 144.1; 144.0; 136.0; 130.1; 130.0; 129.1; 128.3; 127.9; 127.7; 127.1; 127.0; 126.8; 125.1; 119.9; 117.6; 113.2; 69.0; 68.9; 66.6; 58.4; 56.2; 55.2;43.2; 43.1; 24.7; 24.6; 24.4; 24.3; 20.3, 19.5; 19.4.

3.7. Competitive Dialysis Assays

Slide-A-Lyzer Mini Dialysis Units 3500MWCO were purchased from Pierce. A total 200 mL of the dialysate solution containing 1 μM of the compound was used for each competition dialysis assay. A volume of 100 μL of 50 μM monomeric unit of each of oligonucleotide sequence was placed in the

dialysis unit. Potassium phosphate buffer containing 185 mM NaCl, 185 mM KCl, 2 mM NaH_2PO_4, 1 mM Na_2EDTA and 6 mM Na_2HPO_4 at pH 7 was used for all experiments.

The samples were allowed to equilibrate with continuous stirring at room temperature overnight. Dialysis samples were transferred to an Eppendorf tube. In order to measure the compound entered in the dialysis unit, dialysis samples were treated with a snake venom phosphodiesterase to release the intercalating compound as described previously [25].

Finally, the fluorescence of each sample was measured (λ_{ex} and λ_{em} were set to 252 and 435 nm for compounds **1**, **5** and **7** and to 258 and 460 nm for compounds **2**, **3**, **4**, **6** and **8** and normalized for each compound.

3.8. Cell Viability Assays

The *in vitro* cytotoxicity of the compounds (**1**, **2**, **3**, **4**, **5**, **6**, **7** and **8**) was evaluated by colorimetric assays with a tetrazole salt (MTT) on the HTB-38 (human colon carcinoma) cell line. The cell line was cultured in RPMI and supplemented with 10% fetal calf serum and 200 mM L-glutamine. Cells were grown in a humidified atmosphere of air containing 5% CO_2 at 37°. Cells were plated in triplicate wells (1.5×10^4 cells per well) in 100 μL of growth medium in 96-well plates and allowed to proliferate for 24 h. They were then treated with increasing concentrations of the compounds. After 72 h incubation, 20 μM MTT (5 mg/mL in phosphate buffer saline 10%) was added for additional 4 h. Absorbance at 570 nm was measured on a multiwell plate reader after removing the medium and addition of 50 μL of dimethyl sulfoxide. Cell viability was expressed as a percentage of control and IC_{50} was determined as the concentration of the drug that produced 50% reduction of absorbance at 570 nm.

3.9. NMR Spectroscopy

The NMR spectra of oligonucleotides were recorded at 25 °C on a Bruker AV-600 spectrometer equipped with a *z*-gradient triple resonance TXI and were processed with TOPSPIN v.1. The instrument was operated at a frequency of 600.10 MHz for ^1H. ^1H chemical shifts (δ_H) were measured in ppm and referenced to external DSS (sodium 2,2-dimethyl-2-silapentane-5-sulfonate salt) set for 0.00 ppm. Estimated accuracy for protons is within 0.02 ppm. The samples for NMR measurements were dissolved in 500 μL H_2O/D_2O (9:1) containing 25 mM KH_2PO_4, 150 mM KCl and 1 mM EDTA (pH 6.7) for the quadruplex d(5′-TTAGGG-3′)$_4$ and containing 10 mM KH_2PO_4, 70 mM KCl and 0.2 mM EDTA (pH 7.0) for the double helix d(5′-CGATCG-3′)$_2$. The final concentration of the oligonucleotide solutions ranged between 0.7 and 0.6 mM. A stock solution of **2** and **8** was prepared in DMSO-d_6 at the concentrations of 10 and 20 mM, respectively. ^1H-NMR titration was performed by adding increasing amounts of **2** and **8** to the oligonucleotide solutions at an R= [Ligand]/[DNA] ratio equal to 0, 0.25, 0.5, 0.75, 1, 2 and 3.

4. Conclusions

Several compounds with the 5-methylacridine-4-carboxamide core group present in a DNA intercalating dual topoisomerase I/II inhibitor (DACA) derivative were prepared and their

anti-proliferative properties were studied. Solid-phase methods were used for the rapid generation of the 5-methylacridine-4-carboxamide derivatives. As the protonable dimethylamino group was considered relevant for the biological activity [22], we first studied the replacement of this group by natural amino acids with protonable groups like lysine and arginine. Unfortunately, the resulting peptide-acridine compounds lost DNA binding capacity and thus were inactive. In contrast, the threoninol derivative carrying the 5-methylacridine-4-carboxamide unit retained the anti-proliferative properties of the 5-methylacridine-4-carboxylic acid. Linking two units of the 5-methylacridine-4-carboxamide with a threoninol phosphate backbone generated the most active compound, in spite of the presence of the negative phosphate backbone. This finding demostrates that linking several intercalating units with a negative backbone may indeed be a useful strategy to obtain novel DNA-intercalating drugs as the DNA-binding properties are not negatively affected and compounds have increased solubility in aqueous solutions.

Acknowledgments

This work was supported by the Spanish Ministry of Education (grants BFU2007-63287, CTQ2010-20541-C03-01), and the Generalitat de Catalunya (2009/SGR/208). CIBER-BBN is an initiative funded by the VI National R&D&i Plan 2008-2011, Iniciativa Ingenio 2010, Consolider Program, CIBER Actions and financed by the Instituto de Salud Carlos III with assistance from the European Regional Development Fund. SM acknowledges the support of the University of Milano (PUR 2009 Funds) and PRIN09 (2009Prot.2009J54YAP_005). RF is recipient of a FPI contract from the Spanish Ministry of Science.

References

1. Palchaudhuri, R.; Hergerother, P.J. DNA as a target for anticancer compounds: Methods to determine the mode of binding and the mechanism of action. *Curr. Opin. Biotechnol.* **2007**, *18*, 497–503.
2. Neto, B.A.; Lapis, A.A. Recent developments in the chemistry of deoxyribonucleic acid (DNA) intercalators: Principles, design, synthesis, applications and trends. *Molecules* **2009**, *14*, 1725–1746.
3. Neidle, S.; Parkinson, G. Telomere maintenance as a target for anticancer drug discovery. *Nat. Rev. Drug Discov.* **2002**, *1*, 383–393.
4. Mergny, J.L.; Hélène, C. G-quadruplex DNA: A target for drug design. *Nat. Med.* **1998**, *4*, 1366–1367.
5. Perry, P.J.; Read, M.A.; Davies, R.T.; Gowan, S.M.; Reszka, A.P.; Wood, A.A; Kelland, L.R.; Neidle, S. 2,7-Disubstituted aminofluorenone derivatives as inhibitors of human telomerase. *J. Med. Chem*. **1999**, *42*, 2679–2684.
6. Harrison, R.J.; Gowan, S.M.; Kelland, L.R.; Neidle, S. Human telomerase inhibition by substituted acridine derivatives. *Bioorg. Med. Chem. Lett*. **1999**, *9*, 2463–2468.
7. Monchaud, D.; Teulade-Fichou, M.P. A hitchhiker's guide to G-quadruplex ligands. *Org. Biomol. Chem.* **2008**, *6*, 627–636.

8. Ou, T.M.; Lu, Y.J.; Tan, J.H.; Huang, Z.S.; Wong, K.Y.; Gu, L.Q. G-quadruplexes: Targets in anticancer drug design. C*hemMedChem* **2008**, *3*, 690–713.
9. Campbell, N.H.; Patel, M.; Tofa, A.B.; Ghosh, R.; Parkinson, G.N.; Neidle, S. Selectivity in ligand recognition of G-quadruplex loops. *Biochemistry* **2009**, *48*, 1675–1680.
10. Larsen, A.K.; Escargueil, A.E.; Skladanowski, A. Catalytic topoisomerase II inhibitors in cancer therapy. *Pharmacol. Ther.* **2003**, *99*, 167–181.
11. Corbett, K.D.; Berger, J.M. Structure, molecular mechanism, and evolutionary relatioships in DNA topoisomerases. *Annu. Rev. Biophys. Biomol. Struct*. **2004**, *33*, 95–118.
12. Topcu, Z. DNA topoisomerases as targets for anticancer drugs. *J. Clin. Pharm. Ther.* **2001**, *26*, 405–416.
13. Arimondo, P.B.; Hélène, C. Design of new anti-cancer agents based on topoisomerase poisons targeted to specific DNA sequences. *Curr. Med. Chem. Anticancer Agents* **2001**, *1*, 219–235.
14. Adams, A. Crystal structures of acridine complexed with nucleic acids. *Curr. Med. Chem*. **2002**, *9*, 1667–1675.
15. Arya, D.P.; Willis, B. Reaching into the major groove of B-DNA: Synthesis and nucleic acid binding of a neomycin-Hoechst 33258 conjugate. *J. Am. Chem. Soc.* **2003**, *125*, 12398–12399.
16. Fechter, E.; Olenyuk, B.; Dervan, P.B. Design of a sequence specific DNA bis-intercalator. *Angew. Chem. Int. Ed.* **2004**, *43*, 3591–3594.
17. Spicer, J.A.; Gamage, S.A.; Finlay, G.J.; Denny, W.A. Synthesis and evaluation of unsymmetrical bis(arylcarboxamides) designed as topoisomerase-targeted anticancer drugs. *Bioorg. Med. Chem*. **2002**, *10*, 19–29.
18. Gamage, S.A.; Spiecer, J.A.; Atwell, G.J.; Finlay, G.J.; Baguley, B.C.; Denny, W.A. Structure-activity relationships for substituted bis(acridine-4-carboxamides): A new class of anticancer agents. *J. Med. Chem*. **1999**, *42*, 2383–2393.
19. Mucsi, I.; Molnár, J.; Tanaka, M.; Santelli-Rouvier, C.; Patelis, A.M.; Galy, J.P.; Barbe, J. Effect of acridine derivatives on the multiplication of herpes simplex virus. *Anticancer Res.* **1998**, *18*, 3011–3015.
20. Wakelin, L.P.; Adams, A.; Denny, W.A. Kinetic studies of the binding of acridine carboxamide topoisomerase poisons to DNA: Implications for mode of binding of ligands with uncharged chromophores. *J. Med. Chem*. **2002**, *45*, 894–901.
21. Atwell, G.J.; Rewcastle, G.W.; Baguley, B.C.; Denny, W.A. Potential antitumor agents. 50. In vivo solid-tumor activity of derivatives of *N*-[2-(dimethylamino)ethyl]acridine-4-carboxamide. *J. Med. Chem.* **1987**, *30*, 664–669.
22. Atwell, G.J.; Cain, B.F.; Baguley, B.C.; Finlay, G.J.; Denny, W.A. Potential antitumor agents. 43. Synthesis and biological activity of dibasic 9-aminoacridine-4-carboxamides, a new class of antitumor agents. *J. Med. Chem*. **1984**, *24*, 1481–1485.
23. Aviñó, A.; Navarro, I.; Farrera-Sinfreu, J.; Royo, M.; Aymamí, J.; Delgado, A.; Llebaria, A.; Albericio, F.; Eritja, R. Solid-phase synthesis of oligomers carrying several chromophore units linked by phosphodiester backbones. *Bioorg. Med. Chem. Lett.* **2008**, *18*, 2306–2310.

24. Ferrera-Sinfreu, J.; Aviñó, A.; Navarro, I.; Aymamí, J.; Beteta, N.G.; Varón, S.; Pérez-Tomás, R.; Castillo-Avila, W.; Eritja, R.; Albericio, F.; Royo, M. Design, synthesis and antiproliferative properties of oligomers with chromophore units linked by amide backbones. *Bioorg. Med. Chem. Lett.* **2008**, *18*, 2440–2444.
25. Ferreira, R.; Aviñó, A.; Pérez-Tomás, R.; Gargallo, R.; Eritja, R. Synthesis and G-quadruplex binding properties of defined acridine oligomers. *J. Nucleic Acids* **2010**, *2010*, doi:10.4061/2010/489060.
26. Ferreira, R.; Artali, R.; Ferrera-Sinfreu, J.; Albericio, F.; Royo, M.; Eritja, R.; Mazzini, S. Acridine and quindoline oligomers linked through a 4-aminoproline backbone prefer G-quadruplex structures. *Biochim. Biophys. Acta* **2011**, *1810*, 769–776.
27. Asanuma, H.; Shirasuka, K.; Takarada, T.; Kashida, H.; Komiyama, M. DNA-dye conjugates for controllable H* aggregation. *J. Am. Chem. Soc.* **2003**, *125*, 2217–2223.
28. Ocampo, S.; Albericio, F.; Fernández, I.; Vilaseca, M.; Eritja, R. A straightforward synthesis of 5'-peptide oligonucleotide conjugates using N^{α}-Fmoc-protected amino acids. *Org. Lett.* **2005**, *7*, 4349–4352.
29. Gros, J.; Rosu, F.; Amrane, S.; De Cian, A.; Gabelica, V.; Lacroix, L.; Mergny, J.L. Guanines are a quartet's best friends: Impact of base substitutions on the kinetics and stability of tetramolecular quadruplexes. *Nucleic Acids Res.* **2007**, *35*, 3064–3075.
30. Bock, L.C.; Griffin, L.C.; Latham, J.A.;Vermaas, E.H.; Toole, J.J. Selection of single-stranded DNA molecules that bind and inhibit human thrombin. *Nature* **1992**, *355*, 564–566.
31. Wang, Y.; Patel, D.J. Solution structure of the human telomeric repeat d[$AG_3(T_2AG_3)_3$] G-tetraplex. *Structure* **1993**, *1*, 263–282.
32. Siddiqui-Jain, A.; Grand, C.L.; Bears, D.J.; Hurley, L.H. Direct evidence for a G-quadruplex in a promoter region and its targeting with a small molecule to repress *c-myc* transcription. *Proc. Natl. Acad. Sci. USA* **2002**, *99*, 11593–11598.
33. Dai, J.; Dexheimer, T.S.; Chen, D.; Carver, M.; Ambrus, A.; Jones, R.A.; Yang, D. An intermolecular G-quadruplex structure with mixed parallel/antiparallel G-strands formed in the BCL-2 promoter region in solution. *J. Am. Chem. Soc.* **2006**, *128*, 1096–1098.
34. Ren, J.; Chaires, J.B. Sequence and structural selectivity of nucleic acid binding ligands. *Biochemistry* **1999**, *38*, 16067–16075.
35. Ragazzon, P.; Chaires, J.B. Use of competition dialysis in the discovery of G-quadruplex selective ligands. *Methods* **2007**, *43*, 313–323.
36. De Cian, A.; Guittat, L.; Kaiser, M.; Saccà, B.; Amrane, S.; Bourdoncle, A.; Alberti, P.; Teulade-Fichou, M.P.; Lacroix, L.; Mergny, J.L. Fluorescence-based melting aasyas for studying quadruplex ligands. *Methods* **2007**, *42*, 183–195.
37. Tran, P.L.; Largy, E.; Hamon, F.; Teulade-Fichou, M.P.; Mergny, J.L. Fluorescence intercalator displacement assay for screening G4 ligands towards a variety of G-quadruplex structures. *Biochimie* **2011**, *93*, 1288–1296.
38. Guittat, L.; Alberti, P.; Rosu, F.; van Miert, S.; Thetiot, E.; Pieters, L.; Gabelica, V.; De Pauw, E.; Ottaviani, A.; Riou, J.F.; Mergny, J.L. Interactions of cryptolepine and neocryptolepine with unusual DNA structures. *Biochimie* **2003**, *85*, 535–547.

39. Lu, Y.J.; Ou, T.M.; Tan, J.H.; Hou, J.Q.; Shao, W.Y.; Peng, D.; Sun, N.; Wang, X.D.; Wu, W.B.; Bu, X.Z.; *et al*. 5-*N*-Methylated quindoline derivatives as telomeric G-quadruplex stabilizing ligands: Effects of 5-*N* positive charge on quadruplex binding affinity and cell proliferation. *J. Med. Chem.* **2008**, *51*, 6381–6392.
40. Spicer, A.; Gamage, S.A.; Atwell, G.J.; Finlay, G.J.; Baguley, B.C.; Denny, W.A. Structure-activity relationships for acridine-substituted analogues of the mixed topoisomerase I/II inhibitor *N*-[2-(dimethylamino)ethyl]acridine-4-carboxamide. *J. Med. Chem*. **1997**, *40*, 1919–1929.

Sample Availability: Samples of the compounds **1**, **2**, **5** and **6** are available from the authors.

© 2012 by the authors; licensee MDPI, Basel, Switzerland. This article is an open access article distributed under the terms and conditions of the Creative Commons Attribution license (http://creativecommons.org/licenses/by/3.0/).

Discussió general i conclusions

Discussió general

Des de que hi ha evidències que els quàdruplex de guanina es poden formar en el genoma humà, per exemple en els telòmers o en zones promotores d'oncogens, l'interès pel seu estudi i la seva utilització com a diana terapèutica ha anat augmentat progressivament. S'ha postulat que l'estabilització dels quàdruplex de guanina està relacionada amb la regulació transcripcional d'alguns gens. Per aquest motiu, en els últims anys ha hagut un gran interès en el disseny de lligands amb afinitat pels quàdruplex de guanina presents en zones promotores d'oncogens, per tal d'obtenir nous fàrmacs contra el càncer. Per una altra banda, més d'un 85% de les cèl·lules cancerígenes presenten un gran nivell de l'enzim telomerasa. Ja fa un temps que es va postular que el disseny d'inhibidors contra la telomerasa podria ser una bona alternativa per obtenir nous fàrmacs contra el càncer. Però desgraciadament, aquesta aproximació no ha tingut l'èxit esperat, ja que l'acció sobre la telomerasa necessita un temps molt llarg per tal de trobar un efecte terapèutic. Actualment es veu que les estructures de quàdruplex són una millor diana terapèutica i és per aquest motiu que hi ha un gran interès en dissenyar lligands selectius per quàdruplex de guanina.

La primera part d'aquesta tesi es basa en el el desenvolupament d'una nova metodologia sintètica per obtenir estructures de G-quàdruplex molt estables. Es descriu el disseny i la síntesi de molècules amb quatre cadenes riques en guanines unides per una unitat ramificadora. Aquesta metodologia permet la síntesis d'estructures de G-quàdruplex formades per quatre cadenes on es pot modificar una o vàries posicions d'una sola cadena, per exemple introduint el derivat 8-aminoguanina. Aquesta estratègia també permet introduir una cadena amb una orientació oposada respecte a les altres tres. Quan totes les cadenes estan en la mateixa orientació, s'obté un quàdruplex paral·lel simètric. Quan una de les cadenes es troba amb una orientació oposada a les altres, s'obté un G-quàdruplex paral·lel o 3+1 segons el catió de la solució. També es descriu la presència d'estructures bimoleculars que poden tenir interès per aplicacions biomèdiques ja que alguns aptàmers contra el HIV són estructures bimoleculars de quàdruplex de guanina que tenen afinitat per la proteïna gp120.

A continuació es presenta una revisió de les metodologies d'espectroscòpia de masses aplicades als G-quàdruplex. L'ESI-MS en condicions natives permet determinar sense ambigüitats l'estequiometria de macromolècules i s'ha convertit en una tècnica molt utilitzada en l'estudi de G-quàdruplex per determinar el nombre de cadenes implicades en l'estructura o per detectar i quantificar complexes amb lligands. Es demostra que les estructures paral·leles de G-quàdruplex són més estables en fase gas que les estructures antiparal·leles utilitzant espectroscòpia de mobilitat iònica i estudiant la preservació dels ions d'amoni en l'estructura. L'estudi de la formació de G-quàdruplex induïda per co-dissolvents demostra que els dissolvents més emprats a ESI-MS afavoreixen la formació de G-quàdruplex i que l'estructura que s'obté depèn de la naturalesa d'aquest co-dissolvent.

El tercer capítol es troba entre el primer i el segon bloc i es basa en l'estudi estructural i d'estabilitat dels complexes formats entre derivats 9-amino acridines, que es troben en avaluació preclínica i el G-quàdruplex telomèric humà. S'ha observat que aquests compostos s'uneixen selectivament a les seqüències formadores de G-quàdruplex que es troben en regions promotores d'oncogens i en seqüències telomèriques. Un estudi detallat per RMN permet proposar un model del complex format, on les 9-amino acridines es troben entre les tètrades d'adenina i guanina del G-quàdruplex telomèric, formant interaccions π-π i enllaços d'hidrogen. Estudis de dinàmica molecular demostren que el model proposat és estable. També es demostra que aquests compostos indueixen una estabilitat del G-quàdruplex degut a les diferents interaccions de les parts que formen els lligands i que aquestes interaccions energèticament favorables estan directament relacionades amb l'activitat biològica d'aquests compostos.

L'altre gran bloc de la tesi es basa en la preparació i en el desenvolupament de nous lligands selectius a estructures de G-quàdruplex. S'han descrit vàries metodologies per obtenir oligòmers de compostos heterocíclis amb propietats d'unió al DNA amb la intenció de modular la selectivitat per diverses estructures de DNA així com la seva activitat biològica. La metodologia utilitzada en tots els casos ha estat la metodologia de síntesis en fase sòlida.

En aquest cas s'ha descrit una nova estratègia per obtenir oligòmers d'acridina amb un esquelet de PNA. Aquest mètode, basat en la generació de l'esquelet de la cadena i posterior acoblament de l'agent intercalant, és més ràpid i efectiu que el descrit prèviament sense la necessitat de construir el monòmer de cada intercalant. Els experiments de diàlisis competitiva mostren diferencies d'afinitat d'aquests compostos pels G-quàdruplex, especialment per les seqüències de G-quàdruplex que es troben en regions promotores d'oncogens. Desafortunadament, els compostos sintetitzats seguint aquesta nova metodologia no presenten activitat antitumoral.

A continuació, es van determinar les propietats d'unió al DNA d'una sèrie completa d'oligòmers, amb un esquelet d'aminoprolina, que contenien fins a tres unitats d'acridina i/o quindolina. Els oligòmers de quindolina mostren una gran afinitat per les estructures de tríplex i G-quàdruplex. En canvi, els oligòmers d'acridina presenten una major selectivitat per les estructures de G-quàdruplex, però amb una afinitat menor. L'afinitat dels oligòmers de la 4-aminoprolina amb acridina per les estructures de G-quadruplex és similar a l'afinitat descrita pels oligòmers d'acridina amb esquelet de PNA, indicant que els dos esquelets proporcionen unes propietats similar als compostos. S'ha realitzat un estudi detallat per dinàmica molecular i per RMN del complex format pel dímer de la quindolina amb una estructura de G-quàdruplex telomèrica. Aquest complex s'estabilitza per interaccions π-π, entre els anells aromàtics del dímer i les nucleobases del G-quàdruplex. Aquest complex pot ser el punt de

partida pel disseny de noves molècules amb una gran afinitat pels telòmers i amb propietats anticancerígenes.

A l'últim capítol es descriu la síntesis de diversos derivats de l'acridina DACA, un conegut inhibidor de la topoisomerasa I/II. Quan es substitueix el grup protonable dimetilamino de l'acridina DACA per uns amino àcids naturals es perd la capacitat d'unió al DNA així com l'activitat antitumoral del compost original. En canvi, els oligòmers obtinguts amb el cor de l'acridina DACA presenten una gran afinitat pel DNA i conserven l'activitat biològica. Es demostra que les propietats d'unió al DNA no es veuen afectades per la presència de càrregues negatives en l'esquelet dels oligòmers, mentre es millora la solubilitat.

Últimament l'interès per obtenir lligands capaços de discriminar entre quàdruplex *vs* dúplex s'ha desplaçat per dissenyar compostos capaços de diferenciar entre diverses topologies de quàdruplex, amb l'objectiu d'obtenir compostos més selectius i eficaços. Encara que hi queda un gran camí per obtenir potents fàrmacs on la seva diana terapèutica siguin els quadruplex de guanina, alguns d'aquest lligands selectius a aquestes estructures ja es troben en els primeres fases d'avaluació clíniques.

Conclusions

1. S'han preparat oligonucleòtids ramificats que contenen quatre cadenes riques amb guanina. La metodologia desenvolupada construeix primer una cadena i a continuació s'addiciona una molècula que genera tres funcions alcohols (triplicador o trebler) que són la base de la síntesis de les tres cadenes restants. Aquesta metodologia permet per primer cop la introducció individual d'anàlegs de les bases (per exemple 8-aminoguanina) i la preparació de quàdruplex amb tres cadenes paral·leles i una antiparal·lela.
2. L'anàlisi estructural per RMN i espectroscòpia de masses dels oligonucleòtids ramificats demostra per primer cop l'existència de dímers intermoleculars.
3. L'estudi detallat per espectrometria de masses de seqüències de 12 bases de DNA relacionades amb els telòmers humà demostra que les estructures paral·leles de quàdruplex de guanina són més estables en fase gas que les estructures antiparal·leles.
4. L'addició de co-dissolvents a seqüències de 12 bases de DNA relacionades amb els telòmers humà afavoreix la formació de quàdruplex de guanina i l'estructura que s'obté depèn de la naturalesa d'aquest co-dissolvent.
5. S'ha estudiat la interacció de 9-amino acridines que estan en avaluació preclínica amb diverses seqüències de DNA utilitzant la diàlisi competitiva. Es demostra una afinitat important de les acridines per seqüències formadores de quàdruplex entre les que es poden trobar seqüències telòmeriques i seqüències de promotors d'oncogens. Estudis de RMN confirmen l'afinitat de les acridines per les seqüències telòmeriques. A partir de les dades de RMN s'ha construït un model del complex acridina-seqüència telomèrica on s'observa la interacció de l'acridina amb les tètrades d'adenina i guanina del quàdruplex paral·lel formant interaccions π-π i enllaços d'hidrogen. Estudis de dinàmica molecular demostren que el model és estable.
6. S'ha demostrat per RMN i per dinàmica molecular que les 9-amino acridines indueixen una estabilitat del G-quàdruplex degut a les diferents interaccions de les parts que formen els lligands i que aquestes interaccions energèticament favorables estan directament relacionades amb l'activitat biològica.
7. S'han preparat oligòmers d'acridina amb un esquelet de (2-aminoetil)-glicina utilitzant una metodologia de síntesis en fase sòlida. Els compostos sintetitzats tenen afinitat per les estructures de quàdruplex però no presenten activitat antiproliferativa.
8. S'ha estudiat la interacció d'una sèrie d'oligòmers d'acridina i/o quindolina amb seqüències de DNA per diàlisis competitiva. La majoria dels derivats estudiats tenen afinitat per estructures de quàdruplex però els derivats de quindolina tenen molta més afinitat. Estudis de RMN confirmen aquesta afinitat amb el compost format per dos quindolines que presentava l'afinitat per quàdruplex més elevada de tota la sèrie. A partir de les dades de

RMN s'ha construït un model del complex dímer quindolina-seqüència telomèrica on s'observa les interaccions π-π entre els anells aromàtics del dímer i les nucleobases del quàdruplex.

9. S'ha preparat diversos compostos d'acridina derivats del N-[2-(Dimetilamino)etil]acridina-4-carboxamida (DACA), un inhibidor de la topoisomerasa I/II, utilitzant una metodologia de síntesis en fase sòlida. El més actiu dels compostos sintetitzats té una activitat antiproliferativa de l'ordre de 25 μM. S'ha avaluat l'afinitat relativa dels compostos sintetitzats per seqüències de DNA demostrant que els compostos tenen una elevada afinitat pel DNA però no són selectius per una estructura en concret.

Resum de la memòria

La tesi gira a l'entorn del estudi del quàdruplex de guanina i la síntesis i avaluació de lligands selectius a aquestes estructures.

En el capítol 1 es descriu una metodologia per obtenir estructures de G-quàdruplex molt estables. Aquesta metodologia permet introduir modificacions en una sola cadena o modificar la polaritat d'una cadena respecte les altres tres. En el segon capítol es presenta una revisió de les metodologies d'espectroscòpia de masses aplicades als G-quàdruplex i s'estudia la formació de G-quàdruplex induïda per co-dissolvents. En el tercer capítol es descriu el complex format pel G-quàdruplex telomèric humà amb unes acridines en avaluació preclínica, així com els estudis estructurals i d'estabilitat realitzats per RMN i per dinàmica molecular.

Els altres capítols formen la part de la tesi dedicada al desenvolupament de nous lligands selectius a estructures de G-quàdruplex amb interès biològic. Així doncs, en el quart capítol es descriu una nova estratègia per obtenir oligòmers d'acridina amb un esquelet de PNA i s'estudia les seves propietats d'unió a diverses estructures de DNA així com les seves propietats antitumorals. En el capítol 5 es determinen les propietats d'unió al DNA d'una sèrie completa d'oligòmers d'acridina i/o quindolina. També es realitza un estudi per RMN i per dinàmica molecular del complex format pel dímer de la quindolina i un G-quàdruplex. En l'últim capítol es descriu un nou mètode per obtenir uns derivats d'acridina DACA, un inhibidor de la topoisomerasa I/II. Es van realitzar experiments de diàlisis competitiva, RMN i de viabilitat cel·lular per determinar-ne les seves propietats d'unió al DNA a més de les seves propietats antiproliferatives.